AN INVESTIGATION ON THE APPLICATION OF TWO AND THREE DIMENSIONAL LIMIT EQUILIBRIUM ANALYSES IN SLOPE STABILITY

ŞEV DURAYLILIĞINDA İKİ VE ÜÇ BOYUTLU LİMİT DENGE ANALİZLERİNİN UYGULANMASI ÜZERİNE BİR ARAŞTIRMA

BEKİR SALİH FIRINCIOĞLU

Prof. Dr. MURAT ERCANOĞLU
Supervisor

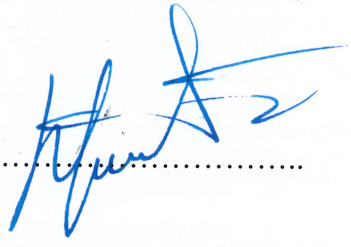
Submitted to Graduate School of Science and Engineering of Hacettepe University as a Partial Fulfillment to the Requirements for the Award of the Degree of Master of Science in Geological Engineering

2018

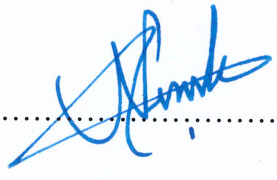
This work named "**An Investigation on the Application of Two and Three Dimensional Limit Equilibrium Analyses in Slope Stability**" by **BEKİR SALİH FIRINCIOĞLU** has been approved as a thesis for the Degree of **MASTER OF SCIENCE IN GEOLOGICAL ENGINEERING** by the below mentioned Examining Committee Members.

Prof. Dr. Tamer TOPAL
Head ..... 

Prof. Dr. Murat ERCANOĞLU
Supervisor ..... 

Prof. Dr. Harun SÖNMEZ
Member ..... 

Prof. Dr. Dilek TÜRER
Member ..... 

Prof. Dr. Nihat Sinan IŞIK
Member ..... 

This thesis has been approved as a thesis for the Degree of **MASTER OF SCIENCE IN GEOLOGICAL ENGINEERING** by the Board of Directors of the Institute for Graduate School of Science and Engineering.

Prof. Dr. Menemşe GÜMÜŞDERELİOĞLU
Director of the Institute of
Graduate School of Science and Engineering

To my family,

without them this work wouldn't have been possible.

YAYINLAMA VE FİKRİ MÜLKİYET HAKLARI BEYANI

Enstitü tarafından onaylanan lisansüstü tezimin/raporumun tamamını veya herhangi bir kısmını, basılı (kağıt) ve elektronik formatta arşivleme ve aşağıda verilen koşullarla kullanıma açma iznini Hacettepe üniversitesine verdiğimi bildiririm. Bu izinle Üniversiteye verilen kullanım hakları dışındaki tüm fikri mülkiyet haklarım bende kalacak, tezimin tamamının ya da bir bölümünün gelecekteki çalışmalarda (makale, kitap, lisans ve patent vb.) kullanım hakları bana ait olacaktır.

Tezin kendi orijinal çalışmam olduğunu, başkalarının haklarını ihlal etmediğimi ve tezimin tek yetkili sahibi olduğumu beyan ve taahhüt ederim. Tezimde yer alan telif hakkı bulunan ve sahiplerinden yazılı izin alınarak kullanması zorunlu metinlerin yazılı izin alarak kullandığımı ve istenildiğinde suretlerini Üniversiteye teslim etmeyi taahhüt ederim.

☐ **Tezimin/Raporumun tamamı dünya çapında erişime açılabilir ve bir kısmı veya tamamının fotokopisi alınabilir.**
(Bu seçenekle teziniz arama motorlarında indekslenebilecek, daha sonra tezinizin erişim statüsünün değiştirilmesini talep etseniz ve kütüphane bu talebinizi yerine getirse bile, tezinin arama motorlarının önbelleklerinde kalmaya devam edebilecektir.)

☒ **Tezimin/Raporumun 29.05.2021 tarihine kadar erişime açılmasını ve fotokopi alınmasını (İç Kapak, Özet, İçindekiler ve Kaynakça hariç) istemiyorum.**
(Bu sürenin sonunda uzatma için başvuruda bulunmadığım taktirde, tezimin/raporumun tamamı her yerden erişime açılabilir, kaynak gösterilmek şartıyla bir kısmı ve ya tamamının fotokopisi alınabilir)

☐ **Tezimin/Raporumun ..... tarihine kadar erişime açılmasını istemiyorum, ancak kaynak gösterilmek şartıyla bir kısmı veya tamamının fotokopisinin alınmasını onaylıyorum.**

☐ **Serbest Seçenek/Yazarın Seçimi**

29 / 05 / 2018



(İmza)

Bekir Salih Fırıncıoğlu

ETHICS

In this thesis study, prepared in accordance with the spelling rules of Graduate Studies in Science of Hacettepe University,

I declare that

- all the information and documents have been obtained in the base of the academic rules
- all audio-visual and written information and results have been presented according to the rules of scientific ethics
- in case of using others Works, related studies have been cited in accordance with the scientific standards
- all cited studies have been fully references
- I did not do any distortion in the data set
- and any part of this thesis has not been presented as another thesis study at this or any other university

28/05/2018



BEKİR SALİH FIRINCIOĞLU

ABSTRACT

AN INVESTIGATION ON THE APPLICATION OF TWO AND THREE DIMENSIONAL LIMIT EQUILIBRIUM ANALYSES IN SLOPE STABILITY

Bekir Salih FIRINCIOĞLU

Master of Science, Department of Geological Engineering

Supervisor: Prof. Dr. Murat ERCANOĞLU

May 2018, 251 pages

In this study, it was aimed at comparing the two and three-dimensional limit equilibrium methods, which were applied to different slope geometries and a real case study. Also, each method individually investigated with the aid of computer codes. Four very well-known and one inspired hypothetical slope geometries have been chosen from the literature for the investigations. Many combinations of scenarios have been integrated to these slope geometries including different conditions with groundwater levels, ponded waters, pseudo-static condition and external loadings. Total of 164 scenarios has been modelled in both two and three-dimensions. Morgenstern & Price's procedure was taken as the reference method as it is one of the well-known methods for its accuracy under various conditions.

During the two-dimensional analyses, underestimation and overestimation of the safety factors were noticed in different scenarios with various methods by up to - % 40 and + % 60. The same comparison between the three-dimensional analyses indicated that the safety factors were varying between - % 34 and + % 14 in all of the scenarios. The most intriguing results have been found in between the comparison of two and three-dimensional analyses. The calculated factors of safety were as low as 70 per cent and as much as 540 per cent different in some scenarios.

In addition to the hypothetical cases, a landslided area was chosen for the investigation using the limit equilibrium method at Denizkonak region in Kastamonu, Turkey. The investigations were started with a field study following the laboratory tests. The investigated area was generally formed by highly disintegrated flysch with layered siltstones. Therefore, Hoek-Brown failure criterion and Geological Strength Index were chosen for the strength and visual definition of the flysch. Two separate, but interdependent, landslides were observed at the investigated area, and possible cross-sections before the failures were drawn based on the current topography. Back-analyses were performed to obtain the conditions of failure and found that a high pore-pressure ratio was needed to trigger the landslide.

However, the second landslide has failed with a lower pore-water pressure and the current topography was determined to be on the edge of failure with a slight increase in the pore-pressure ratio. Also, three-dimensional analyses of the landslide area have generated unconservative results.

Keywords: back-analysis, Geological Strength Index, Hoek-Brown failure, limit equilibrium method, landslide, slope stability.

ÖZET

ŞEV DURAYLILIĞINDA İKİ VE ÜÇ BOYUTLU LİMİT DENGE ANALİZLERİNİN UYGULANMASI ÜZERİNE BİR ARAŞTIRMA

Bekir Salih FIRINCIOĞLU

Yüksek Lisans, Jeoloji Mühendisliği Bölümü

Tez Danışmanı: Prof. Dr. Murat ERCANOĞLU

Mayıs 2018, 251 sayfa

Şev duraysızlıklarına ilişkin değerlendirmeler, gerek insan yaşamı, gerekse yapılan ve/veya yapılması tasarlanan mühendislik yapıları için son derece önemli bir konudur. Bu konuya ilişkin çok sayıda yaklaşım, teori ve uygulama bulunmakla birlikte, geçmişteki temel yaklaşım, duraysızlıkların olduğu ve/veya olası olduğu yerlerde güvenlik katsayısı hesaplamalarının yapılıp, gerekiyorsa önlemlerin alınmasına yönelik uygulamaları içermektedir. Günümüzde ise, öncelikle daha büyük alanların, genel olarak analiz edilmesi/haritalanması, daha sonra ayrıntılı analizlerin yapılması şeklinde olup, genelden özele inen bir yöntembilimin izlenmesi yönündedir. Bu şekilde izlenen bir yöntemin, ekonomi ve zaman açısından önemli kazanımlar getirdiği, literatürde sıklıkla ifade edilmektedir.

Gerek insan yapımı, gerekse de doğal yollarla şekillenmiş olan her türlü yer yüzeyi şekli, eğime sahip olması ve gerekli diğer kaydırıcı etkenlerin sağlanması durumunda kaymaya karşı duyarlı durumdadır. Bu yer yüzeyi yapılarının kaymaya karşı olan güvenliğinin hesaplanması ve buna yönelik iyileştirme çalışmalarının yapılması, olası maddi zararların azaltılması ve insan yaşamını kısıtlayıcı unsurların giderilmesi ve en önemlisi, insan yaşamının güvenliği açısından çok önemli bir yer tutmaktadır. Bu tip duraysızlıkların tespit edilip ve modellenebilmesi için birçok teori ortaya sunulmuştur. Bu teoriler arasından limit denge teorisi neredeyse 100 yılı aşkın bir süredir kullanılmakla birlikte, çeşitli vakalar üzerinde uygulanarak, güvenilirliğini uzun yıllar önce kanıtlamıştır.

Şev duraysızlıkları, ya da geniş anlamıyla heyelanlar, tüm dünyada olduğu gibi, Türkiye'de de önemli zararlara yol açan doğa kaynaklı afet türlerinden biridir. Gerek nüfus artışı, gerekse doğal tehlikenin içerildiği alanlarda yapılan veya yanlış seçilen yerleşim alanları, bu doğal afet türünün sayısında da son 50 yıl içinde önemli bir artışa neden olmuştur. Dünyada ve ülkemizde, özellikle son 20 yıl içinde bu konuyla ilgili olarak, çok sayıda proje, uygulama ve araştırma yapılmış ve hayata geçirilmiştir. Bununla birlikte, karar vericilerin,

planlamacıların ve yöneticilerin konuya daha fazla önem vermeleri ve uygulamada bu tür çalışmaları dikkate alarak hayata geçirmeleri de son derece büyük bir önem arz etmektedir.

Yukarıda değinilen hususlar gözetilerek, bu tez çalışması kapsamında, limit denge yöntemlerinin şev duraylılığı problemlerine uygulanması üzerine kapsamlı bir araştırma yapılmıştır. Bu araştırma hipotetik şevlerle birlikte, geçmişte heyelana maruz kalmış bir alanı da kapsamaktadır. Limit denge yöntemleri ilk kullanıldığı yıllarda iki boyutlu kesitler üzerinde kullanılıyor olsa da, ilerleyen senelerde üç boyutlu modeller üzerinde çalışmalar yapılmış ve teoriler geliştirilmiştir. Günümüze kadar çok sayıda iki ve üç boyutlu yöntem geliştirilmiş olsa da, bunlardan sadece bazıları günümüzde sıklıkla kullanılmaktadır.

Son 20 sene içerisinde bilgisayar kullanımının son derece yaygınlaşmış olması ve gerek yazılımsal, gerekse de donanımsal özelliklerin son derece gelişmiş olması nedeniyle, mühendislik uygulamalarının pratikleştirilmesi için paket programlar piyasaya sürülmüştür. Bu çalışma kapsamında, Kanada kökenli Rocscience firmasının piyasa sürdüğü *Slide* ve *Slide*^{3} isimli programlar iki ve üç boyutlu şevlerin modellenmesi ve güvenlik katsayının hesaplanabilmesi için kullanılmıştır.

Tez çalışmasında, iki ve üç boyutlu analizler için toplamda 10 farklı yöntemden yararlanılmıştır. Bu yöntemler literatürde teorik çalışmalar için sıklıkla kullanılan ve iyi tanınmış olan 5 farklı şev geometrisi üzerinde uygulanmıştır. Bu şev geometrileri üzerine yeraltı suyu seviyesi, şev önünde su birikintisi, sismik ivme ve dış yükler eklenerek farklı kombinasyonlar üretilmiştir. Bu kombinasyonlar neticesinde iki ve üç boyutlu analizlerde kullanılmak üzere toplamda 164 farklı model oluşturulmuştur. Bu modeller üzerinde kayma yüzeyinin şekline göre uygun olan yöntemler ayrı ayrı uygulanmış ve karşılığında elde edilen güvenlik katsayıları kaydedilmiştir.

Bu araştırmalar sırasında güvenlik katsayısının kıyaslanabilmesi için dünyaca kabul görmüş, neredeyse her kayma koşuluna uyarlanabilen Morgenstern & Price'ın yöntemi referans değer olarak alınmıştır. Bu çalışmalar sonrasında her bir yöntemin ürettiği sonuç yüzdece ayrı ayrı incelenmiştir. İncelemeler iki ve üç boyutlu yöntemlerin karşılıklı kıyaslanmasına ek olarak kendi içlerinde de kıyaslanmıştır. İki boyutlu analizlerin tüm senaryolar üzerinde kıyaslanmaları sonucunda, bazı yöntemler güvenlik katsayısını % 40'a kadar daha düşük üretirken bazı durumlarda da % 60'a kadar daha yüksek hesaplamıştır. Bu durum üç boyutlu analizlerde de kendi içerisinde incelenmiş ve güvenlik katsayısı bazı durumlarda % 34 daha düşük sonuç verirken, bazen de % 14 daha yüksek sonuç verdiği saptanmıştır. Analiz sonuçlarının belki de en ilgi çekici bulgusu, aynı yöntemlerin iki ve üç boyutlu modeller üzerindeki performanslarının incelenmesi ile elde edilmiştir. Buna göre, iki boyutlu analizlerde hesaplanan güvenlik katsayılarına göre üç boyutlu analizler bazı durumlarda % 70 daha tutucu sonuç üretirken bazen de % 540'a kadar daha yüksek bir güvenlik katsayısı üretmiştir.

Tez kapsamında seçilen limit denge yöntemi, Kastamonu ilinin Cide ilçesinin Denizkonak beldesindeki bir paleoheyelan sahası üzerinde uygulanmıştır. Burada yapılan saha gözlemleri sırasında arazide farklı zamanda gelişen iki ayrı heyelanın varlığı tespit edilmiştir. Arazi gözlemleri ve insansız hava aracı ile çekilen fotoğraflara dayalı olarak, bunlardan ilkinin dönel tipte kayması ile birlikte, diğerinin kayan heyelan malzemesi içerinde yeniden duraysızlığını yitirerek akma tipi bir hareket gösterdiği tespit edilmiştir. Yapılan saha incelemesi sırasında bölgeye siltli ve killi birimlerin ardalanması ile gelişen aşırı bozunmuş ve ayrışmış filiş özelliğindeki birimin egemen olduğu belirlenmiştir. Ayrıca, arazi gözlemleri sırasında heyelan bölgesinin batı sınırında mostra vermiş litolojik birimlerin heyelan malzemesine göre dayanımındaki yüksek farklılık ve yamaç eğimindeki ani artışlar, olası bir yapısal unsurun varlığını işaret etmektedir.

Heyelanların kayma sırasındaki koşullarının incelenebilmesi için güncel topoğrafya üzerinden kesit alınmış ve bu kesite göre kayma öncesine ait iki farklı topoğrafya çizilmiştir. Kesitlerin modellenmesi sırasında saha gözlemleri temel alınarak, yenilme ölçütü olarak Hoek-Brown seçilmiştir. Sahadan alınan örnekler üzerinden disk makaslama indeksi deneyi yapılmış ve tek eksenli sıkışma dayanımı ile birim hacim ağırlık tayin edilmiştir. Çizilen ilksel geometri üzerinden yapılan geriye dönük analizler ile ilk heyelanın kayma anında jeolojik dayanım indeksi 20 olarak tespit edilmiştir. Bu sonuç, literatür ve saha gözlemleri ile de uyumludur. Yapılan analizler, ilk kayma gerçekleşmeden önce gözenek basıncı oranının en az 0.44 olduğu, ancak, örselenmiş malzeme içerisinde gerçekleşen ikinci kaymanın yaklaşık 0.24 gözenek basıncı oranıyla kaydığı tespit edilmiştir. Güncel topoğrafya üzerinde yapılan çalışmalar bölgenin gözenek basıncı oranının 0.33'ü geçmesi durumunda halen kaymaya karşı duyarlı olduğunu göstermektedir. Bu sonuçlar iki ve üç boyutlu analizlerin kıyaslanması üzerine iki boyutlu yöntemlerin daha tutucu sonuç vermesi neticesinde seçilmiştir.

Anahtar Kelimeler: geriye dönük analiz, Jeolojik Dayanım İndeksi, Hoek-Brown yenilme ölçütü, limit denge analizleri, heyelan, şev duraylılığı.

ACKNOWLEDGMENT

I would like to express my deepest gratitude to my supervisor, Professor Dr. Murat Ercanoğlu, who created the opportunity for this thesis to actualized. He consistently expressed his deep patience and steered this work to right direction whenever needed. Without his guidance and support of any kind this thesis would not have been possible.

I would like to thank to Professor Dr. Harun Sönmez, who contributed to this work with his deep sight and knowledge during the field investigation and as well as in other areas whenever needed.

I would like to thank to my beloved, Buke Oğul, who expressed her deepest supports whenever needed.

This thesis is supported by Hacettepe University Scientific Research Projects Coordination Unit with the project number of FHD-2018-16818.

TABLE OF CONTENTS

Page

ABSTRACT i
ÖZET iii
ACKNOWLEDGMENT vi
TABLE OF CONTENTS vii
LIST OF FIGURES x
LIST OF TABLES xvii
NOTATION & ABBREVIATIONS xxiii
UNIT CONVERSION TABLE xxviii
1. INTRODUCTION 1
2. LITERATURE REVIEW 3
2.1 State of The Art 3
2.1.1 Mass movement of the Mount St. Helens 3
2.1.2 The Vajont slide 8
2.1.3 Carsington Dam failure 9
2.1.4 Kettleman Hills failure 13
2.2 Other Studies on Limit Equilibrium Method 18
3. METHODOLOGY 27
3.1 Failure Criterions 27
3.1.1 Mohr-Coulomb criterion 27
3.1.2 Hoek-Brown criterion 28
3.1.2.1 An introduction of the criterion 28
3.1.2.2 The application of the criterion 29
3.2 Limit Equilibrium Procedures 35
3.2.1 Single body procedures 36
3.2.1.1 $\phi = 0$ method 36
3.2.2 Method of slices 36
3.2.2.1 Ordinary method of slices 37
3.2.2.2 Bishop's method 38
3.2.2.3 Morgenstern & Price's method 40
3.2.2.4 Spencer's method 40
3.2.2.5 Janbu's method 42
3.2.2.6 Sarma's method 44

3.2.2.7 Chen & Morgenstern's method 45
3.2.2.8 General limit equilibrium method of slices (GLE method) 46
3.2.3 Miscellaneous other methods 48
3.2.4 Comparison of limit equilibrium methods 51
3.2.5 Three-dimensional effect 54
3.2.5.1 Three-dimensional slope stability methods 55
3.2.5.1.1 Hovland's method 56
3.2.5.1.2 Chen & Chameau's method 56
3.2.5.1.3 Hungr's method 57
3.2.5.1.4 Lam & Fredlund's method 58
3.2.5.1.5 Huang & Tsai's method 59
3.2.5.1.6 Cheng & Yip's method 60
3.2.5.2 Miscellaneous other 3D methods 60
3.2.5.3 Comparison of three-dimensional methods 63
4. APPLICATION OF LIMIT EQUILIBRIUM PROCEDURES 68
4.1 The Analyses 70
4.1.1 Hypothetical case I 70
4.1.2 Hypothetical case II 85
4.1.3 Hypothetical case III 104
4.1.4 Hypothetical case IV 120
4.1.5 Hypothetical case V 123
4.1.6 Case VI 139
4.1.6.1 Introduction of the area 139
4.1.6.2 Field investigation 142
4.1.6.3 Laboratory testing 151
4.1.6.4 The stability analyses 154
5. DISCUSSIONS 166
5.1 Hypothetical Case I 166
5.2 Hypothetical Case II 168
5.3 Hypothetical Case III 170
5.4 Hypothetical Case IV 171
5.5 Hypothetical Case V 172
5.6 Case VI 173
6. CONCLUSIONS AND RECOMMENDATIONS 175

7. REFERENCES 177
APPENDICES 190
CURRICULUM VITAE 251

LIST OF FIGURES

Page

Figure 2.1. North slope of Mount St. Helens showing slide blocks I & II with fracture systems. [1] 4

Figure 2.2. Displacements against time. [4] 4

Figure 2.3. Direct shear test results. [4] 5

Figure 2.4. Cross section of Mount St Helens with assumed boundaries. [4] 6

Figure 2.5. The layers that affected the sliding surface. [13] 8

Figure 2.6. Cross section the failure site showing before (1) and after (2) the failure. [14] 8

Figure 2.7. Overall factor of safety against the extent of failure progression: (a) and (b) indicates the value for K=1 and K=2, respectively. [17] 9

Figure 2.8. Cross section of the Carsington Dam [18] 10

Figure 2.9. Plan view of the Carsington Dam and location of the slip. [18] 10

Figure 2.10. Geological profile in the ground area. [18] 11

Figure 2.11. A cross-section of Carsington Dam after failure [18] 12

Figure 2.12. The cross-section of the dam for the stability analyses [18] 13

Figure 2.13. Landfill Unit B-19 of Phase I-A (a) The plan view (b) Cross-section of C-1/C-2 (c) Cross-section of X-1/X-2. [21] 14

Figure 2.14. The pre-failure topography of the area [21] 15

Figure 2.15. Computed factors of safety for selected sections [21] 16

Figure 2.16. Plan view of the multiple block system used in the 3D analysis [21] 17

Figure 2.17. Plan view of the multi-block analysis with computed results. [21] 18

Figure 3.1 Fitting two different straight lines into failure envelope. A-line fitted onto low ranges of normal stresses while B-line fitted on overall envelope. [67] 27

Figure 3.2. The transition between intact rock material to rock mass. [68] 28

Figure 3.3. The modified GSI system. [75] 30

Figure 3.4. The relationship between two proposed disturbance factors. [75] 33

Figure 3.5. Evaluation of the disturbance factor. [76] 34

Figure 3.6. Slope and slip surface for the ϕ=0 method. (Modified from [84], [85]) 36

Figure 3.7. Typical slice with forces in Fellenius method. (Modified from [85]) 37

Figure 3.8. Forces acting on a slice of a soil mass. [53] 38

Figure 3.9. Polygon of forces on a typical slice. [53] 39

Figure 3.10. An enlarged sketch of the slice. [91] 41

Figure 3.11. Obtaining the factor of safety. [91] 42

Figure 3.12. Correction factor with respect to the ratio of the shear surface. [54] 44

Figure 3.13. Forces acting on circular slip surface. [57] 46

Figure 3.14. Forces for the noncircular case. [57] 47

Figure 3.15. The relationship between inclinations of interslice forces and slope surface. [85] 48

Figure 3.16. Slope profile. [123] 51

Figure 3.17. Typical sliding mass divided into soil columns. [134] 55

Figure 3.18. Typical soil column. [134] 56

Figure 3.19. Soil column after simplifying assumptions. [140] 59

Figure 4.1 Total combinations for different scenarios. 69

Figure 4.2 Cross-section of the homogeneous slope with a pre-defined slip surface. 70

Figure 4.3 Three-dimensional model of hypothetical case I. 70

Figure 4.4 Modelling of the low GWT elevation. 72

Figure 4.5 Three-dimensional model of the investigated slope. Blue and brown surfaces indicate the GWT and slip surface, respectively 72

Figure 4.6 Demonstration of the external loading. 73

Figure 4.7 Three-dimensional model of the slope for the scenario-*c*. External loadings indicated by red arrows. 74

Figure 4.8 Same slope profile as the analysis-*b* with an additional seismic activity. 74

Figure 4.9 Cross-section of the slope and applied external forces. 75

Figure 4.10 Cross-section of the slope profile with ponded water in front. 75

Figure 4.11 Three-dimensional profile of the scenario-*f*. 76

Figure 4.12 Three-dimensional profile of the scenario-*g*. 77

Figure 4.13 The slope profile with the combinations of all the scenarios. 78

Figure 4.14 Cross-section of the slope profile with high GWT elevation. 79

Figure 4.15 Three-dimensional model of the investigated slope for the scenario-*j*. 80

Figure 4.16 Three-dimensional model of the scenario-*k*. 80

Figure 4.17 Cross-section of the slope profile for the scenario-*m*. 81

Figure 4.18 The slope profile for the scenario-*n*. 82

Figure 4.19 Three-dimensional model of the scenario-*n*. 83

Figure 4.20 Three-dimensional model for the scenario-*p*. 83

Figure 4.21 Showing all of the combinations in cross-section. 84

Figure 4.22 Three-dimensional model of the scenario-*t*. 85

Figure 4.23 Cross-section of the slope with predefined circular slip surface which consists of fifty slices. 86

Figure 4.24 Three-dimensional model of the hypothetical case II. Brown area indicates the slip surface. 86

Figure 4.25 Indicating groundwater table level.....90

Figure 4.26 Three-dimensional slope geometry. Faint blue line indicates the GWT level. 90

Figure 4.27 Showing the location of the external loadings on top. 92

Figure 4.28 Three-dimensional model of the case II, scenario-*c*. 92

Figure 4.29 Cross-section of the slope profile with seismic activity.....93

Figure 4.30 Slope profile with external loadings on top and seismic activity. 93

Figure 4.31 Cross-section of the slope profile and ponded water at front. 94

Figure 4.32 Three-dimensional geometry of the case II, scenario-*f*. Faint blue surface indicates the water table level. 94

Figure 4.33 Three-dimensional slope geometry of case II, scenario-*g*. 95

Figure 4.34 Combinations of the possible scenarios. 96

Figure 4.35 Cross-section of the investigated slope with high elevation GWT.....97

Figure 4.36 Three-dimensional model of case II, scenario-*j*. 97

Figure 4.37 Three-dimensional model of the case II, scenario-*k*. 99

Figure 4.38 Cross-section of the slope profile with loadings on top.....100

Figure 4.39 Cross-section of the investigated profile. Indicating higher water table and ponded water.....100

Figure 4.40 Three-dimensional slope profile of the case II, scenario-*n*. Faint blue layer indicates the water table level.....101

Figure 4.41 Three-dimensional model of the case II, scenario-*p*. 102

Figure 4.42 Slope profile and other possible combinations.....103

Figure 4.43 Three-dimensional slope geometry of the case II, scenario-*t*. 103

Figure 4.44 Cross-section of the drained slope with external loadings and seismic accelerations. 104

Figure 4.45 Cross-section of the case III. The slip surface has been indicated by the red line. 105

Figure 4.46 Three-dimensional model of the hypothetical case III.....105

Figure 4.47 The cross-section of the slope profile. The blue line indicates the GWT. 107

Figure 4.48 Three-dimensional model of the scenario-*b*, hypothetical case III.....108

Figure 4.49 The slope profile with external loadings on top of the slope. 109

Figure 4.50 Three-dimensional profile of the investigated scenario. 109

Figure 4.51 The investigated cross-section of the slope. 110

Figure 4.52 The cross-section for the scenario-*f*. The dashed line indicates the ponded water. 111

Figure 4.53 Three-dimensional model of the scenario-f.....111

Figure 4.54 Three-dimensional slope profile of the scenario-g, hypothetical case III. 112

Figure 4.55 The cross-section of the slope with investigated external and internal effects. 113

Figure 4.56 The cross-section of the slope with high GWT. 114

Figure 4.57 Three-dimensional model of the scenario-*j,* hypothetical case III..... 114

Figure 4.58 Investigated slope profile of the scenario-*k.* 115

Figure 4.59 The cross-section of the slope for the scenario-*m.* 116

Figure 4.60 The cross-section of the investigated slope. The blue dashed area indicates the ponded water..... 116

Figure 4.61 Three-dimensional model of the scenario-*n.* The ponded water has been indicated by using a letter (w). 117

Figure 4.62 Three-dimensional model of the scenario-*p,* hypothetical case III..... 118

Figure 4.63 The cross-section of the investigated slope. 119

Figure 4.64 Three-dimensional profile of the investigated slope..... 119

Figure 4.65 The fully drained slope profile with loadings and seismic activity. 120

Figure 4.66 The cross-section of the investigated dam. The red line indicates the slip surface 121

Figure 4.67 Three-dimensional model of the hypothetical case III..... 121

Figure 4.68 Three-dimensional profile of the hypothetical case IV. Brown area indicates the sliding surface. 123

Figure 4.69 The slope profile of the case V. 124

Figure 4.70 Three-dimensional model of the hypothetical case V..... 124

Figure 4.71 Three-dimensional profile of the scenario-*a*, hypothetical case V. Brown area indicates the slip surface 126

Figure 4.72 The cross-section of the slope. The blue line indicates the water table. 127

Figure 4.73 Three-dimensional model of the scenario-*b,* hypothetical case V..... 127

Figure 4.74 The location of the external loadings on top of the slope. 128

Figure 4.75 Three-dimensional model of the scenario-*c,* hypothetical case V. 128

Figure 4.76 The investigated slope model for the scenario-*e,* case V. 129

Figure 4.77 The cross-section of the slope for the scenario-*f*, hypothetical case V. 130

Figure 4.78 Three-dimensional model of the scenario-*f*, hypothetical case V. 130

Figure 4.79 Three-dimensional model of the scenario-*g*, hypothetical case V. 131

Figure 4.80 The cross-section of the investigated slope profile for the scenario-*i*, case V. 132

Figure 4.81 The analyzed slope model for the scenario-*j*, case V. 132

Figure 4.82 Three-dimensional model of the scenario-*j*, hypothetical case V. 133

Figure 4.83 Three-dimensional model of the scenario-*k*, hypothetical case V. 134

Figure 4.84 The cross-section of the scenario-*m*, case V. 135

Figure 4.85 The cross-section of the slope for the scenario-n, case V. 135

Figure 4.86 Three-dimensional model of the scenario-*n,* hypothetical case V. 136

Figure 4.87 Three-dimensional model of the scenario-*p*, hypothetical case V. 137

Figure 4.88 The investigated slope model for the scenario-*s*, case V. 137

Figure 4.89 Investigated slope profile of the scenario-*t*, hypothetical case V. 138

Figure 4.90 The slope model for the scenario-*v*, case V. 139

Figure 4.91 The location of the study area. 139

Figure 4.92 Three-dimensional model of the investigated area. 140

Figure 4.93 Elevation map of the inspected area. 140

Figure 4.94 The outcrops of the two landslides. 142

Figure 4.95 Aerial photograph of the two landslides. 143

Figure 4.96 Approximate scarp of the Landslide #1. 143

Figure 4.97 The outcrop of the Landslide #1. Showing a steeply inclined surface. 144

Figure 4.98 The steeply inclined outcrop of the Landslide #1. 144

Figure 4.99 Highly disintegrated and eroded rocks at the ground surface. 145

Figure 4.100 Highly disintegrated and eroded rocks at the slope surface. 145

Figure 4.101 Disintegrated siltstones at the upper side of the photograph. Highly weathered soil-like siltstones at below. 146

Figure 4.102 Highly weathered and disintegrated layered siltstones. 146

Figure 4.103 Weathered and disintegrated layered siltstones. 147
Figure 4.104 Decomposed and weathered marl. 147
Figure 4.105 Tilted over a wooden electric pole. 148
Figure 4.106 Damaged house with minor cracks on the wall. 148
Figure 4.107 Minorly damaged building wall. 149
Figure 4.108 Severely damaged old village house. 149
Figure 4.109 Severely damaged village house due to the landslide. 150
Figure 4.110 Devastated building due to slope instability. 150
Figure 4.111 Severely damaged house pillars due to uplifting caused by the landslide. Red arrows indicate the area of vertical movement. 151
Figure 4.112 The block punch index test apparatus. 152
Figure 4.113 Preparation of the block specimens. 152
Figure 4.114 Prepared specimens for the BPI test 153
Figure 4.115 Cross-section of the investigated area. Dashed and dotted lines indicate post-failure 2D topography. 155
Figure 4.116 Pre-failure model of the investigated area. 155
Figure 4.117 Three-dimensional model of the Landslide#1. Brown area indicates the sliding mass. 156
Figure 4.118 Back-analyses for the very first failure. 156
Figure 4.119 Cross-section of the topography before the second failure. 159
Figure 4.120 Three-dimensional model of the Landslide#2. 159
Figure 4.121 The relationship between the safety factors and the pore-pressure ratio. 160
Figure 4.122 Two-dimensional model of the current topography 162
Figure 4.123 Three-dimensional model of the estimated current topography 162
Figure 4.124 Comparing the safety factors with the pore-pressure ratio 163

LIST OF TABLES

Page

Table 2.1. Geotechnical properties of deposit. [4] 5

Table 2.2. Computed results of factors of safety. [4] 7

Table 2.3. Factors of safety for randomly generated slip surfaces. [4] 7

Table 2.4. Geotechnical properties of fill materials. [18] 11

Table 2.5. The results of the analyses. [18].....13

Table 2.6. Shear strengths and angles of internal friction between interfaces [21].....15

Table 2.7. Computed results of the analyses. [21] 18

Table 3.1. Values of the constant m for intact rock material. Values in parenthesis are estimates. [72].....32

Table 3.2. Results for different methods of analysis. [123].....51

Table 3.3. Comparison of the method of slices.....52

Table 3.4. Characteristics of three-dimensional methods. [191].....63

Table 3.5. Summarized three-dimensional methods. [192] 66

Table 4.1 Available methods in *Slide* and *Slide*^{3}.....69

Table 4.2 Coordinates of the slope profile in x and y-axes 71

Table 4.3 The results of the fully-drained analyses.....71

Table 4.4 Coordinates of the low GWT elevation.....72

Table 4.5 Computed factors of safety for low GWT elevation.....73

Table 4.6 Results of the stability analysis with external loading. 74

Table 4.7 The results of the analyses with seismic activity. 74

Table 4.8 Computed safety factors for scenario-*e*. 75

Table 4.9 Coordinates of the water table in the Cartesian system.....76

Table 4.10 Computed factors of safety for the scenario-*f*.....77

Table 4.11 Computed results of the safety factors for scenario-*g*.....77

Table 4.12 Computed results for the scenario-*h*.....77

Table 4.13 Computed results for the scenario-*i*. 78
Table 4.14 Coordinates of the high GWT elevation. 78
Table 4.15 Computed factors of safety for the scenario-*j*. 80
Table 4.16 Computed results of safety factors for the scenario-*k*. 80
Table 4.17 Computed results of the factors of safety for the scenario-*l*. 81
Table 4.18 The results of the analysis for the scenario-*m*. 81
Table 4.19 Coordinates of the water table from the scenario-*n*. 82
Table 4.20 The computed safety factors for the scenario-*n*. 83
Table 4.21 Computed safety factors for scenario-*p*. 83
Table 4.22 The results of the stability analyses for the scenario-*r*. 84
Table 4.23 Computed safety factors for the scenario-*s*. 84
Table 4.24 The results of the analyses for the scenario-*t*. 84
Table 4.25 Computed results of the scenario-*v*. 85
Table 4.26 Computed results for the scenario-*y*. 85
Table 4.27 Assumed properties of the slope forming materials. 86
Table 4.28 Coordinates of the slope boundary. 86
Table 4.29 The coordinates of the materials boundary for hypothetical case II. 89
Table 4.30 Results of the calculations for the scenario-*a*. 89
Table 4.31 Coordinates of the groundwater table. 91
Table 4.32 Calculated factors of safety for the scenario-*b*. 91
Table 4.33 Coordinates of the external loadings. 92
Table 4.34 Results of the analysis for the scenario-*c*. 92
Table 4.35 Computed safety factors for the scenario-*d*. 93
Table 4.36 Computed safety factors for the scenario-*e*. 94
Table 4.37 Location of the water table. 95
Table 4.38 Computed safety factors for the scenario-*f*. 95

Table 4.39 Computed factors of safety for the scenario-*g.* 96
Table 4.40 The results of the analysis of the scenario-*h.* 96
Table 4.41 Computed safety factors for the scenario-*i.* 96
Table 4.42 Coordinates of the groundwater table. 97
Table 4.43 Results of the stability analysis for scenario-j. 98
Table 4.44 The results of the analysis for the scenario-*k.* 99
Table 4.45 Computed factors of safety for the scenario-*l.* 99
Table 4.46 The results of the analysis for the scenario-*m.* 100
Table 4.47 Coordinates of the water table. 101
Table 4.48 Computed results for the scenario-*n.* 101
Table 4.49 Computed results for the scenario-*p.* 102
Table 4.50 The results of the analysis for the scenario-*r.* 102
Table 4.51 Computed safety factors for the scenario-*s.* 103
Table 4.52 Computed safety factors for the scenario-*t.* 103
Table 4.53 The results of the computations for the scenario-*v.* 104
Table 4.54 The computed factors of safety for the scenario-*y.* 104
Table 4.55 Geotechnical properties of the materials in Case III. 105
Table 4.56 Location of the slip surface 106
Table 4.57 Location of the external and the material boundary, hypothetical case III. 106
Table 4.58 Calculated factors of safety for the scenario-*a.* 107
Table 4.59 The results of the analysis for the scenario-*b.* 107
Table 4.60 The location of the groundwater table. 108
Table 4.61 The calculated safety factors for the scenario-*c.* 108
Table 4.62 The coordinates of the external loadings for the scenario-*c.* 109
Table 4.63 The calculated safety factors for the scenario-*d.* 110
Table 4.64 The results of the analysis for the scenario-*e.* 110

Table 4.65 The location of the water table for the scenario-*f.* 111

Table 4.66 The results of the analysis for the scenario-*f.* 112

Table 4.67 The results of the analysis for the scenario-*g.* 112

Table 4.68 The computed safety factors for the scenario-*h.* 113

Table 4.69 The computed safety factors for the scenario-*i.* 113

Table 4.70 The location of the water table for the scenario-*j.* 114

Table 4.71 The computed safety factors for the scenario-*j.* 115

Table 4.72 The computed safety factors for the scenario-*k.* 115

Table 4.73 The results of the analysis for the scenario-*l.* 115

Table 4.74 The computed safety factors for the scenario-*m.* 116

Table 4.75 The location of the water table 117

Table 4.76 The computed safety factors for the scenario-*n.* 117

Table 4.77 The results of the analysis for the scenario-*p.* 118

Table 4.78 The computed safety factors for the scenario-*r.* 118

Table 4.79 The computed safety factors for the scenario-*s.* 119

Table 4.80 The results of the analysis for the scenario-*t.* 119

Table 4.81 The computed safety factors for the scenario-*v.* 120

Table 4.82 The computed safety factors for the scenario-*y.* 120

Table 4.83 Geotechnical properties of the materials. 121

Table 4.84 The location of the slip surface and external boundary 122

Table 4.85 Coordinates of the material boundaries for the hypothetical case III. 122

Table 4.86 The results of the analysis for the scenario-*a.* 123

Table 4.87 The computed safety factors for the scenario-*b.* 123

Table 4.88 Geotechnical properties of the materials for Case V 124

Table 4.89 The coordinates of slope geometry. 125

Table 4.90 Location of the slip surface for the hypothetical case V. 125

Table 4.91 Computed factors of safety for the scenario-*a*. 126

Table 4.92 The location of the groundwater table for the scenario-*a*, case V. 126

Table 4.93 The results of the analysis for the scenario-*b,* case V. 127

Table 4.94 The coordinates of the external loadings for the scenario-*c,* case V. 128

Table 4.95 The computed safety factors for the scenario-*c,* case V. 128

Table 4.96 Safety factors for the scenario-*d,* case V. 129

Table 4.97 The computed safety factors for the scenario-*e,* case V. 129

Table 4.98 The coordinates of the groundwater table. 130

Table 4.99 The results of the analysis for the scenario-*f*, case V. 131

Table 4.100 The computed safety factors for the scenario-*g,* case V. 131

Table 4.101 The results of the analysis for the scenario-*h,* case V. 131

Table 4.102 The results of the analysis for the scenario-*i*, case V. 132

Table 4.103 The coordinates of the groundwater table for the scenario-*j*. 133

Table 4.104 The results of the analysis for the scenario-*j*, case V. 133

Table 4.105 The computed safety factors for the scenario-*k*, case V. 134

Table 4.106 The results of the analysis for the scenario-*l*, case V. 134

Table 4.107 The computed safety factors for the scenario-*m*, case V. 135

Table 4.108 The coordinates of the water table for the scenario-n. 136

Table 4.109 The results of the analysis for the scenario-*n*, case V. 136

Table 4.110 The computed safety factors for the scenario-*p*, case V. 136

Table 4.111 The computed safety factors for the scenario-*r*, case V. 137

Table 4.112 The results of the analysis for the scenario-*s*, case V. 138

Table 4.113 The results of the analysis for the scenario-*t*, case V. 138

Table 4.114 The computed safety factors for the scenario-*v*, case V. 138

Table 4.115 The computed safety factors for the scenario-*y*, case V. 139

Table 4.116 Total precipitation from 1990 to 2010 for Cide district. 141

Table 4.117 Total precipitation for the last three months of the years. 141

Table 4.118 The results of the laboratory tests. 153

Table 4.119 The input parameters used in the analyses. 154

Table 4.120 The coordinates of the investigated landslide in two and three-dimensions. 157

Table 4.121 The coordinates of the Landslide#2 for modelling purpose. 160

Table 4.122 The coordinates of up-to-date cross-section of the landslide area as the time of this work. 163

NOTATION & ABBREVIATIONS

Notation

Σ	Summation operator
ΔQ, Q	Resultant of interslice forces
ΔW, W	Weight of slice or column
ΔX, X	Vertical forces between slices with boundary values X_n, X_{n+1} or X_L, X_R
h_t	Vertical distance between shear surface and line of thrust
D_n	Estimated number of discontinuity sets
E'	Normal effective for on slice interface
F_0	Initial value for factor of safety before correction
F_{local}	Factor of safety against shear on interslice boundary
J_v	Volumetric joint count
b_m	Dimensionless parameter appears in rock mass constant
b_s	Dimensionless parameter appears in material or rock mass constant
c'	Cohesion with respect to effective stress
c'_P	Cohesion with respect to peak strength
c'_R	Cohesion with respect to residual strength
c_u	Undrained shear strength
f_0	Correction factor
$f_0(x)$	Interslice force inclination function
m_b	Rock mass constant
m_i	Intact rock material constant
m_α	Input parameter for 2D factor of safety
n_α	Input parameter for 3D factor of safety
z_Q	Vertical distance between shear surface and resultant interslice forces
γ_d	Dry unit weight of material
$\theta_x, \theta_y, \theta_z$	Inclination of applied normal force on base of column with respect to x, y and z axes
σ'	Effective stress
σ'_1	Major principal effective stress at failure
σ'_3	Minor principal effective stress at failure
σ_c	Uniaxial compressive strength of intact rock material

σ_n	Normal stress
τ_r	Residual shear strength
ϕ'_P	Angle of internal friction with respect to peak strength
ϕ'_R	Angle of internal friction with respect to residual strength
Δx	Width of column in x direction
Δy	Width of column in y direction
A	Area of base of column
a	Constant depending on the characteristic of rock mass
a	Variable perpendicular distance from base of slice to moment center
A_L, A_R	Resultant of external water force
a_L, a_R	Vertical distance from the resultant of external water force to center of rotation
b	Width of slice
d	Depth of shear surface from *L*
D	Diameter used in the BPI test
D	Input parameter for horizontal seismic force
d_f, *D*	Disturbance factor for rock masses
E, ΔE	Horizontal forces between slices with boundary values E_a, E_b, E_n, E_{n+1}
F	Factor of safety
F	Failure load used in the BPI test
f	Offset arm of normal force
F_f	Factor of safety with respect to force equilibrium
F_{fi}	Computed final value for factor of safety after iteration
F_i	Factor of safety obtained using Spencer's both moment and force equilibrium equation
F_{in}	Initial value for factor of safety before iteration
F_m	Factor of safety with respect to moment equilibrium
F_{mo}	Factor of safety obtained using Spencer's moment equilibrium equation with horizontal interslice forces
G	Resultant of horizontal point load
G	Specific gravity of a material
H	Horizontal inter-column shear force
h	Height of slice

I_r	Infilling rating
k	Critical seismic coefficient
K	Earth pressure coefficient
kW	Horizontal seismic force
L	Direct length of slope from toe to crest
L	Length of shear surface
l	Length of base of slice
m	Mohr-Coulomb power function constant
n	Mohr-Coulomb power function constant
O	The center of circular shear surface
p	Total vertical stress at base of slice
P	Normal force applied to base of slice
P_L, P_R	Normal force applied to side of column
P_v	Vertical external force
R	Radius of circular shear surface
R_r	Roughness rating
r_u	Pore pressure ratio
s	Dimensionless parameter for material and rock mass
S, S_m	Shear force along base of slice
S_x, S_y	Components of shear forces along base of slice
t	Slope of X-b curve
t	Thickness used in the BPI test
U, u	Pore pressure
V	Vertical inter-column shear force on the side of a column
w	Water content
W′	Weight of soil mass
w_L	Liquid limit of a soil sample
w_{opt}	Optimal water content
w_p	Plastic limit of a soil sample
W_r	Weathering rating
x	Horizontal distance between axis of rotation of shear surface and center of gravity of soil mass, slice or column.
x_g, y_g	Coordinates for center of gravity of soil mass
x_i, y_i	Coordinates of midpoint of base of slice

Z	Inclined interslice forces with boundary values Z_n, Z_{n+1}
N	Number of surfaces on a rock block
P'	Effective normal force applied to base of slice
S	Estimated average discontinuity spacing
c	Cohesion
d	Leibniz's notation
dy	Vertical distance from the axis of rotation to center of base of column
$f(x)$	Interslice force inclination function
α	Inclination of base of slice or column
α_{xz}, α_{yz}	Components of inclination of base of column
γ	Average inclination of slope surface
θ	Inclination of interslice forces
θ_i	Inclination of interslice forces when Spencer's both moment and force equilibrium established
λ	Scaling constant
τ	Shear stress
ψ	Known value by iteration for Sarma's procedure
ϕ	Angle of internal friction
ϕ'	Angle of internal friction with respect to effective stress

Abbreviations

2D	Two-dimensional
3D	Three-dimensional
BPI	Block punch index
BPI_c	Corrected block punch index
CF	Clay fraction
Corps.	U.S. Army Corps. of Engineers
DOS	Direction of slide
FEM	Finite Element Method
FOS	Factor of safety
GIS	Geographical Information Systems
GLE	Generalized limit equilibrium

GSI	Geological Strength Index
GWT	Groundwater table
HDPE	High density polyethylene
ISRM	The International Society for Rock Mechanics and Rock Engineering
JanbuC	Janbu's corrected method
JanbuS	Janbu's simplified method
L&K	Lowe & Karafiath's method
LEM	Limit equilibrium method
LL	Liquid limit
MP	Morgenstern & Price's method
OMC	Ordinary method of columns
OMS	Ordinary method of slices
PI	Plasticity index
PL	Plasticity limit
SarmaNV	Sarma's non-vertical slices method
SCR	Surface condition rating
SR	Structure rating
UAV	Unmanned aerial vehicle
UCS	Uniaxial compressive strength
UU	Unconsolidated-undrained

UNIT CONVERSION TABLE

To convert from	to	Multiply by
Feet	m	0.3048
Inches	cm	2.54
Psf	Pa	47.88
lb	kg	0.4536
bars	kPa	100

1. INTRODUCTION

Any earthwork with an inclination, man-made or natural are prone to fail under certain circumstances. Recognition and prevention of possible instabilities are sometimes vital for the continuity of human life, and the consequences of any failure can be devastating for companies in terms of monetary loss. Many theories have been developed since the middle nineteenth century to understand the phenomena of failure on soil and rock masses. One of them is limit equilibrium theory which is a relatively simple and yet convenient and reliable procedure to apply.

Limit equilibrium methods have begun to be developed almost a hundred years ago since then many changes have been made and rigorous solutions have been developed in both two and three-dimensional concepts. Today, it is almost impossible to determine the number of total individual works has been done under this theory. In this thesis, approximately 70 of them have been summarized or mentioned covering both two and three-dimensional studies. This number can be fetched to hundreds by a further extensive work. Also, the usage of the theory for the past fifty years has been summarized with notable works.

In this work, three comparative studies have been made; 2D and 3D methods have been compared separately in terms of the safety factor in their own category. Then the same methods also compared between two and three-dimensional results. The calculations of the safety factors have been done with the aid of computer programs *Slide* and *Slide*^{3} developed by a Canadian company Rocscience Inc. For the comparative purposes, four very well-known and one inspired hypothetical slope geometries have been chosen. Many different scenarios have been integrated into slopes including drained situation, various groundwater levels, ponded waters, earthquake-induced accelerations and external loadings. As a result, 82 scenarios have been created and modelled under two and three-dimensional analyses which make a total of 164 scenarios.

In addition to hypothetical cases, a real case study has been investigated. The investigation area was in Denizkonak village of Cide district in the city of Kastamonu, Turkey. The investigation region is known for several previously occurred landslides and is still susceptible to failure. Two landslides have been identified in the study area during the field investigations. The geology of the area was generally formed by highly disintegrated and weathered layered flysch composed of clayey and silty materials. Also, an unmanned aerial vehicle (UAV) was flown to create a three-dimensional model from almost three hundred

photographs and to investigate the study area from a different perspective. A cross-section of the area was drawn based on the current topographic map and two other cross-sections of the previous landslides was also estimated. The Hoek-Brown failure criterion has been chosen for the strength definition of the material and BPI tests have been performed to determine the uniaxial compressive strength. Back-analyses have been carried out in 2D and 3D to understand the failure conditions of the landslides. Also, current topography was investigated to determine any prone-to-fail situation.

2. LITERATURE REVIEW

Among the many methods of slope stability, limit equilibrium procedure is one of the most used techniques by practicing engineers and researchers. Many instabilities of natural landslides, engineering structures and man-made fills have occurred over the last decades. Some of them had great effects on human life and monetary lost; while others did not affect the modern civilization. In both ways, studying these instabilities by any means advances humankind forward.

2.1 State of The Art

Some of the greatest and the most studied instabilities will be summarized and explained in this chapter to show the usage of the concept of limit equilibrium procedures. A major natural slide, a waste landfill failure, collapsing of a volcanic mountain and a well-known dam failure will be represented in the following lines.

2.1.1 Mass movement of the Mount St. Helens

The north slope of Mount St. Helens bulged for two months from the intrusion of magma. Before the volcanic eruption, this intrusion caused a collapse that created one of the most colossal mass movement in the history.

Voight [1] have investigated the movement mechanism based on the photographs of the failure mass during the event before the explosion. According to Stoffel & Stoffel [2], a new fracture system about 1.5 km length has formed before the failure across the north slope. The first slide of the multiple retrogressive failures, block I, has occurred along the new fracture system [1], [2]. Then, the standing crown after the first failure had collapsed, generating a massive failure referred to as slide block II [3] (Figure 2.1). Retrogressive failure had continued in the crown behind the scarp of the slide block II with numerous and successive failures, namely, slide block III [4].

According to Stoffel & Stoffel [2], summit eruptions were phreatic required high elevation groundwater table; which originated from melting of snow and ice over the mountain.

Deformation measurements done by Lipman et al. [5] indicated that a 1 km wide zone was moving northwards at steady rates of 1.5 – 2.5 m/day. The fracture system that causes slide block I to fail developed along the most intense horizontal displacement [4].

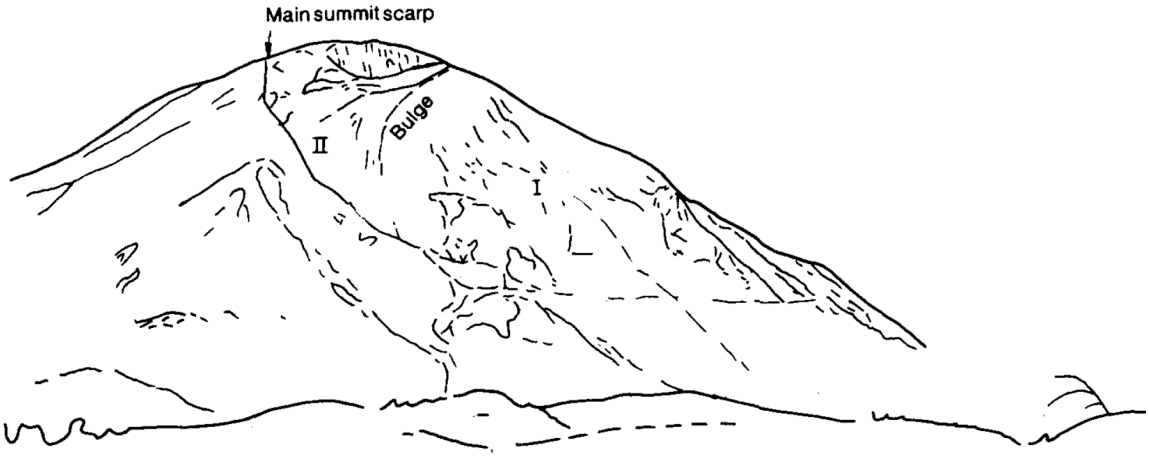


Figure 2.1. North slope of Mount St. Helens showing slide blocks I & II with fracture systems. [1]

Normalized displacements against the time until the failure of the slope was plotted (Figure 2.2) and extrapolation had been done to the curve to suggest an initial movement date [4]. The data from rapid movements indicated that frequent earthquakes were associated with a significant portion of the cumulative displacement [5].

The force of magma intrusion increased shear stress and decreased overall rock mass strength; generating major shear surfaces [4].

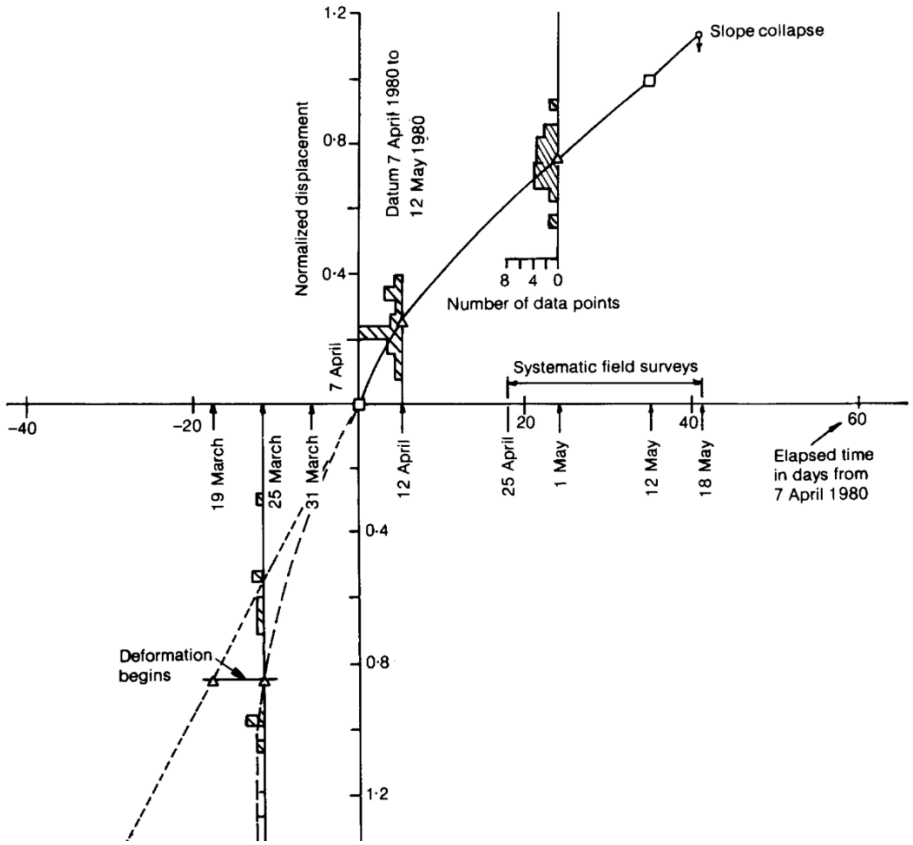


Figure 2.2. Displacements against time. [4]

According to authors, the deposit of failure mass (i.e. avalanche), was heterogeneous and varies from clay-sized particles to blocks over 100m length. Geotechnical properties of the materials have been investigated to characterize the material (Table 2.1).

Table 2.1. Geotechnical properties of deposit. [4]

Property	Mean	Range
Texture		
Percentage (<0.004 mm) clay	4	1 - 7
Percentage silt	11	5 - 21
Percentage sand	42	15 - 69
Median diameter, mm	1.9	0.26 - 9.2
Sorting coefficient	7.1	2.9 - 13
Uniformity coefficient	104	13 – 300
Specific gravity of solids	2.7	2.62 – 2.78
Dry bulk density g/cm^3		
Disturbed	1.68	1.54 – 1.94
Undisturbed	1.80	1.66 – 1.92
Porosity		
Disturbed	0.36	0.27 – 0.42
Undisturbed	0.32	0.28 – 0.37
Void ratio		
Disturbed	0.58	0.37 – 0.72
Undisturbed	0.47	0.38 – 0.60
Relative density, %	54	32 – 70
Water content, %	8.7	5.0 – 14.0
Saturation, %	44	21 – 71
Laboratory permeability, m/s		
Mechanical jostled	8.6 x 10^{-5}	1.8 x 10^{-6} – 2.9 x 10^{-4}
Water jostled	7.3 x 10^{-5}	2.4 x 10^{-6} – 1.5 x 10^{-4}
Field permeability, m/s	9 x 10^{-6}	-

Laboratory direct shear tests were applied to the material samples to gain an overview of the behavior of the deposit under loading; indicating residual strength was generally taking the role on the failure [4]. Also, the authors draw a linear strength plot and the internal friction angle of the material was found to be around 40° – 44° (Figure 2.3).

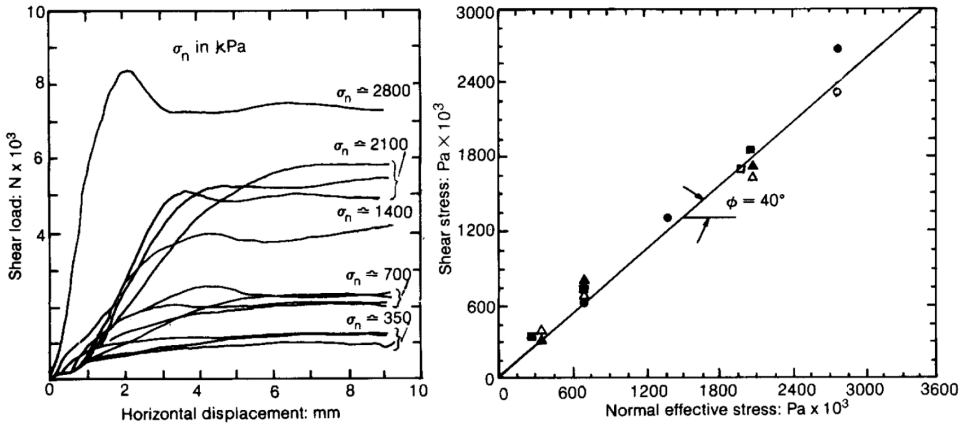


Figure 2.3. Direct shear test results. [4]

Limit equilibrium method had been chosen by the authors [4] to analyze the stability of the initial failure of the mountain with mainly using Bishop's modified procedure and sometimes the ordinary method of slices. Slip surfaces specified to approximate the boundaries of the slide blocks I, II and III are shown by C, B and E, respectively. Slip surfaces D and A were used to examine the influence of position on the block I slide surface (Figure 2.4).

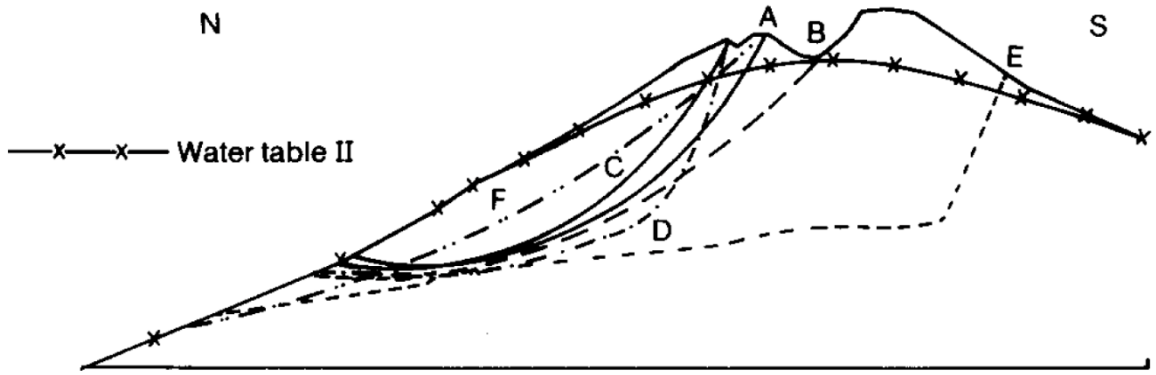


Figure 2.4. Cross section of Mount St Helens with assumed boundaries. [4]

Density of the material forming the slope of the mountain was assumed to be 2.4 gr/cm^3, the angle of internal friction of 40° and cohesion of the material assumed to vary between 0 and 10 bars (i.e. 0 to 1000 kN/m^2). Three different phreatic conditions were assumed; completely dry slope, fully saturated (water table I) and partially saturated (water table II). Pore pressure coefficients r_u taken in the range of 0.2 – 0.4. The computed results for the factor of safety has been given in Table 2.2. The authors suggested to increase the value of FOS by 10 – 20% for three-dimensional effects; where originally proposed by Hovland [6].

Also, the authors had searched for the most critical failure surfaces shaped as cylindrical and sliding block form. Results found to be more critical than the assumed surfaces (Table 2.3). For cohesionless conditions generated slip surfaces found to be too shallow and the resultant values of factors of safety were unrealistically low [4]. For c = 10 bar, the predicted slip surfaces were comparable to the trial surface C and factors of safety were in good agreement with around 4% difference.

Although no strong data available for earthquake record at the time of failure, a surface wave identified with magnitude 5.2 that could serve as a trigger to the mass movement [7], [8]. The researchers suggested that earthquakes with a magnitude of 5 produce near source peak horizontal ground accelerations 0.3 – 0.4k [9]. For a shallow earthquake magnitude of 4.5,

critical acceleration recorded as 0.15*k* [10]. Indicating that the assumption of seismic coefficients greater than 0.2 was not realistic during the instability[4].

Table 2.2. Computed results of factors of safety. [4]

	Cohesion c: bars	*F*			
		A	B	C	D
Water table II (Figure 2.4.)	0	1.11	1.16	1.05	1.37
	1	1.15	1.19	1.09	1.41
	10	1.45	1.47	1.43	1.72
Full Saturation	0	1.00	1.05	0.95	1.28
	10	1.33	1.36	1.33	1.61
Pore pressure coefficient					
$r_u = 0.0$ (dry)	0	1.88	1.94	1.81	2.32
$r_u = 0.2$	0	1.42	1.47	1.36	1.77
$r_u = 0.3$	0	1.19	1.24	1.14	1.50
$r_u = 0.4$	0	0.97	1.01	0.92	1.24
$r_u = 0.3$	1	1.23	1.27	1.18	1.54
$r_u = 0.3$	10	1.52	1.55	1.52	1.84
Seismic coefficient (horizontal) for $r_u = 0.3$					
$k = 0.1$	0	0.99	1.02	0.95	1.20
$k = 0.2$	0	0.84	0.86	0.82	1.00
$k = 0.3$	0	0.74	0.75	0.72	0.86

Table 2.3. Factors of safety for randomly generated slip surfaces. [4]

		Cohesion c: bars	*F*
Circular surfaces (Modified Bishop procedure)	Water table II (Figure 2.4.)	0	0.96
		10	1.38
	Pore pressure coefficient		
	$r_u = 0.3$	0	0.92
	$r_u = 0.3$	10	1.47
Block bounded by Rankine wedges	Water table II (Figure 2.4.)	0	1.00
		10	1.38
	Pore pressure coefficient		
	$r_u = 0.3$	0	1.04
	$r_u = 0.3$	10	1.46

As a result, the performed analyses suggested that there were several reasons behind the failure of the mountain including progressive strength loss associated with the intrusion of the magma, seismicity and gravitational movements [4].

2.1.2 The Vajont slide

In 1963, a catastrophic landslide suddenly occurred on the southern slope of the Vajont dam reservoir. The slide mass had a volume of approximately 270 million m^3; which generated a wave of 140 meters high above the top of the dam, demolishing the near villages and killing almost 2000 people [11].

The mass movement of the slope occurred along bedding plane surfaces [12] with one or more plastic clay layers (Figure 2.5) dominating continuously the slip surface [11].

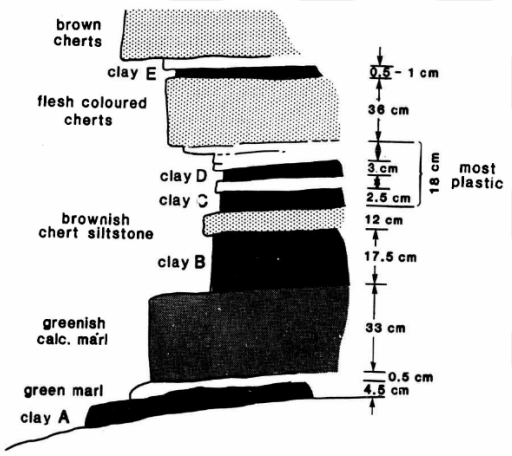


Figure 2.5. The layers that affected the sliding surface. [13]

The slip surface of the landslide assumed as chairlike shaped. The bedding planes were steep at the crest and the toe was flat (Figure 2.6).

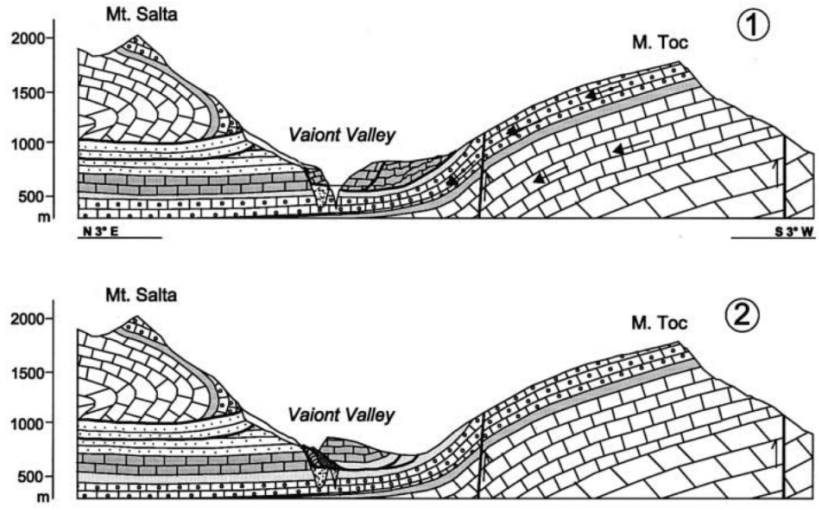


Figure 2.6. Cross section the failure site showing before (1) and after (2) the failure. [14]

Various researchers used limit equilibrium methods to analyze the failure of the slope. Mencl [12], calculated the effective angle of internal friction as 20° or more to maintain the slope in equilibrium. Calculations were done by assuming there was no pore water pressure between the clayey beddings. Lo et al. [15] used Janbu's method [16] to calculate the friction angle during the failure. They assumed that the groundwater level was equal to the water level in the reservoir. They obtained a friction angle as low as 13° to maintain the limit equilibrium.

Chowdhury [17] proposed a different approach to explain the failure of the Vajont valley. He developed a method to simulate the progressive transformation of the slope from a stable condition to one of limit equilibrium. Failure mechanism of the slope assumed to be progressive. The author mentioned that it had generally been accepted the failure started from the crest of the slope and progressed towards the toe. Analyses performed by Chowdhury indicated that the overall factor of safety decreased with an increase of the extent of failure progression up to a minimum value and then increased in F with the failure progression (Figure 2.7).

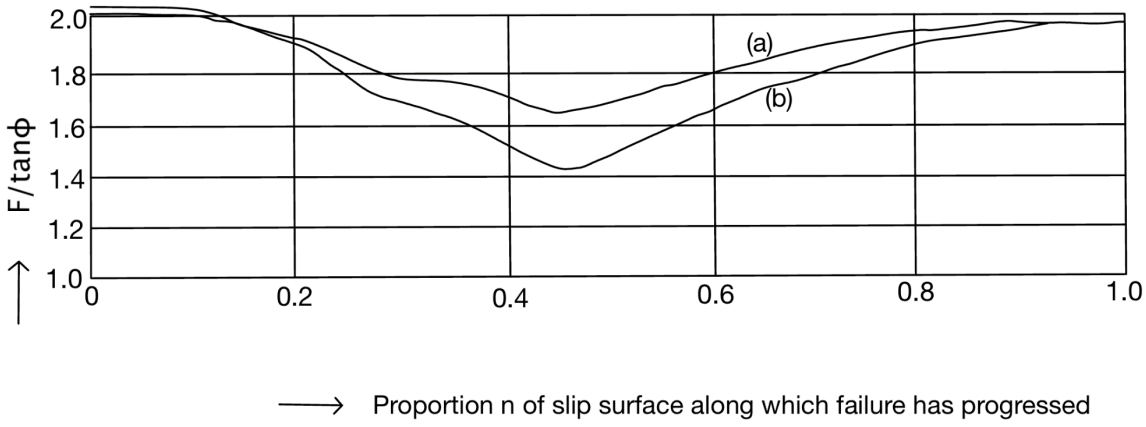


Figure 2.7. Overall factor of safety against the extent of failure progression: (a) and (b) indicates the value for K=1 and K=2, respectively. [17]

2.1.3 Carsington Dam failure

In 1984, before its completion, the upstream slope of the Carsington Dam failed. The initial slip started on the right abutment and spread across the valley to a length of almost 500 meters.

The dam designed to be at 202.37 m above the stream bed; which it failed at elevation 200 – 201 m during the construction period. The dam had a clay core with an upstream extension (the boot) and compacted mudstone at shoulders with drainage blankets of crushed limestone

at every 4 meters height [18]. A typical cross-section of the dam was given below (Figure 2.8).

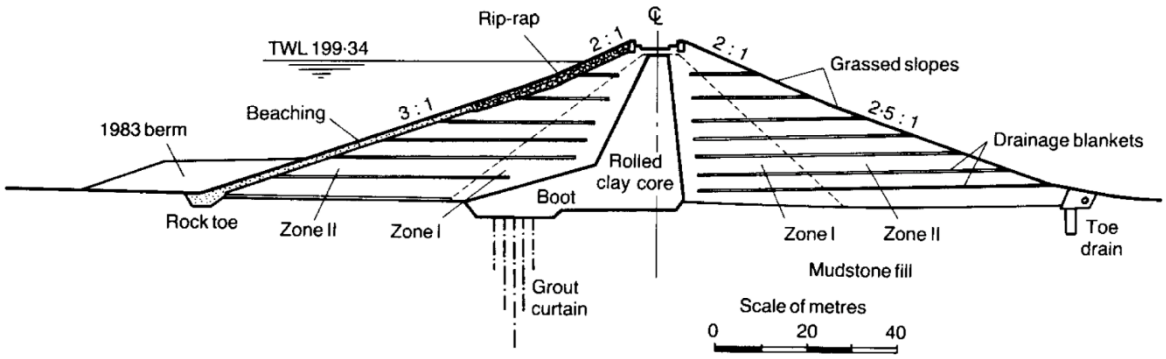


Figure 2.8. Cross section of the Carsington Dam [18]

During the construction, observations of pore pressures and settlements at four different location were made. The initial slip along the dam had a length of 120 m and reached 500 m at the final extent (Figure 2.9); causing large settlements of the crest and outward movements of the upstream toe [18].

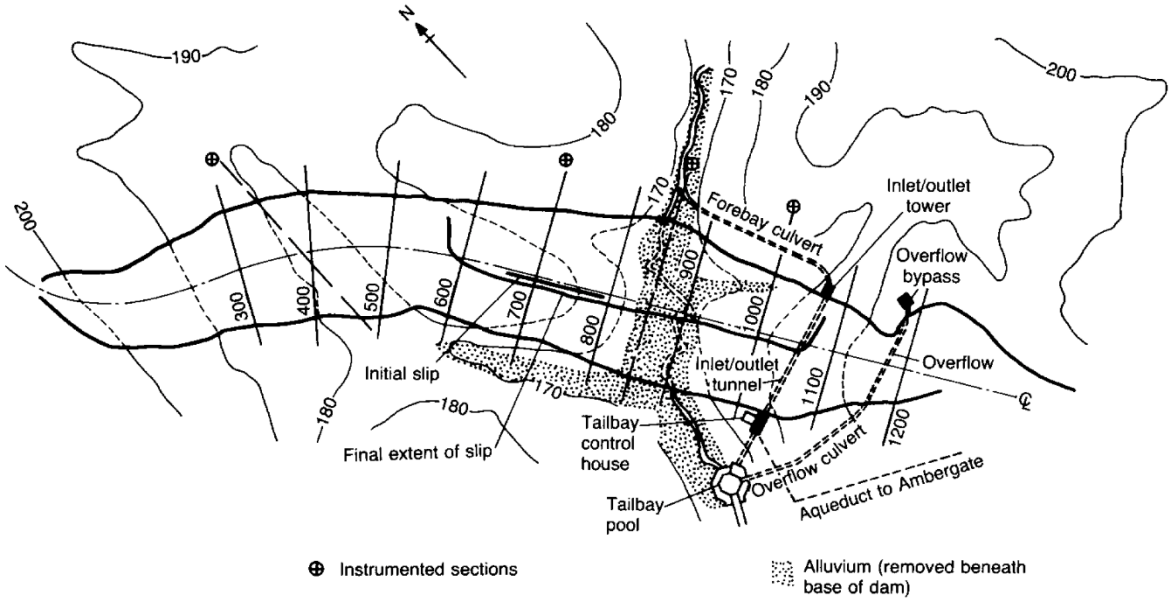


Figure 2.9. Plan view of the Carsington Dam and location of the slip. [18]

Around the construction area, four trial pits were excavated along with the borings for investigation purposes. They showed that around 1-meter thickness a silty clay subsoil (a_1) and plastic yellow-brown clay deposits (a_2) overlying a completely weathered mudstone (b_1). Below this layer, a dark grey clay (b_3) and a brecciated material (b_4) over a weak mudstone (b_5) exist (Figure 2.10). Beneath these layers, a heavily jointed unweathered mudstone (b_6) was encountered during the field research of the authors [18].

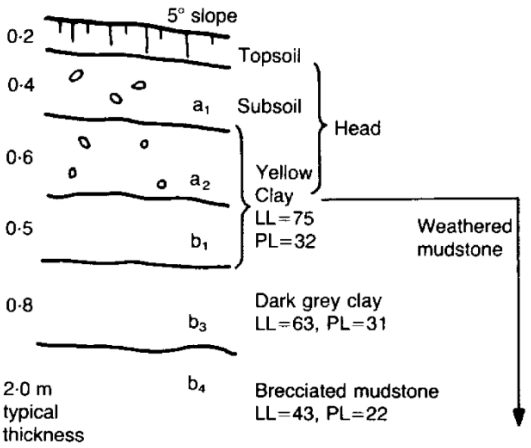


Figure 2.10. Geological profile in the ground area. [18]

Some of the investigated soil layers had been used for the construction of the dam for economical and practical purposes. While investigating the geotechnical properties of the soils, water content, plasticity and clay fraction had been found to increase in value with respect to weathering degree [18]. Properties of fill zones which used in the construction period were given in Table 2.4.

Table 2.4. Geotechnical properties of fill materials. [18]

Property		Core	Zone I	Zone II
Standard compaction	w_{opt}: %	26	20	14
	γ_d: kN/m^3	14.6	16.2	18.1
In situ properties	w: %	34	24	14, 18*
	γ_d: kN/m^3	13.6	15.4	18.3
Liquid limit w_L: %		69	56**	45
Plastic limit w_P: %		31	29	23
Plasticity index (PI): %		38	27	22
Clay fraction (CF): %		56	-	34
Activity (PI/CF)		0.68	-	0.65
Specific gravity G		2.68	2.71	2.71
Peak strength	c'_P: kPa	15	10	17
	ϕ'_P: °	21	22	26
Residual strength	c'_R: kPa	0	-	0*
	ϕ'_R: °	13	-	15*

*From shear zone (small samples)
**Single test only

While exploring the failure, the authors noticed two closely spaced slip surfaces with minor shear surfaces in Yellow Clay (a_2 and b_1). The same type of shear surfaces had also been observed while field investigation and marked as a down-slope movement due to freezing and thawing during solifluction [18]. The observed profile of the dam and the slip surfaces was given in Figure 2.11.

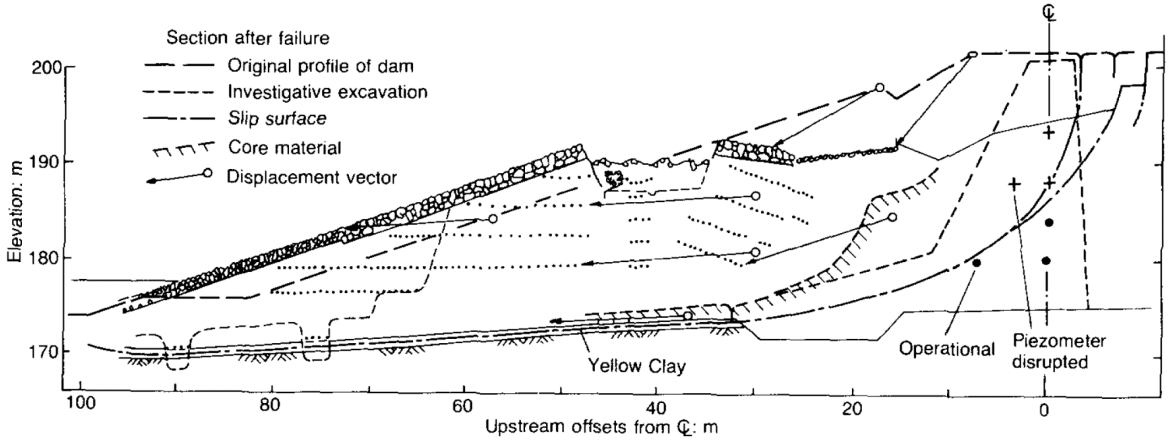


Figure 2.11. A cross-section of Carsington Dam after failure [18]

The laboratory analyses had been done by considering the peak intact strength, peak strength under the effect of solifluction shears and residual strength of the materials. Also, the average shear strain along the slip surface at the time of the failure was calculated using finite element analysis to calibrate the mobilized shear strength parameters [18].

According to Vaughan [19], if the length of the initial failure in a deep-seated slide was greater than the critical length, the soil mass would fail without three-dimensional effect. This is why the limit equilibrium analyses of the dam had been chosen to compute in two-dimensions [18].

The stability of the Carsington Dam was investigated using multiple wedges with six vertical slices. The interslice forces assumed to act at an angle of 10°. The pore pressures in the core and boot were taken from the piezometer readings. Various slip surfaces had been chosen around the observed surface (Figure 2.12). The surface that gives the lowest factor of safety was almost overlaying the actual one [18].

The authors noted that the results of the analyses (Table 2.5) could not be precise; but there would be little changes in computed factors of safety as slip geometry, pore pressures and many input parameters were known. Various inclinations of inter-slice forces had been tried and found to have an insignificant effect on the FOS. The effect of the different solifluction

shears had also been investigated and the results showed that an additional effect of progressive failure would be necessary to initiate the failure [18].

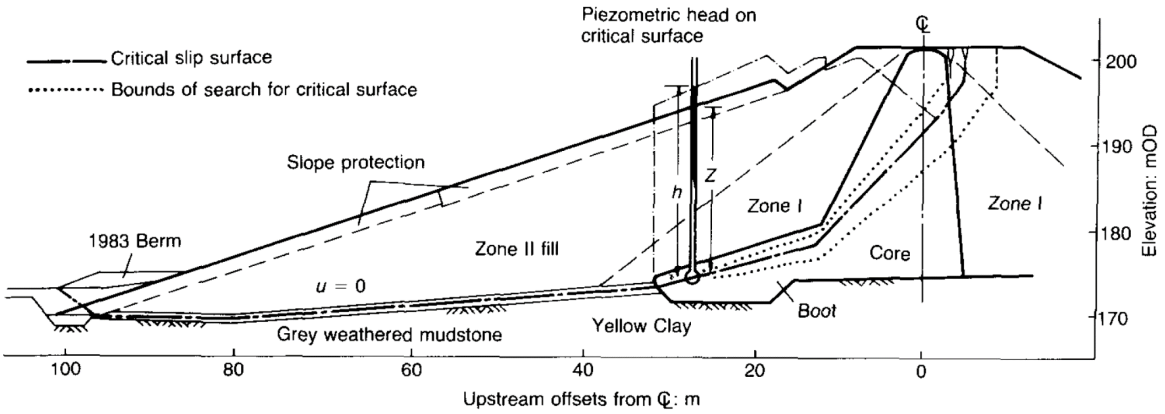


Figure 2.12. The cross-section of the dam for the stability analyses [18]

Almost 75 percent of the slide did not fail at the beginning, failed after significant movement of the initial failure; indicating a progressive slide failure mechanism. Also, the horizontal extension of the failure can be explained by lateral load transfer [19].

Table 2.5. The results of the analyses. [18]

Condition	Core		Yellow Clay		FOS	Reduction: %	Combined reduction: %
	c: kPa	ϕ': °	c: kPa	ϕ': °			
Peak, intact	15	21	10	20	$F_1 = 1.41$		
Peak, with shears	6	20	6	18	$F_2 = 1.21$	$\frac{F_1 - F_2}{F_1} = 14$	
At failure	1.5	19	0	16	$F_3 = 1.00$	$\frac{F_2 - F_3}{F_2} = 17$	$\frac{F_1 - F_3}{F_1} = 29$
Residual	0	13	0	12	$F_R = 0.71$		

2.1.4 Kettleman Hills failure

Kettleman City hosted a Class I hazardous waste treatment and storage facility, generally called as Kettleman City Landfill. Landfill Unit B-19 has an area of 145,7x10^3 m^2 and covers the region called Phase 1-A waste pile. When the pile reached a maximum height of 27 m, an instability occurred. Resulting in lateral displacements of about 10.7 m and vertical settlement of the surface were as much as 4.3 m [20].

To prevent the pollution of the environment with the hazardous material, the base and the sides of the excavated area were lined with a multilayer system of impervious geomembranes, clay layers and drainage layers [21]. The plan view of the Landfill B-19 of Phase I-A area and the cross-sections showing the liner system and the fill were given in the Figure 2.13. below for clarity.

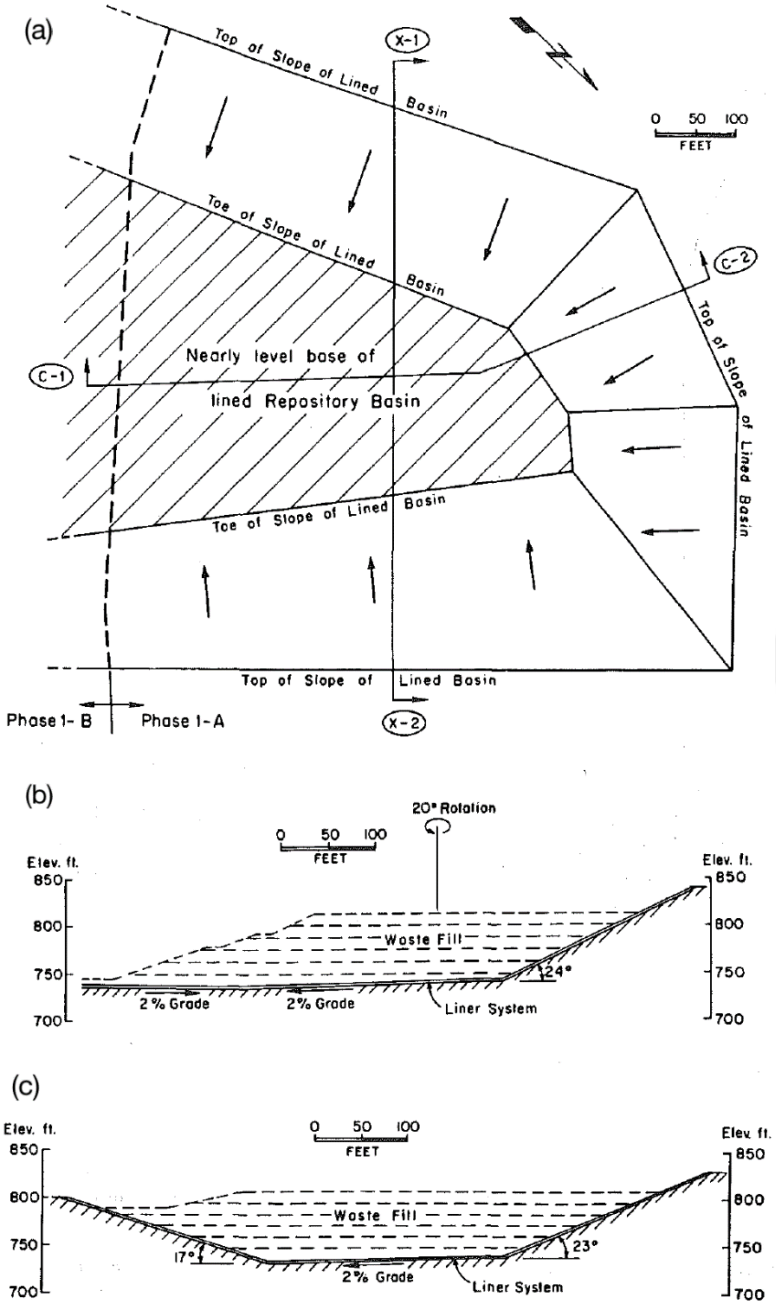


Figure 2.13. Landfill Unit B-19 of Phase I-A (a) The plan view (b) Cross-section of C-1/C-2 (c) Cross-section of X-1/X-2. [21]

The composite flexible-membrane-compacted-clay double-liner system underlying the failure surface was well investigated by Mitchell et al. [20]. The system included geotextile

filter fabric, granular leachate-collection layers, plastic geonet-drainage layers, HDPE (high-density polyethylene) geomembrane liners and compacted clay layers [21].

The most critical surfaces within the system were investigated for stability purposes and found to be among the three components as follows [20]: Between HDPE liner/geotextile layer, HDPE liner/geonet layer and HDPE liner/compacted clay layer. The angles of internal friction and shear strengths between the layers were summarized in Table 2.6.

Table 2.6. Shear strengths and angles of internal friction between interfaces [21]

Interface components	Dry interface conditions	Submerged interface conditions
HDPE liner/geotextile	$\phi'_R \approx 9° \pm 1°$	$\phi'_R \approx 8° \pm 1°$
HDPE liner/geonet	$\phi'_R \approx 8.5° \pm 1°$	$\phi'_R \approx 8.5° \pm 1°$
HDPE liner/clay (presoaked, UU)	-	$\tau_r = 900$ psf $\pm$ 250 psf
Values used for analysis	$\phi'_R = 8.5°$	$\phi'_R \approx 8°$ or $\tau_r = 900$ psf

An average value for the unit weight of waste landfill was assumed by taking the wastes and soils placed in the fill into consideration. All stability analyses were carried out by taking the density of 1.76 g/cm^3 and residual angle of internal friction and residual strength was used. The plan view of the Unit B-19 of Phase I-A before the failure with pre-failure topography has been determined by the investigators (Figure 2.14).

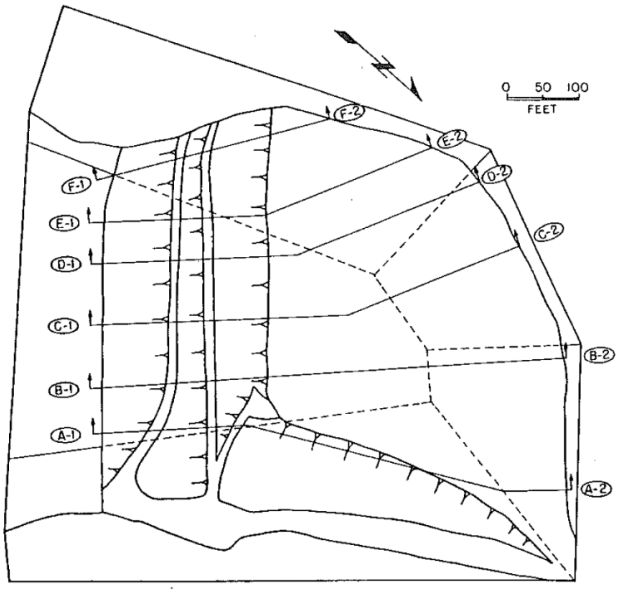


Figure 2.14. The pre-failure topography of the area [21]

All stability analyses have performed by considering two different cases. The first one assumed to be wetting of HDPE liner/compacted clay liner in the lower area of the fill, referred to as "Probable Minimum Clay Liner Wetting Case". In the second case, wetting of the base of the landfill excluding the inclined area was analyzed, called as "Full Base Wetting Case".

Ten different cross-sections have been chosen for stability analyses and six of them can be seen in Figure 2.14. The analyses have been carried in two-dimensions based on the force-equilibrium methods. The inclination of the resultant forces between driving blocks and resisting blocks were assumed to be at 20° [21]. The computed results of the analyses for six different cross-sections under two different cases were given in Figure 2.15; the other four cross-sections also presented the similar results. There were only two sections that gave factors of safety below unity. As these two sections represented only a partial area of the whole failure mass, it was found unlikely that these sections could trigger a progressive failure initially collapsing the whole unit [21]. The authors also weighted each cross-section in proportion to the whole mass to gain a representative overall factor of safety; which resulted in an estimated value of 1.15 to 1.25 [21].

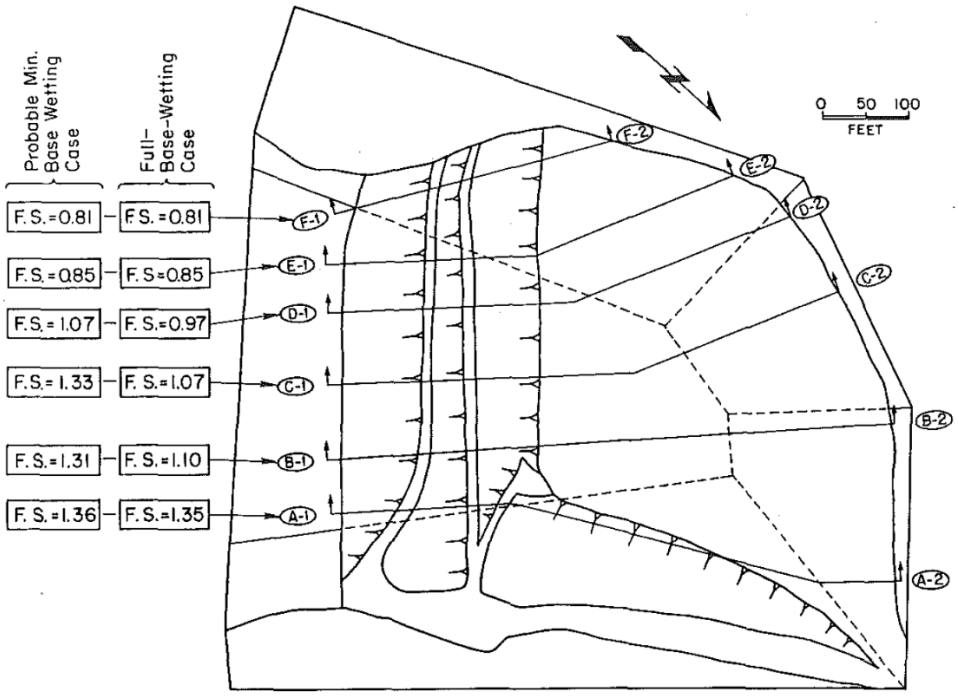


Figure 2.15. Computed factors of safety for selected sections [21]

The authors generally concluded that the sections with factors of safety less than unity were initiated a progressive tearing or dragging effect increasing the likelihood of the horizontal rotation of the mass resulting in reduced lateral pressure [21]. The authors also indicated that

three-dimensional stability analysis would provide a better understanding of the failure and probably give more accurate results.

The authors also declared that three-dimensional analyses would yield factors of safety less than two-dimensional analysis wherein inclined side slopes drive forces to the central toe of the area. Two different approaches were used to analyze the problem. One of them was Multiple Block Analysis; where the fill area divided into five blocks (Figure 2.16) to consider force equilibrium of each block and inter-block forces to resolve the overall potential sliding of the system.

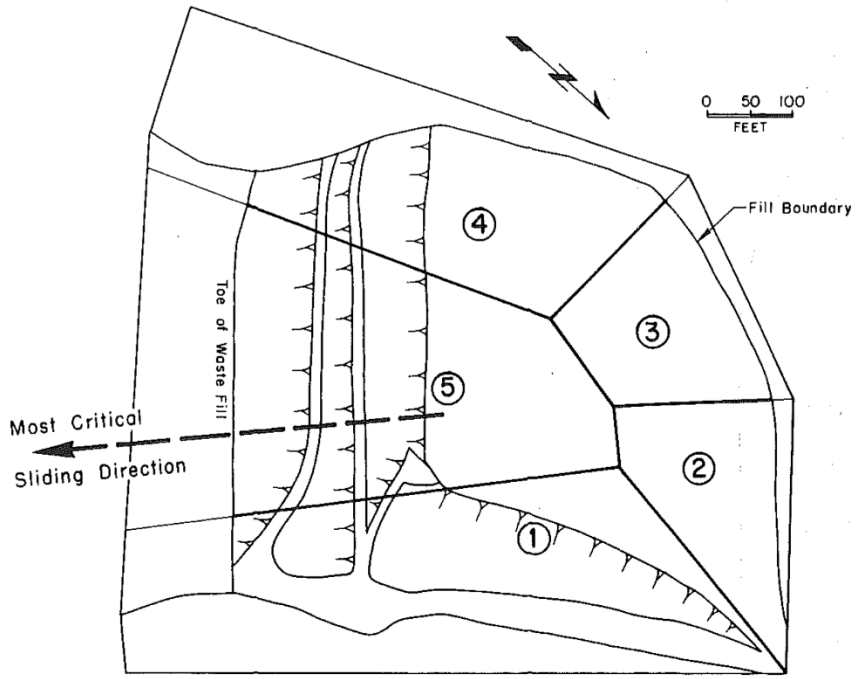


Figure 2.16. Plan view of the multiple block system used in the 3D analysis [21]

In the second approach, blocks in the system were assumed to slide in non-uniform directions and the fill area was divided into 11 different individual blocks with showing cross-sections used previously (Figure 2.17). The calculated overall factor of safety found to be %20 lower than the two-dimensional analyses and %15 lower than the first three-dimensional approach [21]. The same strengths and parameters were used in all three approaches.

However, the authors noted that the equilibrium conditions were not perfectly satisfied. The summed base resultant force was found to be approximately %2 less than the total weight, additional horizontal forces of %3.7 of the total fill weight were also found in the direction of sliding and %1.5 perpendicular to the sliding mass [21].

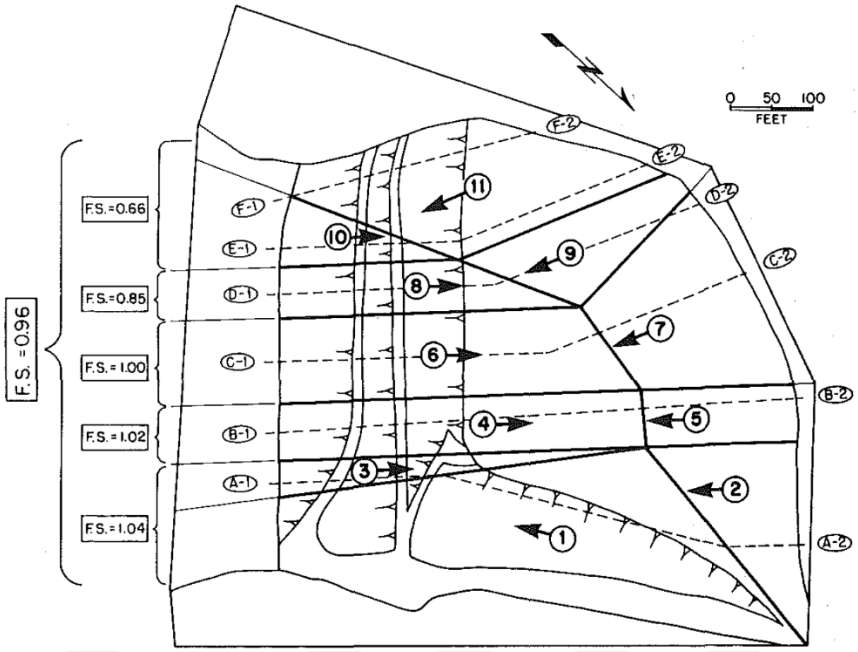


Figure 2.17. Plan view of the multi-block analysis with computed results. [21]

The overall results of the three-dimensional analysis were found to be less than two-dimensional analyses by approximately %10-15 and after consideration of some uncertainties such as human error, laboratory results and engineering judgment, the authors noted that estimated overall factors of safety would be in a range of 0.85 to 1.25 (Table 2.7) [21]. Also, it should be noted that another analysis was done on Kettleman Hills failure and the value for the 3D factor of safety was found to be around %1-8 larger than the two-dimensional analyses [22].

Table 2.7. Computed results of the analyses. [21]

Base liner conditions	Factor of Safety		
	2D Analyses	3D Analyses	Overall best estimate
Probable minimum clay/liner wetting case	1.2 to 1.25*	1.08	≈0.95 to 1.25
Full-base wetting case	1.1 to 1.15*	1.01	≈0.85 to 1.15

*Estimated

2.2 **Other Studies on Limit Equilibrium Method**

Many studies have been performed in slope stability analyses using limit equilibrium procedures, some of them incorporate the procedure for solving cases, some for experimental

purposes and some for purely academic researches. In this chapter, only notable studies after the year 2000 will be represented and summarized shortly in a chronological order.

Italian Alps were hosted a large landslide in glacial deposits in 1993. The sliding mass had a volume of approximately 2 million m^3 and flowed for almost 7 km down to valley after its initial movement. After laboratory tests and image processing techniques, the material forming the slide resembled as a bimrock [23]. Based on the pre-failure and post-failure topographic data, Crosta, the author, performed stability analyses of the slope failure by using limit equilibrium methods. The stability analyses shown that partial saturation of the soils has a significant role in instability.

Bromhead et al. [24] investigated an active landslide on the southwest coast of the Isle of Wight with using Hungr's [25] three-dimensional method of analysis. The base of the sliding surface controlled by a bedding plane; which had an inclination into the slope, preventing it from moving, thus making the slide intriguing for three-dimensional analyses. The authors intended to find the possible direction of sliding by changing it in little orders until a vector of movement achieved that yielded the lowest value for the factor of safety. The study concerned the evolution of landslides with dips into or out of the slope when subjected to strong marine attack and cliff retreat [24]. Also, the analysis confirmed that even where the inclination of the failure surface dips into the slope, failure followed a reasonable direction which could be predicted by using 3D stability analyses.

Dapporto et al. [26] have investigated the riverbanks along the Arno River to determine the failure mechanisms and their causes. The parts of the river stage and pore water pressure distribution for causing the observed failures have been investigated by the authors by using limit equilibrium method. They found out that the stability in riverbanks has mainly controlled by effective strengths parameters. Also, they have concluded that high pore-water pressures were not a necessity in a bank failure.

Kockar & Akgun [27] have investigated engineering geological aspects of the materials surrounding Ilıksu 1 and Ilıksu 2 tunnel projects along the Antalya – Alanya highway. The shear strength parameters of the materials obtained by using the Rock Mass Rating system (RMR) [28]. The authors have performed kinematic analyses on slopes to find out any possible instabilities and limit equilibrium analyses were performed to find out the instabilities that controlled mainly by pore water pressure. Results of the kinematic analyses showed that both wedge failure and planar failure could be expected at various areas of the Ilıksu tunnel 1; but the limit equilibrium analyses indicated no instability [27]. The authors

used a slope stability software called Slope/W for limit equilibrium analyses in complex lithologies and structures. The results showed that the exit portal of the Ilıksu tunnel 1 and, both exit and entrance portal of Ilıksu tunnel 2 were prone to a slope failure. The authors have proposed different support systems for the instabilities.

Leynaud et al. [29] have done researches on the continental slope offshore Helland Hansen area in middle Norway. The authors have investigated the previously failed landslides and static stability of the present slopes using limit equilibrium approach. They pointed out that the present-day slopes under gravitational acceleration were stable. A pseudo-static acceleration of 0.175 g and residual shear strength parameters must be in control for a previously occurred slide, the Storegga slide [29].

Cetin et al. [30] have represented a study on the investigation of a seismically induced landslide at Degirmendere during the well-known 1999 Kocaeli earthquake in Turkey. The horizontal seismic acceleration was adopted as 0.35 g. After the investigations of the slope with limit equilibrium analyses by the authors, the corresponding factor of safety was found to be 0.55; indicating the earthquake had a critical role in the slope failure.

Işık et al. [31] have investigated a landslide occurred during severe rainstorms at the city of Sinop on the Black Sea shore. The rainstorm triggered ground movements and the slope was subjected to external loads from the buildings. The sliding occurred in stiff clay and according to inclinometer measurements, the shape of the slip surface was circular. The results of the authors' study indicated that severe rainfall, surcharge loads by the buildings and low shear strength of the materials forming the slope have a critical role in the initial movement. Also, the residual shear strength was in control on the slip surface due to the continuation of the movement. After investigating the worst-case scenario for future considerations, the authors have achieved a factor of safety of 1.24. They have proposed a toe rock buttress and surface drainage systems to prevent a future instability.

Ten cut slopes were planned along the motorway between Ankara – Pozantı and have been investigated for geotechnical properties of the surrounding materials, excavatability and for the stability aspects by Kentli & Topal [32]. The overall slope angles of the cut slopes and bench slopes have proposed as 32° – 71° and 41° – 90°, respectively by the combination of the long-term limit equilibrium analyses and kinematic analyses [32].

Teoman et al. [33] have investigated the slope stability problems along the E90 highway, Turkey. Mineralogical and geotechnical properties of the soils have been assessed before the

investigation of causes and failure mechanism of three slope failures. The failed slopes formed by mainly clayey and silty materials with some sands and gravels. The short-term limit equilibrium analyses with considering earthquake forces on the slopes did not indicate any instability. However, the long-term stability analyses showed a critical factor of safety value of 1.08; indicating a possible future failure. The broken irrigation pipes were the cause of the failures; thus, the pore water pressure decreased the static stability. The authors have proposed maintenance of the pipes along with surface drainages and replacement of the failed material by rocky blocks.

Apuani et al. [34] have represented the stability analysis of an active volcanic island, Stromboli. Two-dimensional limit equilibrium methods have been performed to assess the stability conditions by taking the depth of the slip surface as 150 m to 350 m; corresponding the previous collapses volumes. The study showed that the investigated rock mass under seismic conditions was stable. The intrusive magma pressure and shallow submarine slides may be the controlling factors in previous instabilities.

Crosta et al. [35] have investigated an earthquake-induced landslide in volcanic deposits in Central America, generally called as The Las Colinas landslide. The critical horizontal seismic acceleration was adopted approximately as 0.4 g. The authors have used limit equilibrium procedure for the stability analysis without groundwater; which yielded factors of safety in between 1.4 and 1.8. The authors also concluded that the materials forming the landslide were reduced in grain size by fragmentation and grain crushing, which eventually allowed the failure mass to perform flow-like landslide in almost dry conditions.

Singh et al. [36] have investigated the affected dams in India during the 2001 Bhuj Earthquake. They have selected limit equilibrium procedure for the stability analyses with computer program XSTABL. The modified Bishop's method has been used for the calculations. The authors have taken the factor of safety as unity to obtain the critical seismic acceleration that affected the individual dams.

Neuffer & Schultz [37] have presented a study of the mechanism of slope failures occurred in Mars. The investigated area contains many landslides in basaltic wall rock and softly layered deposits. Their investigation with limit equilibrium analyses demonstrates that the wall rock landslides required an artesian pressure of at least %41 of overburden pressure and ground acceleration of 0.19 Mars g for failure. The authors concluded that to initiate the failures in wall rocks, Marsquakes or impacts would be necessary as high artesian pressures

in the corresponding area would not be possible. Although, the failures in softly layered deposits did not require a triggering mechanism.

Gens & Alonso [38] have investigated the failure conditions of the Aznalcóllar dam. The internal friction angles of failure materials were taken as 17° - 18° and without any cohesive forces. The phreatic surface was determined according to open pipes located under the dam. The authors have calculated the factor of safety of the downstream slope of the dam using limit equilibrium procedure. The corresponding value founded as 1.40.

Bilgehan & Kiliç [39] have investigated the landslides along the North Anatolian fault zone in Amasya province, Turkey. The instabilities mainly triggered by undercutting of the river and change in pore water pressures. The authors have installed plastic pipes into the boreholes to determine the groundwater levels and the location the slip surface. The findings indicated that some failures occurred as retrogressively, and rotational failures were also present. The static stability of the slopes has been calculated with limit equilibrium methods, which yielded a factor of safety of 0.96 [39]. Toe buttress and a surface drainage system have been recommended by the authors for remedial measures.

Chugh et al. [40] have presented a study on the slope failure of a municipal solid waste landfill near Cincinnati, Ohio, USA. The failure mechanism for the analyses was based on the field observations. It was also implemented into limit equilibrium procedure to simulate the translational type of the failure. The computed value of the factor of safety was approximately equaled to unity. Also, the internal angle of friction of the materials was found as 12° using the limit equilibrium methods.

Ulusay et al. [41] have investigated the geotechnical aspects of the Kuzulu landslide near Sivas province, Turkey, which caused fifteen deaths and destruction of thirty houses. The field investigations of the authors indicated that the failure has occurred in volcanic deposits and the failure surface took place between volcanics and the underlying limestone; later the movement acted as a flow-like instability until it stopped at the Kuzulu village. The residual strength of the materials has been adopted by the authors as the failure developed progressively. The limit equilibrium procedures have been also used to back-calculate the required pore water pressure ratio for the initial instability.

Steiakakis et al. [42] have presented a study on the investigation of a waste fill dump of the South Field Mine in Greece. The average inclination of the waste fill slope was %10 with a total height of 110 meters. High pore-water pressures existed through the slope and the base

of the fill deposit includes a clay layer with low shear strength. The authors have done calculations of stability of the waste dump by using limit equilibrium procedure and concluded that the slope was stable until a critical pore-water pressure has reached. The clay layer did not affect the overall stability.

Ozdemir & Delikanli [43] have investigated a slope instability near the town of Yaka at Isparta province, Turkey. The inclination, aspect and the elevation of the slope were generated using Geographical Information Systems (GIS) based digital elevation model. During the field observations, the shape of the slip surface was found to be circular with a maximum depth of 3 meters. The geotechnical properties of the materials were adopted based on undrained peak and residual shear strength data. Limit equilibrium procedure has been chosen by the authors for the stability analysis which yielded stable results under dry conditions and unstable results with high pore-water pressures. The authors concluded that the investigated slope could easily lose the stability with any triggering mechanism, considering the factor of safety was close to unity.

Arikan et al. [44] have presented a study on the assessment of the stability of open pit mine slopes at Cakmakkaya and Damar, Turkey. Limit equilibrium procedure has been used by the authors for back analyzing on the failed slopes. The groundwater conditions and pairs of possible shear strength parameters have been achieved. The factors of safety against various slope angles have been determined. After the investigation, the authors have proposed remedial measures such as slope flattening, surface drainage and long-term monitoring of the groundwater conditions.

Kohv et al. [45] have investigated one of the largest landslide in recent years in Estonia. Locations of the slip surfaces have been determined using the borehole data. The modelling of the landslide has been done by limit equilibrium procedure; which utilized Spencer's method. According to analysis, six separate retrogressive slope failures occurred. The authors indicated that the low strength clay underlying the slip surface was responsible for the initial failures.

Kargar slope failure at Iran in highly fractured rock mass has been investigated by Sharifzadeh et al. [46]. According to the authors, the slope was being supported by shotcrete and grouted by rock bolts before the failure. Limit equilibrium methods have been used to back analyze the failed slope. Also, Hoek-Brown failure criterion with geological strength index has been applied in the back-analyses to calculate the shear strength parameters. The

authors found out that in the preliminary design of the slope, exaggerated strength parameters have been used than the actual ones, which eventually caused the slope to fail.

Wei et al. [47] have presented a study on incorporating different slope stability analyses. The normal and shear stresses have been computed by using finite element method, then, limit equilibrium analysis has been used to calculate the corresponding factor of safety.

Tutluoglu et al. [48] have analyzed a slope failure in a lignite mine at Elbistan – Çöllolar, Turkey. The authors have performed back analyses on a critical weak layer under the lignite seam using two-dimensional limit equilibrium procedure and three-dimensional finite difference models. The results of the analyses indicated that two-dimensional limit equilibrium method overestimated the angle of internal friction of the clay by %30 than the 3D finite difference method.

Xie et al. [49] have demonstrated a three-dimensional slope stability analysis for a lava lobe on Unzen volcano. The authors have integrated GIS based grid data with limit equilibrium methods to obtain safety factors for the inspected area. The critical slip surfaces were located using Monte Carlo random variables technique. The investigated lava lobe was found to be in a stable condition.

Kayabasi & Gokceoglu [50] investigated the instability problems occurred in an open pit lignite mine, Can, at Canakkale province, Turkey. The data of the failures have been taken from the field investigations. The limit equilibrium procedure has been performed by the authors to assess the stability problems and to back-calculate the shear strength parameters. Based on the analyses, the authors concluded that active – passive wedge type failure was responsible for the instabilities. The causes of the failure were determined as the excavation of the toe and low strength surfaces among the lithological units. Also, the authors made suggestions for remedial measures such as decreasing the inclination of the toe, safe benching and a drainage system.

Leong & Rahardjo [51] presented a study on the investigation of the two instabilities of Bukit Batok slope at Singapore. The analyses have been done by using different limit equilibrium methods such as OMS [52], Bishop's routine [53], Janbu's simplified [54], Spencer's method [55], Morgenstern & Price's method [56] and GLE [57]. All methods performed in both two-dimensions and three-dimensions using a software called SVSlope. Mohr–Coulomb failure criterion has been chosen by the authors to define the strengths. The analyses have been performed by using different pairs of shear strength parameters. The

results of the analyses indicated that the first (1989) and the second (1991) failures have occurred due to increasing of the pore water pressure. The difference between the values of the factors of the safety was found to be decreasing with increasing of the pore-water pressures. Also, 3D analyses yielded smaller value for the factor of safety than 2D analyses, at which the strength of the materials was controlled by low cohesive forces.

Singh et al. [58] have investigated the road-cut slopes along a highway at Uttarakhand state, India. After field observations, five locations were chosen to perform the stability analyses. Limit equilibrium procedure and finite element method have been selected by the authors to determine the instabilities. The results indicated that only one slope was stable, others were found to be prone to collapse.

Alemdag et al. [59] investigated the failure mechanism of a large and rapid planar failure at Gumushane, Turkey. The initial movement was initiated by an excavation and blasting for housing purposes. According to the authors, observations during field investigations, the failure mechanism was controlled by three fault planes. The results of the kinematical and limit equilibrium analyses showed that the slope was prone to fail after excavation without blasting.

Ozcan et al. [60] have investigated geotechnical aspects and the stability of downstream slope of a tailing dam at a mine in Turkey. The dam was planned to be heightened about 7 meters to improve its storage capacity. The authors have performed static and pseudo-static stability analyses based on the limit equilibrium procedure. The results indicated that the calculated factor of safety of the dam decreases gradually by heightening of the dam; but the ranges of FOS was found to be suitable for heightening.

Ozbay & Cabalar [61] have investigated the slope stabilities occurred at a lignite mine in Elbistan, which already mentioned previously in another study [48]. The authors paid attention to evaluate the failure mechanisms of the two separate landslides by using finite element method and limit equilibrium procedure. The results of the analyses showed that slopes have factors of safety around unity even with low pore-water pressures. The authors indicated that the first failure was probably due to rising of the groundwater level, which followed by the other landslide, progressively.

Alemdag et al. [62] have demonstrated the utilization of limit equilibrium procedures and finite element methods on a slope debris in Turkey. The geotechnical properties of the materials were derived from the field investigations and laboratory tests. The results of the

analyses suggested that both methods were in good agreement; but finite element method yielded more conservative results.

Topsakal & Topal [63] have investigated a re-activated landslide area in Turkey to determine the best remedial measures. Limit equilibrium procedure has been performed to back calculated the geotechnical properties of the mobilized material along the sliding surface. Corresponding to results of the analyses, the authors have suggested implementing pre-stresses anchors for remedial measures.

Babanouri & Dehghani [64] have investigated the stability of the right abutment of the Latian Dam in Iran. Limit equilibrium methods with various critical sliding surface locating techniques have been performed to analyze the stability. The effect of rock mass properties, seismic forces and pore water pressure have been studied by the authors. The results indicated that the right abutment was prone to slide. The authors suggested that decreasing the inclination of the upper part of the abutment by 15° would improve the stability

3. METHODOLOGY

3.1 Failure Criterions

3.1.1 Mohr-Coulomb criterion

The Mohr-Coulomb failure criterion is widely accepted in slope stability applications. It is first developed by Coulomb in 1776 and modified by Mohr later in 1882. Kliche [65] described the criterion as "a rock failure criterion that assumes there is a functional relationship between the normal and shear stresses acting on a potential failure surface". Also, the criterion can be used on soils and smooth-planar discontinuity planes [66].

Although, the criterion is generally based on a linear failure envelope (Equation 1), in some cases, where low confining pressures and normal stress levels exist, the use of a nonlinear envelope could be necessary (Equation 2). Using straight lines on a non-linear failure envelope generate improper shear strength parameters and cannot represent the overall failure envelope (Figure 3.1)

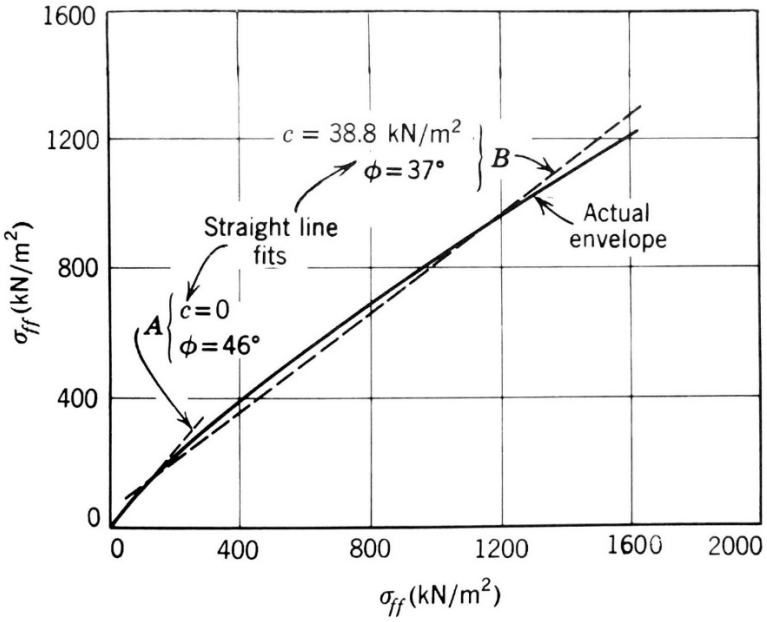


Figure 3.1 Fitting two different straight lines into failure envelope. A-line fitted onto low ranges of normal stresses while B-line fitted on overall envelope. [67]

$$\tau = c' + \sigma' tan\phi \quad (1)$$

$$\tau = m(\sigma')^n \quad (2)$$

3.1.2 Hoek-Brown criterion

In rock engineering, the stability of the deep excavations or underground openings depends on the behavior of the surrounding rock mass as a whole unit. In some cases, rock mass has numerous joint systems that it can act as an isotropic medium. The Figure 3.2 shows the transition between an intact rock material to isotropic rock mass around an underground opening.

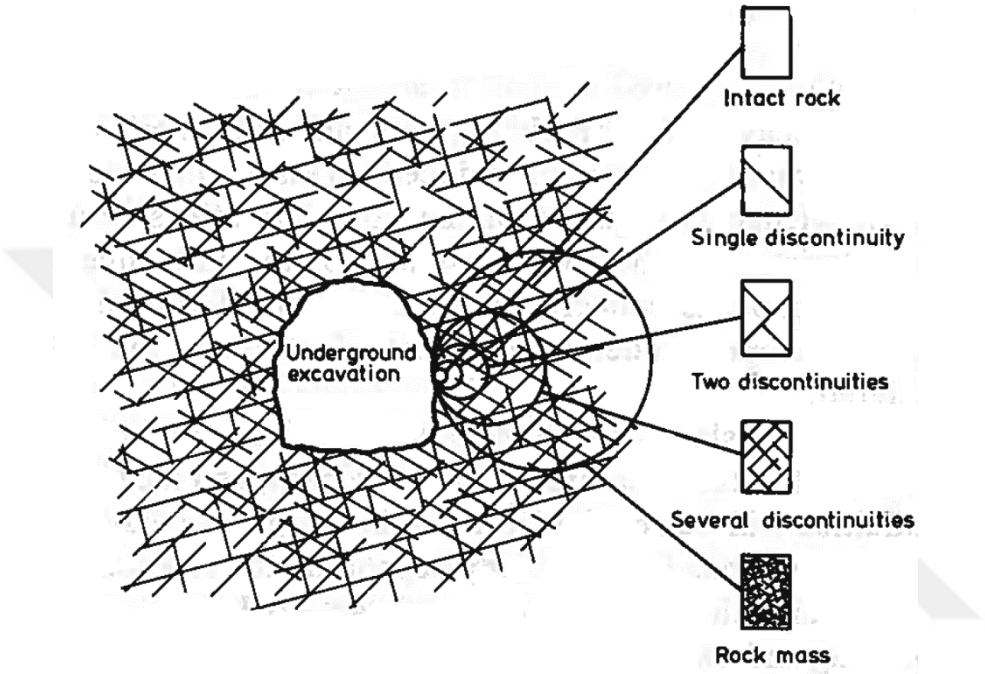


Figure 3.2. The transition between intact rock material to rock mass. [68]

Hoek & Brown [68] have developed an empirical failure criterion for rock masses to be used for practical engineering purposes with using many experimental and empirical study results. The relationship between principal stresses at failure was demonstrated and widely accepted because of the absence of any other criterion.

3.1.2.1 An introduction of the criterion

While the original criterion has been presented in the year 1980, it has undergone many changes over the years until the final edition in 2002 has been proposed. The summary of the changes over the years will be discussed in the next paragraphs, but for clarity, only the recent changes that is still being used today will be represented.

The empirical failure criterion has been studied by many researchers and undergone many changes over the years after the original work was presented by Hoek & Brown in 1980 [68]. Later, Hoek [69] have represented the relationship between the criterion and the normal and

shear stresses at failure; which originally derived by Dr. Bray. The re-examination of the relationship was adopted by Hoek & Brown [70] by introducing the concept of "undisturbed" and "disturbed" rock masses into the criterion, which followed by Hoek et al. [71], the idea of the very poor-quality rock masses should have zero tensile strength. Then, Hoek [72] introduced suggestions about strength parameters with using Mohr envelope; also, a variable coefficient *a* was introduced to adjust the shape of the stress plot in Mohr envelope. Hoek & Brown [73] have compiled the previous works into a new study with illustrative examples. Later, Sonmez & Ulusay [74] have introduced a disturbance factor to assign the rock mass parameters. Finally, the last modifications to the criterion have been proposed by Sonmez & Ulusay [75] and Hoek et al. [76], simultaneously.

In addition to modification of the criterion, Geological Strength Index (GSI) was developed over the years to compensate the geological features of the rock masses. The first introduction was from Hoek [72], followed by Hoek et al. [77]. Later, Hoek et al. [78] have implemented "foliated – laminated" category into the GSI chart; which subsequently removed due to impractical usage. Modifications have been done by Sonmez & Ulusay [74] for a better indication of the exact GSI values. Hoek & Marinos [79] have extended the index for weak rock masses. The final edition of the GSI chart has been demonstrated by Sonmez & Ulusay [75].

3.1.2.2 The application of the criterion

The empirical criterion was originally developed to be used in rock masses, where discontinuity spacing is minimal and complex instabilities were expected. If the instability is controlled by one or two discontinuity sets, the criterion cannot be used. Also, there can be a single fault zone or shear zone in the rock mass. In such conditions, the behavior of the rock mass can be predicted by using the criterion and the discontinuity plane should be considered separately in terms of strength criterion [71].

The failure criterion in terms of principal stresses have been generalized by Hoek [72] and expressed as

$$\sigma_1' = \sigma_3' + \sigma_c(m_b \frac{\sigma_3'}{\sigma_c} + s)^a \qquad 3$$

The parameter *s* becomes 1 for intact rock materials and approaches to zero as the quality of the rock mass decreases (i.e. completely eroded materials and aggregates have zero *s* value). The parameter *a* is taken as 0.5, where the behavior of the rock mass is controlled by well-interlocked rock materials.

The GSI value depends on the structure and surface conditions of the rock mass and used to obtain the value of the rock mass parameters. Generally used modified GSI system including intact rock materials and massive rock masses was proposed by Sonmez & Ulusay [75] and demonstrated below (Figure 3.3).

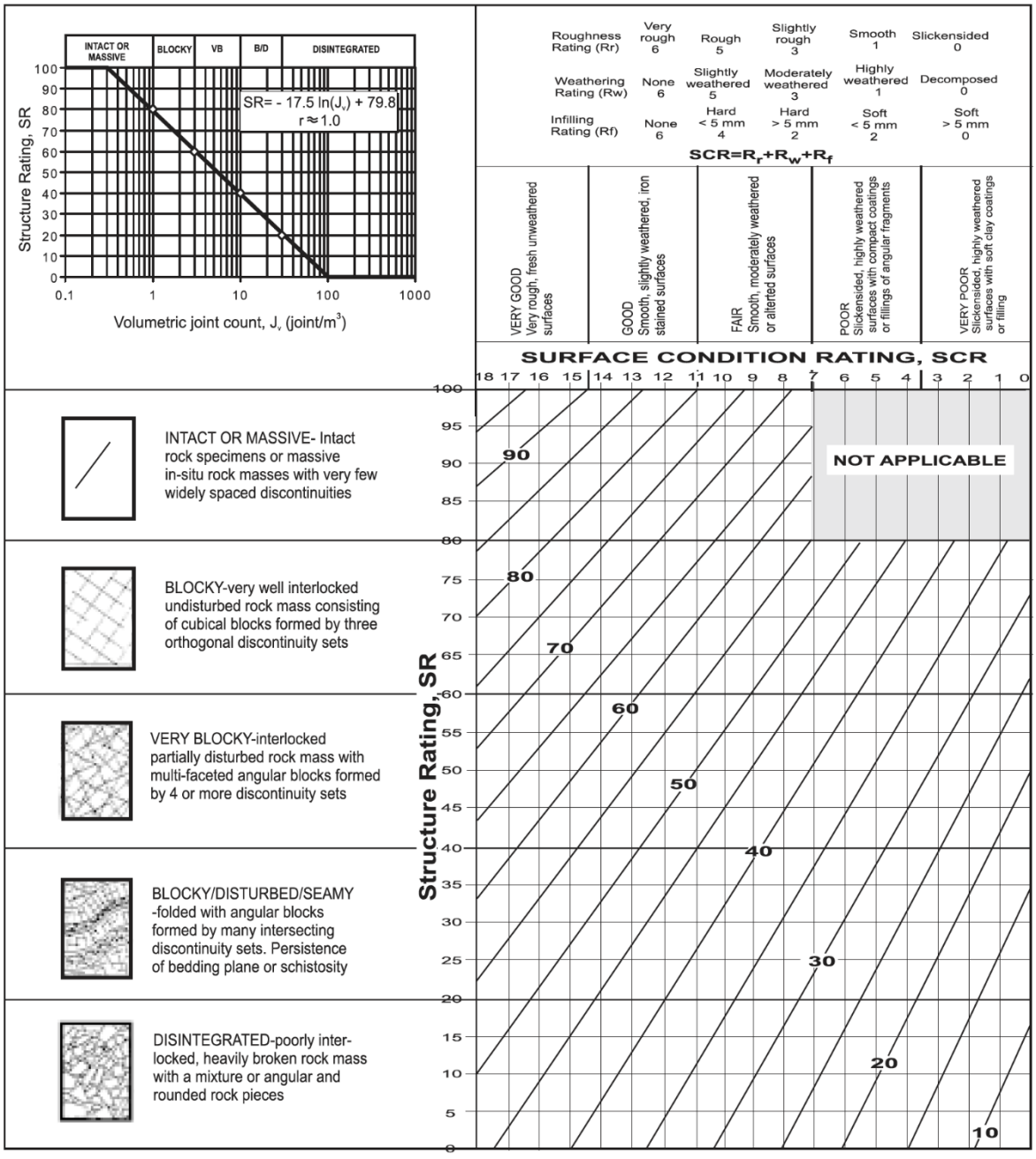


Figure 3.3. The modified GSI system. [75]

Determining the Structure Rating requires the value for Volumetric Joint Count rating has to be known. Sonmez & Ulusay [74], [75] proposed several approaches in their studies to calculate the value, but one approach will be demonstrated considering the authors' suggestions.

While making the suggestions, authors assume that the interested rock mass is homogenous and isotropic. The number of discontinuity sets on a rock mass can be assessed by the following expressions.

$$D_n = \frac{N}{2} \tag{4}$$

$$J_v = D_n\left(\frac{1}{S}\right) \tag{5}$$

Another rating system to assess the overall GSI value is Surface Condition Rating (SCR). It can be calculated by summing the roughness rating (R_r), weathering rating (W_r) and the infilling rating (I_r); which can be found in the GSI chart.

The dimensionless parameter *a* can be found by using Sonmez & Ulusay [75] proposition:

$$a = 0.5 \quad (GSI \geq 30) \tag{6}$$

$$a = 0.65 - \left(\frac{GSI}{200}\right) \quad (GSI < 30) \tag{7}$$

or by Hoek et al.'s [76]:

$$a = \frac{1}{2} + \frac{1}{6}\left(e^{-\frac{GSI}{15}} - e^{-\frac{20}{3}}\right) \tag{8}$$

Sonmez & Ulusay [74] presented formulations for the rock mass constants m_b and *s* as the following.

$$\frac{m_b}{m_i} = exp\left(\frac{GSI - 100}{b_m}\right) \tag{9}$$

$$s = exp\left(\frac{GSI - 100}{b_s}\right) \tag{10}$$

where b_m and b_s can be found by the following expressions by incorporating the disturbance factor d_f.

$$b_m = 3.14ln\left(\frac{d_f}{d_f + 340(1 - d_f)}\right) + 28 \tag{11}$$

$$b_s = 0.67ln\left(\frac{d_f}{d_f + 340(1 - d_f)}\right) + 9 \tag{12}$$

Several suggestions have been made to find the intact rock material parameter, m_i. Hoek [72] presented a table for various types of rocks and the corresponding m_i value (Table 3.1).

Table 3.1. Values of the constant m for intact rock material. Values in parenthesis are estimates. [72]

Rock type	Class	Group	Texture			
			Course	Medium	Fine	Very fine
SEDIMENTARY	Clastic		Conglomerate (22)	Sandstone 19	Siltstone 9	Claystone 4
			← Greywacke → (18)			
	Non-Clastic	Organic	← Chalk → 7			
			← Coal → (8-21)			
		Carbonate	Breccia (20)	Sparitic Limestone (10)	Micritic Limestone 8	
		Chemical		Gypstone 16	Anhydrire 13	
METAMORPHIC	Non Foliated		Marble 9	Hornfels (19)	Quartzite 24	
	Slightly foliated		Migmatite (30)	Amphibolite 31	Mylonites (6)	
	Foliated*		Gneiss 33	Schists (10)	Phyllites (10)	Slate 9
IGNEOUS	Light		Granite 33		Rhyolite (16)	Obsidian (19)
			Granodiorite (30)		Dacite (17)	
	Dark		Diorite (28)		Andesite 19	
			Gabbro 27	Dolerite (19)	Basalt (17)	
			Norite 22			
	Extrusive pyroclastic type		Agglomerate (20)	Breccia (18)	Tuff (15)	

*These values are for intact rock specimens tested normal to bedding or foliation.

Other widely accepted suggestion for finding the intact rock material parameter m_i have been proposed by Hoek & Brown [70]. Authors concluded that using triaxial test data for the intact rock material can yield the value for m_i and σ_c with regression analysis as following.

$$\sigma_c = \sqrt{\frac{\sum y}{n} - \frac{\sum x}{n}\left(\frac{\sum xy - \left(\frac{\sum x \sum y}{n}\right)}{\sum x^2 - \frac{(\sum x)^2}{n}}\right)} \qquad 13$$

$$m_i = \frac{1}{\sigma_c}\left(\frac{\sum xy - (\sum x \sum y)/n}{\sum x^2 - \frac{(\sum x)^2}{n}}\right) \quad 14$$

where; x = σ_3', y = $(\sigma_1' - \sigma_3')^2$ and n represents the number of σ_1' and σ_3' data pairs.

The degree of representation of the above statistical evaluation can be found by calculating the following expression.

$$r^2 = \frac{(\sum xy - (\sum x \sum y)/n)^2}{(\sum x^2 - (\sum x)^2/n)(\sum y^2 - (\sum y)^2/n} \quad 15$$

Also, the rock mass constants m_b and s can be found by Hoek et al.'s [76] presentation by the following formulas:

$$m_b = m_i exp\left(\frac{GSI - 100}{28 - 14D}\right) \quad 16$$

$$s = exp\left(\frac{GSI - 100}{9 - 3D}\right) \quad 17$$

Evaluation of the disturbance factor proposed by Hoek et al. [76] can be assessed from Figure 3.5 and the relationship of the two proposed factors is given in Figure 3.4.

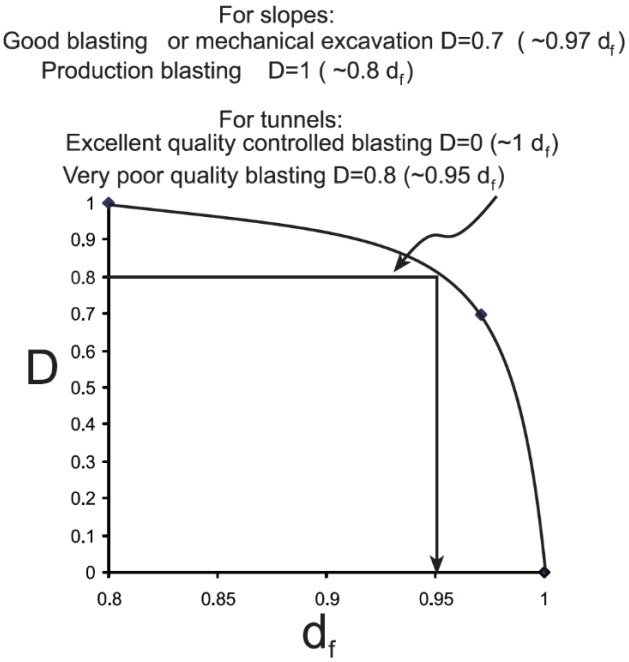


Figure 3.4. The relationship between two proposed disturbance factors. [75]

Appearance of rock mass	Description of rock mass	Suggested value of D
	Excellent quality controlled blasting or excavation by Tunnel Boring Machine results in minimal disturbance to the confined rock mass surrounding a tunnel.	$D = 0$
	Mechanical or hand excavation in poor quality rock masses (no blasting) results in minimal disturbance to the surrounding rock mass. Where squeezing problems result in significant floor heave, disturbance can be severe unless a temporary invert, as shown in the photograph, is placed.	$D = 0$ $D = 0.5$ No invert
	Very poor quality blasting in a hard rock tunnel results in severe local damage, extending 2 or 3 m, in the surrounding rock mass.	$D = 0.8$
	Small scale blasting in civil engineering slopes results in modest rock mass damage, particularly if controlled blasting is used as shown on the left hand side of the photograph. However, stress relief results in some disturbance.	$D = 0.7$ Good blasting $D = 1.0$ Poor blasting
	Very large open pit mine slopes suffer significant disturbance due to heavy production blasting and also due to stress relief from overburden removal. In some softer rocks excavation can be carried out by ripping and dozing and the degree of damage to the slopes is less.	$D = 1.0$ Production blasting $D = 0.7$ Mechanical excavation

Figure 3.5. Evaluation of the disturbance factor. [76]

Also, the normal stress and the shear stress in terms of principal stresses can be calculated by using Balmer's equations [80].

$$\sigma_n' = \frac{\sigma_1' + \sigma_2'}{2} - \frac{\sigma_1' - \sigma_2'}{2} \times \frac{\frac{d\sigma_1'}{d\sigma_3'} - 1}{\frac{d\sigma_1'}{d\sigma_3'} + 1} \quad 18$$

$$\tau = (\sigma_1' - \sigma_3') \times \frac{\sqrt{\frac{d\sigma_1'}{d\sigma_3'}}}{\frac{d\sigma_1'}{d\sigma_3'} + 1} \quad 19$$

where

$$\frac{d\sigma_1'}{d\sigma_3'} = 1 + am_b \left(\frac{m_b \sigma_3'}{\sigma_c + s} \right)^{a-1} \quad 20$$

3.2 **Limit Equilibrium Procedures**

When a slope is prone to collapse, or, in other words, the available shear strength of materials above the failure surface is equal to mobilized shear strength (F=1), the slope can be said to be in a limiting equilibrium condition. The calculations which are performed under this condition called limit equilibrium methods.

There are two different approaches in this method to satisfy the static equilibrium of a slope. Some methods consider the equilibrium of the entire soil above the slip surface as a whole body as it is in the ϕ=0 method. In other methods, the soil mass is divided into vertical, horizontal or even radial slices of a certain number and equilibrium equations are solved for each individual slice. This procedure is generally called as the *method of slices* and is being used for almost a century.

Although there are many procedures based on the method of slices, depending on the number of equilibrium equations to be satisfied, they can be divided into four categories [81]: methods that satisfy only overall moment equilibrium, overall moment and overall force equilibrium, force equilibrium of each slice, and both moment and force equilibrium of each slice.

3.2.1 Single body procedures

These procedures take the soil mass above the slip surface as a whole unit and consider the equilibrium conditions for that unit.

3.2.1.1 $\phi = 0$ method

This is the most basic method of all limit equilibrium methods and can be easily calculated by hand. Developed by Fellenius [82], [83] for undrained analysis. In this method, failure surface is assumed to be a part of a circular arc and moments are taking into consideration at the center of the circle to calculate a factor of safety (Figure 3.6). The internal friction angle is assumed to be zero and the shear strength along the failure surface is defined by undrained shear strength; thus, the only strength parameter in this method is the cohesion.

The factor of safety for this type of slope can be calculated by taking the ratio of resisting and overturning moments about the center of the slip surface (Equation 21).

$$F = \frac{c_u LR}{W'x} \qquad 21$$

To avoid any confusion, this method is also called as Swedish Circle Method, Circular Arc Method, Undrained Analysis Method and Total Stress Analysis.

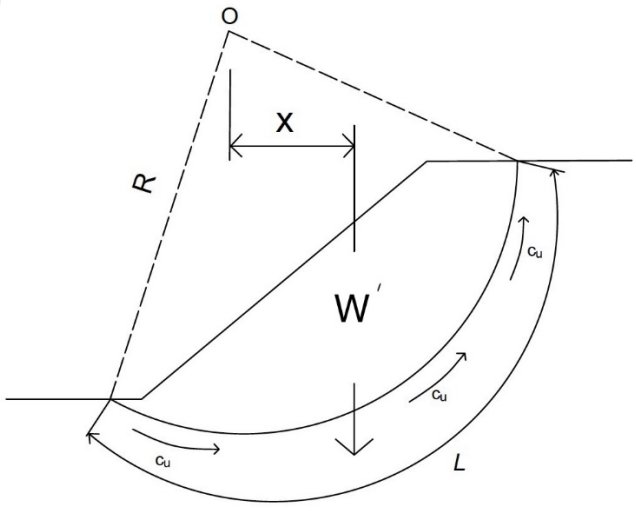


Figure 3.6. Slope and slip surface for the ϕ=0 method. (Modified from [84], [85])

3.2.2 Method of slices

This procedure can be done by dividing the sliding soil mass into several slices and considering the force and moment equilibrium for each of the slice and also for the whole sliding body. Slices generally have been taken as vertically; but can be taken as horizontally, radially and as a wedge-shaped.

3.2.2.1 Ordinary method of slices

Ordinary method of slices (OMS) is the first slice technique developed by Fellenius [86], [52] for stability analyses of circular slip surfaces and has also been referred to as the Fellenius Method or Swedish Method of Slices. In this method, interslice forces considered to act at a parallel inclination to the base of the slice and neglects the interslice forces in the vertical direction (Figure 3.7). This simple assumption prevents interslice equilibrium where adjacent slices have different base inclinations. This inconsistency causes wrong calculation of the effective stresses at the base of each slice, and there is not a single direction in which the force equilibrium is satisfied.

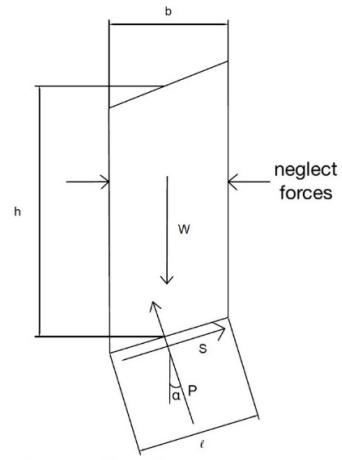


Figure 3.7. Typical slice with forces in Fellenius method. (Modified from [85])

In this method factor of safety can be obtained by resolving moments and substituting the effective normal stress into Mohr-Coulomb equation which gives:

$$F = \frac{\sum[c'l + (Wcos\alpha - ul)tan\phi']}{\sum Wsin\alpha} \qquad 22$$

The part of the equation which represents effective normal stress ($\sigma' = Wcos\alpha - ul$) on the slip surface can lead to unrealistically low and sometimes negative values [85]. Whitman and Bailey [87] suggest that the term may be taken as zero when its value becomes negative. Also to avoid this error Turnbull and Hvorslev [88] proposed a different procedure by replacing the weight of the slice in terms of effective weight which takes into account the vertical uplifting force due to the pore water pressure on the base of the slice. Which leads the following expression for *F*:

$$F = \frac{\sum[c'l + (Wcos\alpha - ulcos^2\alpha)tan\phi']}{\sum Wsin\alpha} \qquad 23$$

Although this expression gives reasonable values for normal force distribution along a slip surface, its inaccuracy as much as %50-60 still exists for problems in which slip surface is deep with a relatively low slope angle, where high pore-water pressures present [53], [85], [87].

3.2.2.2 Bishop's method

In his PhD. Thesis, Bishop [89] stated that on a typical earth dam with idealized elastic properties for materials, local overstress will occur when the value of the factor of safety is below 1.8. Later from his PhD. Research, Bishop [53] pointed out that many slopes and dams with stability problems have a factor of safety lower than this. This is why he concluded that a state of plastic equilibrium must be considered to exist throughout at least part of the slope.

In this method, failure is usually assumed to be on a continuous slip surface and because of determination of the most critical surface has some difficulties and relying on multiple variables, a simplified shape as a circular arc was adopted and the problem is assumed to be on a plane strain condition[1]. Bishop, also inspired from Fellenius's method in which soil mass above the sliding surface is separated in vertical slices, but he made a simplifying assumption, the forces between the slices act horizontally so there are no shear forces occurring between them. Illustration of the forces acting on a slice of a soil mass bounded by the circular arc of ABCD of radius R and center O are given below. (Figure 3.8)

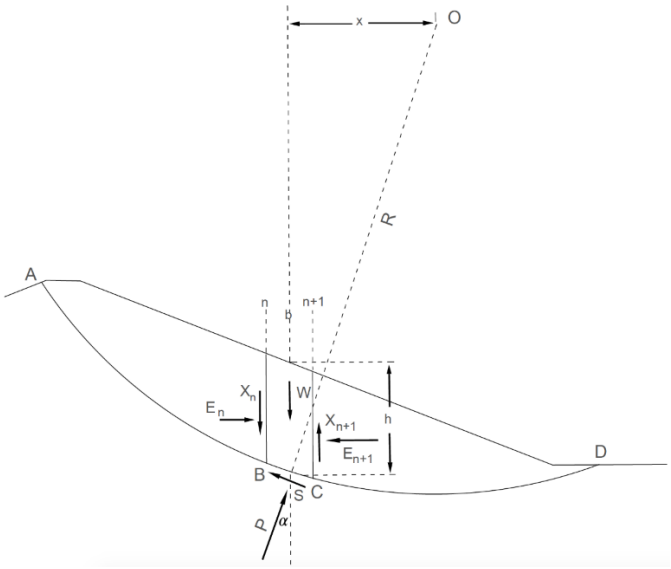


Figure 3.8. Forces acting on a slice of a soil mass. [53]

[1] In soil mechanics, continuous masses of earth with a constant cross-section whose outer boundaries are perpendicular to a single vertical plane. Every slice of earth-oriented parallel to this plane is acted upon by the same external and internal forces. The thickness of the slice is not changed by a change in a state of stress in the slice. Such type of deformation is known as plane strain condition. [224]

Bishop later resolves the forces vertically acting on a typical slice from a polygon of forces (Figure 3.9) and re-arranging the equation to obtain the effective normal force (*P'*), he obtains:

$$P' = \frac{W + X_n - X_{n+1} - l\left(ucos\alpha + \frac{c'}{F}sin\alpha\right)}{cos\alpha + \frac{tan\phi'.sin\alpha}{F}} \qquad 24$$

By replacing this effective normal force with the Fellenius's conventional method and putting $l=b\sec\alpha$ and $x=R\sin\alpha$, an equation for the factor of safety can be obtained:

$$F_f = \frac{1}{\sum W sin\alpha}.\sum\left[\{c'b + tan\phi'.(W - ub + (X_n - X_{n+1}))\}.\frac{sec\alpha}{1 + \frac{tan\phi'.tan\alpha}{F_i}}\right] \qquad 25$$

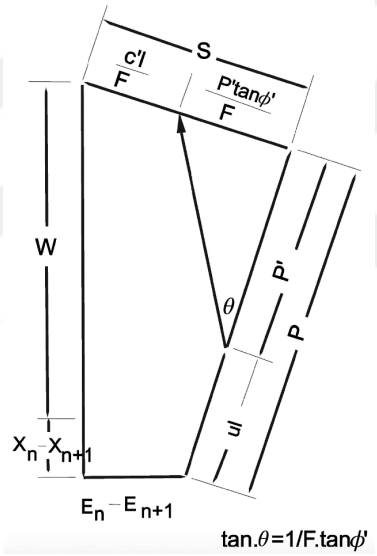


Figure 3.9. Polygon of forces on a typical slice. [53]

The values for $(X_n - X_{n+1})$ to be found by successive approximation and must satisfy the condition of $\sum(X_n - X_{n+1})= 0$ which gives a rigorous solution to the problem. By doing so, this gives additional complexity to the method and the value of *F* is to be found insignificant, less than %1 difference in a typical case [53]. That is why Bishop recommends assuming $(X_n - X_{n+1})= 0$ for a routine work then taking an initial value for *F* until the condition for $F_f \leq F_i$ - 0.001 is met after few consecutive trials.

While there seem to be two different procedures for this method, to avoid confusion, where the vertical forces are not taking into consideration the procedure called *Bishop's simplified method* or *Bishop's routine method.* The other procedure considers all of the forces acting on a slice and satisfies full static equilibrium, which later called as *Complete Bishop's*

method. In the complete procedure, Bishop showed what steps and assumptions would be necessary, however, no specific details were stated and were not described completely.

3.2.2.3 Morgenstern & Price's method

Although Bishop's method has been used widely since its first publication, its restrictions to circular failure surfaces and satisfying force equilibrium only in vertical direction can't be ignored. To overcome the limitations of previous limit equilibrium methods, Morgenstern and Price [56] developed a method with satisfying all the equilibrium conditions to analyze, any failure surfaces with arbitrary shapes, any configuration composed of soils with different shear strength properties and slopes with complex pore pressure distributions.

In order to remove the indeterminacy of the normal pressure along the slip surface, Morgenstern & Price eliminated it from equilibrium equations, thus making the internal forces more indeterminate. The other two assumptions have been made about the position of the line of thrust and the relation between the interslice forces (E, X) assumed to be as:

$$X = \lambda f(x) E \tag{26}$$

After some research and calculations, the authors also pointed out that for homogeneous slopes with circular slips, differences between the internal force distributions would not affect the factor of safety drastically. Thus, the interslice for function doesn't have a key role in analyzing this type of slopes. For a non-circular surface with homogeneous material, the computed factor of safety found to be %8 less than other studies [54], [90].

3.2.2.4 Spencer's method

In his original work, Spencer [91] intended to develop a method that satisfies both overall force and moment equilibrium conditions and also force equilibrium for each slice with taking the inter-slice forces into account, but it was limited to circular failure surfaces only. Later then, Spencer [55] refined his method by satisfying moment equilibrium for each slice and adapting to failure surfaces with arbitrary shapes. Figure 3.10 shows Spencer's typical slice of mean height h and width b with the forces acting upon it.

By resolving all of the interslice force components on a single slice, Spencer obtained the resultant of the interslice forces as:

$$Q = \frac{\frac{c'b}{F} sec\alpha + \frac{tan\phi'}{F}(Wcos\alpha - ubsec\alpha) - Wsin\alpha}{\cos(\alpha - \theta)\left[1 + \frac{tan\phi'}{F}\tan(\alpha - \theta)\right]} \tag{27}$$

Spencer indicated that, because of the external forces on the embankment are in equilibrium, the sum of the horizontal and vertical components of the interslice forces must also be zero (Equation 28, 29). Also, the sum of the moments of external forces for circular failure surfaces about the center of rotation is zero, the sum of the moments of the interslice forces about the center of rotation must also be zero (Equation 30).

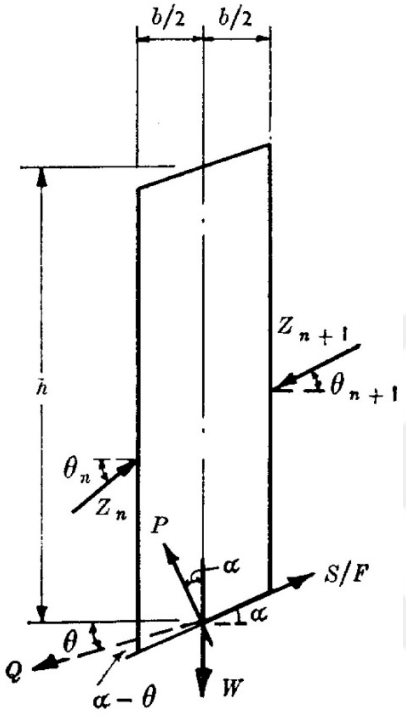


Figure 3.10. An enlarged sketch of the slice. [91]

$$\sum[Qcos\theta] = 0 \tag{28}$$

$$\sum[Qsin\theta] = 0 \tag{29}$$

$$\sum[Qcos(\alpha - \theta)] = 0 \tag{30}$$

Spencer pointed out that the values of F and θ must be found which satisfy all three equations above. In his original work to simplify the solution greatly, Spencer assumed that the interslice forces are parallel, which makes the sum of the horizontal and vertical components of the interslice forces become identical (Equation 31) and leaving only equation 30 and 31 to solve. Then, several values of θ has been taken and corresponding values for the factor of safety for both force equilibrium (F_f) and moment equilibrium (F_m) equations have been obtained and plotted on a graph. Also, the factor of safety for horizontal interslice forces considering the moment equation has been marked as F_{mo}. The intersection point of the two

curves gives the value of the factor of safety (F_i) which satisfies both condition and the present inclination of interslice forces (θ_i) (Figure 3.11).

$$\sum Q = 0 \qquad 31$$

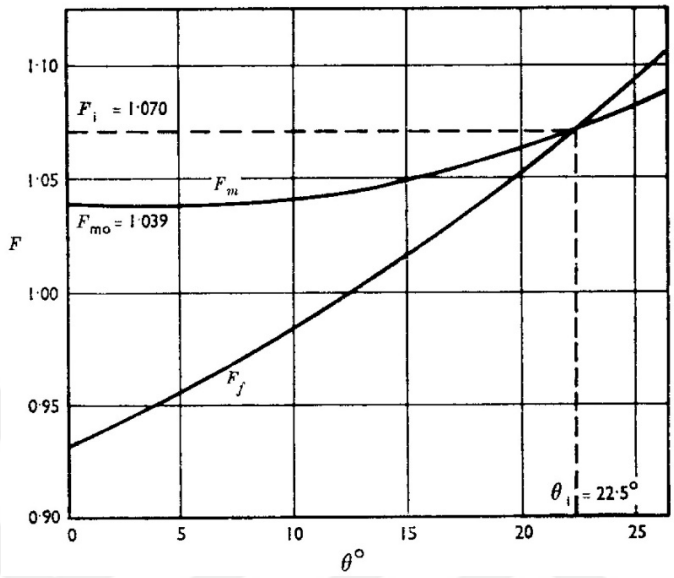


Figure 3.11. Obtaining the factor of safety. [91]

According to the graph above, Spencer has found that the inclination value of interslice forces in static equilibrium is less than the slope's inclination. Other than this, the factor of safety obtained from the force equilibrium equation is greatly affected by the inclination of interslice forces; but the factor of safety obtained from the moment equilibrium equation is affected slightly which gives a clear indication for the reason why Bishop's method gives more accurate results [91].

3.2.2.5 Janbu's method

Basic principles of the method of slices have been first discussed by Janbu [16] at a conference in Stockholm. Two years later Janbu, Bjerrum and Kjaernsli [54] published a method for calculating the factor of safety of slopes with arbitrarily shaped slip surfaces also satisfying horizontal and vertical force equilibrium of each slice with an assumption of zero interslice shear forces present, known as Janbu's Simplified method. Finally, a more rigorous method has been developed by Janbu [92] to satisfy all force and moment equilibrium of sliding body, known as Janbu's Generalized method or Janbu's Rigorous method. Although this method appeared to be rigorous, Sarma [93] pointed out that the position of the normal stress on the uppermost slice is not being taken into account, preventing overall moment equilibrium to be satisfied.

Janbu stated that static equilibrium must be both satisfied for individual slices and the whole sliding body. In order to accomplish, he derived some formulations to show a combination of horizontal and vertical equilibrium for each slice (Equation 32), an equation of vertical interslice forces (Equation 33) which yields moment equilibrium for a slice of infinitesimal width and an equation to maintain overall horizontal equilibrium (Equation 34).

$$\Delta E = \Delta Q + (p + t)\Delta b tan\alpha - \tau \Delta b(1 + tan^2\alpha) \quad 32$$

$$X = -Etan\theta + h_t \frac{dE}{db} - z_Q \frac{dQ}{db} \quad 33$$

Where $p = \Delta W/\Delta$b and $t = \Delta$X$/\Delta$b.

$$\sum_{a}^{b} \Delta E = E_b - E_a \quad 34$$

Janbu also introduced that to obtain an overall average factor of safety for a selected shear surface, the formulation below (Equation 35) should be used. Values for the factors of safety for both sides must be determined by an iteration procedure same as Bishop's method.

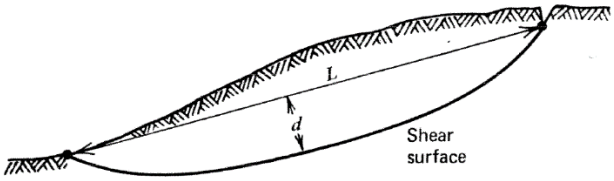
$$F = \frac{\sum_a^b \left[\frac{c' + (p + t - u)tan\phi'}{1 + (1/F)tan\phi' tan\alpha}\right] \Delta b(1 + tan^2\alpha)}{E_a - E_b + \sum_a^b [\Delta Q + (p + t)tan\alpha \Delta b]} \quad 35$$

As mentioned earlier, Janbu et al. [54] developed a simplified method for analyzing shear surfaces with arbitrary shapes. In order to overcome the consequences of zero interslice shear forces, they introduced a correction factor (f_0) to somewhat convert the founded factor of safety to a more rigorous one. Approximated value for the final factor of safety can simply be found by the following equation.

$$F = f_0 F_0 \quad 36$$

Restricted to homogenous soil profiles, f_0 value can be selected from Figure 3.12 which is developed by comprehensive investigation of around 40 different soil profiles.

After using the correction value of the simplified method, it is shown by Janbu [92] that a value for the factor of safety obtained is very close to the more rigorous method. Janbu also indicated that the simplified method yielded deeper shear surfaces than the rigorous method and should be used only for saving time when no computer is available. In his book, Bromhead [94] indicates that the simplified method originally developed to use in slopes with a low inclination and advises using only narrow slices with this method.



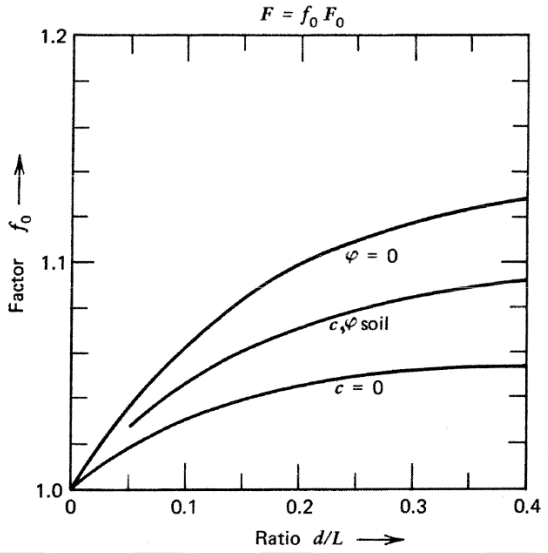


Figure 3.12. Correction factor with respect to the ratio of the shear surface. [54]

3.2.2.6 Sarma's method

Instead of focusing on determination of factor of safety that will bring the soil mass to a failure, Sarma [95] approached the calculation of stability problems of slopes differently, by computing the critical horizontal acceleration that is required to maintain the slope in a state of limiting equilibrium. Also, Sarma intended to develop this method simple enough to be calculated by hand and as accurate as Morgenstern-Price procedure with no computer program would be necessary.

Sarma proposed the following equation for each slice to satisfy the complete force equilibrium of slope.

$$\sum \Delta X tan(\phi' - \alpha) + \sum kW = \sum D \qquad 37$$

in which D stands for

$$D = Wtan(\phi' - \alpha) + \frac{c'bcos\phi' sec\alpha - r_u W sin\phi' sec\alpha}{\cos(\phi' - \alpha)} \qquad 38$$

Also, Sarma chooses the center of gravity of the sliding mass to take moments for the sake of simplification with coordinates of x_g and y_g. Moment equilibrium equation is expressed in terms of complete force equilibrium equation as following

$$\sum \Delta X\left[(y_i - y_g)tan(\phi' - \alpha) + (x_i - x_g)\right] = \sum W(x_i - x_g) + \sum D(y_i - y_g) \quad 39$$

Defining X in the form of

$$\Delta X = \lambda\psi \quad 40$$

Substituting into force and moment equilibrium equations to obtain λ and k.

$$\lambda = \frac{\sum W(x_i - x_g) + \sum D(y_i - y_g)}{\sum \psi\left[(y_i - y_g)tan(\phi' - \alpha) + (x_i - x_g)\right]} \quad 41$$

$$k = \frac{\sum D - \lambda \sum \psi tan(\phi' - \alpha)}{\sum W} \quad 42$$

As Sarma considers the equilibrium along interslice boundaries, the relationship between interslice forces has been given similar to Morgenstern & Price's method as:

$$X = \frac{\lambda E'}{F_{local}} \quad 43$$

3.2.2.7 Chen & Morgenstern's method

This method is essentially the same as the Morgenstern & Price's procedure, but with a refinement. Chen & Morgenstern [96] show that assumptions of the inclinations of the interslice forces or location of the line of thrust at the boundaries of slopes have some certain limitations which have been ignored in the previous works. They concluded that at the two ends of the shear surface the interslice forces must become parallel to the inclination of the surface of the slope. They proposed the following relationship between the forces on the slice interface to overcome the limitations.

$$X = [\lambda f(x) + f_0(x)]E \quad 44$$

Where $f(x)$ and $f_0(x)$ are two different functions to define the distribution of interslice force inclinations. Both functions are predefined by the user, which Chen & Morgenstern specify that the function $f(x)$ is equal to zero at both ends of the shear surface and $f_0(x)$ is the tangent of the inclination of the slope at each end.

3.2.2.8 General limit equilibrium method of slices (GLE method)

Generally, two-dimensional limit equilibrium methods have some similarities and differences which have been obscure. Fredlund et al. [57] present a general limit equilibrium formulation to show that each method presented earlier is actually a special case of the formulation and share the same theoretical background. This formulation procedure is referred to as GLE method and can be applied to shear surfaces with arbitrary shapes and satisfies all equilibrium conditions.

For circular shear surface analysis, a typical slope with forces acting on it has been presented (Figure 3.13) and the corresponding factors of safety with respect to moment and force equilibrium has been given.

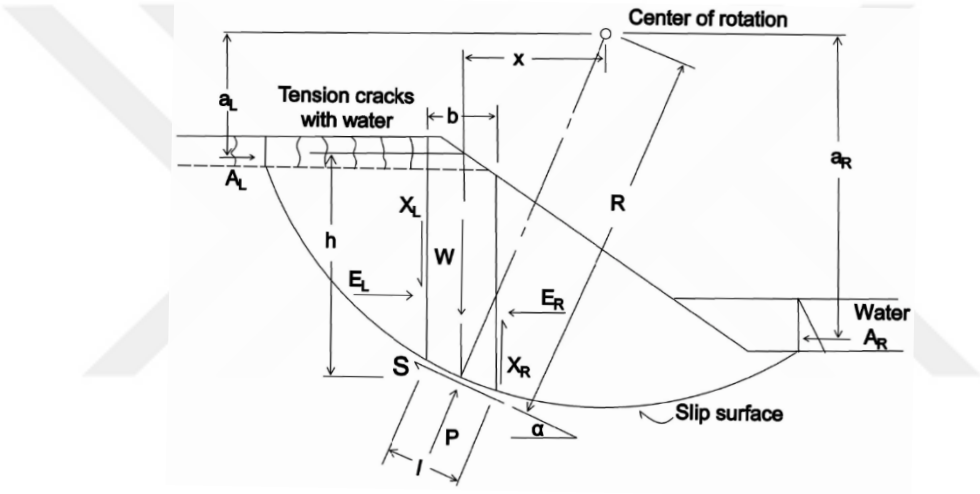


Figure 3.13. Forces acting on circular slip surface. [57]

The factor of safety with respect to moment equilibrium, F_m:

$$F_m = \frac{\sum[c'l + (P - ul)tan\phi']R}{\sum Wx \pm Aa} \quad 45$$

The factor of safety with respect to force equilibrium, F_f:

$$F_f = \frac{\sum[c'l + (P - ul)tan\phi']cos\alpha}{\sum Psin\alpha \pm A} \quad 46$$

The normal force on the base of the slice, P can be computed from:

$$P = \frac{W - (X_R - X_L) - \frac{c'lsin\alpha}{F} + \frac{ultan\phi'sin\alpha}{F}}{m_\alpha} \quad 47$$

where

$$m_\alpha = cos\alpha + \frac{sin\alpha tan\phi'}{F} \quad 48$$

The authors indicated that the factor of safety in normal force equation can be either respect to moment or force equilibrium depending on which condition is being solved. Also, common methods that are being used widely can be categorized in terms of the assumption of interslice forces and the equilibrium condition that is satisfied.

For noncircular shear surface analysis, a figure has been given below to indicate the forces and the components (Figure 3.14). While force equilibrium and normal force equation remained unchanged, the moment equilibrium equation has changed drastically. The radius (*R*) is now subject to change depending on the location and the normal force has now an offset arm, f.

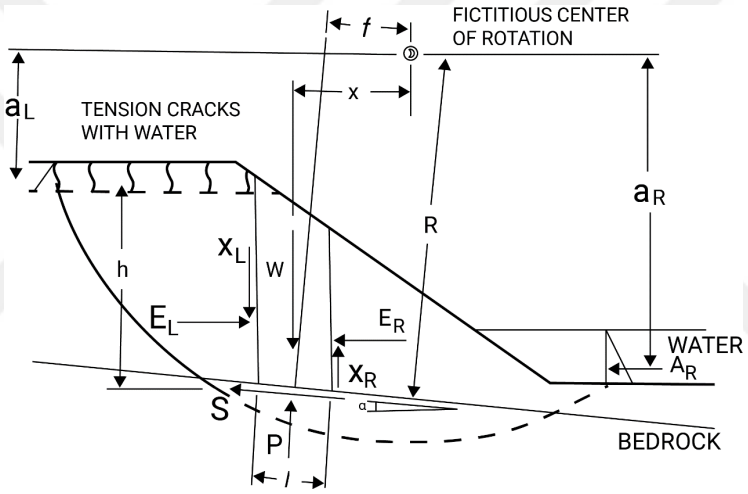


Figure 3.14. Forces for the noncircular case. [57]

The factor of safety equation with respect to moment equilibrium for noncircular is given below.

$$F_m = \frac{\sum[c'l + (P - ul)tan\phi']R}{\sum Wx - \sum Pf \pm Aa} \quad 49$$

The authors concluded that proposed equations are the basic equations for limit equilibrium analysis and almost all methods use the same principle. Comparisons show that calculation of factor of safety gives identical values for many methods and almost identical with Morgenstern & Price's method which uses integration to apply the normal force to the base of the slice instead assuming it acting through the center of the base of the slice [57].

3.2.3 Miscellaneous other methods

The limit equilibrium methods have been developing since the beginning of 20th century and have a history of almost hundred years. As there are dozens of methods available to this date, it is almost impossible to gather and summarize them all. Also, most of them are beyond the scope of this thesis. Still, many methods will be explained or at least mentioned in this chapter.

One of the most well-known method here is Corps of Engineers Method [97], [98], [99]. This method satisfies force equilibrium in vertical and horizontal direction and does not satisfy moment equilibrium. The interslice forces are assumed to be either equal to the average surface inclination of slope or parallel to the inclination of the surface. Also, interslice force inclinations may vary between slices or may be the same for all (Figure 3.15). Reasonable results can be achieved by taking the angles flatter as steeper angles give overestimated values for the factor of safety. The relationship between interslice forces is given below.

$$X = \gamma E \qquad 50$$

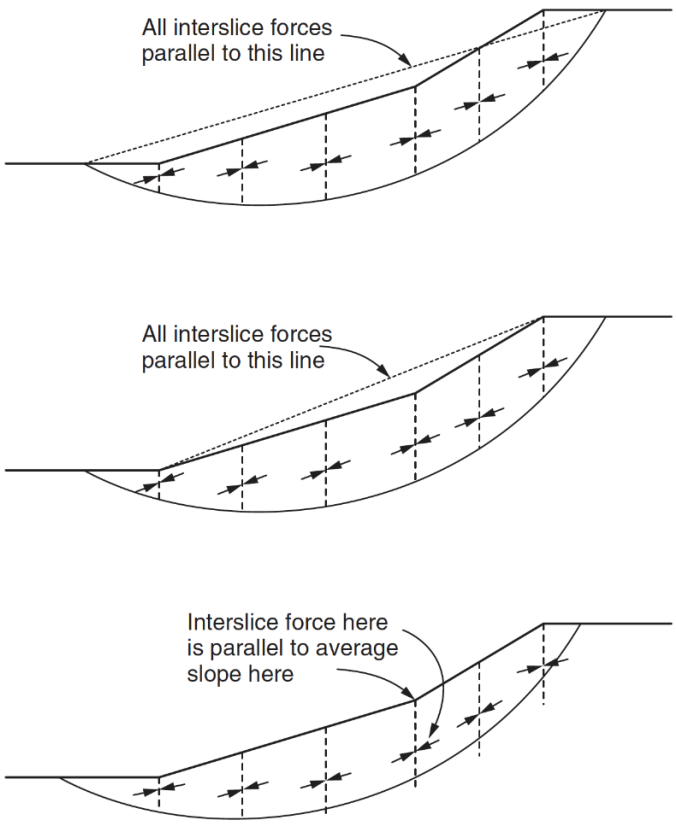


Figure 3.15. The relationship between inclinations of interslice forces and slope surface. [85]

Lowe and Karafiath's method [100] satisfies force equilibrium only and assumes the inclination of interslice forces to be equal to the average inclination of slope surface and inclination of the base of the considered slice (Equation 51). Although moment equilibrium is not satisfied, the method gives very similar results as rigorous methods.

$$X = \left(\frac{\gamma + \alpha}{2}\right) E \tag{51}$$

Maksumovic [101] tried to eliminate the difficulties of applying external forces from Morgenstern & Price's method with using the same approximate integration formula. In order to simplify the problem, he divided pore water pressure distribution along the slice into small separate triangles. Also, he implemented the same principle into the slice to resolve the moments and forces for simple evaluation.

Bailey & Christian's method [102] is very similar to Fellenius's method which interslice forces are neglected and assumed to be zero. Thus, taking only moment equilibrium into consideration. The difference between Fellenius's method is avoiding the occurrence of negative pore water pressures by taking the weight of a slice as the effective weight which is also proposed by Turnbull and Hvorslev [88].

Terzaghi & Peck [103] proposed a method for general shear surface analysis with considering the moment equilibrium of a soil mass about an external point. Interslice shear forces assumed to be zero and the factor of safety is given as:

$$F = \frac{\sum [cb + (W + \Delta X - ub) tan\phi] \left(\frac{a}{m_\alpha}\right)}{\sum Wx - \sum \left[W + \Delta X + (ubtan\phi - cb)\frac{tan\alpha}{F}\right]\left(\frac{f}{m_\alpha}\right)} \tag{52}$$

where

$$m_\alpha = \left(1 + \frac{tan\alpha tan\phi}{F}\right) cos\alpha \tag{53}$$

This method has been considered by Terzaghi & Peck to approximate the actual slip surface of a slope and then using a more accurate method for the rest of the calculations.

Correia [104] approached the relationship between internal forces differently by eliminating the horizontal force on the slice interface and considering the shape of interslice shear force distribution by a scaling factor with dimension of force, not its magnitude. (Equation 54).

$$X = \lambda f(x) \tag{54}$$

Chugh [105] proposed a method similar to Spencer's method with respect to statically determinacy and assumptions about interslice force directions. He implemented a constant acceleration from earthquake forces through the center of a slice and can be horizontal or inclined.

Law & Lumb [106] developed a method to analyze progressive failures and suggested to use both peak strength parameters and residual strength parameters for soils which helps to analyze some cases that were difficult with common methods. This method also satisfies all kind of equilibrium conditions thus making it a rigorous method.

Leshchinsky [107] presented a method based on Baker & Garber's [108] variational limiting equilibrium analysis. The normal force distribution along the shear surface is described with an ordinary differential equation then determined through a process of minimization of the factor of safety. This method also satisfies all three limiting equilibrium conditions.

Greenwood [109] aimed to develop a method similar to Fellenius's method simple enough for hand calculation by implementing the horizontal earth pressure coefficient (K) into the general theory of limit equilibrium. The method can be applied to general shapes of slip surfaces and neglects forces on slice boundaries.

As mentioned earlier, there are still so many methods of limiting equilibrium for slope stability analysis such as Skempton's [110] method for undrained analysis. Kenney [90] also developed a method for slip surfaces of arbitrary shapes. Taylor's [111], [112] work for the early development of the method of slices technique. Bell's [113] proposition for general slip surfaces which assumes normal force distribution along the shear surface. Nonveiller [114] extended Bishop's method for general slip surfaces by altering the moment center. Some considerable work had been done by Taylor [111], Terzaghi [115] and Fröhlich [116] for slip surfaces shaped as a logarithmic spiral. Yang et al. [117] approached differently by taking the sliding mass as a whole unit instead dividing it into slices.

There are such methods that use non-vertical slices to determine statical equilibrium such as Seed & Sultan [118] uses slices shaped like a wedge, Sarma [93] also adopts wedges as slices which is considered as a rigorous solution. Horizontal slices adopted by Shahgholi et al. [119], Nouri et al. [120]. Radial and inclined slices have been considered by Kumar et al. [121] and Patra & Basudhar [122], respectively.

3.2.4 Comparison of limit equilibrium methods

As there are many methods involving limit equilibrium conditions for slope stability analysis, comparisons had been made between them to clarify the resultant values for the factor of safety [123], [124]. Also, common points and differences had been well presented and compared by Espinoza et al. [125], Zhu et al. [126] and Nash [127], . For further interest, Fredlund [128], Morgenstern [129], Mostyn & Small [130] has reviewed many different methods from different aspect for stability analysis.

Fredlund & Krahn [123] has taken six commonly used methods into the analysis to compare with six different situations; where geometry, soil properties and pore water conditions vary. The slope profile which considered in the analysis includes both circular and non-circular failure surfaces (Figure 3.16).

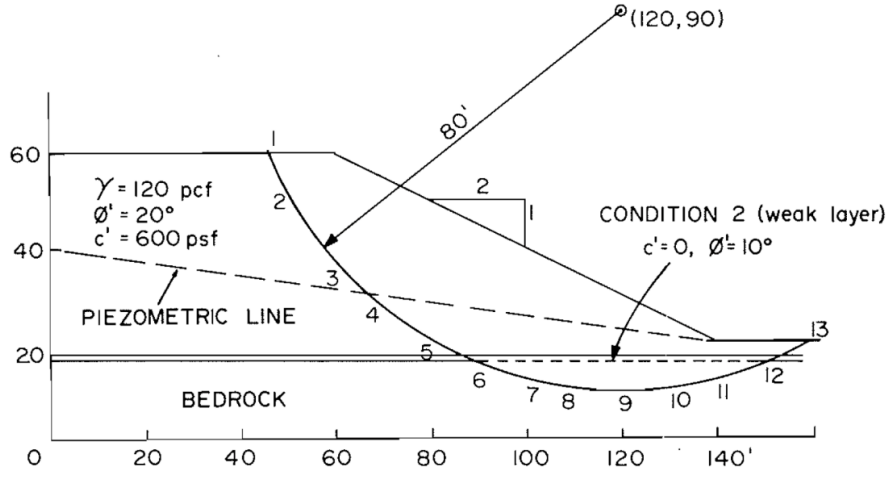


Figure 3.16. Slope profile. [123]

The computed results for the six different situations have been given below (Table 3.2). The average difference in terms of the factor of safety is about % 0.1; which represents a clear insight that no matter how many conditions satisfied the differences between rigorous and simple methods has negligible outcomes in terms of practical use.

Table 3.2. Results for different methods of analysis. [123]

Case no.	Example problem*	Ordinary method	Simplified Bishop method	Spencer's method			Janbu's simplified method	Janbu's rigorous method**	Morgenstern-Price method $f(x)$ = constant	
				F	θ	λ			F	λ
1	Simple 2:1 slope, 40 ft (12m) high, ϕ'=20°, c'=600 psf (29 kPa)	1.928	2.080	2.073	14.81	0.237	2.041	2.008	2.076	0.254

2	Same as 1 with a thin, weak layer with ϕ'=10°, c'=0	1.288	1.377	1.373	10.49	0.185	1.448	1.432	1.378	0.159
3	Same as 1 except with r_u=0.25	1.607	1.766	1.761	14.33	0.255	1.735	1.708	1.765	0.244
4	Same as 2 except with r_u=0.25 for both materials	1.029	1.124	1.118	7.93	0.139	1.191	1.162	1.124	0.116
5	Same as 1 except with a piezometric line	1.693	1.834	1.830	13.87	0.247	1.827	1.776	1.833	0.234
6	Same as 2 except with a piezometric line for both materials	1.171	1.248	1.245	6.88	0.121	1.333	1.298	1.250	0.097

*Width of slice is 0.5 ft. (0.3m) and the tolerance on the nonlinear solution is 0.001.
**The line of thrust is assumed at 0.333.

There are still many limit equilibrium methods for stability analysis which is not included in this work. It can be confusing to understand main similarities and differences between various methods. In order to overcome this situation, an extensive comparison has been made (Table 3.3). The table below shows which equilibrium conditions satisfied for each method. Also, ease of applicability and applied shape of the critical shear surface has been demonstrated.

Table 3.3. Comparison of the method of slices.

Method	Equilibrium Conditions			Shape of critical shear surface	Calculation by hand
	Force Equilibrium		Overall Moment Equilibrium		
	Vertical	Horizontal			
Fellenius (OMS)	×	×	✓	Circular	✓
Bishop's simplified	✓	×	✓	Circular	✓
Bishop's rigorous	✓	✓	✓	Circular	✓
Bailey & Christian	×	×	✓	Any	✓
Terzaghi & Peck	✓	×	✓	Any	✓

Bell's method	✓	✓	✓	Any	×
Nonveiller's method	✓	✓	✓	Any	×
Correia's method	✓	✓	✓	Any	×
Greenwood's method	×	×	✓	Any	✓
Maksumovic's method	✓	✓	✓	Any	×
Janbu's simplified	✓	✓	×	Any*	✓
Janbu's rigorous	✓	✓	×	Any	✓
Morgenstern & Price	✓	✓	✓	Any	×
Spencer's method	✓	✓	✓	Any	×
Chugh's method	✓	✓	✓	Any	×
GLE method	✓	✓	✓	Any	×
Sarma	✓	✓	✓	Any	×
Chen & Morgenstern	✓	✓	✓	Any	×
Law & Lumb	✓	✓	✓	Any**	✓
Leshchinsky's method	✓	✓	✓	Any	×
Corps. Of Engineers	✓	✓	×	Any	✓
Lowe & Karafiath	✓	✓	×	Any	✓
Seed & Sultan	✓	✓	×	Any	✓
Sarma's wedge method	✓	✓	×	Any	✓

Shahgholi et al.	✓	×	×	Any	✓
Kumar et al.	×	×	✓	Circular	✓

*Restricted to elongated shallow slip surfaces.
**Developed for progressive failures.

3.2.5 Three-dimensional effect

Slope stability analysis by limit equilibrium method generally has been done by considering plane strain assumption which yields a two-dimensional factor of safety for the problem considered, but, in reality, failures of engineering designs such as embankments, vertical cuts, retaining walls and as well as slopes happens to be in three dimensions. Consideration of this difference can't be neglected.

While there are some advantages of evaluating failures on three dimensional, it comes with some drawbacks. Calculating a slope failure in three dimensions requires precise formulation of equilibrium of forces and moments in every direction (i.e. x, y, z.); which adds significant complexity to the problem and essentially requires a computational power. The direction of the slide must be determined correctly to achieve satisfactory results. Also, determination of three-dimensional shear surface accurately, where failure takes place in, is another problem in 3D calculations for the factor of safety because failures do not necessarily occur on a symmetrical surface. In addition, Cheng & Lau [131] claims that many 3D methods in practice today are numerically unstable under transverse horizontal forces.

Implementing a three-dimensional effect on slope stability analysis may have various disadvantages and difficulties. However, the advantages of performing a 3D analysis make it more intriguing. As much as it is a drawback to determine the true sliding surface, it will make the problem more practical. A 3D failure surface would give accurate results as it can be represented by spatial variability. Also, applying a three-dimensional analysis would be more representative in terms of the calculated values. While investigating a large-scale rock wedge failure with variable surface properties on the slip surface, the routine method [132] for wedge stability analysis can be used with assuming the slip surfaces to be uniform and planar. These assumptions would give inaccurate results and a 3D approach should be preferred [133]. In addition, Chen et al. [133] pointed out that a 3D analysis will represent better the behavior of soil and rock structures especially in stability problems controlled by discontinuities, where the slope has a special geometry such as including a tunnel portal into

analysis; which a 2D cross-sections can't represent because of the plane strain assumption. Also, back calculating strengths from three-dimensional geometry with using 3D analysis instead of conventional two-dimensional analysis would yield more accurate results [85].

Also, the end effects in geometry such as a curvature plays an important role on the three-dimensional stability. Cheng & Lau [131] stated that concavity in a slope increases the factor of safety while convexity decreases. Leshchinsky & Baker [154] has pointed out in their research that for cohesionless soils, there are no end effects as the failure surface coincide with the slope surface. However, they also concluded that the end effects were more pronounced in highly cohesive soils.

3.2.5.1 Three-dimensional slope stability methods

Starting from the development of two-dimensional methods, implementing a 3D effect has gained attraction over the time. Dozens of 3D methods have been developed over the years. The progress of these methods is very similar to 2D analyses, where assumptions are made about inter-slice forces, the shape of the slip surface, the position of normal force on the base of the slice, the position of the line of thrust etc. Early developments have started with simple geometries which contain simple soil properties. By the meantime methods have been adopted from the successful two-dimensional methods such as Fellenius's, Bishop's, Spencer's, Morgenstern & Price's etc. This time instead of using slices, the sliding soil mass is divided into several vertical columns (Figure 3.17).

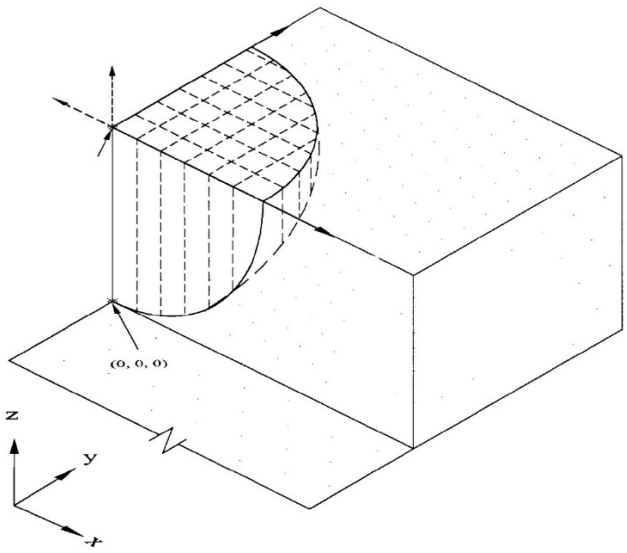


Figure 3.17. Typical sliding mass divided into soil columns. [134]

A typical soil column (Figure 3.18) is used in the 3D analysis to consider the forces acting on it; then resolving the forces to maintain force equilibrium in desired directions and to maintain moment equilibrium becomes much easier.

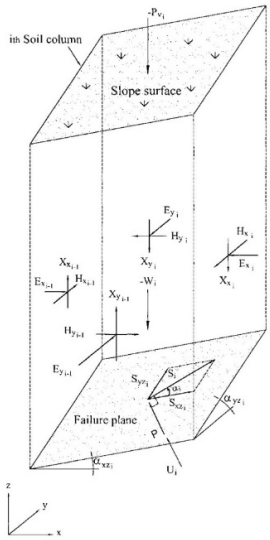


Figure 3.18. Typical soil column. [134]

For simplicity only commonly used and well-known methods will be presented next.

3.2.5.1.1 Hovland's method

Hovland [6] developed this method for slopes with frictional and cohesive soils; also known as the ordinary method of columns (OMC). The inter-column forces and pore water pressures are not taking into consideration; this method is basically a 2D version of Fellenius's method [86] extended into three dimensions. The slip surfaces are assumed to be either cone-shaped or wedge-shaped. After his analysis, he concluded that the ratio of the factors of safety between two and three-dimensional method is prone to change significantly with varying shear strength parameters and the shape of the slip surface. Azzouz & Baligh [135] indicated that this method tends to underestimate the normal force, thus the shear stress, on steep slip surfaces.

3.2.5.1.2 Chen & Chameau's method

In this method [136], failure surface is assumed to be symmetrical and the inter-column forces have a constant inclination from toe to the crest of the soil mass. The inter-column shear forces have the same inclination as the base of the column. Both moment and force equilibrium conditions are satisfied. These assumptions are very much the same as Spencer's procedure, making it an extension of Spencer's method [91] into three dimensions.

After their analyses, they concluded that 3D effects are more significant at smaller lengths of failure mass and where soils have high cohesion values and low internal friction angles. The 3D factor of safety (FOS) was found to be less than the 2D factor of safety for cohesionless soils. Although, this finding is found to be erroneous by other studies [137],[138].

3.2.5.1.3 Hungr's method

Hungr intended to develop a method [25] using directly Bishop's 2D routine procedure [53] with the exact same assumptions. Thus, the method neglects vertical inter-column shear forces; but inter-column normal forces and horizontal shear forces remains the same. Only the vertical force equilibrium condition for each column and the overall moment equilibrium is satisfied, neglecting horizontal force equilibrium as Bishop's method. Hungr expected this method would work very well as it does in the two-dimensional analysis.

Hungr derived the normal force equation (Equation 55) acting on the base of the column from vertical force equilibrium.

$$P = \frac{W - \frac{cAsin\alpha_{yz}}{F} + \frac{uAtan\phi sin\alpha_{yz}}{F}}{n_\alpha} \quad 55$$

where

$$n_\alpha = cos\alpha\left(1 + \frac{sin\alpha_{yz}tan\phi}{Fcos\alpha}\right) \quad 56$$

According to Hovland [6], the area of the base of the column, *A*, can be found by the following equation.

$$A = \Delta x \Delta y \frac{\sqrt{1 + sin^2\alpha_{xz}sin^2\alpha_{yz}}}{cos\alpha_{xz}cos\alpha_{yz}} \quad 57$$

Also, the overall moment equilibrium equation with respect to the factor of safety can be found by the following expression.

$$F = \frac{\sum[(W - uAcos\alpha)tan\phi + cAcos\alpha]}{\left(\sum W sin\,\alpha_{yz}\right)n_\alpha} \quad 58$$

Hungr et al. [139] combined Janbu's simplified method [54] with Bishop's method in another study. This time, he also derived the factor of safety (Equation 59) from the horizontal force equilibrium with using the exact same assumptions as Bishop's method.

$$F = \frac{\sum[cAcos\alpha_{yz} + (P - uA)tan\phi cos\alpha_{yz}]}{\sum Pcos\alpha tan\alpha_{yz} + \sum kW + G} \quad 59$$

3.2.5.1.4 Lam & Fredlund's method

A generalized model based on general limit equilibrium (GLE) method has been implemented into three-dimensional study by Lam and Fredlund [140]. Inter-column resultant force directions have been simulated with the use of inter-column force functions of arbitrary shape. Modelling of the geometry of the slope, the stratigraphy, the potential sliding surface and the pore water pressure distribution has been determined by a well-known geostatistical procedure, called Kriging technique. The direction of movement and a possible change in the direction of the sliding mass is not stated. The point of application of the normal force on the base of the column assumed to be at the center. Also, similar to Morgenstern & Price's method [56] inter-column force functions have been used to determine the relationship between inter-column shear forces and the related normal forces on each face of the column.

A typical soil column after the assumptions has been given in Figure 3.19 below. The normal force applied to the base of the column can be found by the following expression.

$$P = \frac{W - (X_L - X_R) - (V_L - V_R) - \frac{Ac'sin\alpha}{F} + \frac{Utan\phi'sin\alpha}{F}}{n_\alpha} \quad 60$$

where

$$n_\alpha = cos\theta_y + \frac{tan\phi' sin\alpha}{F} \quad (61)$$

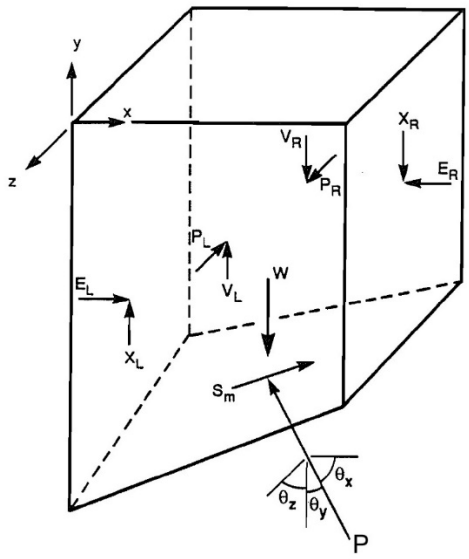


Figure 3.19. Soil column after simplifying assumptions. [140]

The factor of safety with respect to moment equilibrium obtained by summing the moments of the forces about the axis of the rotation.

$$F_m = \frac{\sum(Ac' + Ptan\phi' - Utan\phi')(cos\alpha dy + sin\alpha x)}{\sum\left(Pcos\theta_x dy + Pcos\theta_y x + Wx\right)} \quad (62)$$

The factor of safety with respect to the summation of forces in x-direction obtained as shown below.

$$F_f = \frac{\sum(Ac' + Ptan\phi' - Utan\phi')cos\alpha}{\sum Pcos\theta_x} \quad (63)$$

After their research with a case history, they found out that doing back analysis in two dimensions overestimate the shear strength parameters of the soil.

3.2.5.1.5 Huang & Tsai's method

The authors have developed a new 3D slope stability analysis based on two-directional moment equilibrium [134]. It is possible to determine the direction of sliding (DOS) for semispherical and composite failure surfaces along with calculating the factor of safety. Three equations were used in order to determine DOS and the corresponding factor of safety: two equations derived from moment equilibrium in x and y directions and the final third equation takes into account the overall moment equilibrium of the sliding soil mass. This

method ignores the horizontal inter-column forces and it is the first three-dimensional asymmetrical Bishop method, where soil columns assumed to move apart from each other.

Also, Huang et al. [141] proposed a method based on two-directional force and moment equilibrium to analyze a slope stability problem with an arbitrary slip surface. This method is based on the assumptions and formulations of a two-dimensional analysis, Janbu's rigorous method [92]. The direction of sliding (or the resultant shear force) can be calculated directly instead of assuming. This method also neglects the horizontal inter-column shear forces.

3.2.5.1.6 Cheng & Yip's method

A three-dimensional asymmetric slope stability method based on extensions of Bishop's routine, Janbu's simplified and Morgenstern & Price's method has been developed by Cheng and Yip [142]. The slip surface was assumed to be spherically shaped for all methods and an arbitrary inter-column force function has been adopted from Morgenstern & Price's procedure to calculate the inter-column shear forces.

3.2.5.2 Miscellaneous other 3D methods

Plenty of three-dimensional limit equilibrium analyses for slope stability have been developed after gaining some popularity with the well-known methods such as Hovland's. While development of 3D methods has started with simple problems; now, there are rigorous methods that satisfy full static equilibrium.

Common methods have been represented in the previous chapter; still, there are dozens of three-dimensional methods yet to be mentioned. Such as, Sherard et al. [143] and Lambe & Whitman [144] tried to convert a two-dimensional factor of safety into three-dimensional by the weighted-average procedure. The very first 3D method developed by Anagnosti [145] for general slip surfaces as an extension of Morgenstern-Price's procedure.

Baligh & Azzouz [146] presented a method based on an extension of circular arc method, assuming the slip surface as a cylindrical center part with conical or ellipsoidal ends. Later expanding the method for cohesive and frictional slopes with additional assumptions [147] and finally extending the original method to consider the effect of applied loads on the stability of slopes [148].

According to Hungr [25], the extension of Bishop's method into 3D with the exact same assumptions have been also developed by Hutchison [149] and by Humphrey & Dunne [150].

Dennhardt & Forster [151] proposed a method from symmetrical slopes with ellipsoidal slip surface. Symmetrical external load on top of the slope has been considered and distribution of normal force on slip surface was assumed.

Leshchinsky et al. [152] proposed a three-dimensional mathematical approach to slope stability analysis by taking the variational calculus and combining it with limiting equilibrium approach. The authors used the Kopacsy's [153] proposition and improved it. Later, Leshchinsky & Baker [154] and Baker & Leshchinsky [155] modified and improved the original work. Also, Ugai [156] developed a method using variational calculus and limit equilibrium method (LEM) for symmetrical vertical cuts. The same methodology has been adopted by Leshchinsky & Mullet [157], [158] for vertical corner cuts and vertical cuts with longitudinal extension.

Gens et al. [159] presented a method to analyze homogeneous, isotropic and purely cohesive slopes (i.e. undrained analysis). Slip surface was assumed to be cylindrical with center part as plane-shaped or curved at both ends. Also, the factor of safety has been calculated by considering the overall moment equilibrium of the sliding mass.

A different approach for the stability of concave slopes has been proposed by Xing [160], by considering the limit equilibrium condition of slopes in plan-view. Both moment and force equilibrium conditions for the sliding soil mass has been satisfied.

Ugai [161] and Ugai & Hosobori [162] proposed several three-dimensional methods extended from the well-known two-dimensional method of analysis such as Fellenius's OMS, Spencer's method, Janbu's simplified method and Bishop's routine method.

Leshchinsky & Huang [163] developed a two-dimensional method which is modified from Leshchinsky's [164] generalized variational limit equilibrium analysis based on Baker & Gaber's [108] work to deal with general slip surfaces. Later, Leshchinsky & Huang [165] presented a three-dimensional method to extend their 2D analysis into three-dimensional method developed earlier by Leshchinsky et al. [152]. The presented 3D method satisfies all limit equilibrium equations and based on variational approach. The normal stress on the slip surface (general shape, but symmetrical) is found and obtained mathematically.

Cavounidis and Kalogeropoulus [166] developed a 3D method as an extension of Azzouz & Baligh's method [147] to examine vertical cuts in cohesive soils. Slip surface assumed to be cylindrical at center part and conically shaped at both ends. The factor of safety is derived from taking the moment equilibrium of the sliding body into consideration.

Yamagami & Jiang [167], [168] and Jiang & Yamagami [169] have developed the first method for asymmetric problems, where the sliding direction is determined instead of being assumed or using a plane of symmetry. The slip surface is adopted as a general shape and the inclinations of resultant inter-column forces are related with the inclination of the base of the corresponding column. Horizontal and vertical force equilibrium have been satisfied in this method.

Chang [170] proposed a 3D method of analysis for the stability of slopes based on the sliding mechanism of the Kettleman Hills landfill slope. This method also adopts limit equilibrium concept and assumes the sliding body as multiple adjoining inclined blocks. The factor of safety is derived from the force equilibrium of both individual blocks and the whole sliding body. Same landfill failure has been analyzed by Seed et al. [21], [171] by considering the sliding mass as a block system where blocks contact each other vertically and the forces between them act horizontally. Vertical equilibrium was satisfied for each block and horizontal equilibrium was satisfied for the whole system. This method is basically a wedge analysis extended into three-dimensions. Also, Byrne et al. [172] presented a three-dimensional procedure based on Janbu's method [173] to investigate the same failure mechanism.

Chen et al. [174] presented a three-dimensional method as an extension of Spencer's method into three-dimensions. The shape of the slip surface was assumed to be circular and the inclination of resultant inter-column forces was assumed to be constant. In order to determine the factor of safety overall moment equilibrium and force equilibriums were satisfied.

Jiang & Yamagami [175] also extended Spencer's method into three-dimensions by taking the concept of limit equilibrium and variational analysis into consideration. General assumptions of Spencer's method also applied in this method. The direction of the slide (i.e. the direction of shear stress) assumed to be perpendicular to the longitudinal extent of the slope. Horizontal force equilibrium and overall moment equilibrium have been satisfied in this method.

Zheng [176], [177] proposed a rigorous three-dimensional method where the whole sliding body taking into consideration instead of individual columns. The slip surface was assumed to be general shaped and all six equilibrium conditions were satisfied. Also, Sun et al. [178] and Zheng [179] proposed a method as an extension of Morgenstern & Price's procedure into three-dimensions.

In addition, there are few methods that satisfies all equilibrium conditions such as Zhu & Qian [180], Zhou & Chen [181] and Lu & Zhu [182]. Also, Feng et al. [183], Chen et al. [184], Zhang et al. [185], [186], [187], Sun et al. [188] proposed three-dimensional methods that satisfies 4 – 5 equilibrium conditions.

3.2.5.3 Comparison of three-dimensional methods

It is obvious that, over decades, many limit equilibrium methods have been developed in both two-dimensions and three-dimensions. Some only work with very simple geometries and plain subsurface conditions; but some works with exceptionally complicated geometries and geological conditions.

While the methods being presented almost all of them have been compared with others and the values of the factor of safety indicate that many of them have close to each other. Even the most rigorous methods do not have much difference to mean considerable in a practical sense.

Chakraborty & Goswami [189] has done a literature review for three-dimensional slope stability analyses and summarize the methods with respect to slopes with cohesive soils and application of external loadings. Wines [190] discussed the reasons for the differences between two and three-dimensional results.

Kalatehjari & Ali [191] have reviewed many of the existing three-dimensional slope stability analyses based on limit equilibrium method. Also, they have presented a summary and characteristics of them with respect to the main origin of the method, consideration of the direction of the slide, application (i.e. restrictions) of the method and the adopted shape of the slip surface (Table 3.4).

Table 3.4. Characteristics of three-dimensional methods. [191]

3D Method	Derivation	DOS	Application	Slip Surface
Anagnosti [145]	Morgenstern & Price's method	No	Generalized	Generalized

Baligh & Azzouz [146]	Circular arc	No	Simple slopes	Cylindrical center part with conical or ellipsoidal ends
Hovland [6]	Fellenius's method	No	Symmetrical	Cone/Wedge shaped
Azzouz & Baligh [147]	Circular arc	No	Simple slopes	Cylindrical center part with conical or ellipsoidal ends
Chen & Chameau [136]	Spencer's method	No	Symmetrical	Cylindrical center part with ellipsoidal ends
Azzouz & Baligh [148]	Circular arc	No	Simple slopes	Cylindrical center part with conical or ellipsoidal ends
Dennhardt &Forster [151]	LEM	No	Symmetrical	Ellipsoidal
Leshchinsky et al. [152]	LEM and variational analysis	No	Symmetrical	Spherical and cylindrical
Ugai [156]	LEM and variational analysis	No	Vertical cuts	Cylindrical with curved caps
Leshchinsky & Baker [154]	LEM and variational analysis	No	Symmetrical	Cylindrical with curved ends
Baker & Leshchinsky [155]	LEM and variational analysis	No	Conical heaps	Cylindrical with cap ends/expansion of 2D log-spiral
Hungr [25]	Bishop's modified method	No	Symmetrical	Rotational with circular central section
Gens et al. [159]	Swedish circle	No	Simple slopes	Cylindrical with planar ends
Leshchinsky & Mullet [158]	LEM and variational analysis	No	Vertical cuts	Expansion of log-spiral function
Ugai [161]	Fellenius's, modified Bishop's, Janbu's and Spencer's methods	No	Symmetrical	Based on the method
Xing [160]	Spencer's method	No	Symmetrical	Symmetrical elliptic surface with circular vertical cut
Hungr et al. [139]	Simplified Bishop's and Janbu's methods	No	Symmetrical	Symmetrical rotational
Leshchinsky & Huang [165]	2D method of Leshchinsky & Huang	No	Symmetrical	General symmetrical/extension of log-spiral

Cavounidis & Kalogeropoulus [166]	3D method of Azzouz & Baligh	No	Symmetrical	Cylindrical with conical end caps
Lam & Fredlund [140]	2D general LEM	No	Symmetrical	Generalized rotational surfaces
Yamagami & Jiang [167], [168]	Simplified Janbu's method	Yes	Generalized	Generalized
Huang & Tsai [134]	LEM and two directional FOS	No	Complicated	Semispherical/partly spherical composite
Huang et al. [141]	Janbu's method and two directional FOS	Yes	Generalized	Generalized
Chen et al. [174]	Spencer's method	No	Generalized	Generalized rotational
Jiang & Yamagami [175]	Spencer's method based on variational analysis	No	Symmetrical	Rotational surfaces
Cheng & Yip [142]	Bishop's, Janbu's and Morgenstern & Price's methods	Yes	Generalized	Spherical
Zheng [177]	LEM	No	Generalized	Generalized
Sun et al. [188]	Morgenstern & Price's method	No	Generalized	Generalized

Duncan [192] has well summarized three-dimensional slope stability methods that published until the time of his work. He divided the methods into three categories by the types of problems addressed: curved slopes in plan-view or containing corners, slopes with loadings on top; and the last, slopes with failure surfaces bounded by physical boundaries.

Summarized three-dimensional methods have been given below (Table 3.5). Duncan has drawn attention to three important conclusions from these studies. Almost all cases provide a greater 3D factor of safety than two-dimensional. Except, Hovland [6], Chen & Chameau [136] and Seed et al. [21]. The reason behind this exception for Hovland's method is that it is based on an extension of the ordinary method of slices, which does not take into account the vertical side forces. Chen & Chameau's results have been found erroneous by other studies, as mentioned in the corresponding topic. Seed et al.'s presentation has been found to be inaccurate because all conditions of equilibrium did not satisfy and there was a horizontal force imbalance which resulted in up to % 25 difference in the final calculated value of factor of safety. The second conclusion is, 2D & 3D analyses should give the same factor of safety for homogeneous cohesionless slopes [137], [154]. As a final conclusion,

while doing back calculation of strengths neglecting 3D effects would result in overestimated strength parameters [193], [165].

Table 3.5. Summarized three-dimensional methods. [192]

Authors	Method	Strength	Geometry of slope/slip surface	3D effects found
Anagnosti [145]	Extended Morgenstern & Price	c, ϕ	Unrestricted/unrestricted	$F_3 = 1.5\ F_2$ in one case
Baligh & Azzouz [146]	Extended circular arc	$\phi = 0$	Simple slopes/surfaces of revolution	$F_3 > F_2$
Giger & Krizek [194]	Upper bound theory of perfect plasticity	c, ϕ	Slopes with corners/log spiral	$F_3 > F_2$
Giger & Krizek [195]	Upper bound theory of perfect plasticity	c, ϕ	Slopes with corners/log spiral (with loads on top of slope)	$F_3 > F_2$
Baligh et al. [196]	Extended circular arc	$\phi = 0$	Simple loaded slopes/surfaces of revolution	$F_3 > F_2$
Hovland [6]	Extended OMS	c, ϕ	Unrestricted/unrestricted	$F_3 < F_2$ for some cases
Azzouz et al. [193]	Extended Swedish circle	$\phi = 0$	Four real embankments/surfaces of revolution	$F_3 = 1.07\ F_2$ to $1.30\ F_2$
Chen & Chameau [197]	Extended Spencer and finite element	c, ϕ	Unrestricted/unrestricted	Spencer results are similar to FEM
Chen & Chameau [136]	Extended Spencer	c, ϕ	Unrestricted/unrestricted	$F_3 < F_2$ for some cases
Azzouz & Baligh [148]	Extended Swedish circle	$\phi = 0$	Same as Baligh & Azzouz with loads on top	$F_3 > F_2$
Dennhardt & Forster [151]	Assumed *s* on slip surface	c, ϕ	Slopes with loads/unrestricted	$F_3 > F_2$
Leshchinsky et al. [152]	LEM and variational analysis	c, ϕ	Unrestricted	$F_3 > F_2$
Ugai [156]	LEM and variational analysis	$\phi = 0$	Vertical slopes/cylindrical	$F_3 > F_2$
Leshchinsky & Baker [154]	LEM and variational analysis	c, ϕ	Slopes constrained in 3rd dimension/unrestricted	$F_3 > F_2$ for c > 0, $F_3 = F_2$ for c = 0

Baker & Leshchinsky [155]	LEM and variational analysis	c, ϕ	Conical heaps/unrestricted	$F_3 > F_2$
Cavounidis [138]	LEM	c, ϕ	Unrestricted/unrestricted	F_3 must be > F_2
Hungr [25]	Extended Bishop's modified	c, ϕ	Unrestricted/surfaces of revolution	$F_3 > F_2$
Gens et al. [159]	Extended Swedish circle	$\phi = 0$	Simple slopes/surfaces of revolution	$F_3 > F_2$
Leshchinsky & Mullet [158]	LEM and variational analysis	c, ϕ	Vertical slopes with corners/unrestricted	$F_3 > F_2$
Ugai [161]	Extended OMS, Bishop's modified, Janbu and Spencer	c, ϕ	Unrestricted/unrestricted	$F_3 > F_2$, except for OMS
Xing [160]	LEM	c, ϕ	Unrestricted/ellipsoidal	$F_3 > F_2$
Michalowski [198]	Kinematical theorem of limit plasticity	c, ϕ	Unrestricted/unrestricted	$F_3 > F_2$
Seed et al. [21]	Ad hoc 2D and 3D	c, ϕ	One particular case, the Kettleman Hills failure	$F_3 < F_2$
Leshchinsky & Huang [165]	LEM and variational analysis	c, ϕ	Unrestricted/unrestricted	$F_3 > F_2$

4. APPLICATION OF LIMIT EQUILIBRIUM PROCEDURES

Limit equilibrium procedures are commonly used by engineers and academicians to obtain a safety factor for a critical slope profile. Also, it is widely used for back-calculation of the shear strength parameters, investigation of the overall causes of the instabilities, and, sometimes for the remedial purposes.

Here in this thesis, two (2D) and three-dimensional (3D) limit equilibrium methods will be performed using a slope stability software *Slide 7.0* (2D) and *Slide*^{3} (3D). The main aim of the analyses is to investigate the changes in the safety factor for multiple scenarios.

Five different hypothetical slope profiles have been chosen for the investigations, where four of them are very well-known profiles in the literature that is used generally for searching the critical slip surface [199]–[208]. The slope profiles have been investigated by considering different phreatic conditions, external loadings, frontal-water pressure from ponded-water, and fully-drained slope profile. Also, pseudo-static analyses have been performed to investigate the effect of earthquake-induced seismic accelerations.

Every possible conditions were implemented into the analyses to mimic the real-life scenarios such as a simple slope without any internal or external pressures applied and complex scenarios as inclined multi-layered slopes where high pore-water pressure, external loadings, ponded water pressure and active seismic conditions control the overall stability of the slope.

Total of 20 different scenarios were investigated for each of the four different hypothetical slope profiles (Figure 4.1) and 2 scenarios for a dam profile with an empty reservoir where no pore-water pressures exist. According to this, 82 different cases were performed in both two and three-dimensional limit equilibrium analyses; making a total of 164 individual cases.

Only predefined slip surfaces were used in the hypothetical analyses instead of critical slip surface searching methods for the reason that the main purpose of the thesis is to investigate the possible changes in the safety of a slope, and not to acquire the minimum factor of safety.

For two-dimensional analyses where the slip surface is expected to be circular due to lithological and structural conditions, Fellenius's method, Bishop's routine method, Spencer's method, Janbu's simplified and corrected methods, Corp's of engineers, GLE method (same as Morgenstern & Price's method in the software), Lowe & Karafiath's method were used. Where the conditions indicate a noncircular slip surface, Fellenius's and

Bishop's method will be excluded. For three-dimensional analyses with a circular slip surface, Bishop's routine method, Janbu's simplified method, Spencer's method and GLE/MP method will be used. Bishop's routine method will be excluded where a noncircular slip surface present. The summary of the applicable methods is presented in Table 4.1.

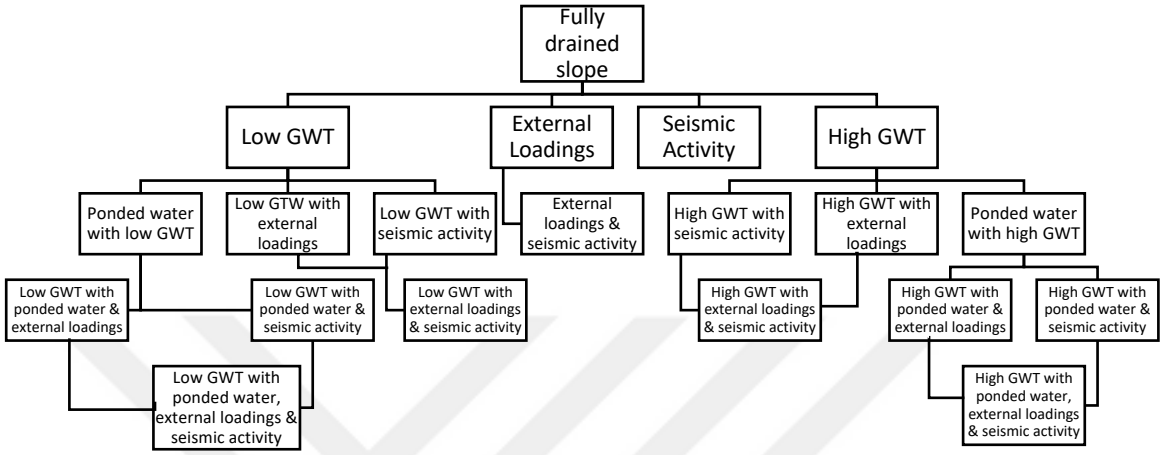


Figure 4.1 Total combinations for different scenarios.

Table 4.1 Available methods in *Slide* and *Slide*[3]

2D Methods		3D Methods	
Circular	Noncircular	Circular	Noncircular
Fellenius (OMS)	-	-*	-
Bishop's routine	-	Bishop's routine	-
Janbu's simplified method	Janbu's simplified method	Janbu's simplified method	Janbu's simplified method
Janbu's corrected method	Janbu's corrected method	-*	-*
Spencer's method	Spencer's method	Spencer's method	Spencer's method
GLE/MP	GLE/MP	GLE/MP	GLE/MP
Corps. of Engineers***	Corps. of Engineers***	-*	-*
Lowe & Karafiath	Lowe & Karafiath	-*	-*
-	Sarma	-*	-*
-	SarmaNV**	-*	-*

*Not available in *Slide*[3].
**Wedge-shaped, non-vertical slices. [93]
***EM 1110-2-1902, 1970.

In the analyses, the number of slices was kept constant. The slope profiles were divided into 50 slices and maximum of 50 vertical columns in both *x* and *y* directions for two-dimensional and three-dimensional analyses, respectively. Number of iterations to achieve the factor of

safety is fixed to 75. The tolerance between the initial factor of safety (F_{in}) and the final computed factor of safety (F_{fi}) is set to % 0.1 and gradually increased to % 1 until the convergence has been achieved. The interslice force function defined as a half part of a sinusoid. When tensile stresses present along the slip surface, the corresponding shear strength was taken as zero to prevent negative values.

4.1 The Analyses

4.1.1 Hypothetical case I

The slope profile was originally introduced by Yamagami & Ueta [200] in a comparative study of locating the critical slip surface. The profile is a one-stepped simple geometry (Figure 4.2 and Figure 4.3) and consists of a low-strength homogeneous soil. The dry unit weight of the material is 17.64 kN/m^3, saturated unit weight 18.50 kN/m^3, cohesion and the angle of internal friction is 9.8 kPa and 10°, respectively.

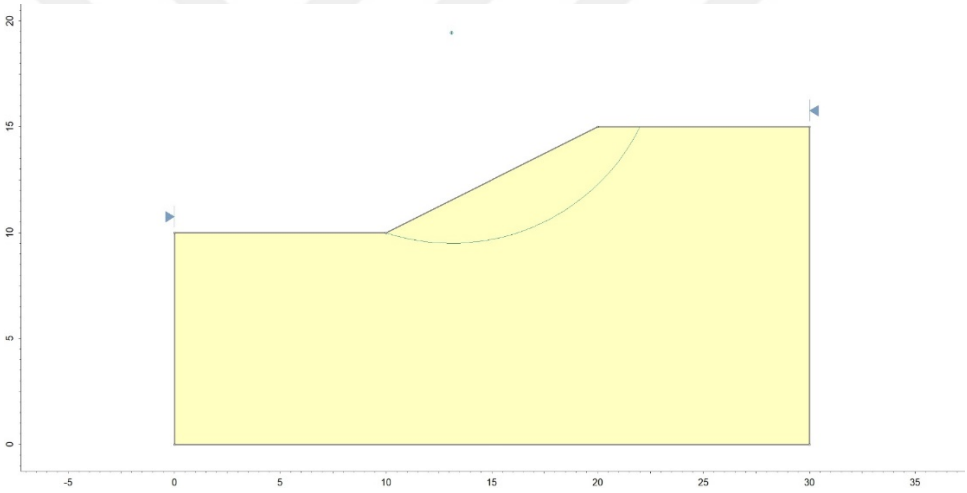


Figure 4.2 Cross-section of the homogeneous slope with a pre-defined slip surface.

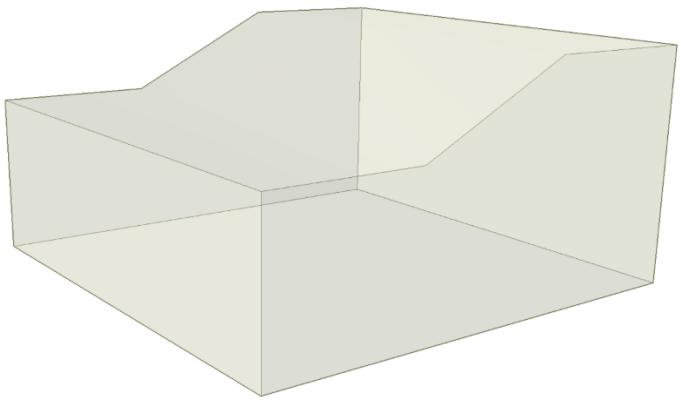


Figure 4.3 Three-dimensional model of hypothetical case I.

Coordinates of the predefined slip surface in the two-dimensional Cartesian system are (10.00, 10.00) and (22.00, 15.00); which, the first coordinate defines *x*-axis and the second defines *y*-axis. Also, the coordinates of the external boundary of the slope profile are given in Table 4.2. The analyses were performed with suitable methods to circular slip surfaces as mentioned earlier in Table 4.1.

Table 4.2 Coordinates of the slope profile in *x* and *y*-axes

External Boundary				
2D		3D		
x-axis	*y*-axis	*x*-axis	*y*-axis	*z*-axis
30	0	30	0	0
30	15	30	30	0
20	15	30	0	15
10	10	30	30	15
0	10	20	0	15
0	0	20	30	15
		10	0	10
		10	30	10
		0	0	10
		0	30	10
		0	0	0
		0	30	0

a – Fully drained situation

The first analysis was performed by assuming a fully drained slope material without any pore-fluid pressure, external loadings or seismic activity. The results of the analysis are given in below (Table 4.3).

Table 4.3 The results of the fully-drained analyses.

	OMS	Bishop	Spencer	Corps.	JanbuS	JanbuC	L&K	GLE/MP
F (2D)	1.3070	1.3544	1.3526	1.4038	1.2685	1.3557	1.3915	1.3526
F (3D)	-	1.5330	1.5290	-	1.4124	-	-	1.5299

b – Homogeneous slope with low elevation groundwater table

In this analysis, the groundwater level was kept at low elevation in order to maintain low pore-water pressure (Figure 4.4 & Figure 4.5).

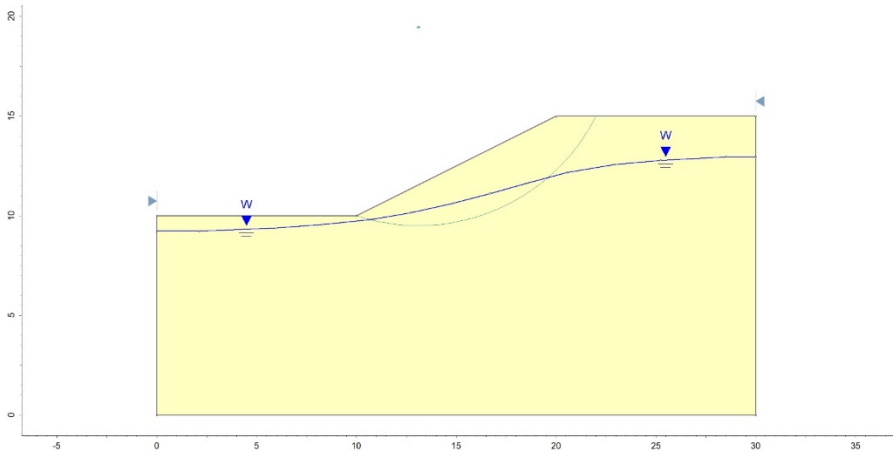


Figure 4.4 Modelling of the low GWT elevation.

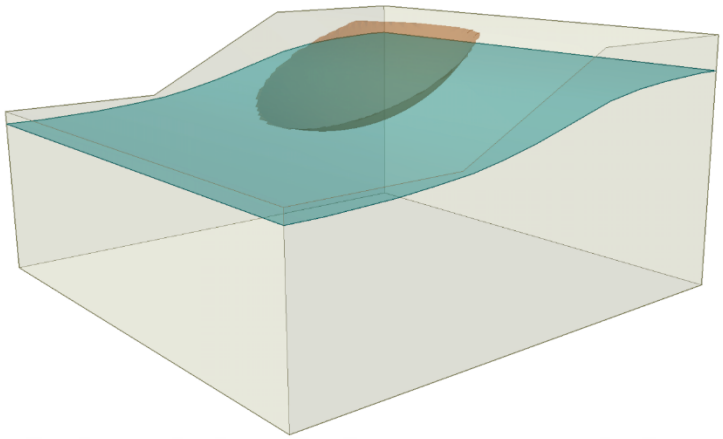


Figure 4.5 Three-dimensional model of the investigated slope. Blue and brown surfaces indicate the GWT and slip surface, respectively

The pore-water unit weight has been taken as 9.810 kN/m^3. The coordinates of the corresponding groundwater table are given in Table 4.4.

Table 4.4 Coordinates of the low GWT elevation.

Groundwater table				
2D		3D		
x-axis	*y*-axis	*x*-axis	*y*-axis	*z*-axis
0	9.23569	0	0	9.23569
2.13200	9.23569	0	30.00000	9.23569
5.99600	9.37800	2.13200	0	9.23569
8.28700	9.56000	2.13200	30.00000	9.23569
10.70700	9.79622	5.99600	0	9.37800
12.74500	10.15300	5.99600	30.00000	9.37800
14.83100	10.60900	8.28700	0	9.56000
16.68900	11.11100	8.28700	30.00000	9.56000
18.46800	11.60100	10.70700	0	9.79622
20.54300	12.17100	10.70700	30.00000	9.79622
22.92500	12.55800	12.74500	0	10.15300

25.24000	12.77500	12.74500	30.00000	10.1530
28.50000	12.94600	14.83100	0	10.60900
30.00000	12.94600	14.83100	30.00000	10.60900
		16.68900	0	11.11100
		16.68900	30.00000	11.11100
		18.46800	0	11.60100
		18.46800	30.00000	11.60100
		20.54300	0	12.17100
		20.54300	30.00000	12.17100
		22.92500	0	12.55800
		22.92500	30.00000	12.55800
		25.24000	0	12.77500
		25.24000	30.00000	12.77500
		28.50000	0	12.94600
		28.50000	30.00000	12.94600
		30.00000	0	12.94600
		30.00000	30.00000	12.94600

The results of the stability analyses are given below (Table 4.5).

Table 4.5 Computed factors of safety for low GWT elevation.

	OMS	Bishop	Spencer	Corps.	JanbuS	JanbuC	L&K	GLE/MP
F (2D)	1.32428	1.2819	1.2801	1.3324	1.2077	1.2908	1.3193	1.2803
F (3D)	-	1.4922	1.4891	-	1.3776	-	-	1.4843

c - Homogeneous slope with low elevation of groundwater table and external loading on top

This analysis was performed by assuming the same principle as the analysis-*b*, except this time there is a direct pressure to the top of the slope (Figure 4.6 & Figure 4.7). The external loading acts perpendicular to the boundary with a magnitude of 150 kPa. The coordinates of the loading for two-dimensional case, are (25.00, 15.00) and (21.50, 15.00). Also, the results of the analysis are given in Table 4.6.

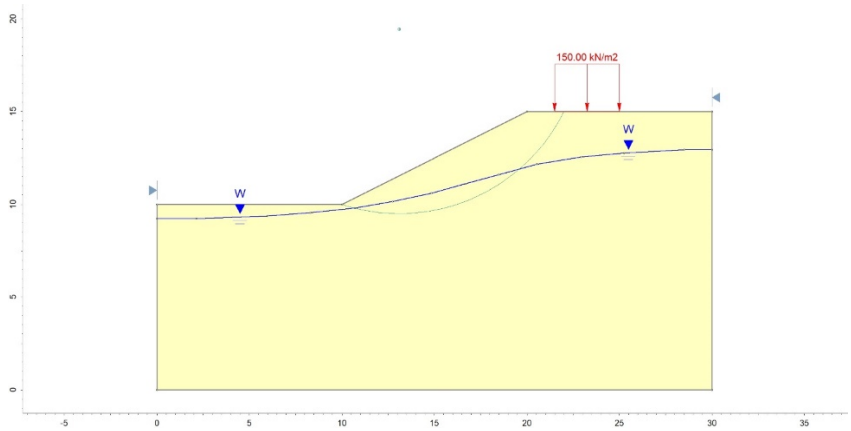


Figure 4.6 Demonstration of the external loading.

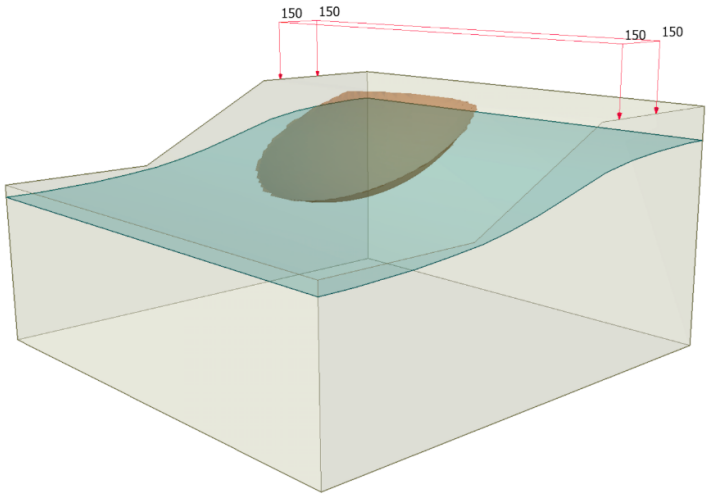


Figure 4.7 Three-dimensional model of the slope for the scenario-*c*. External loadings indicated by red arrows.

Table 4.6 Results of the stability analysis with external loading.

	OMS	Bishop	Spencer	Corps.	JanbuS	JanbuC	L&K	GLE/MP
F (2D)	0.9170	0.9903	0.9791	0.9694	0.8310	0.8882	0.9670	0.9821
F (3D)	-	1.3219	1.2714	-	1.1566	-	-	1.2980

d – Homogeneous slope with low elevation GWT and seismic activity

Analysis performed with the same groundwater table as the previous analyses with an additional seismic activity (Figure 4.8). According to Melo & Sharma [209], the seismic coefficients in horizontal and vertical direction have an average ratio of 1/4. In the analyses, the horizontal and vertical seismic coefficients were taken as 0.1 and 0.025, respectively. The results of the analyses are given in Table 4.7.

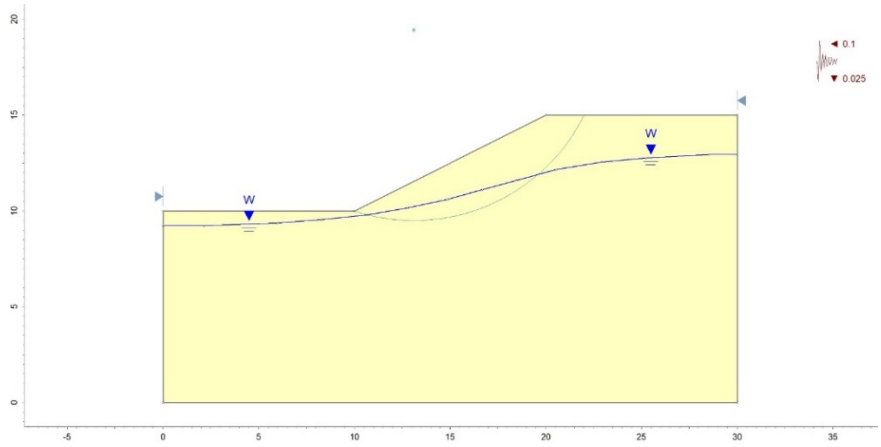


Figure 4.8 Same slope profile as the analysis-*b* with an additional seismic activity.

Table 4.7 The results of the analyses with seismic activity.

	OMS	Bishop	Spencer	Corps.	JanbuS	JanbuC	L&K	GLE/MP
F (2D)	0.9937	1.0263	1.0255	1.0339	0.9559	1.0217	1.0196	1.0252
F (3D)	-	1.1858	1.1706	-	1.0734	-	-	1.1818

e – Homogeneous slope with low elevation GWT, external loading and seismic activity

In this analysis, pore-water pressure, external loading and seismic activity were applied at the same time with the same conditions in previous analyses (Figure 4.9). Corresponding factors of safety to this scenario are given in Table 4.8.

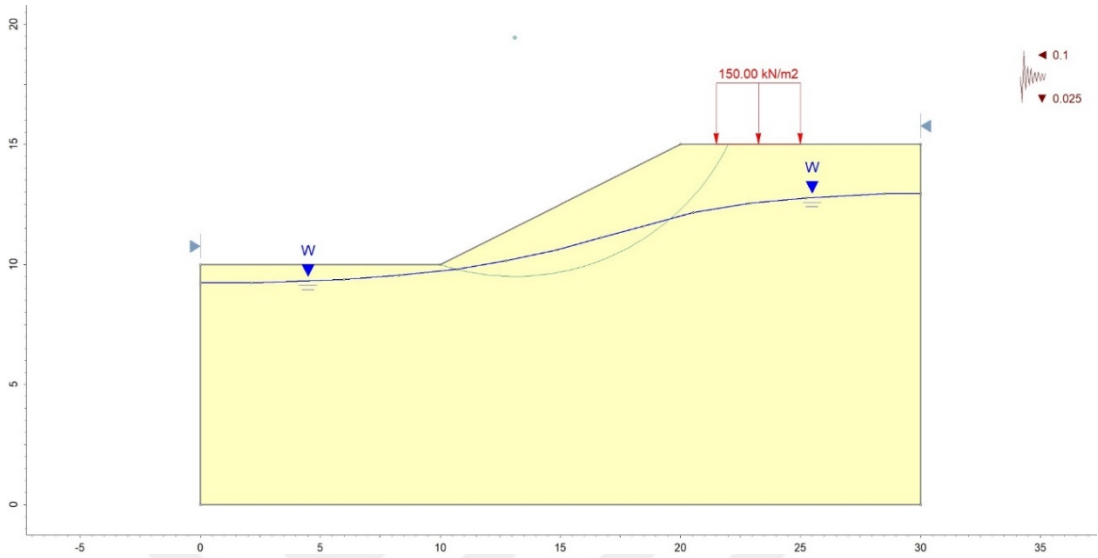


Figure 4.9 Cross-section of the slope and applied external forces.

Table 4.8 Computed safety factors for scenario-*e*.

	OMS	Bishop	Spencer	Corps.	JanbuS	JanbuC	L&K	GLE/MP
F (2D)	0.7768	0.8380	0.8300	0.8089	0.7119	0.7609	0.8045	0.8320
F (3D)	-	1.0835	1.0413	-	0.9519	-	-	1.0676

f – Homogeneous slope with low elevation of GWT and ponded water in front

This analysis has been done by considering only the forces accumulating from pore-water pressures and ponded water. The groundwater level is kept at low elevation and the ponded water is shallow in depth (Figure 4.10 and Figure 4.11). Neither seismic activity nor the external loadings were applied. Also, the coordinates of the water table are given in Table 4.9.

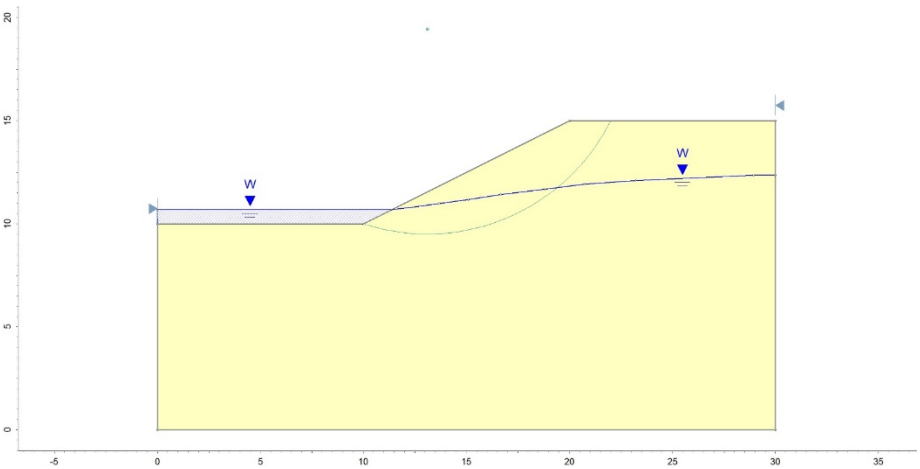


Figure 4.10 Cross-section of the slope profile with ponded water in front.

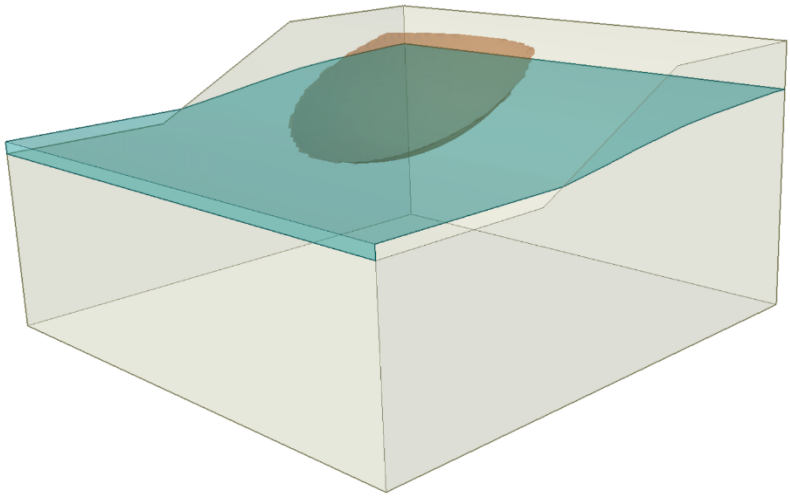


Figure 4.11 Three-dimensional profile of the scenario-*f*.

Table 4.9 Coordinates of the water table in the Cartesian system.

Water table				
2D		3D		
x-axis	*y*-axis	*x*-axis	*y*-axis	*z*-axis
0	10.000	0	0	10.000
0	10.682	0	30.000	10.000
11.364	10.682	0	0	10.682
12.419	10.816	0	30.000	10.682
13.670	10.983	11.364	0	10.682
15.086	11.173	11.364	30.000	10.682
16.666	11.411	12.419	0	10.816
18.798	11.683	12.419	30.000	10.816
20.735	11.92	13.670	0	10.983
23.199	12.099	13.670	30.000	10.983
28.926	12.363	15.086	0	11.173
30.000	12.363	15.086	30.000	11.173
		16.666	0	11.411
		16.666	30.000	11.411
		18.798	0	11.683
		18.798	30.000	11.683
		20.735	0	11.920
		20.735	30.000	11.920
		23.199	0	12.099
		23.199	30.000	12.099
		28.926	0	12.363
		28.926	30.000	12.363
		30.000	0	12.363
		30.000	30.000	12.363

The factors of safety corresponding to various methods was calculated in the stability analysis and the results are given in below. (Table 4.10)

Table 4.10 Computed factors of safety for the scenario-*f*.

	OMS	Bishop	Spencer	Corps.	JanbuS	JanbuC	L&K	GLE/MP
F (2D)	1.2292	1.2669	1.2662	1.3247	1.1951	1.2773	1.3051	1.2653
F (3D)	-	1.4652	1.4642	-	1.3576	-	-	1.4618

g – Homogeneous slope with low elevation GWT, ponded water in front and external loading

The water pressures from pore-pressures and ponded water were kept the same as the scenario-*e* and an additional external loading on the top of the slope was applied (Figure 4.12). The results of the analysis are given in Table 4.11.

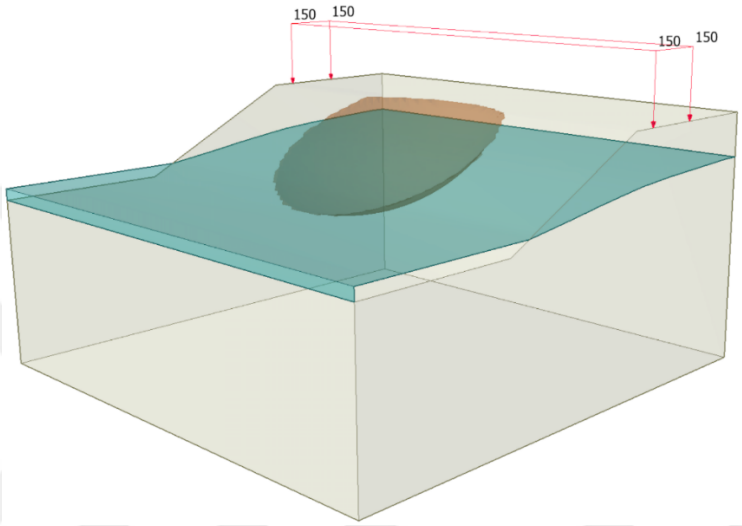


Figure 4.12 Three-dimensional profile of the scenario-*g*.

Table 4.11 Computed results of the safety factors for scenario-*g*.

	OMS	Bishop	Spencer	Corps.	JanbuS	JanbuC	L&K	GLE/MP
F (2D)	0.9027	0.9746	0.9640	0.9573	0.8186	0.8749	0.9502	0.9671
F (3D)	-	1.3007	1.2518	-	1.1352	-	-	1.2763

h – Homogeneous slope with low elevation GWT, ponded water in front and seismic activity

This analysis is the same as scenario-*f* but with an additional seismic activity to investigate the effects of an earthquake. The computed results for this analysis is given in Table 4.12.

Table 4.12 Computed results for the scenario-*h*.

	OMS	Bishop	Spencer	Corps.	JanbuS	JanbuC	L&K	GLE/MP
F (2D)	0.9774	1.0081	1.0077	1.0197	0.9407	1.0054	1.0001	1.0071
F (3D)	-	1.1625	1.1522	-	1.0551	-	-	1.1603

i – Homogeneous slope with low elevation of GWT, ponded water in front, external loading on top and seismic activity

This is the scenario where all of the combinations applied to the slope profile (Figure 4.13). The properties of the water table, external loading and seismic activity are the same as the previous analyses. The results of the computed safety factors are given in Table 4.13.

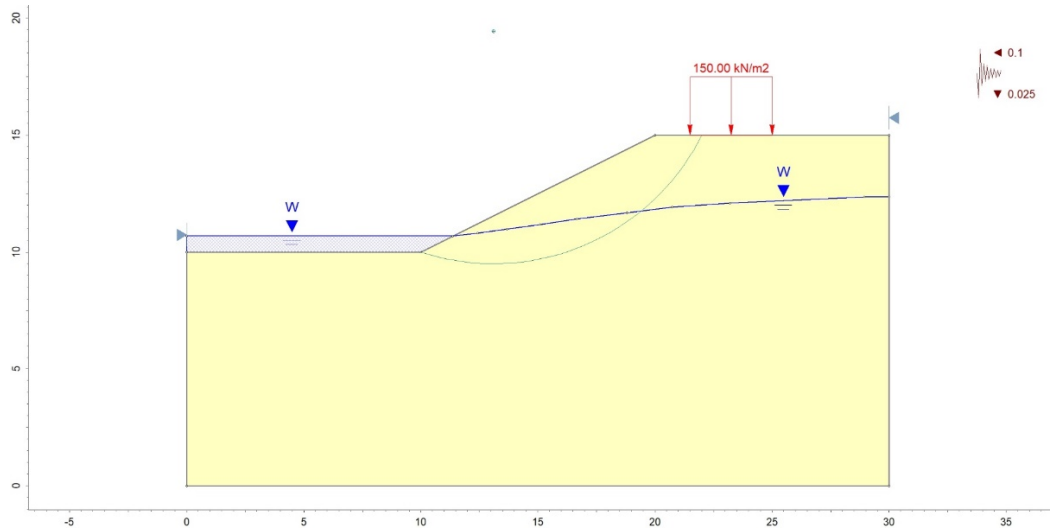


Figure 4.13 The slope profile with the combinations of all the scenarios.

Table 4.13 Computed results for the scenario-*i*.

	OMS	Bishop	Spencer	Corps.	JanbuS	JanbuC	L&K	GLE/MP
F (2D)	0.7621	0.8216	0.8141	0.7953	0.6992	0.7472	0.7877	0.8161
F (3D)	-	1.0633	1.0221	-	0.9357	-	-	1.0475

j – Homogeneous slope with high elevation groundwater table

In this analysis, the groundwater level was kept at low elevation in order to maintain low pore-water pressure (Figure 4.14 & Figure 4.15). The coordinates of the water table are given in Table 4.14.

Table 4.14 Coordinates of the high GWT elevation.

Water table				
2D		3D		
x-axis	*y*-axis	*x*-axis	*y*-axis	*z*-axis
0	8.60000	0	0	8.60000
1.28800	8.62900	0	30.00000	8.60000
3.63000	8.78300	1.28800	0	8.62900
4.93600	8.92200	1.28800	30.00000	8.62900
6.39100	9.10500	3.63000	0	8.78300
7.49600	9.29600	3.63000	30.00000	8.78300
8.32700	9.47100	4.93600	0	8.92200
9.41600	9.77800	4.93600	30.00000	8.92200
10.06440	9.97906	6.39100	0	9.10500
11.20600	10.46600	6.39100	30.00000	9.10500
12.80300	11.11000	7.49600	0	9.29600
14.33900	11.70400	7.49600	30.00000	9.29600
15.85000	12.21800	8.32700	0	9.47100
17.28700	12.66400	8.32700	30.00000	9.47100
18.66200	13.00500	9.41600	0	9.77800
19.83900	13.26500	9.41600	30.00000	9.77800
21.09110	13.52090	10.06440	0	9.97906

22.40200	13.72900	10.06440	30.00000	9.97906
23.81400	13.94600	11.20600	0	10.46600
25.43100	14.17500	11.20600	30.00000	10.46600
26.75000	14.31800	12.8030	0	11.11000
27.51200	14.39200	12.80300	30.00000	11.11000
28.73700	14.46470	14.33900	0	11.70400
30.00000	14.46470	14.33900	30.00000	11.70400
		15.85000	0	12.21800
		15.85000	30.00000	12.21800
		17.28700	0	12.66400
		17.28700	30.00000	12.66400
		18.66200	0	13.00500
		18.66200	30.00000	13.00500
		19.83900	0	13.26500
		19.83900	30.00000	13.26500
		21.09110	0	13.52090
		21.09110	30.00000	13.52090
		22.40200	0	13.72900
		22.40200	30.00000	13.72900
		23.81400	0	13.94600
		23.81400	30.00000	13.94600
		25.43100	0	14.17500
		25.43100	30.00000	14.17500
		26.75000	0	14.31800
		26.75000	30.00000	14.31800
		27.51200	0	14.39200
		27.51200	30.00000	14.39200
		28.73700	0	14.46470
		28.73700	30.00000	14.46470
		30.00000	0	14.46470
		30.00000	30.00000	14.46470

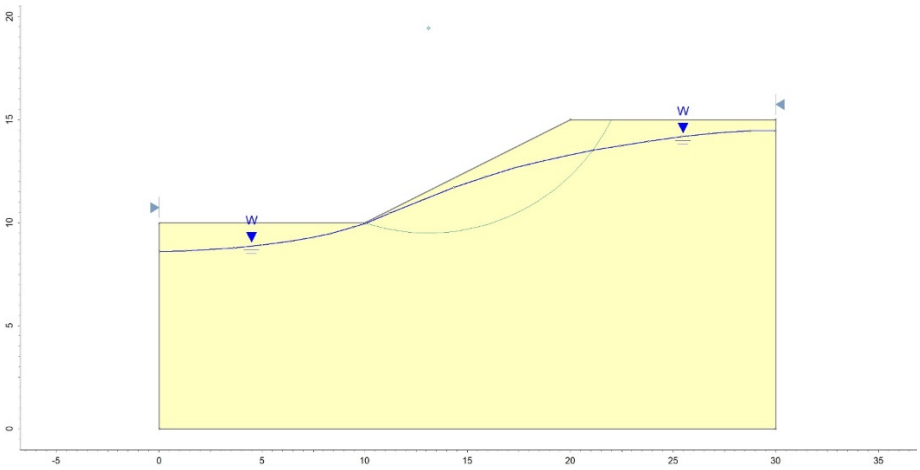


Figure 4.14 Cross-section of the slope profile with high GWT elevation.

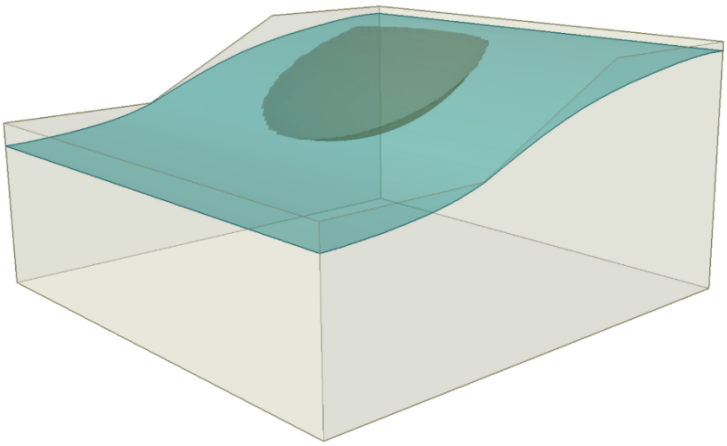


Figure 4.15 Three-dimensional model of the investigated slope for the scenario-*j*.

The results of the stability analysis and the corresponding factors of safety are given in Table 4.15.

Table 4.15 Computed factors of safety for the scenario-*j*.

	OMS	Bishop	Spencer	Corps.	JanbuS	JanbuC	L&K	GLE/MP
F (2D)	1.1231	1.1375	1.1371	1.1881	1.0783	1.1525	1.1696	1.1368
F (3D)	-	1.3435	1.3381	-	1.2486	-	-	1.3425

k - Homogeneous slope with high elevation groundwater table and external loading on top

In this scenario, the groundwater level was at high elevation and an external loading applied to the top of the slope (Figure 4.16). The magnitude and coordinates of the load are the same as the previous analyses. The results of the analyses are given in below. (Table 4.16)

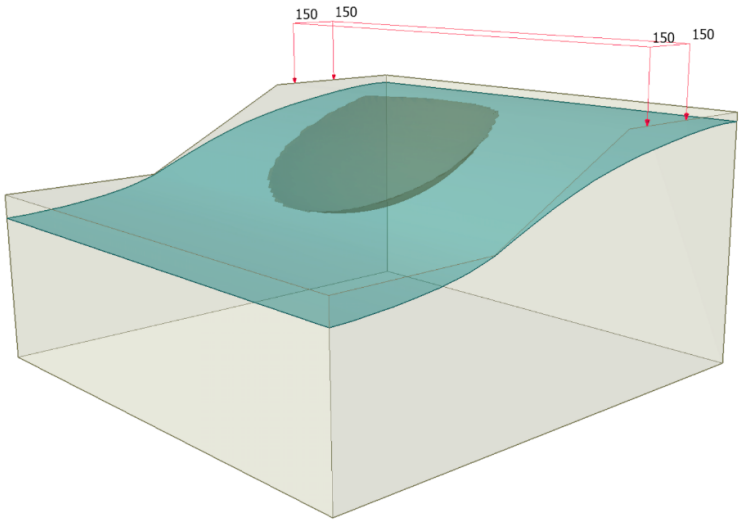


Figure 4.16 Three-dimensional model of the scenario-*k*.

Table 4.16 Computed results of safety factors for the scenario-*k*.

	OMS	Bishop	Spencer	Corps.	JanbuS	JanbuC	L&K	GLE/MP
F (2D)	0.8351	0.8883	0.8788	0.8740	0.7529	0.8045	0.8708	0.8816
F (3D)	-	1.2002	1.1513	-	1.0516	-	-	1.1809

l – Homogeneous slope with high elevation groundwater table and seismic activity

In this analysis, high groundwater table generates a high pore-water pressure along with a seismic activity. The ratio and the values of the horizontal and vertical seismic coefficients have been taken the same as the previous analyses. The computed safety factors for this scenario is given in Table 4.17.

Table 4.17 Computed results of the factors of safety for the scenario-*l*.

	OMS	Bishop	Spencer	Corps.	JanbuS	JanbuC	L&K	GLE/MP
F (2D)	0.8969	0.9096	0.9097	0.9215	0.8520	0.9106	0.9056	0.9090
F (3D)	-	1.0623	1.0537	-	0.9685	-	-	1.0648

m – Homogeneous slope with high elevation GWT, external loading and seismic activity

This analysis has been performed by assuming a high pore-water pressure, an external loading on top of the slope and a seismic activity applying at the same time (Figure 4.17). The results of the analysis are given in Table 4.18.

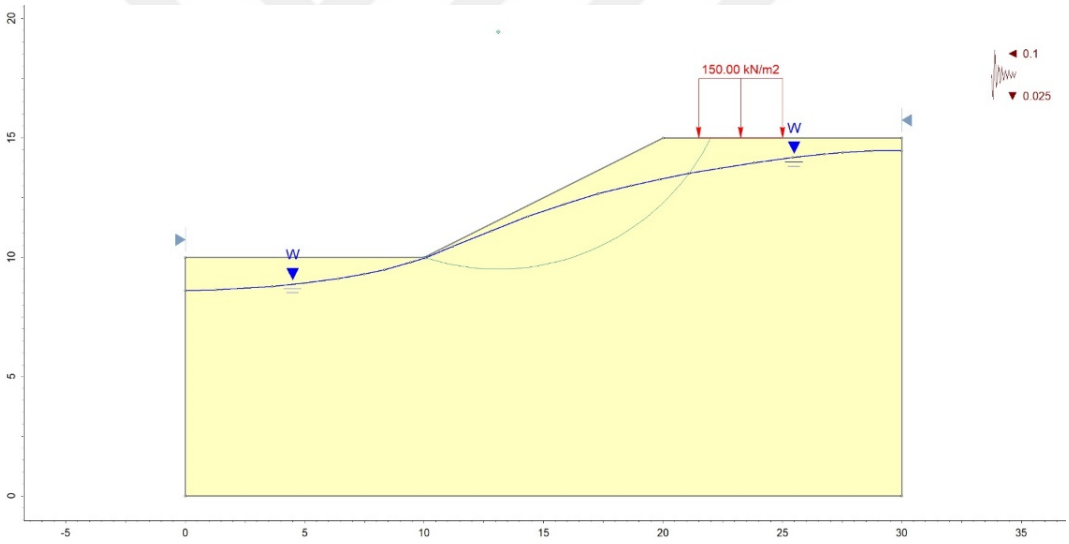


Figure 4.17 Cross-section of the slope profile for the scenario-*m*.

Table 4.18 The results of the analysis for the scenario-*m*.

	OMS	Bishop	Spencer	Corps.	JanbuS	JanbuC	L&K	GLE/MP
F (2D)	0.7062	0.7503	0.7443	0.7229	0.6432	0.6875	0.7229	0.7455
F (3D)	-	0.9819	0.9420	-	0.8617	-	-	0.9625

n – Homogeneous slope with high elevation GWT and ponded water in front

In this analysis, the water table level is kept at high elevation and the ponded water is deep in depth (Figure 4.18 & Figure 4.19). Neither seismic activity nor the external loadings were applied. Also, the coordinates of the water table are given in Table 4.19.

Table 4.19 Coordinates of the water table from the scenario-*n*.

Water table				
2D		3D		
x-axis	*y*-axis	*x*-axis	*y*-axis	*z*-axis
0	10.0000	0	0	10.0000
0	14.0070	0	30.0000	10.0000
18.0149	14.0075	0	0	14.0070
18.2930	14.0490	0	30.0000	14.0070
19.4760	14.2210	18.0149	0	14.0075
21.0760	14.4020	18.0149	30.0000	14.0075
22.8080	14.5300	18.2930	0	14.0490
24.5010	14.6090	18.2930	30.0000	14.0490
26.2150	14.6744	19.4760	0	14.2210
29.0820	14.6744	19.4760	30.0000	14.2210
30.0000	14.6744	21.0760	0	14.4020
		21.0760	30.0000	14.4020
		22.8080	0	14.5300
		22.8080	30.0000	14.5300
		24.5010	0	14.6090
		24.5010	30.0000	14.6090
		26.2150	0	14.6744
		26.2150	30.0000	14.6744
		29.0820	0	14.6744
		29.0820	30.0000	14.6744
		30.0000	0	14.6744
		30.0000	30.0000	14.6744

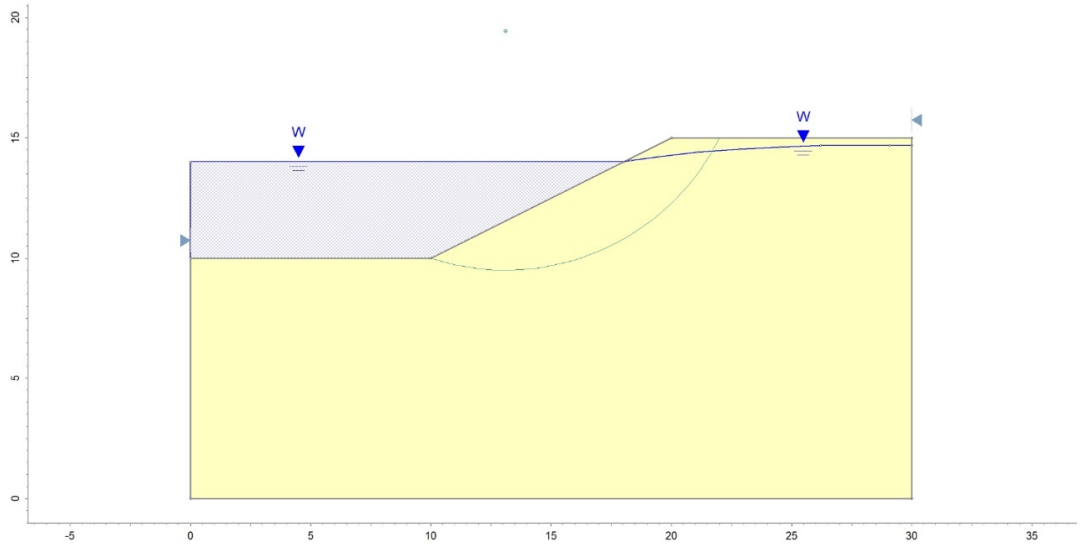


Figure 4.18 The slope profile for the scenario-*n*.

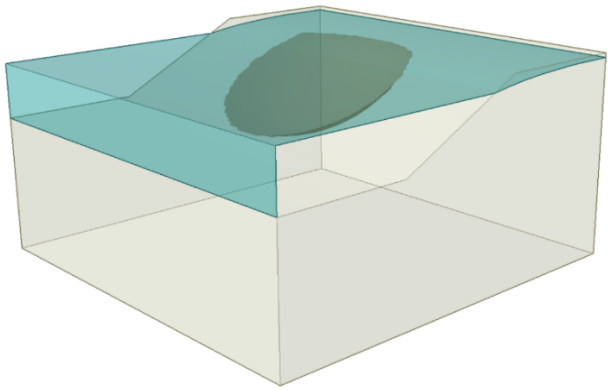


Figure 4.19 Three-dimensional model of the scenario-*n*.

The computed factors of safety to corresponding methods in stability analysis are given in Table 4.20.

Table 4.20 The computed safety factors for the scenario-*n*.

	OMS	Bishop	Spencer	Corps.	JanbuS	JanbuC	L&K	GLE/MP
F (2D)	1.8059	1.8496	1.8463	2.5383	1.6947	1.8113	1.9469	1.8461
F (3D)	-	2.4285	2.4503	-	2.1769	-	-	2.4263

p – Homogeneous slope with high elevation GWT, ponded water in front and external loading

This analysis was performed by assuming a high pore-water pressure along with a direct water pressure from the front side of the slope and an external loading with a magnate of 150 kPa on top of the boundary (Figure 4.20). The results of the stability analysis are given in Table 4.21.

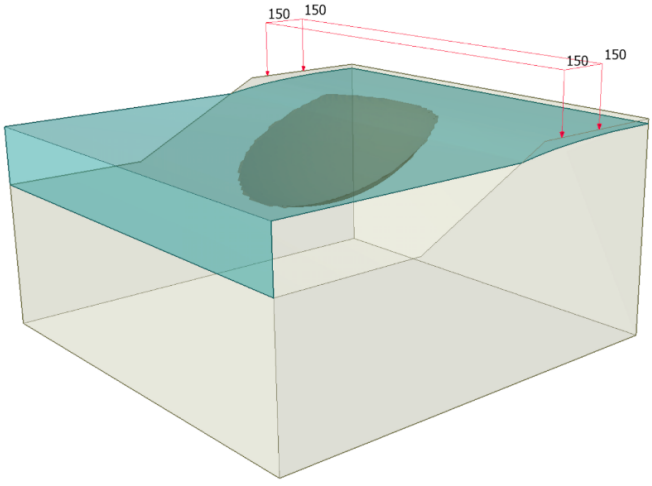


Figure 4.20 Three-dimensional model for the scenario-*p*.

Table 4.21 Computed safety factors for scenario-*p*.

	OMS	Bishop	Spencer	Corps.	JanbuS	JanbuC	L&K	GLE/MP
F (2D)	1.1244	1.2174	1.2027	1.3522	0.9614	1.0276	1.1582	1.2049
F (3D)	-	1.9029	1.8398	-	1.5356	-	-	1.8699

r – Homogeneous slope with high elevation GWT, ponded water in front and seismic activity

This analysis is the same as the scenario-*n* with an additional seismic activity. The results of the stability analyses are given in Table 4.22.

Table 4.22 The results of the stability analyses for the scenario-*r*.

	OMS	Bishop	Spencer	Corps.	JanbuS	JanbuC	L&K	GLE/MP
F (2D)	1.2631	1.2946	1.2926	1.5434	1.1806	1.2618	1.2857	1.2918
F (3D)	-	1.6456	1.6517	-	1.4365	-	-	1.6319

s – Homogeneous slope with high elevation GWT, ponded water in front, external loading on top and seismic activity

This analysis consists of all of the combinations mentioned previously and differing from scenario-*i* only by the level of the water table (Figure 4.21). The results of the analysis are given in Table 4.23.

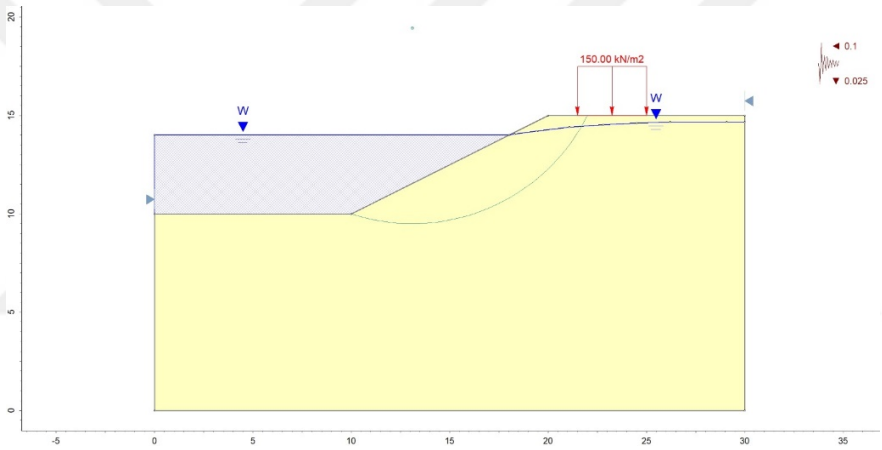


Figure 4.21 Showing all of the combinations in cross-section.

Table 4.23 Computed safety factors for the scenario-*s*.

	OMS	Bishop	Spencer	Corps.	JanbuS	JanbuC	L&K	GLE/MP
F (2D)	0.8922	0.9638	0.9540	1.0268	0.7848	0.8388	0.8989	0.9558
F (3D)	-	1.3928	1.3558	-	1.1370	-	-	1.3482

t – Homogeneous slope with external loading on top

This analysis has been done by considering only an external load on the top of the drained slope (Figure 4.22). The results of the analysis are given in Table 4.24.

Table 4.24 The results of the analyses for the scenario-*t*.

	OMS	Bishop	Spencer	Corps.	JanbuS	JanbuC	L&K	GLE/MP
F (2D)	0.9611	1.0415	1.0301	1.0160	0.8682	0.9279	1.0142	1.0323
F (3D)	-	1.3568	1.3090	-	1.1902	-	-	1.3349

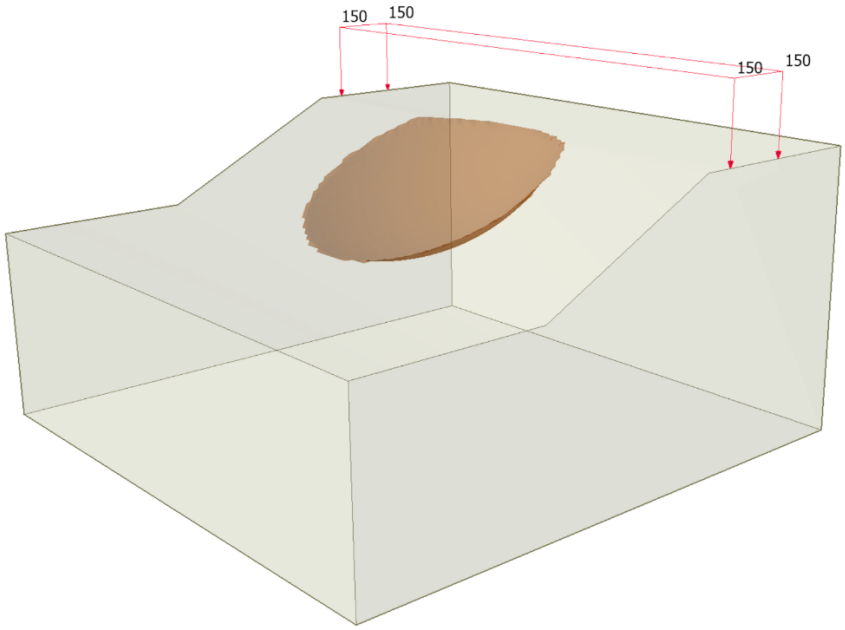


Figure 4.22 Three-dimensional model of the scenario-*t*.

v – Homogeneous slope with external loading on top and seismic activity

This analysis consists of both external loading on top of the slope and seismic activity. Computed factors of safety for each method available is given in Table 4.25.

Table 4.25 Computed results of the scenario-*v*.

	OMS	Bishop	Spencer	Corps.	JanbuS	JanbuC	L&K	GLE/MP
F (2D)	0.8152	0.8829	0.8733	0.8492	0.7449	0.7962	0.8458	0.8763
F (3D)	-	1.1152	1.0721	-	0.9744	-	-	1.0974

y – Homogeneous slope with seismic activity

This analysis only examines the effects of an earthquake-induced forces. The computed factors of safety for each method is given Table 4.26.

Table 4.26 Computed results for the scenario-*y*.

	OMS	Bishop	Spencer	Corps.	JanbuS	JanbuC	L&K	GLE/MP
F (2D)	1.0463	1.0860	1.0858	1.0906	1.0057	1.0749	1.0760	1.0845
F (3D)	-	1.2225	1.2091	-	1.1002	-	-	1.2164

4.1.2 Hypothetical case II

This case represents multi-step geometry as in open-pit mines. It consists of 3 different lithological units with a low inclination relative to horizontal (Figure 4.23 & Figure 4.24). One of the materials has a very low strength characteristic and acts as a weak thin layer between relatively hard strata. The properties of the materials are given in Table 4.27.

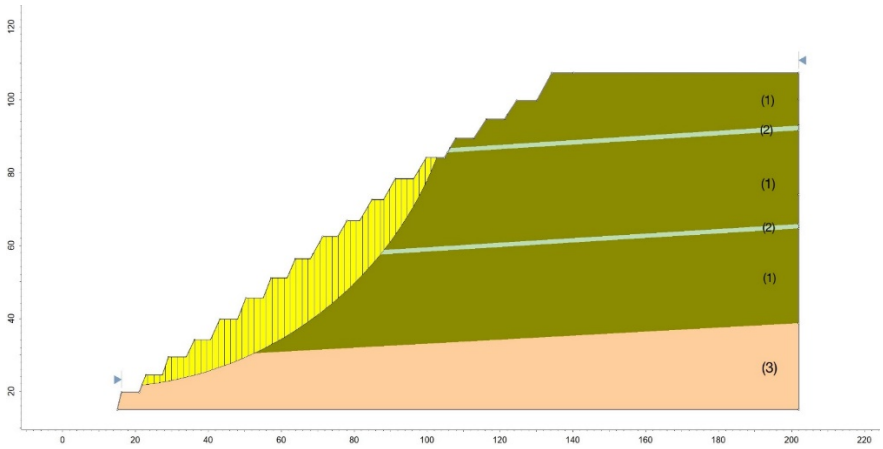


Figure 4.23 Cross-section of the slope with predefined circular slip surface which consists of fifty slices.

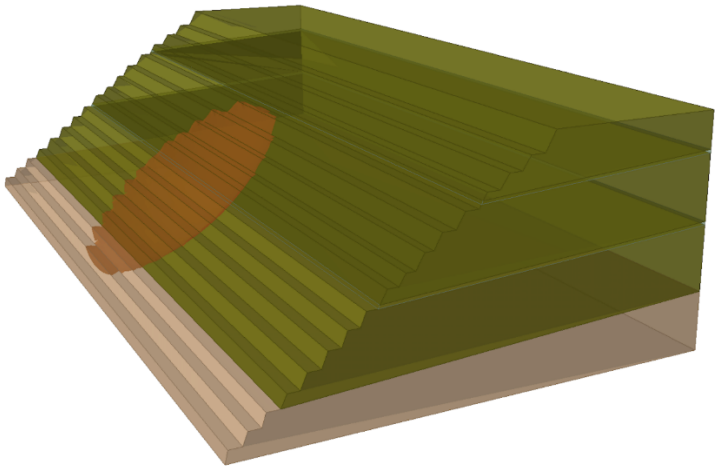


Figure 4.24 Three-dimensional model of the hypothetical case II. Brown area indicates the slip surface.

Table 4.27 Assumed properties of the slope forming materials.

Property	Material 1	Material 2	Material 3
Unit weight (kN/m^3)	20	14	17
Saturated unit weight (kN/m^3)	21.2	14.8	18
Cohesion (kPa)	28	3	17
Angle of internal friction (°)	45	14	35

In the two and three-dimensional Cartesian coordinate system, the center of the pre-defined circular failure surface is (10.44, 120.02) and (10.44, 187.00, 120.02), respectively. The lower and the upper part of the failure surface is on (21.77, 21.73) and (102.65, 84.14), respectively. The coordinates of the external boundary of the slope and slope-forming materials are also given in Cartesian system Table 4.28 and Table 4.29, respectively.

Table 4.28 Coordinates of the slope boundary.

External boundary				
2D		3D		
x-axis	*y*-axis	*x*-axis	*y*-axis	*z*-axis
201.9870	15.0000	201.9870	0	15.0000

201.9870	38.7730	201.9870	374.0000	15.0000
201.9870	64.7457	201.9870	0	38.7730
201.9870	65.9864	201.9870	374.0000	38.7730
201.9870	74.0099	201.9870	0	64.7457
201.9870	91.7110	201.9870	374.0000	64.7457
201.9870	92.9517	201.9870	0	65.9864
201.9870	100.2310	201.9870	374.0000	65.9864
201.9870	107.4440	201.9870	0	74.0099
140.1760	107.4440	291.9870	374.0000	74.0099
134.3090	107.4440	201.9870	0	91.7110
130.1040	99.8410	201.9870	374.0000	91.7110
124.5750	99.8410	201.9870	0	92.9517
122.0130	95.8815	201.9870	374.0000	92.9517
121.3170	94.8050	201.9870	0	100.2310
116.3800	94.8050	201.9870	374.0000	100.2310
112.8250	89.4730	201.9870	0	107.4440
107.8880	89.4730	201.9870	374.0000	107.4440
106.3210	86.7427	140.1760	0	107.4440
105.6610	85.5940	140.1760	374.0000	107.4440
104.8270	84.1410	134.3090	0	107.4440
99.7910	84.1410	134.3090	374.0000	107.4440
96.3350	78.3160	130.1040	0	99.8410
91.3000	078.3160	130.1040	374.0000	99.8410
88.1400	72.5890	124.5750	0	99.8410
84.8820	72.5890	124.5750	374.0000	99.8410
81.5250	66.7630	122.0130	0	95.8815
78.0690	66.7630	122.0130	374.0000	95.8815
75.5010	62.5170	121.3170	0	94.8050
71.3540	62.5170	121.3170	374.0000	94.8050
68.6532	57.5917	116.3800	0	94.8050
67.9970	56.3950	116.3800	374.0000	94.8050
63.8500	56.3950	112.8250	0	89.4730
61.6780	51.1620	112.8250	374.0000	89.4730
57.2350	51.1620	107.8880	0	89.4730
55.0620	45.6330	107.8880	374.0000	89.4730
50.3230	45.6330	106.3210	0	86.7427
48.0520	39.8070	106.3210	374.0000	86.7427
43.1150	39.8070	105.6610	0	85.5940
40.6460	34.1790	105.6610	374.0000	85.5940
36.2030	34.1790	104.8270	0	84.1410
33.9320	29.4400	104.8270	374.0000	84.1410
29.0940	29.4400	99.7910	0	84.1410
27.4150	24.5030	99.7910	374.0000	84.1410
22.8730	24.5030	96.3350	0	78.3160
20.9970	19.7630	96.3350	374.0000	78.3160
16.1590	19.7630	91.3000	0	78.3160
15.0000	15.0000	91.3000	374.0000	78.3160
		88.1400	0	72.5890

		88.1400	374.0000	72.5890
		84.8820	0	72.5890
		84.8820	374.0000	72.5890
		81.5250	0	66.7630
		81.5250	374.0000	66.7630
		78.0690	0	66.7630
		78.0690	374.0000	66.7630
		75.5010	0	62.5170
		75.5010	374.0000	62.5170
		71.3540	0	62.5170
		71.3540	374.0000	62.5170
		68.6532	0	57.5917
		68.6532	374.0000	57.5917
		67.9970	0	56.3950
		67.9970	374.0000	56.3950
		63.8500	0	56.3950
		63.8500	374.0000	56.3950
		61.6780	0	51.1620
		61.6870	374.0000	51.1620
		57.2350	0	51.1620
		57.2350	374.0000	51.1620
		55.0620	0	45.6330
		55.0620	374.0000	45.6330
		50.3230	0	45.6330
		50.3230	374.0000	45.6330
		48.0520	0	39.8070
		48.0520	374.0000	39.8070
		43.1150	0	39.8070
		43.1150	374.0000	39.8070
		40.6460	0	34.1790
		40.6460	374.0000	34.1790
		36.2030	0	34.1790
		36.2030	374.0000	34.1790
		33.9320	0	29.4400
		33.9320	374.0000	29.4400
		29.0940	0	29.4400
		29.0940	374.0000	29.4400
		27.4150	0	24.5030
		27.4150	374.0000	24.5030
		22.8730	0	24.5030
		22.8730	374.0000	24.5030
		20.9970	0	19.7630
		20.9970	374.0000	19.7630
		16.1590	0	19.7630
		16.1590	374.0000	19.7630
		15.0000	0	15.0000
		15.0000	374.0000	15.0000

Table 4.29 The coordinates of the materials boundary for hypothetical case II.

Material boundary				
2D		3D		
x-axis	*y*-axis	*x*-axis	*y*-axis	*z*-axis
33.9320	29.4400	33.9320	0	29.4400
201.9870	38.7730	33.9320	374.0000	29.4400
67.9970	56.3950	201.9870	0	38.7730
201.9870	64.7457	201.9870	374.0000	38.7730
68.6532	57.5917	67.9970	0	56.3950
201.9870	65.9864	67.9970	374.0000	56.3950
105.6610	85.5940	201.9870	0	64.7457
201.9870	91.7110	201.9870	374.0000	64.7457
106.3210	86.7427	68.6532	0	57.5917
201.9870	92.9517	68.6532	374.0000	57.5917
		201.9870	0	65.9864
		201.9870	374.0000	65.9864
		105.6610	0	85.5940
		105.6610	374.0000	85.5940
		201.9870	0	91.7110
		201.9870	374.0000	91.7110
		106.3210	0	86.7427
		106.3210	374.0000	86.7427
		201.9870	0	92.9517
		201.9870	374.0000	92.9517

a – Fully drained situation

This analysis is performed with suitable methods by assuming the absence of the water pressure acting on or in to slope. The results of the stability analysis are given in Table 4.30.

Table 4.30 Results of the calculations for the scenario-*a.*

	OMS	Bishop	JanbuC	Spencer	Corps	L&K	GLE/MP	JanbuS
F (2D)	1.4897	1.5713	1.5623	1.5568	1.5647	1.5529	1.5544	1.4795
F (3D)	-	1.6977	-	1.6829	-	-	1.6874	1.6041

b – Low elevation groundwater table

In this case, shallow groundwater table has been added to the cross-section to investigate the effects of the pore-water pressure (Figure 4.25 & Figure 4.26). The coordinates of the GWT and the results of the analysis are given in Table 4.31 and Table 4.32, respectively.

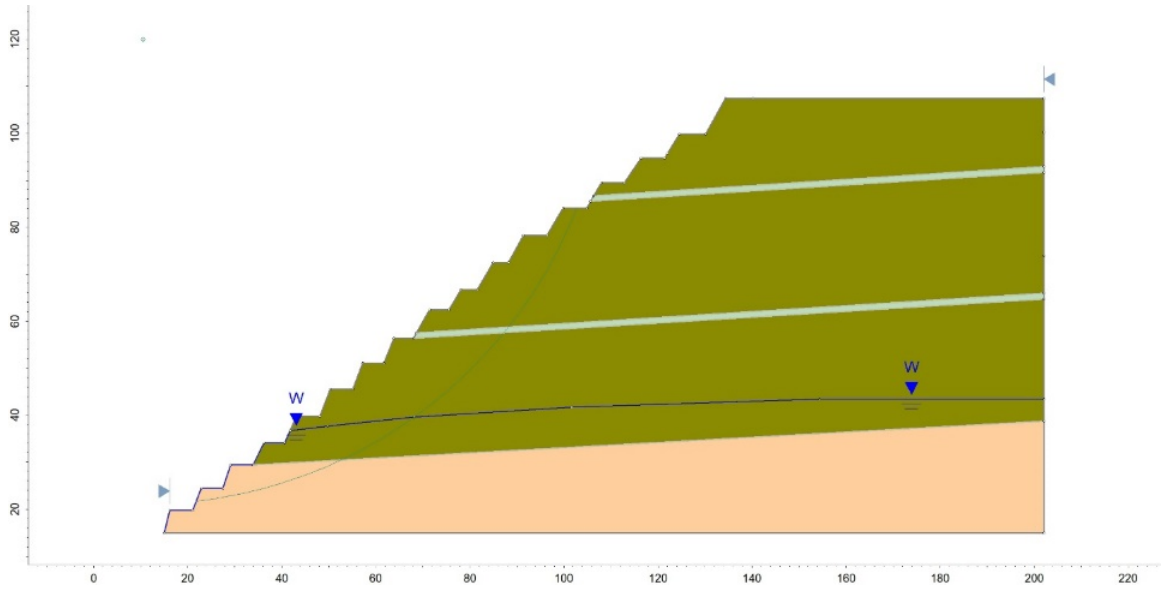


Figure 4.25 Indicating groundwater table level.

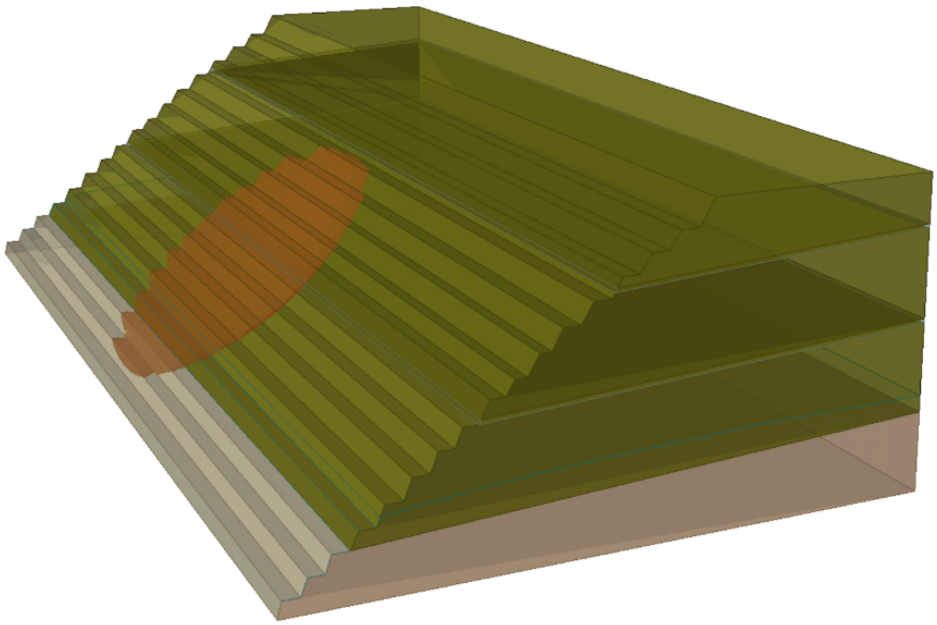


Figure 4.26 Three-dimensional slope geometry. Faint blue line indicates the GWT level.

Table 4.31 Coordinates of the groundwater table.

Groundwater table				
2D		3D		
x-axis	*y*-axis	*x*-axis	*y*-axis	*z*-axis
15.0000	15.0000	15.0000	0	15.0000
16.1590	19.7630	15.0000	374.0000	15.0000
20.9970	19.7630	16.1590	0	19.7630
22.8730	24.5030	16.1590	374.0000	19.7630
27.4150	24.5030	20.9970	0	19.7630
29.0940	29.4400	20.9970	374.0000	19.7630
33.9320	29.4400	22.8730	0	24.5030
36.2030	34.1790	22.8730	374.0000	24.5030
40.6460	34.1790	27.4150	0	24.5030
41.7720	36.7456	27.4150	374.0000	24.5030
49.8550	37.6750	29.0940	0	29.4400
68.0717	39.5987	29.0940	374.0000	29.4400
101.6510	41.7990	33.9320	0	29.4400
154.2150	43.5258	33.9320	374.0000	29.4400
201.9870	43.5258	36.2030	0	34.1790
		36.2030	374.0000	34.1790
		40.6460	0	34.1790
		40.6460	374.0000	34.1790
		41.7720	0	36.7456
		41.7720	374.0000	36.7456
		49.8550	0	37.6750
		49.8550	374.0000	37.6750
		68.07170	0	39.5987
		68.07170	374.0000	39.5987
		101.6510	0	41.7990
		101.6510	374.0000	41.7990
		154.2150	0	43.5258
		154.2150	374.0000	43.5258
		201.9870	0	43.5258
		201.9870	374.0000	43.5258

Table 4.32 Calculated factors of safety for the scenario-*b*.

	OMS	Bishop	JanbuC	Spencer	Corps	L&K	GLE/MP	JanbuS
F (2D)	1.3240	1.3300	1.3568	1.3321	1.3334	1.3203	1.3308	1.2849
F (3D)	-	1.4860	-	1.4858	-	-	1.4930	1.4299

c – Low elevation groundwater table with external loading on top

In this scenario, external loadings have been applied to the top of the slope while the pore-water pressures have remained the same as the previous analysis (Figure 4.27 & Figure 4.28). The location of the external loading and the results of the analysis are given in Table 4.33 and Table 4.34, respectively.

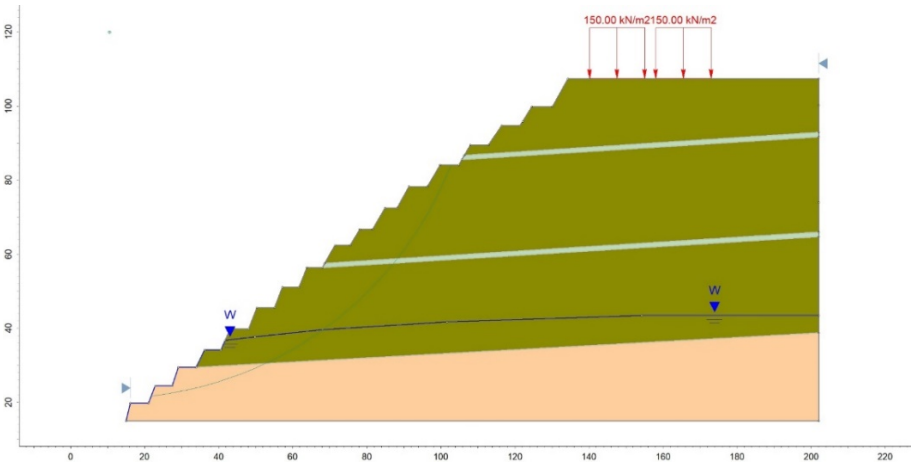


Figure 4.27 Showing the location of the external loadings on top.

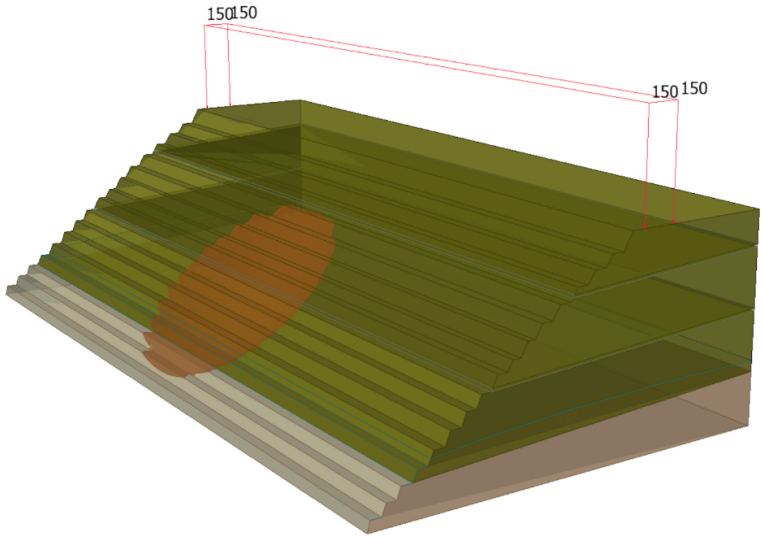


Figure 4.28 Three-dimensional model of the case II, scenario-*c*.

Table 4.33 Coordinates of the external loadings.

External loadings				
2D		3D		
x-axis	*y*-axis	*x*-axis	*y*-axis	*z*-axis
155.000	107.444	155.000	0	107.444
140.176	107.444	155.000	374.000	107.444
173.000	107.444	140.176	0	107.444
158.000	107.444	140.176	374.000	107.444
		173.000	0	107.444
		173.000	374.000	107.444
		158.000	0	107.444
		158.000	374.000	107.444

Table 4.34 Results of the analysis for the scenario-*c*.

	OMS	Bishop	JanbuC	Spencer	Corps	L&K	GLE/MP	JanbuS
F (2D)	1.3240	1.3300	1.3568	1.3321	1.3334	1.3203	1.3308	1.2849
F (3D)	-	1.4860	-	1.4858	-	-	1.4930	1.4299

d – Low elevation groundwater table with seismic activity

In addition to scenario-*b*, the effect of an earthquake has been investigated by implementing horizontal and vertical seismic coefficients into the analysis (Figure 4.29). The effects of the earthquake-induced forces can be seen in Table 4.35.

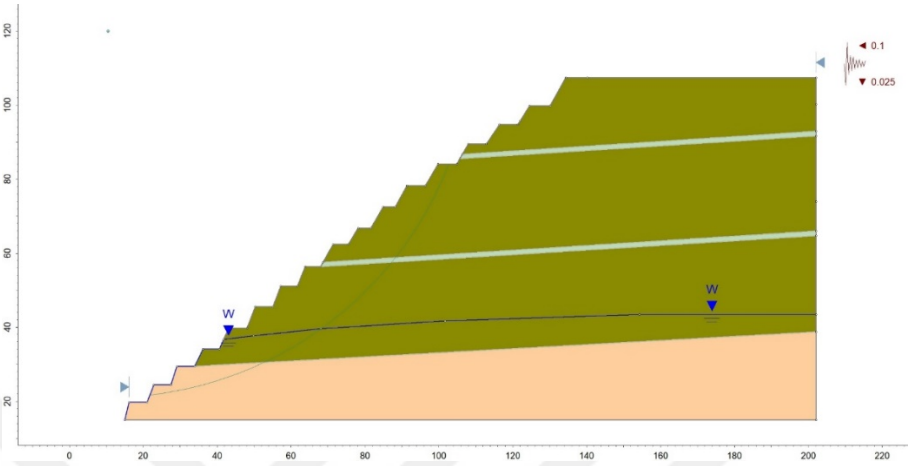


Figure 4.29 Cross-section of the slope profile with seismic activity.

Table 4.35 Computed safety factors for the scenario-*d*.

	OMS	Bishop	JanbuC	Spencer	Corps	L&K	GLE/MP	JanbuS
F (2D)	1.0948	1.1018	1.1096	1.1052	1.0874	1.0762	1.1116	1.0508
F (3D)	-	1.2290	-	-*	-	-	-*	1.1631

*did not converge.

e – Low elevation groundwater table with external loadings and seismic activity

In this analysis, the effect of both external loadings and seismic activity has been investigated on the factor of safety with various methods (Figure 4.30). The properties of the loadings and seismic activity were kept the same as before. Also, the results of the analysis are given in Table 4.36.

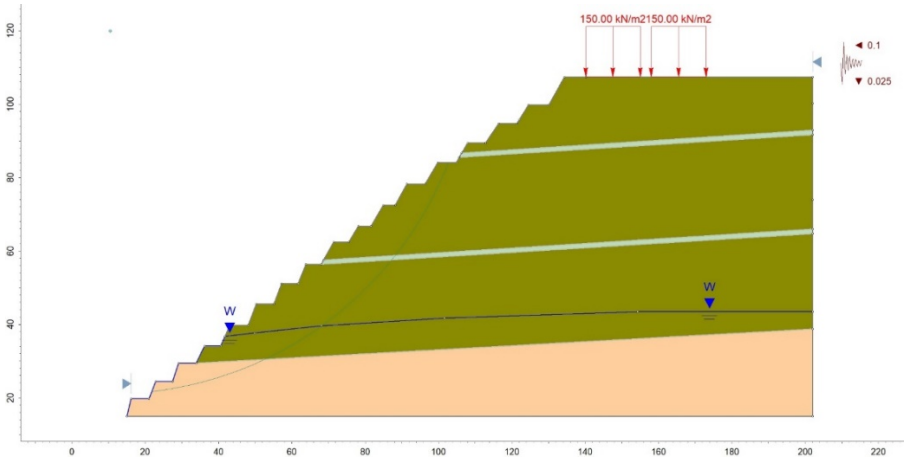


Figure 4.30 Slope profile with external loadings on top and seismic activity.

Table 4.36 Computed safety factors for the scenario-*e*.

	OMS	Bishop	JanbuC	Spencer	Corps	L&K	GLE/MP	JanbuS
F (2D)	1.0948	1.1018	1.1096	1.1052	1.0874	1.0762	1.1116	1.0508
F (3D)	-	1.2290	-	-*	-	-	-*	1.1631

*did not converge.

f – Low elevation groundwater with ponded water at front of the slope

This analysis consists of a ponded water at front of the slope and a low groundwater table elevation (Figure 4.31 & Figure 4.32). There are no external loadings and seismic activity. The coordinates of the water table and the results of the stability analysis are given in Table 4.37 and Table 4.38, respectively.

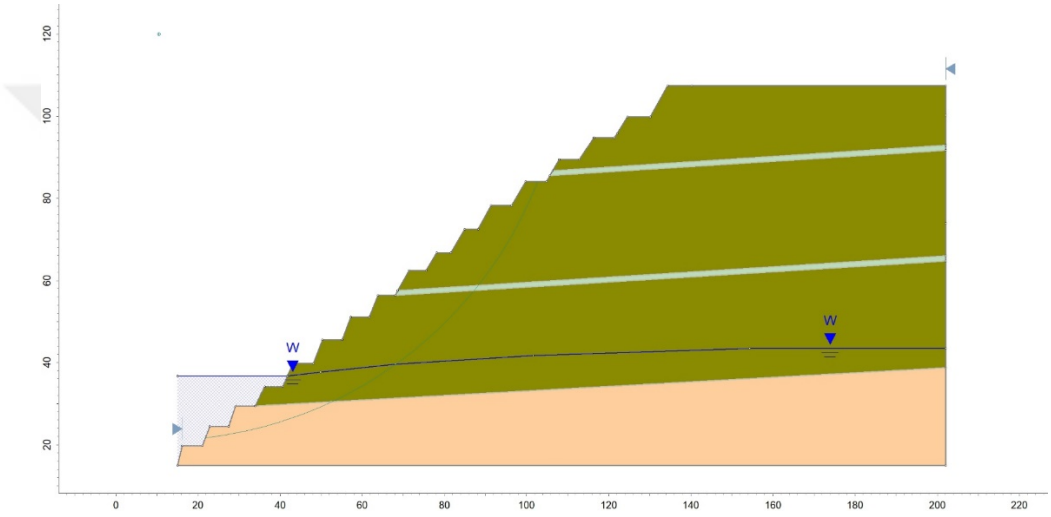


Figure 4.31 Cross-section of the slope profile and ponded water at front.

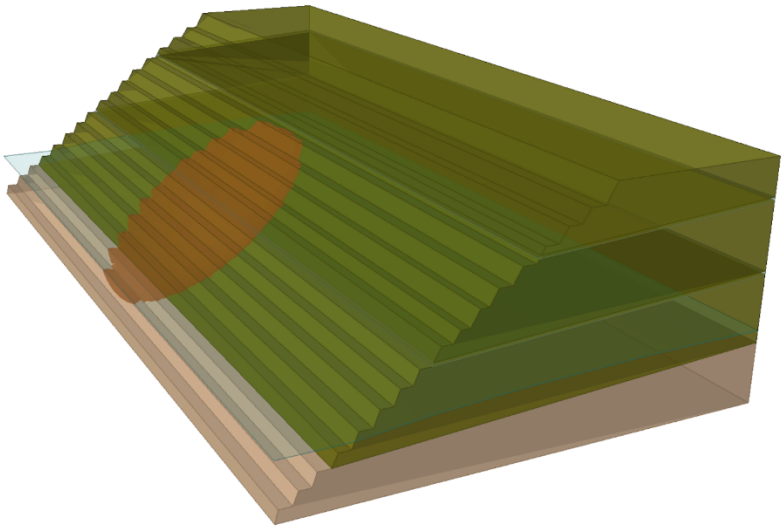


Figure 4.32 Three-dimensional geometry of the case II, scenario-*f*. Faint blue surface indicates the water table level.

Table 4.37 Location of the water table.

Water table				
2D		3D		
x-axis	*y*-axis	*x*-axis	*y*-axis	*z*-axis
15.0000	36.7460	15.0000	0	36.7460
41.7720	36.7456	15.0000	374.0000	36.7460
49.8550	37.6750	41.7720	0	36.7456
68.0717	39.5987	41.7720	374.0000	36.7456
101.6510	41.7990	49.8550	0	37.6750
154.2150	43.5258	49.8550	374.0000	37.6750
201.9870	43.5258	68.0717	0	39.5987
		68.0717	374.0000	39.5987
		101.6510	0	41.7990
		101.6510	374.0000	41.7990
		154.2150	0	43.5258
		154.2150	374.0000	43.5258
		201.9870	0	43.5258
		201.9870	374.0000	43.5258

Table 4.38 Computed safety factors for the scenario-*f*.

	OMS	Bishop	JanbuC	Spencer	Corps	L&K	GLE/MP	JanbuS
F (2D)	1.4212	1.4842	1.4824	1.4734	1.5040	1.4751	1.4699	1.4038
F (3D)	-	1.7191	-	1.7194	-	-	1.6993	1.6098

*did not converge

g - Low elevation groundwater with ponded water at front and external loadings on top

This analysis has been performed by considering the same profile as the previous analysis and additional loadings on top (Figure 4.33). The results of the analysis are given below. (Table 4.39)

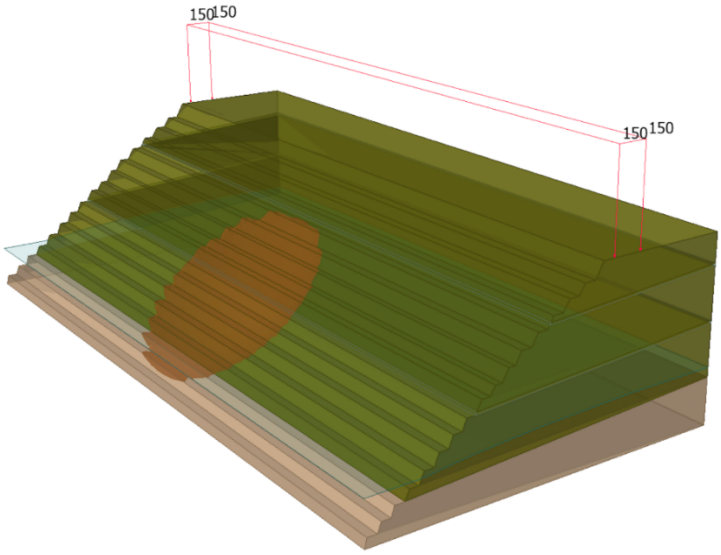


Figure 4.33 Three-dimensional slope geometry of case II, scenario-*g*.

Table 4.39 Computed factors of safety for the scenario-*g*.

	OMS	Bishop	JanbuC	Spencer	Corps	L&K	GLE/MP	JanbuS
F (2D)	1.4212	1.4842	1.4824	1.4734	1.5040	1.4751	1.4699	1.4038
F (3D)	-	1.7191	-	1.7194	-	-	1.6993	1.6098

*did not converge

h - Low elevation groundwater with ponded water at the front and seismic activity

In this analysis, only the effect of an earthquake has been investigated in addition to the scenario-*f*. The computed safety factors are given in Table 4.40.

Table 4.40 The results of the analysis of the scenario-*h*.

	OMS	Bishop	JanbuC	Spencer	Corps	L&K	GLE/MP	JanbuS
F (2D)	1.1639	1.2178	1.2046	1.2124	1.2159	1.1913	1.2077	1.1407
F (3D)	-	1.4068	-	1.3964	-	-	1.3941	1.3012

i - Low elevation groundwater with ponded water at the front, external loadings on top and seismic activity

This analysis considers the effects of all possible scenarios such as pore-water and frontal water pressure, external loadings and pseudo-static condition (Figure 4.34). The results of the calculations are given in Table 4.41.

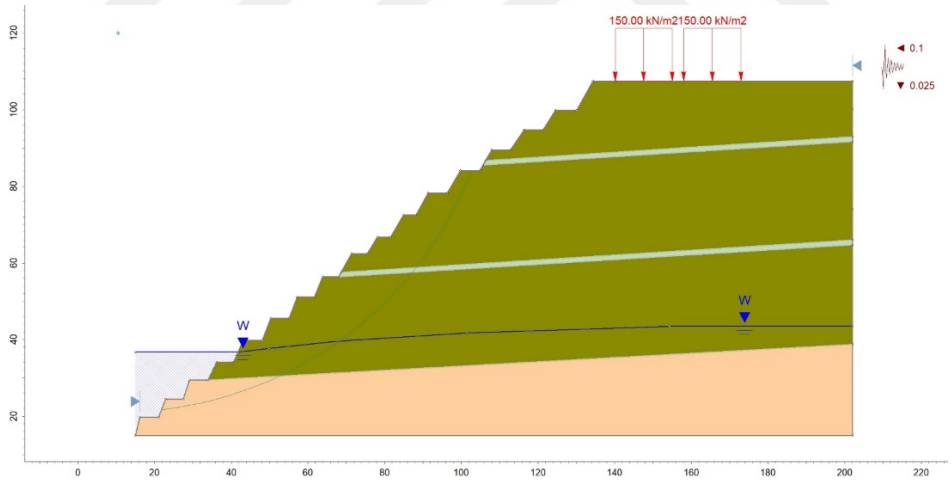


Figure 4.34 Combinations of the possible scenarios.

Table 4.41 Computed safety factors for the scenario-*i*.

	OMS	Bishop	JanbuC	Spencer	Corps	L&K	GLE/MP	JanbuS
F (2D)	1.1639	1.2178	1.2046	1.2124	1.2159	1.1913	1.2077	1.1407
F (3D)	-	1.4068	-	1.3964	-	-	1.3941	1.3012

j – High elevation groundwater table

In this analysis, the groundwater table has been raised to increase the pore-water pressure (Figure 4.35 & Figure 4.36). The location of the water table is given in Cartesian coordinate

system in Table 4.42. Also, the results of the stability analysis and the effects of the higher pore-water pressure can be seen in Table 4.43.

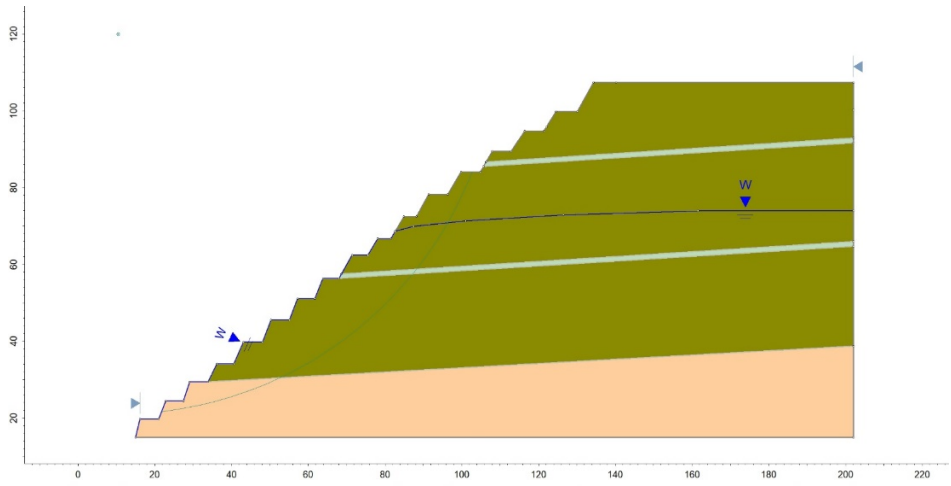


Figure 4.35 Cross-section of the investigated slope with high elevation GWT.

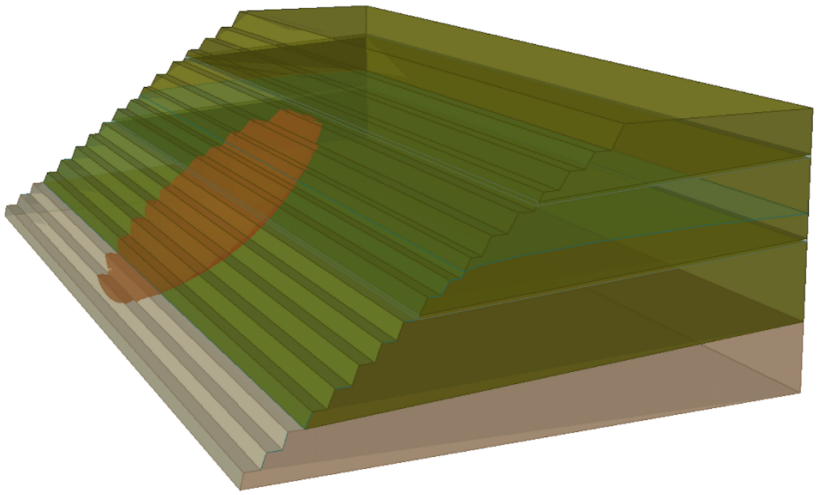


Figure 4.36 Three-dimensional model of case II, scenario-*j*.

Table 4.42 Coordinates of the groundwater table.

Groundwater table				
2D		3D		
x-axis	*y*-axis	*x*-axis	*y*-axis	*z*-axis
15.0000	15.0000	15.0000	0	15.0000
16.1590	19.7630	15.0000	374.0000	15.0000
20.9970	19.7630	16.1590	0	19.7630
22.8730	24.5030	16.1590	374.0000	19.7630
27.4150	24.5030	20.9970	0	19.7630
29.0940	29.4400	20.9970	374.0000	19.7630
33.9320	29.4400	22.8730	0	24.5030
36.2030	34.1790	22.8730	374.0000	24.5030
40.6460	34.1790	27.4150	0	24.5030
43.1150	39.8070	27.4150	374.0000	24.5030
48.0520	39.8070	29.0940	0	29.4400

50.3230	45.6330	29.0940	374.0000	29.4400
55.0620	45.6330	33.9320	0	29.4400
57.2350	51.1620	33.9320	374.0000	29.4400
61.6780	51.1620	36.2030	0	34.1790
63.8500	56.3950	36.2030	374.0000	34.1790
67.9970	56.3950	40.6460	0	34.1790
71.3540	62.5170	40.6460	374.0000	34.1790
75.5010	62.5170	43.1150	0	39.8070
78.0690	66.7630	43.1150	374.0000	39.8070
81.5250	66.7630	48.0520	0	39.8070
82.6381	68.6948	48.0520	374.0000	39.8070
87.4550	69.9990	50.3230	0	45.6330
100.9800	71.4380	50.3230	374.0000	45.6330
126.4940	72.8770	55.0620	0	45.6330
161.6000	74.0099	55.0620	374.0000	45.6330
201.9870	74.0099	57.2350	0	51.1620
		57.2350	374.0000	51.1620
		61.6780	0	51.1620
		61.6780	374.0000	51.1620
		63.8500	0	56.3950
		63.8500	374.0000	56.3950
		67.9970	0	56.3950
		67.9970	374.0000	56.3950
		71.3540	0	62.5170
		71.3540	374.0000	62.5170
		75.5010	0	62.5170
		75.5010	374.0000	62.5170
		78.0690	0	66.7630
		78.0690	374.0000	66.7630
		81.5250	0	66.7630
		81.5250	374.0000	66.7630
		82.6381	0	68.6948
		82.6381	374.0000	68.6948
		87.4550	0	69.9990
		87.4550	374.0000	69.9990
		100.9800	0	71.4380
		100.9800	374.0000	71.4380
		126.4940	0	72.8770
		126.4940	374.0000	72.8770
		161.6000	0	74.0099
		161.6000	374.0000	74.0099
		201.9870	0	74.0099
		201.9870	374.0000	74.0099

Table 4.43 Results of the stability analysis for scenario-j.

	OMS	Bishop	JanbuC	Spencer	Corps	L&K	GLE/MP	JanbuS
F (2D)	0.9291	0.6948	0.6915	0.7017	0.7226	-*	0.6985	0.6549
F (3D)	-	0.6661	-	0.7175	-	-	-*	0.5823

*did not converge

k – High elevation groundwater table and external loadings on top of the slope

In addition to raising the groundwater table, external loadings have been applied to the top of the slope. The location of the loadings is the same as the previous analysis for the Case 2 (Figure 4.37). Also, the results of the stability analysis are given in Table 4.44.

Table 4.44 The results of the analysis for the scenario-*k*.

	OMS	Bishop	JanbuC	Spencer	Corps	L&K	GLE/MP	JanbuS
F (2D)	0.9291	0.6948	0.6915	0.7017	0.7226	-*	0.6985	0.6549
F (3D)	-	0.6661	-	0.7175	-	-	-*	0.5823

*did not converge

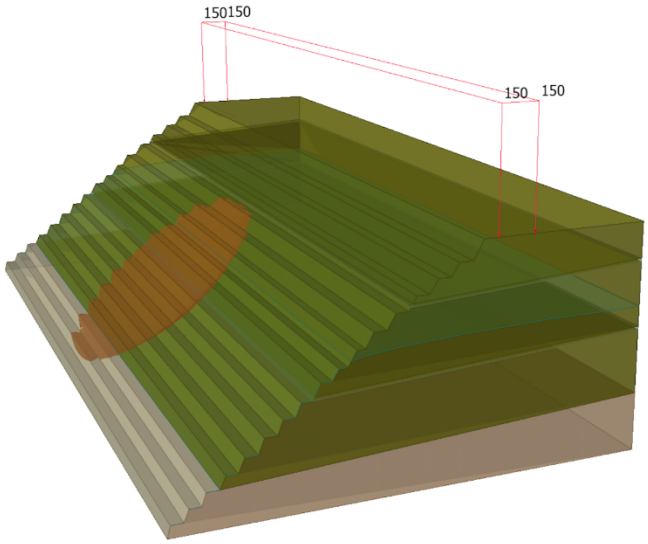


Figure 4.37 Three-dimensional model of the case II, scenario-*k*.

l - High elevation groundwater table and seismic activity

In addition to scenario-*j*, earthquake-induced seismic accelerations have been implemented to the analysis. The effect of the seismic activity can be seen at Table 4.45.

Table 4.45 Computed factors of safety for the scenario-*l*.

	OMS	Bishop	JanbuC	Spencer	Corps	L&K	GLE/MP	JanbuS
F (2D)	0.7524	0.5616	0.5442	0.5808	0.5890	0.7619	0.5751	0.5153
F (3D)	-	0.5094	-	-*	-	-	-*	0.3891

*did not converge.

m – High elevation groundwater table with external loadings on top and seismic activity

This analysis consists of both the effects of external loadings and seismic accelerations (Figure 4.38). The computed safety factors of the scenario are given in Table 4.46.

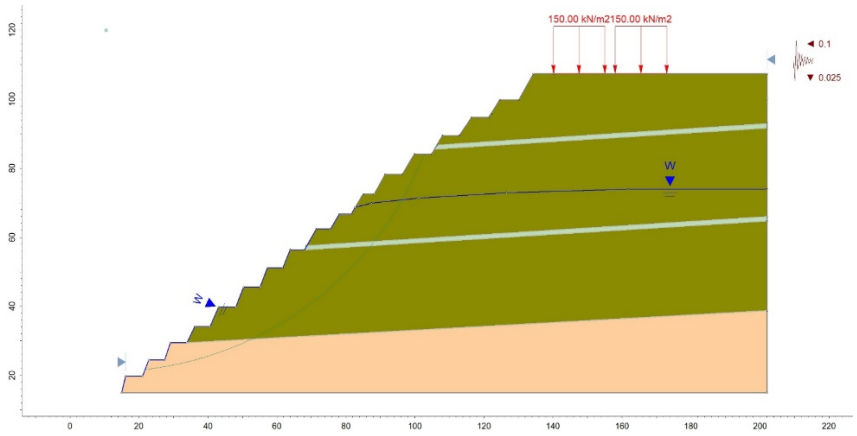


Figure 4.38 Cross-section of the slope profile with loadings on top.

Table 4.46 The results of the analysis for the scenario-*m*.

	OMS	Bishop	JanbuC	Spencer	Corps	L&K	GLE/MP	JanbuS
F (2D)	0.7524	0.5616	0.5442	0.5808	0.5890	0.7619	0.5751	0.5153
F (3D)	-	0.5094	-	-*	-	-	-*	0.3891

*did not converge.

n – High elevation groundwater table with ponded water at front of the slope

In this analysis, there is a frontal water pressure coming from ponded water in addition to scenario-*j* (Figure 4.39 & Figure 4.40). The coordinates of the water table and the results of the analysis are given in Table 4.47 and 4.48, respectively.

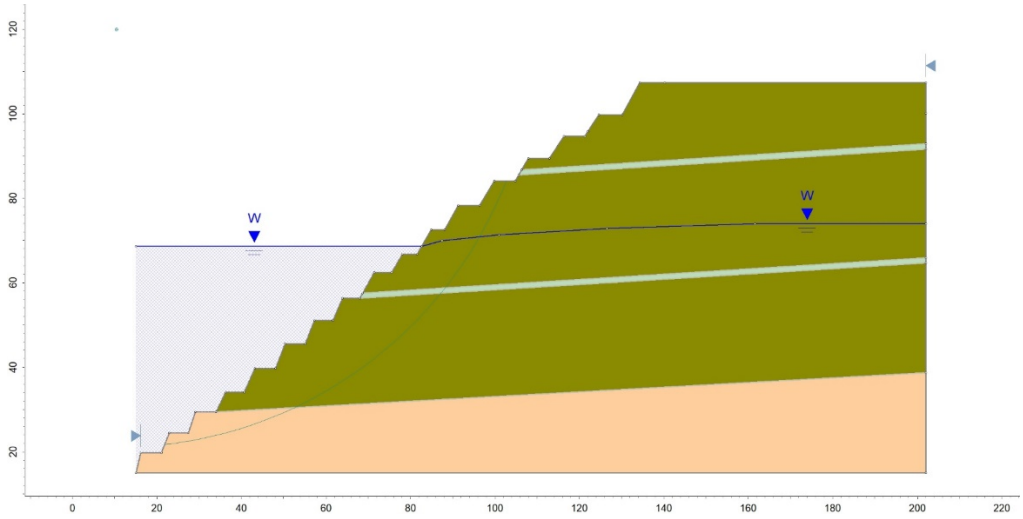


Figure 4.39 Cross-section of the investigated profile. Indicating higher water table and ponded water.

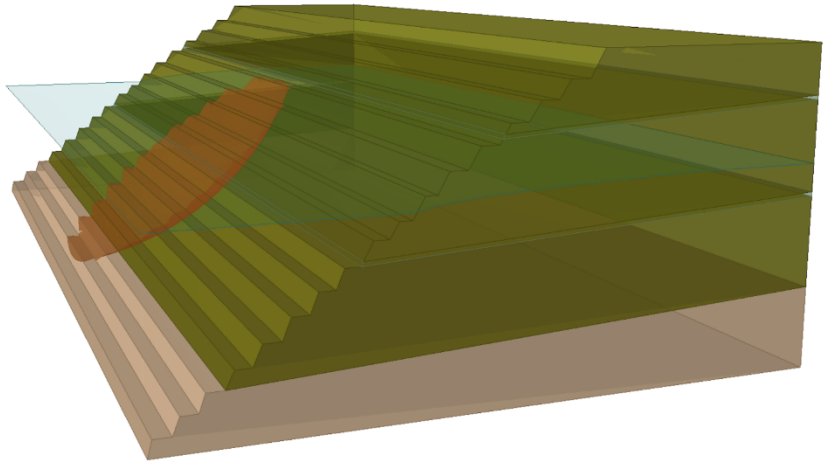


Figure 4.40 Three-dimensional slope profile of the case II, scenario-*n*. Faint blue layer indicates the water table level.

Table 4.47 Coordinates of the water table.

Water table				
2D		3D		
x-axis	*y*-axis	*x*-axis	*y*-axis	*z*-axis
15.0000	68.6950	15.0000	0	68.6950
82.6381	68.6948	15.0000	374.0000	68.6950
87.4550	69.9990	82.6381	0	68.6948
100.9800	71.4380	82.6381	374.0000	68.6948
126.4940	72.8770	87.4550	0	69.9990
161.6000	74.0099	87.4550	374.0000	69.9990
201.9870	74.0099	100.9800	0	71.4380
		100.9800	374.0000	71.4380
		126.4940	0	72.8770
		126.4940	374.0000	72.8770
		161.6000	0	74.0099
		161.6000	374.0000	74.0099
		201.9870	0	74.0099
		201.9870	374.0000	74.0099

Table 4.48 Computed results for the scenario-*n*.

	OMS	Bishop	JanbuC	Spencer	Corps	L&K	GLE/MP	JanbuS
F (2D)	1.5237	1.6003	1.5646	1.5683	2.0270	-*	1.5624	1.4817
F (3D)	-	10.2607	-	9.5858	-	-	9.6150	6.3338

*did not converge

p - High elevation groundwater table with ponded water and external loadings on top

In this analysis, external loadings have been applied on top of the slope in addition to scenario-*n* (Figure 4.41). The results of the computation are given in Table 4.49.

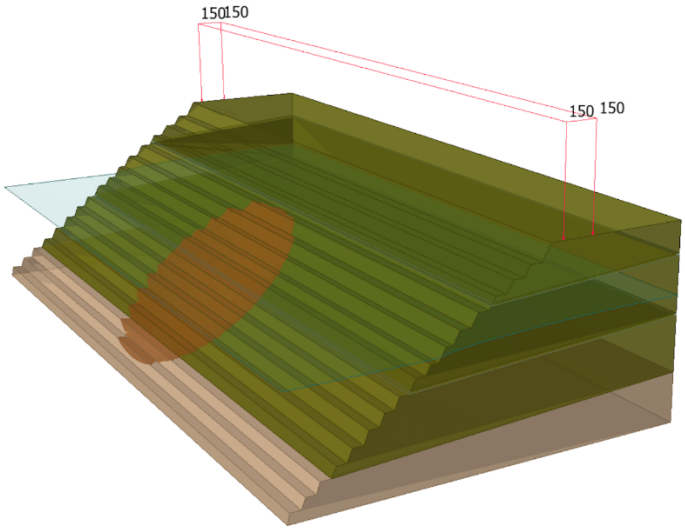


Figure 4.41 Three-dimensional model of the case II, scenario-*p*.

Table 4.49 Computed results for the scenario-*p*.

	OMS	Bishop	JanbuC	Spencer	Corps	L&K	GLE/MP	JanbuS
F (2D)	1.5237	1.6003	1.5646	1.5683	2.0270	-*	1.5624	1.4817
F (3D)	-	10.2607	-	9.5858	-	-	9.6150	6.3338

*did not converge

r - High elevation groundwater table with ponded water and seismic activity

This analysis was performed by assuming an additional seismic activity to scenario-*n*. The effects of the seismic accelerations can be seen in Table 4.50.

Table 4.50 The results of the analysis for the scenario-*r*.

	OMS	Bishop	JanbuC	Spencer	Corps	L&K	GLE/MP	JanbuS
F (2D)	1.1378	1.2003	1.1616	1.1778	1.4492	1.2505	1.1713	1.1000
F (3D)	-	4.6725	-	4.3772	-	-	4.3956	3.5059

s - High elevation groundwater table with ponded water at the front, external loadings on top of the slope and seismic activity

This analysis consists of all possible previous scenarios including the effects of external loadings, all kind of water pressures and an earthquake effect (Figure 4.42). The results of the analysis are given in Table 4.51.

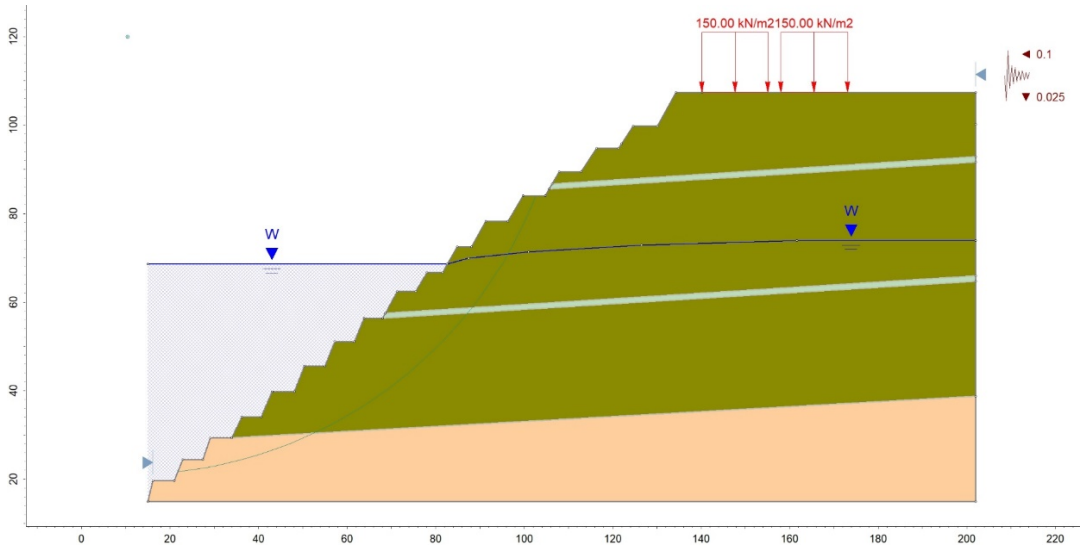


Figure 4.42 Slope profile and other possible combinations.

Table 4.51 Computed safety factors for the scenario-*s*.

	OMS	Bishop	JanbuC	Spencer	Corps	L&K	GLE/MP	JanbuS
F (2D)	1.1378	1.2003	1.1616	1.1778	1.4492	1.2505	1.1713	1.1000
F (3D)	-	4.6725	-	4.3772	-	-	4.3956	3.5059

t – Drained profile and external loadings on top of the slope

This analysis has been performed by assuming only external loadings on a fully drained slope (Figure 4.43). The corresponding results to this condition are given in Table 4.52.

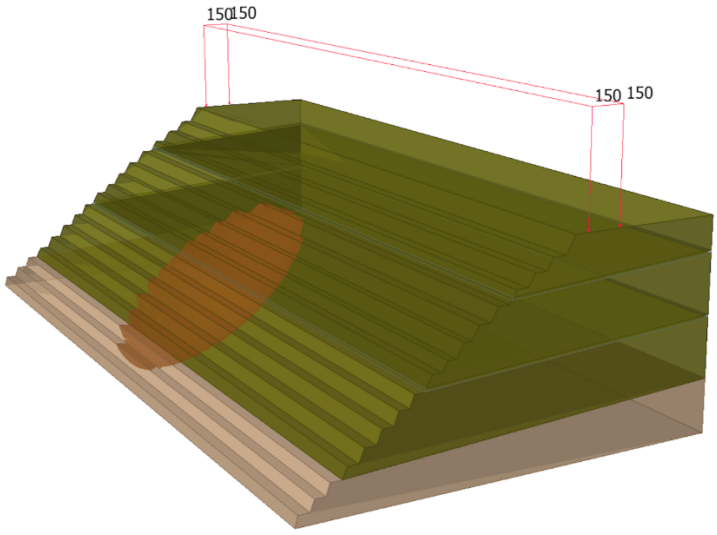


Figure 4.43 Three-dimensional slope geometry of the case II, scenario-*t*.

Table 4.52 Computed safety factors for the scenario-*t*.

	OMS	Bishop	JanbuC	Spencer	Corps	L&K	GLE/MP	JanbuS
F (2D)	1.4897	1.5713	1.5623	1.5568	1.5647	1.5529	1.5544	1.4795
F (3D)	-	1.6977	-	1.6829	-	-	1.6874	1.6041

v – Fully drained slope with external loadings on top and seismic activity

In addition to scenario-*a*, external loadings on top of the slope and seismic activity have been applied to the model (Figure 4.44). The results of this combination are given in Table 4.53.

Table 4.53 The results of the computations for the scenario-*v*.

	OMS	Bishop	JanbuC	Spencer	Corps	L&K	GLE/MP	JanbuS
F (2D)	1.2398	1.3166	1.2939	1.3053	1.2931	1.2891	1.3031	1.2253
F (3D)	-	1.4189	-	1.4083	-	-	1.4122	1.3222

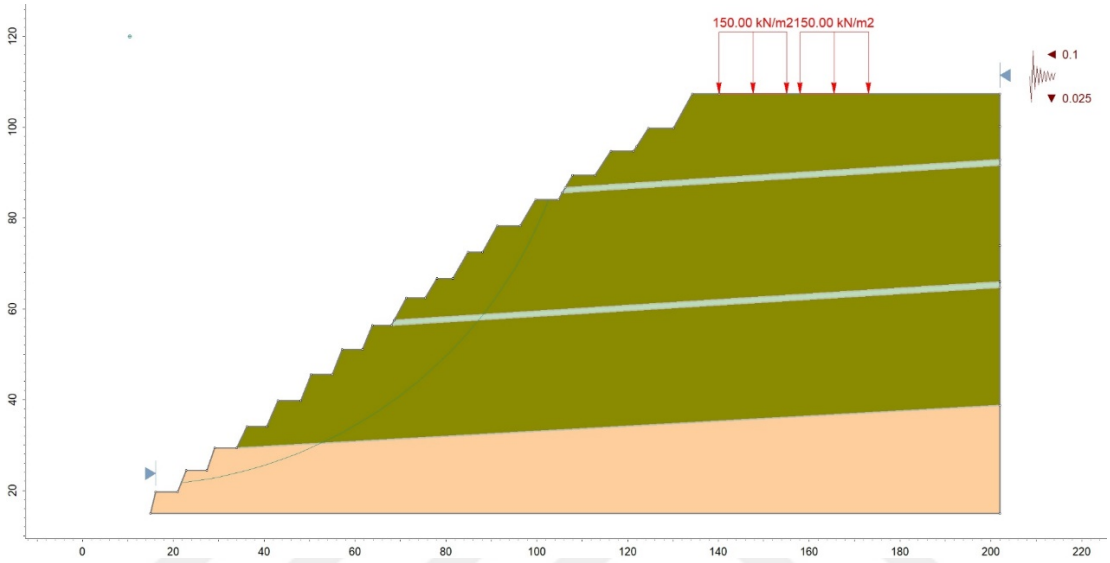


Figure 4.44 Cross-section of the drained slope with external loadings and seismic accelerations.

y – Fully drained slope and seismic activity

In this analysis, there is only a seismic activity in addition to scenario-*a.* The results of the effect can be seen in Table 4.54.

Table 4.54 The computed factors of safety for the scenario-*y*.

	OMS	Bishop	JanbuC	Spencer	Corps	L&K	GLE/MP	JanbuS
F (2D)	1.2398	1.3166	1.2939	1.3053	1.2931	1.2891	1.3031	1.2253
F (3D)	-	1.4189	-	1.4083	-	-	1.4122	1.3222

4.1.3 Hypothetical case III

This is a well-known case from reputable studies such as Arai & Tagyo [199], Sridevi & Deep [202] and Greco [203], which generally used to obtain the most critical slip surface. The slope consists of 3 different inclined lithological units and one of them interposed between relatively higher strength strata (Figure 4.45 & Figure 4.46).

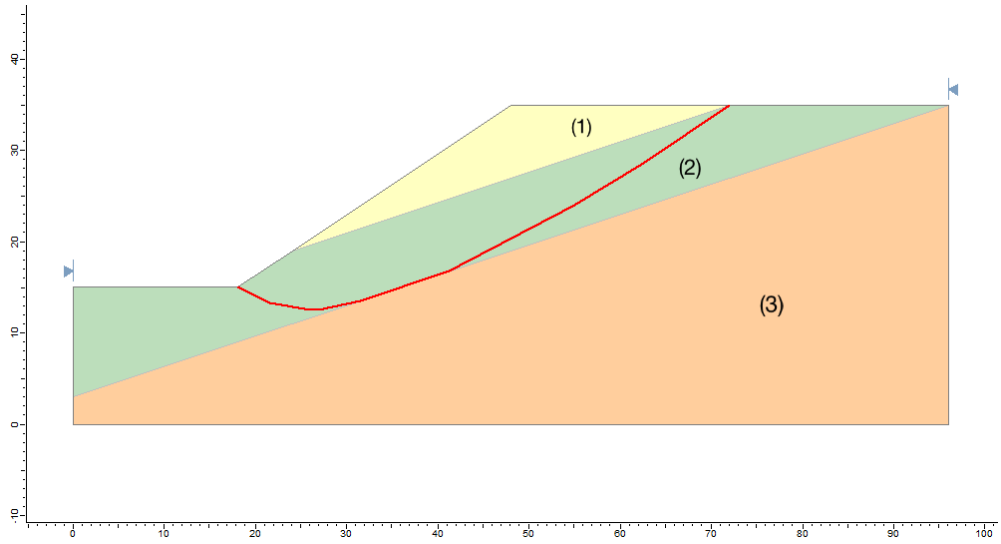


Figure 4.45 Cross-section of the case III. The slip surface has been indicated by the red line.

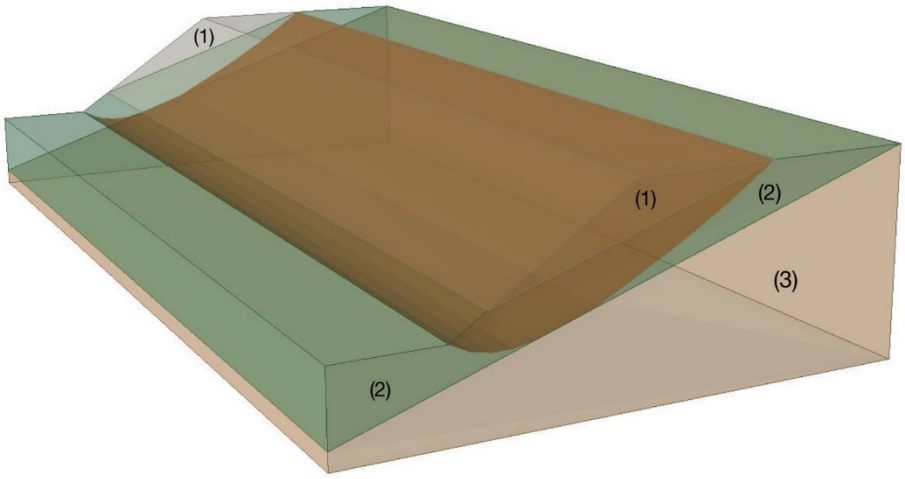


Figure 4.46 Three-dimensional model of the hypothetical case III.

The slope-forming materials were assumed to have the same unit weights and different shear strength parameters (Table 4.55).

Table 4.55 Geotechnical properties of the materials in Case III.

Property	Material 1	Material 2	Material 3
Unit weight (kN/m3)	18.82	18.82	18.82
Saturated unit weight (kN/m^3)	19.60	19.60	19.60
Cohesion (kPa)	29.4	9.8	294
Angle of internal friction (°)	12	5	40

The mobilized soil mass has been assumed to slide on the hardest material which consequently defines a non-circular slip surface. The exact location of the slip surface (Table

4.56), external and material boundary (Table 4.57) of the slope have been given in two and three-dimensional Cartesian coordinate system.

Table 4.56 Location of the slip surface.

Slip surface				
2D		3D		
x-axis	*y*-axis	*x*-axis	*y*-axis	*z*-axis
18.0000	15.0000	18.0000	0	15.0000
21.5610	13.2740	18.0000	192.0000	15.0000
26.0230	12.5110	21.5610	0	13.2740
26.9000	12.5110	21.5610	192.0000	13.2740
31.4954	13.4985	26.0230	0	12.5110
41.2399	16.7466	26.0230	192.0000	12.5110
54.7310	23.9570	26.9000	0	12.5110
62.6050	28.6600	26.9000	192.0000	12.5110
72.0000	35.0000	31.4954	0	13.4985
		31.4954	192.0000	13.4985
		41.2399	0	16.7466
		41.2399	192.0000	16.7466
		54.7310	0	23.9570
		54.7310	192.0000	23.9570
		62.6050	0	28.6600
		62.6050	192.0000	28.6600
		72.0000	0	35.0000
		72.0000	192.0000	35.0000

Table 4.57 Location of the external and the material boundary, hypothetical case III.

External boundary					Material boundary				
2D		3D			2D		3D		
x-axis	*y*-axis	*x*-axis	*y*-axis	*z*-axis	*x*-axis	*y*-axis	*x*-axis	*y*-axis	*z*-axis
96	0	96	0	0	0	3	0	0	3
96	35	96	192	0	96	35	0	192	3
72	35	96	0	35	24	19	96	0	35
48	35	96	192	35	72	35	96	192	35
24	19	72	0	35			24	0	19
18	15	72	192	35			24	192	19
0	15	48	0	35			72	0	35
0	3	48	192	35			72	192	35
0	0	24	0	19					
		24	192	19					
		18	0	15					
		18	192	15					
		0	0	15					
		0	192	15					
		0	0	3					
		0	192	3					
		0	0	0					
		0	192	0					

a – Fully drained situation

In this analysis, there is no water pressure acting on or in to the slope. The corresponding factors of safety is given in Table 4.58.

Table 4.58 Calculated factors of safety for the scenario-*a.*

	JanbuS	JanbuC	Spencer	Corps.	L&K	GLE/MP	Sarma	SarmaNV
F (2D)	0.8129	0.8512	1.0341	0.9982	1.0656	1.0473	0.9129	0.8505
F (3D)	0.7409	-	0.9323	-	-	0.9139	-	-

b – Low elevation groundwater table

This analysis has been performed by assuming a low elevation groundwater table without any ponded water in front (Figure 4.47 & Figure 4.48). The results of the calculation and coordinates of the water table are given in Table 4.59 and Table 4.60, respectively.

Table 4.59 The results of the analysis for the scenario-*b.*

	JanbuS	JanbuC	Spencer	Corps.	L&K	GLE/MP	Sarma	SarmaNV
F (2D)	0.7645	0.8006	0.9773	0.9424	1.0085	0.9915	0.8556	0.8021
F (3D)	0.7158	-	0.9041	-	-	0.8842	-	-

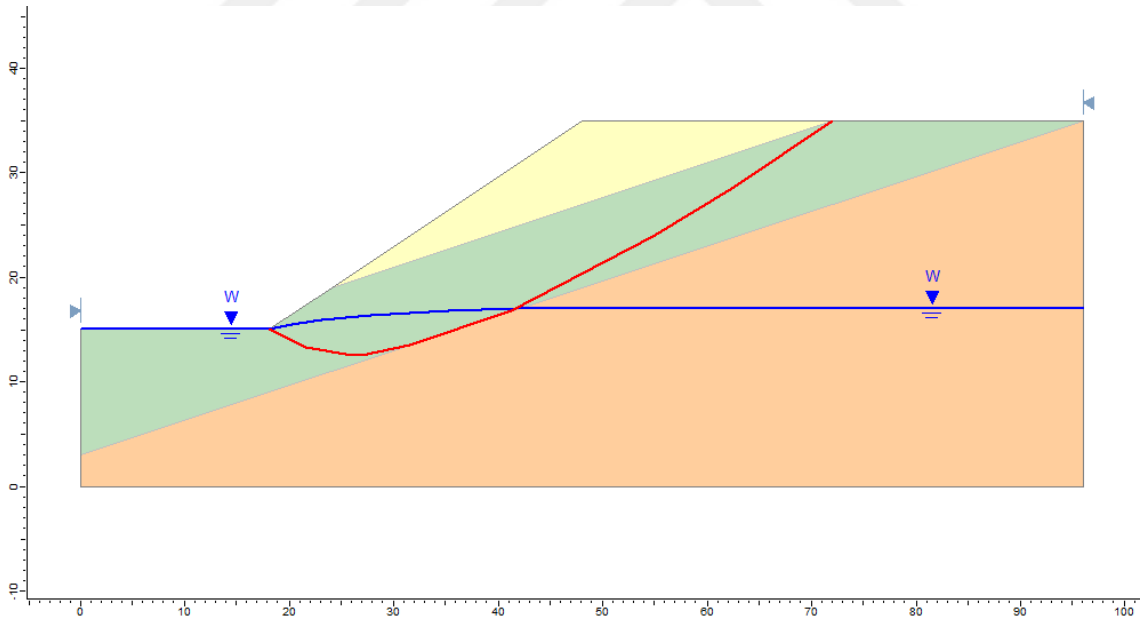


Figure 4.47 The cross-section of the slope profile. The blue line indicates the GWT.

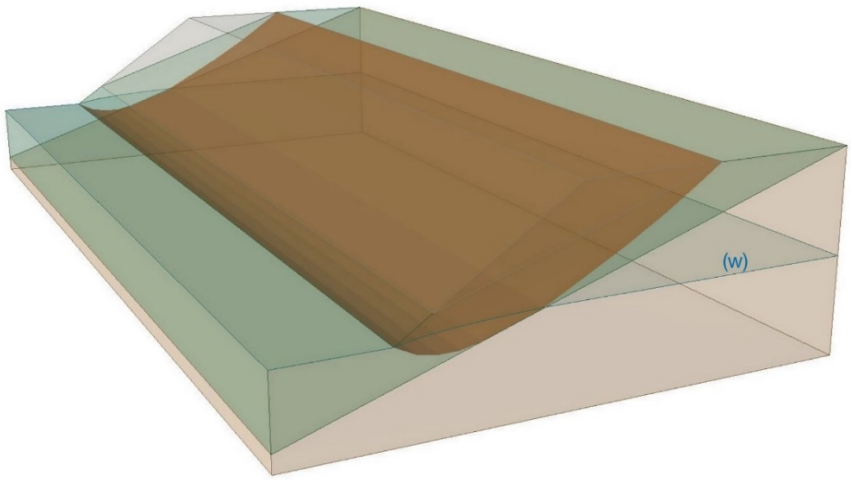


Figure 4.48 Three-dimensional model of the scenario-*b*, hypothetical case III.

Table 4.60 The location of the groundwater table.

Groundwater table				
2D		3D		
x-axis	*y*-axis	*x*-axis	*y*-axis	*z*-axis
0	15.0000	0	0	15.0000
18.0000	15.0000	0	192.0000	15.0000
20.2060	15.4630	18.0000	0	15.0000
23.1230	15.9090	18.0000	192.0000	15.0000
27.7560	16.3210	20.2060	0	15.4630
35.2040	16.7670	20.2060	192.0000	15.4630
41.6631	16.9728	23.1230	0	15.9090
96.0000	16.9728	23.1230	192.0000	15.9090
		27.7560	0	16.3210
		27.7560	192.0000	16.3210
		35.2040	0	16.7670
		35.2040	192.0000	16.7670
		41.6631	0	16.9728
		41.6631	192.0000	16.9728
		96.0000	0	16.9728
		96.0000	192.0000	16.9728

c – Low elevation groundwater table with external loading on top of the slope

In this analysis, external loadings on top of the slope assumed to act in addition to pore-water pressure (Figure 4.49 & Figure 4.50). The calculated safety factors with including the effect of loadings and the location of the external loadings are given in Table 4.61 and Table 4.62, respectively.

Table 4.61 The calculated safety factors for the scenario-*c*.

	JanbuS	JanbuC	Spencer	Corps.	L&K	GLE/MP	Sarma	SarmaNV
F (2D)	0.6210	0.6502	0.8363	0.7851	0.8519	0.8606	0.7341	0.6392
F (3D)	0.5866	-	0.7774	-	-	0.7673	-	-

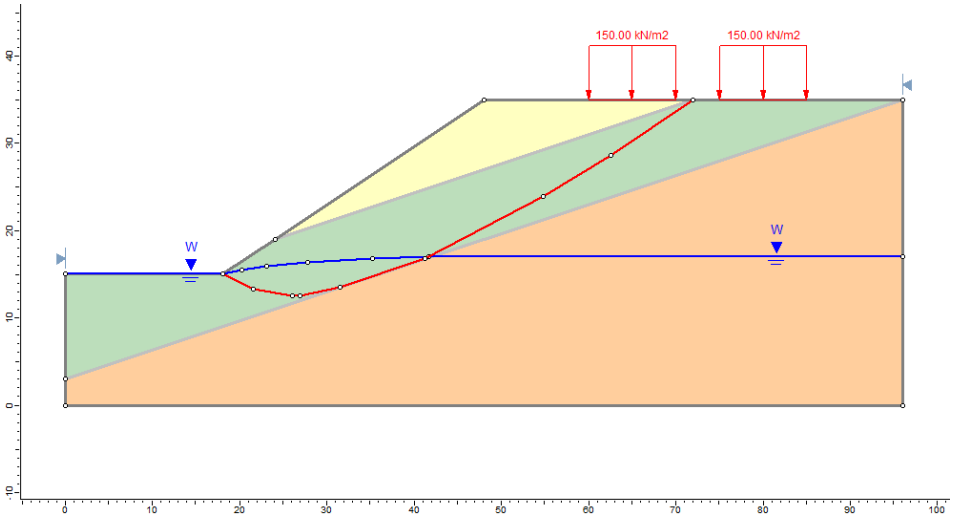


Figure 4.49 The slope profile with external loadings on top of the slope.

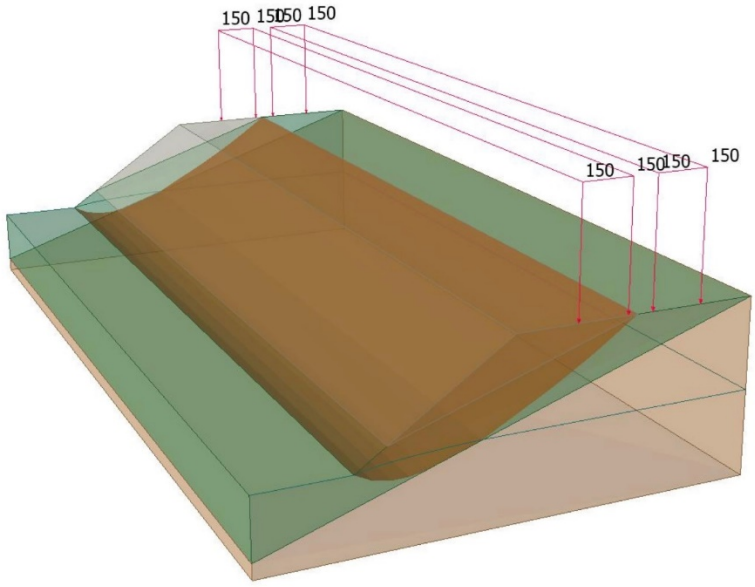


Figure 4.50 Three-dimensional profile of the investigated scenario.

Table 4.62 The coordinates of the external loadings for the scenario-*c*.

External loadings				
2D		3D		
x-axis	*y-axis*	*x*-axis	*y*-axis	*z*-axis
70	35	70	0	35
60	35	70	192	35
85	35	60	0	35
75	35	60	192	35
		85	0	35
		85	192	35
		75	0	35
		75	192	35

d – Low elevation groundwater table with seismic activity

This analysis has been performed by assuming earthquake-induced accelerations acting at the slope. The horizontal and vertical seismic coefficients have been taken as 0.1 and 0.025, respectively. The corresponding effect on the factors of safety by various methods has been given in Table 4.63.

Table 4.63 The calculated safety factors for the scenario-*d*.

	JanbuS	JanbuC	Spencer	Corps.	L&K	GLE/MP	Sarma	SarmaNV
F (2D)	0.5819	0.6094	0.8571	0.7356	0.8000	0.8786	0.6904	0.6192
F (3D)	0.5454	-	0.7799	-	-	0.7440	-	-

e – Low elevation groundwater table with external loadings on top of the slope and seismic activity

In this analysis, both external loadings and seismic activity assumed to affect the overall stability of the slope in addition to pore-water pressures (Figure 4.51). The results of the calculated safety factors have been given in Table 4.64.

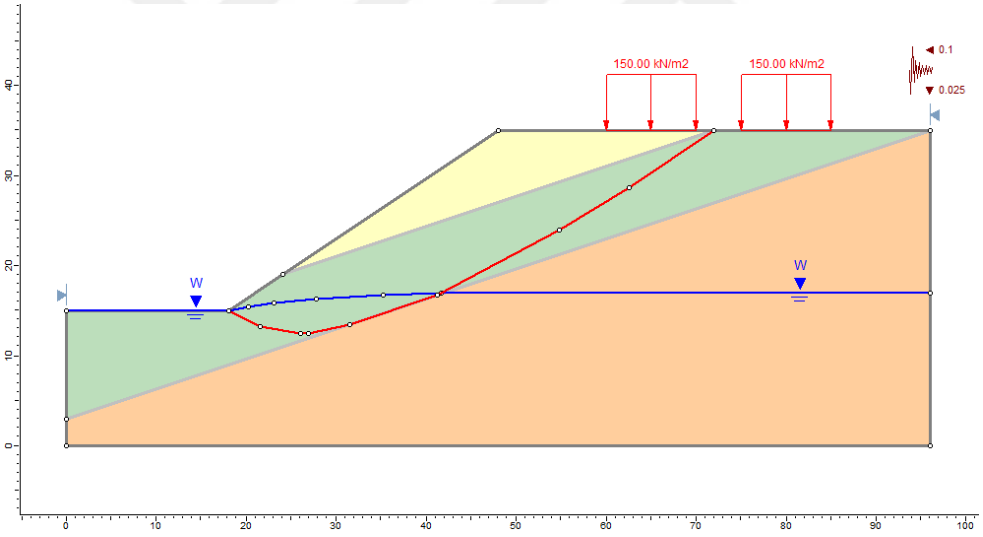


Figure 4.51 The investigated cross-section of the slope.

Table 4.64 The results of the analysis for the scenario-*e*.

	JanbuS	JanbuC	Spencer	Corps.	L&K	GLE/MP	Sarma	SarmaNV
F (2D)	0.4967	0.5201	0.7472	0.6411	0.7061	0.7814	0.6142	0.5214
F (3D)	0.4650	-	0.6857	-	-	0.6682	-	-

f – Low elevation water table with ponded water at front of the slope.

In this analysis, ponded water at the front of the slope acts as a passive resisting force to the sliding soil mass (Figure 4.52 & Figure 4.53). The coordinates of the water table and the computed safety factors are given in Table 4.65 and Table 4.66, respectively.

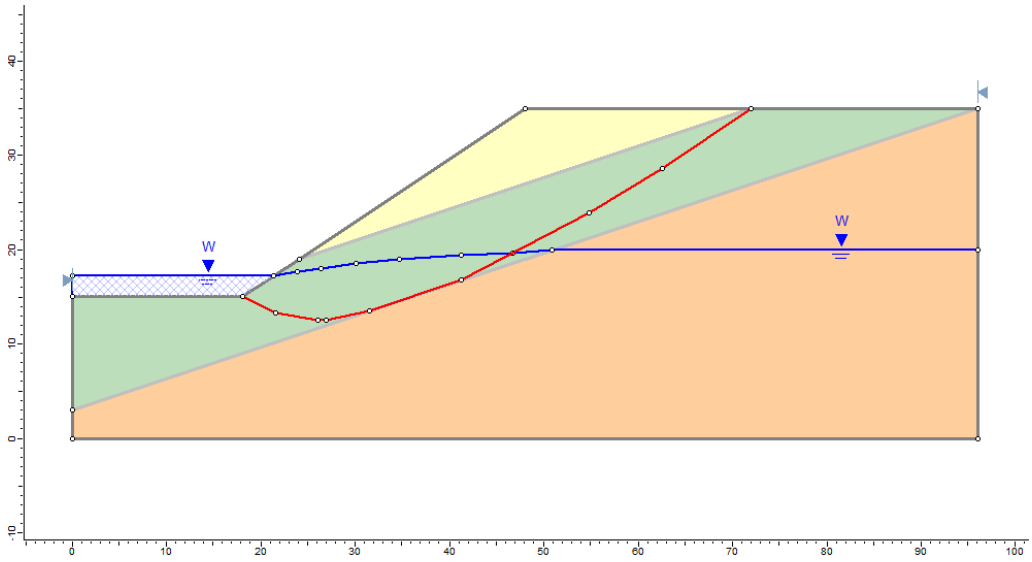


Figure 4.52 The cross-section for the scenario-*f*. The dashed line indicates the ponded water.

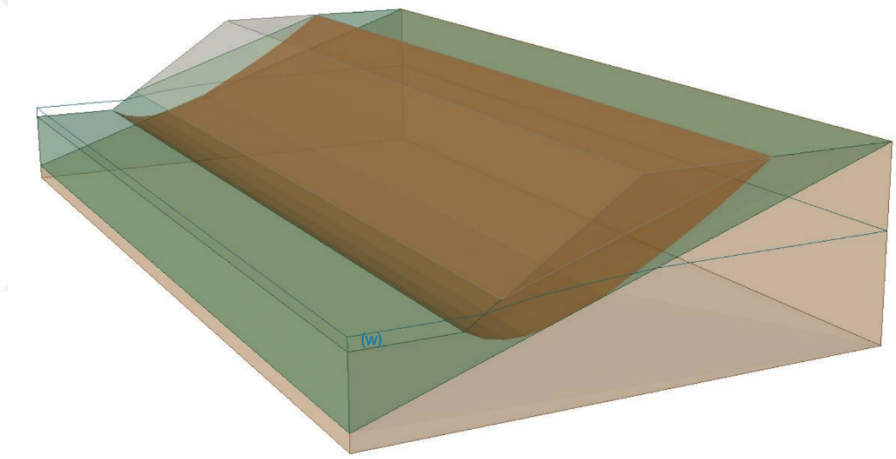


Figure 4.53 Three-dimensional model of the scenario-f.

Table 4.65 The location of the water table for the scenario-*f*.

Water table				
2D		3D		
x-axis	*y*-axis	*x*-axis	*y*-axis	*z*-axis
0	15.0000	0	0	15.0000
0	17.1770	0	192.0000	15.0000
21.2655	17.1770	0	0	17.1770
23.8740	17.6310	0	192.0000	17.1770
26.4010	18.0310	21.2655	0	17.1770
30.1040	18.5560	21.2655	192.0000	17.1770
34.6080	18.9320	23.8740	0	17.6310
41.1880	19.4070	23.8740	192.0000	17.6310
46.7336	19.6828	26.4010	0	18.0310
50.8180	19.9393	26.4010	192.0000	18.0310
96.0000	19.9393	30.1040	0	18.5560

		30.1040	192.0000	18.5560
		34.6080	0	18.9320
		34.6080	192.0000	18.9320
		41.1880	0	19.4070
		41.1880	192.0000	19.4070
		46.7336	0	19.6828
		46.7336	192.0000	19.6828
		50.8180	0	19.9393
		50.8180	192.0000	19.9393
		96.0000	0	19.9393
		96.0000	192.0000	19.9393

Table 4.66 The results of the analysis for the scenario-*f*.

	JanbuS	JanbuC	Spencer	Corps.	L&K	GLE/MP	Sarma	SarmaNV
F (2D)	0.7708	0.8071	0.9854	0.9559	1.0196	0.9995	0.8651	0.8013
F (3D)	0.6953	-	0.8800	-	-	0.8590	-	-

g – Low elevation water table with ponded water at the front and external loadings on top of the slope.

In addition to the scenario-*f*, external loadings have been applied on the top of the slope (Figure 4.54). The computed factors of safety have been in given Table 4.67.

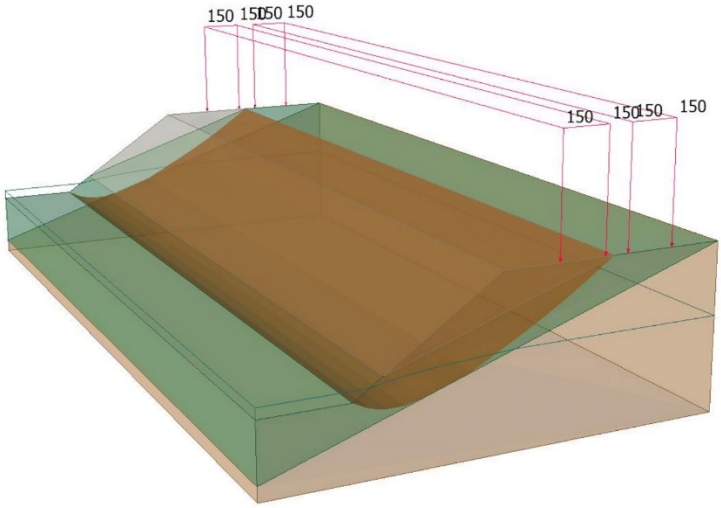


Figure 4.54 Three-dimensional slope profile of the scenario-g, hypothetical case III.

Table 4.67 The results of the analysis for the scenario-*g*.

	JanbuS	JanbuC	Spencer	Corps.	L&K	GLE/MP	Sarma	SarmaNV
F (2D)	0.6243	0.6537	0.8423	0.7942	0.8595	0.8717	0.7412	0.6977
F (3D)	0.5651	-	0.7572	-	-	0.7473	-	-

h – Low elevation water table with ponded water at the front and seismic activity

This analysis has been performed by assuming an additional seismic activity to the scenario-*f*. The corresponding results for the earthquake effect are given in Table 4.68.

Table 4.68 The computed safety factors for the scenario-*h*.

	JanbuS	JanbuC	Spencer	Corps.	L&K	GLE/MP	Sarma	SarmaNV
F (2D)	0.5844	0.6119	0.8582	0.7431	0.8061	0.8895	0.6957	0.6142
F (3D)	0.5231	-	0.7561	-	-	0.7209	-	-

i – Low elevation water table with ponded water at the front, external loadings on top and seismic activity.

This scenario consists of all of the previously investigated effects such as loadings, seismicity and pore-pressure. (Figure 4.55). The results of the analysis have been given in Table 4.69.

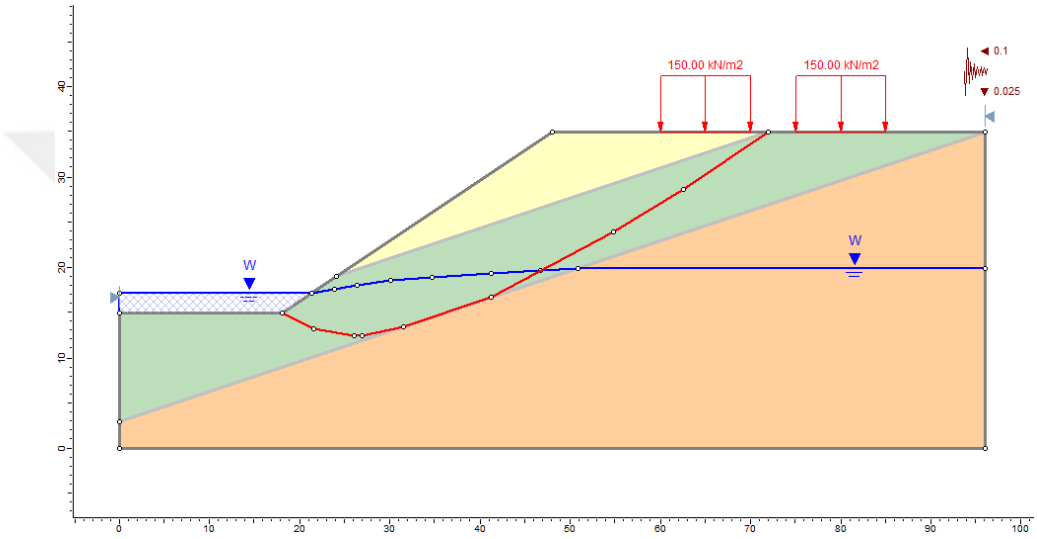


Figure 4.55 The cross-section of the slope with investigated external and internal effects.

Table 4.69 The computed safety factors for the scenario-*i*.

	JanbuS	JanbuC	Spencer	Corps.	L&K	GLE/MP	Sarma	SarmaNV
F (2D)	0.4978	0.5213	0.7486	0.6466	0.7108	0.7832	0.6213	0.5263
F (3D)	0.2511	-	-*	-	-	-*	-	-

*did not converge.

j – High elevation groundwater table

In this analysis, high pore-water pressures exist due to high groundwater table elevation (Figure 4.56 & Figure 4.57). The coordinates of the water table and the results of the analysis are given in Table 4.70 and Table 4.71, respectively.

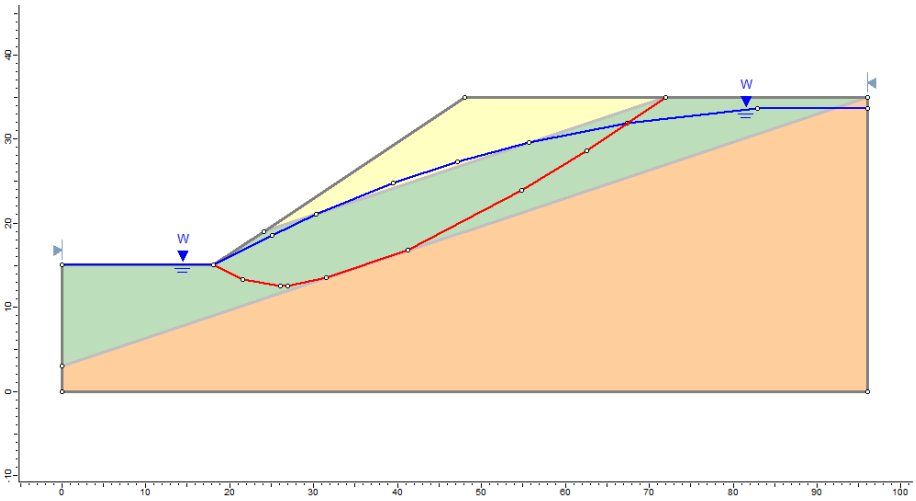


Figure 4.56 The cross-section of the slope with high GWT.

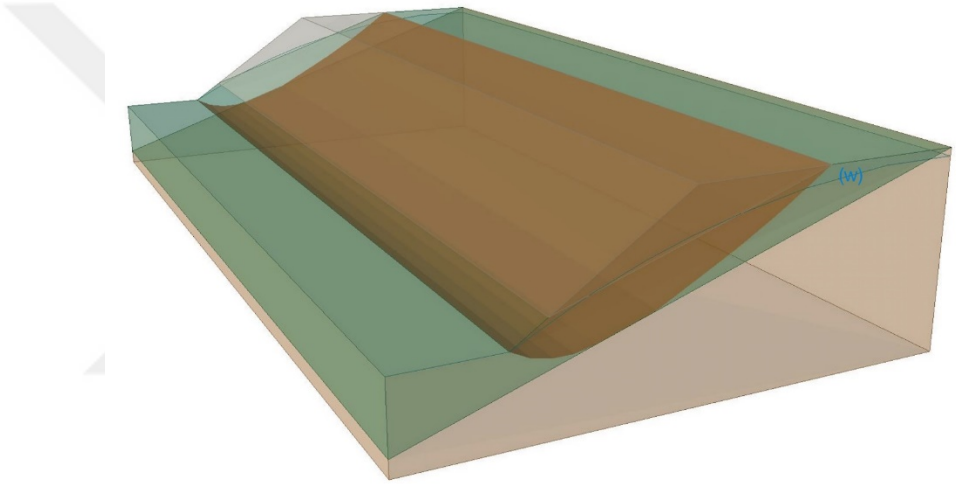


Figure 4.57 Three-dimensional model of the scenario-*j*, hypothetical case III.

Table 4.70 The location of the water table for the scenario-*j*.

Groundwater table				
2D		3D		
x-axis	*y*-axis	*x*-axis	*y*-axis	*z*-axis
0	15.0000	0	0	15.0000
18.0000	15.0000	0	192.0000	15.0000
25.0700	18.5370	18.0000	0	15.0000
30.3149	21.1050	18.0000	192.0000	15.0000
39.4740	24.7950	25.0700	0	18.5370
47.1430	27.3370	25.0700	192.0000	18.5370
55.7041	29.5680	30.3149	0	21.1050
67.4048	31.8990	30.3149	192.0000	21.1050
82.8380	33.5820	39.4740	0	24.7950
96.0000	33.5820	39.4740	192.0000	24.7950
		47.1430	0	27.3370
		47.1430	192.0000	27.3370
		55.7041	0	29.5680

		55.7041	192.0000	29.5680
		67.4048	0	31.8990
		67.4048	192.0000	31.8990
		82.8380	0	33.5820
		82.8380	192.0000	33.5820
		96.0000	0	33.5820
		96.0000	192.0000	33.5820

Table 4.71 The computed safety factors for the scenario-*j*.

	JanbuS	JanbuC	Spencer	Corps.	L&K	GLE/MP	Sarma	SarmaNV
F (2D)	0.6341	0.6640	0.8345	0.8028	0.8693	0.8498	0.7173	0.6649
F (3D)	0.2856	-	0.3199	-	-	0.2922	-	-

k – High elevation groundwater table with external loadings on top of the slope

This analysis has been performed by additional external loadings on top of the slope (Figure 4.58). The results of the analyses have been given in Table 4.72.

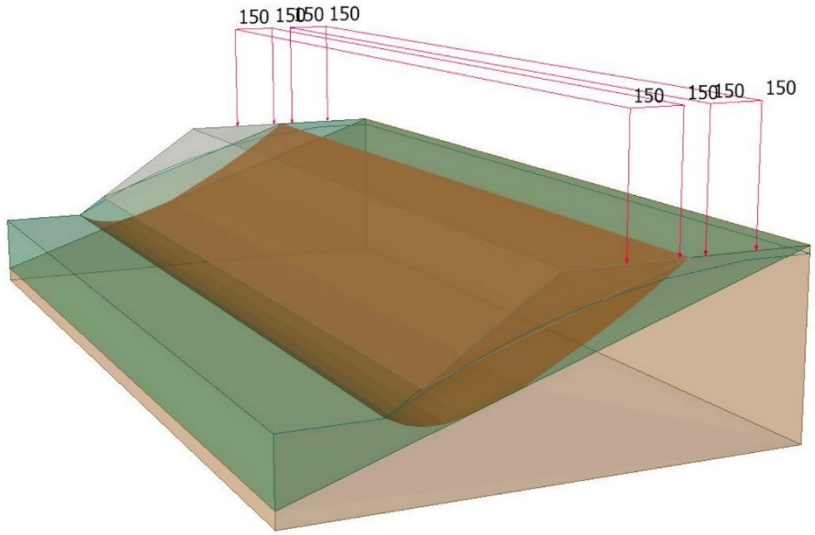


Figure 4.58 Investigated slope profile of the scenario-*k*.

Table 4.72 The computed safety factors for the scenario-*k*.

	JanbuS	JanbuC	Spencer	Corps.	L&K	GLE/MP	Sarma	SarmaNV
F (2D)	0.5210	0.5455	0.7234	0.6758	0.7426	0.7487	0.6260	0.5637
F (3D)	0.2683	-	0.2849	-	-	0.2771	-	-

l – High elevation groundwater table with seismic activity

In this analysis, earthquake-induced seismic forces have been implemented into the analysis. The effect of this forces can be seen in the calculation results. (Table 4.73)

Table 4.73 The results of the analysis for the scenario-*l*.

	JanbuS	JanbuC	Spencer	Corps.	L&K	GLE/MP	Sarma	SarmaNV
F (2D)	0.4803	0.5030	0.7453	0.6270	0.6919	0.7714	0.5852	0.5134
F (3D)	0.2237	-	0.2265	-	-	0.2374	-	-

m – High elevation water table with external loadings on top and seismic activity

This analysis has been performed by considering high pore-water pressures along with external loadings and earthquake forces (Figure 4.59). The effect of these parameters to the factor of safety for various methods are given in Table 4.74.

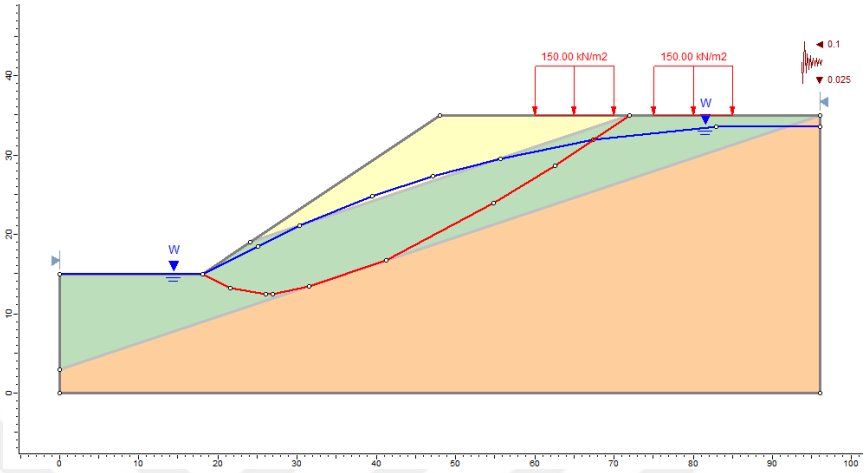


Figure 4.59 The cross-section of the slope for the scenario-*m*.

Table 4.74 The computed safety factors for the scenario-*m*.

	JanbuS	JanbuC	Spencer	Corps.	L&K	GLE/MP	Sarma	SarmaNV
F (2D)	0.4150	0.4345	0.6558	0.5515	0.6169	0.6920	0.5296	0.4433
F (3D)	0.2191	-	0.2427	-	-	0.2305	-	-

n – High elevation water table with ponded water at front of the slope

This analysis has been performed by assuming high pore-water pressures acting in slope and high elevation ponded water that resists to driving forces (Figure 4.60 & Figure 4.61). The coordinates of the water table and calculated safety factors are given in Table 4.75 and Table 4.76, respectively.

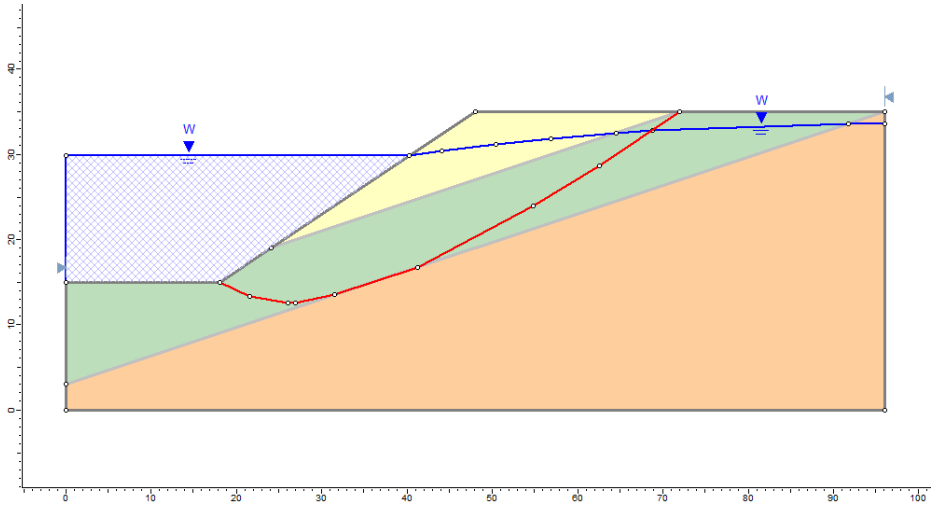


Figure 4.60 The cross-section of the investigated slope. The blue dashed area indicates the ponded water.

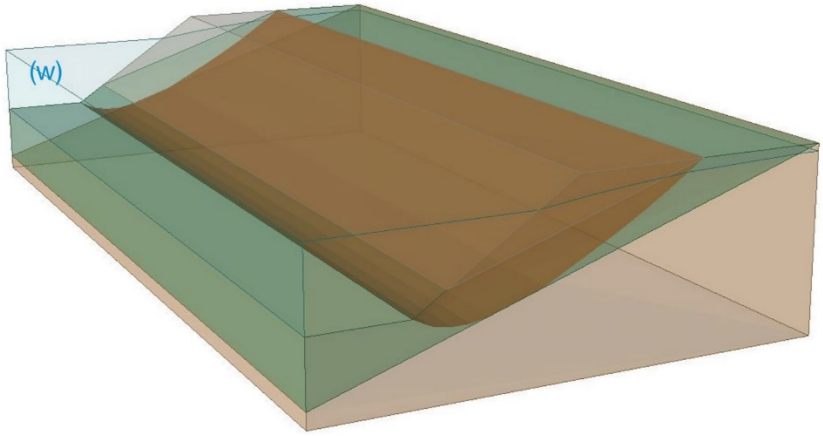


Figure 4.61 Three-dimensional model of the scenario-*n*. The ponded water has been indicated by using a letter (w).

Table 4.75 The location of the water table.

Water table				
2D		3D		
x-axis	*y*-axis	*x*-axis	*y*-axis	*z*-axis
0	15.0000	0	0	15.0000
0	29.8350	0	192.0000	15.0000
40.2530	29.8353	0	0	29.8350
44.0700	30.3350	0	192.0000	29.8350
50.3990	31.1720	40.2530	0	29.8353
56.8330	31.8520	40.2530	192.0000	29.8353
64.4987	32.4996	44.0700	0	30.3350
68.7855	32.8308	44.0700	192.0000	30.3350
91.7448	33.5816	50.3990	0	31.1720
96.0000	33.5816	50.3990	192.0000	31.1720
		56.8330	0	31.8520
		56.8330	192.0000	31.8520
		64.4987	0	32.4996
		64.4987	192.0000	32.4996
		68.7855	0	32.8308
		68.7855	192.0000	32.8308
		91.7448	0	33.5816
		91.7448	192.0000	33.5816
		96.0000	0	33.5816
		96.0000	192.0000	33.5816

Table 4.76 The computed safety factors for the scenario-*n*.

	JanbuS	JanbuC	Spencer	Corps.	L&K	GLE/MP	Sarma	SarmaNV
F (2D)	0.9361	0.9802	1.1357	1.3352	1.3200	1.1224	1.0593	0.9969
F (3D)	0.4215	-	-*	-	-	-*	-	-

*did not converge.

p - High elevation water table with ponded water at the front and external loadings on top of the slope.

This analysis has been performed by assuming the same condition as the scenario-*n* with additional external loadings on top of the slope (Figure 4.62). The results of the computations are given in Table 4.77.

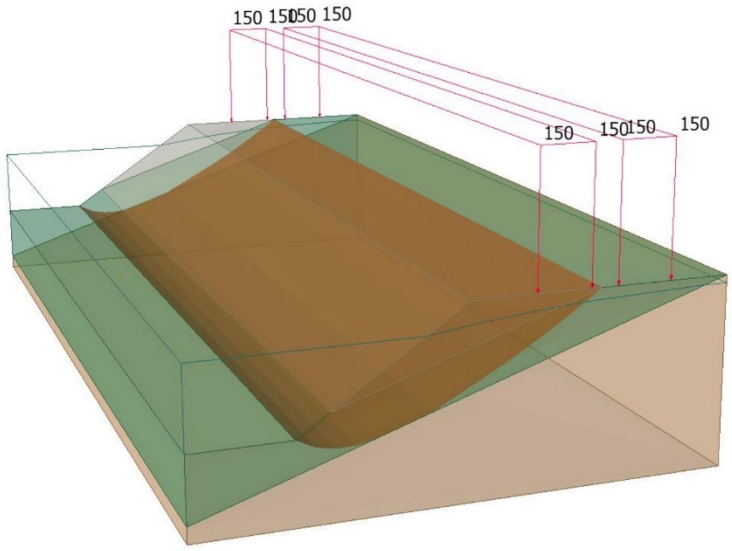


Figure 4.62 Three-dimensional model of the scenario-*p,* hypothetical case III.

Table 4.77 The results of the analysis for the scenario-*p.*

	JanbuS	JanbuC	Spencer	Corps.	L&K	GLE/MP	Sarma	SarmaNV
F (2D)	0.6986	0.7315	0.9048	0.9856	1.0335	0.9050	0.8411	0.7736
F (3D)	0.3454	-	0.3797	-	-	0.3627	-	-

r – High elevation water table with ponded water at the front and seismic activity

In this analysis, there are earthquake-induced accelerations in addition to the scenario-*n.* The computed safety factors with earthquake forces are given in Table 4.78.

Table 4.78 The computed safety factors for the scenario-*r.*

	JanbuS	JanbuC	Spencer	Corps.	L&K	GLE/MP	Sarma	SarmaNV
F (2D)	0.6412	0.6714	0.8498	0.8977	0.9353	0.8498	0.7740	0.7050
F (3D)	0.2843	-	0.3445	-	-	0.3041	-	-

s – High elevation water table with ponded water at the front, external loadings on top and seismic activity.

In this analysis, all combinations have been put together to investigate their effect on the factors of safety (Figure 4.63). The effect of internal and external parameters on the factor of safety is given in Table 4.79.

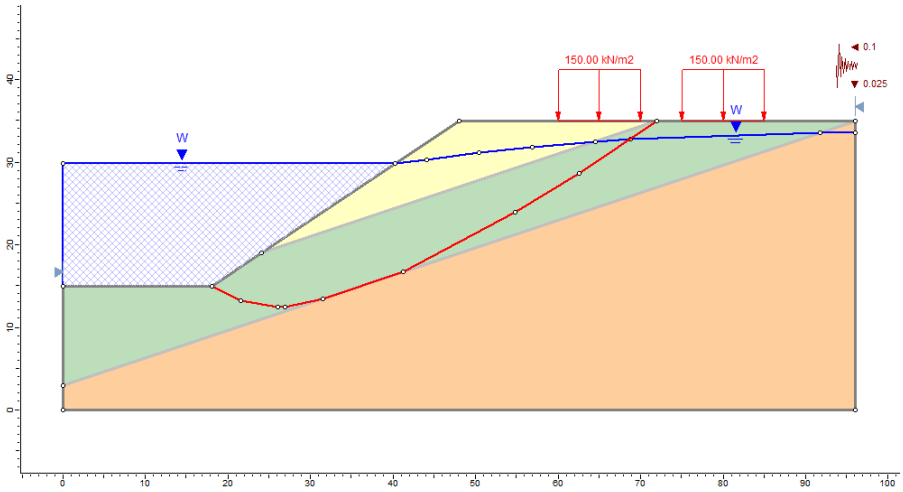


Figure 4.63 The cross-section of the investigated slope.

Table 4.79 The computed safety factors for the scenario-*s*.

	JanbuS	JanbuC	Spencer	Corps.	L&K	GLE/MP	Sarma	SarmaNV
F (2D)	0.5221	0.5467	0.7253	0.7345	0.7957	0.7367	0.6625	0.5938
F (3D)	0.2660	-	0.3004	-	-	0.2822	-	-

t – Fully drained slope with external loadings on top

There are no internal or external water pressures in this analysis, only the effect of external loadings has been investigated (Figure 4.64). The results of the calculations have been given in Table 4.80.

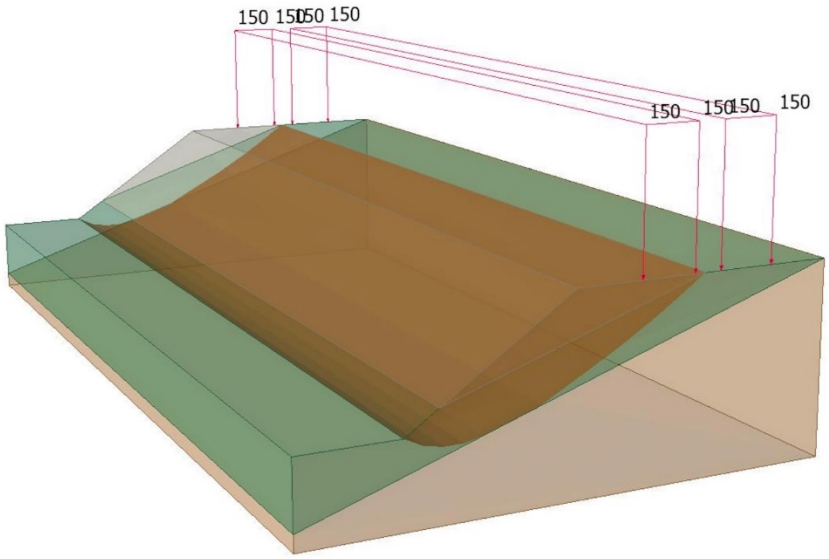


Figure 4.64 Three-dimensional profile of the investigated slope.

Table 4.80 The results of the analysis for the scenario-*t*.

	JanbuS	JanbuC	Spencer	Corps.	L&K	GLE/MP	Sarma	SarmaNV
F (2D)	0.6583	0.6893	0.8813	0.8291	0.8977	0.9047	0.7806	0.6838
F (3D)	0.6064	-	0.8001	-	-	0.7907	-	-

v – Fully drained slope with eternal loadings on top and seismic activity

This analysis has been performed by considering no water pressure. The effect of both external loadings and seismic activity on a fully drained slope has been investigated (Figure 4.65). The results of the analysis are given in Table 4.81.

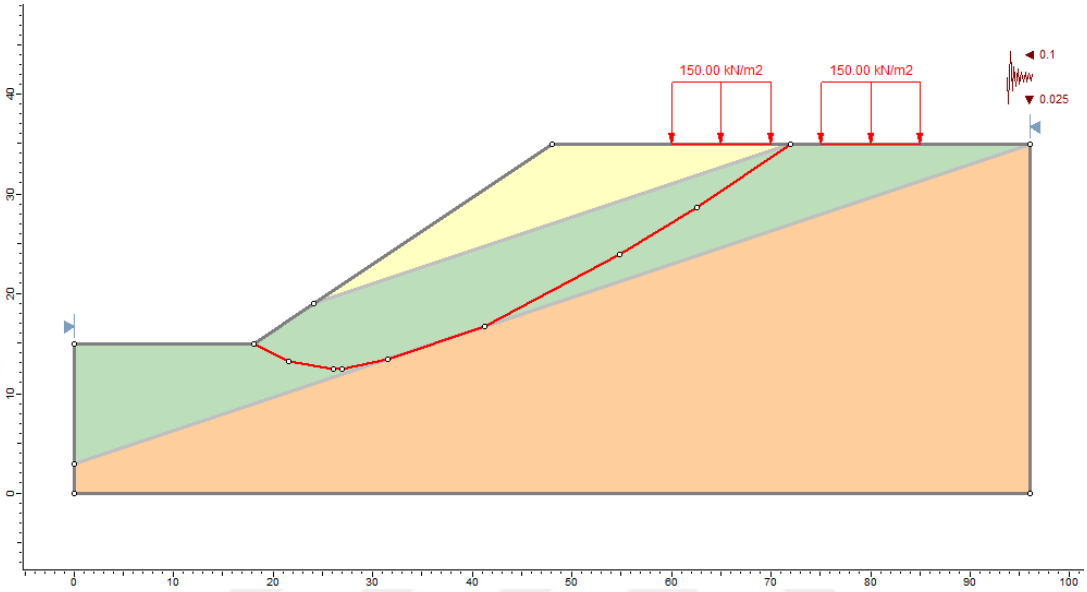


Figure 4.65 The fully drained slope profile with loadings and seismic activity.

Table 4.81 The computed safety factors for the scenario-*v*.

	JanbuS	JanbuC	Spencer	Corps.	L&K	GLE/MP	Sarma	SarmaNV
F (2D)	0.5272	0.5521	0.7838	0.6780	0.7440	0.8154	0.6561	0.5860
F (3D)	0.4883	-	0.7079	-	-	0.6935	-	-

y – Fully drained slope with seismic activity

In this analysis, only the effect of earthquake forces has been investigated on a fully drained slope profile. The results of such an effect are given in Table 4.82.

Table 4.82 The computed safety factors for the scenario-*y*.

	JanbuS	JanbuC	Spencer	Corps.	L&K	GLE/MP	Sarma	SarmaNV
F (2D)	0.6199	0.6491	0.9006	0.7798	0.8440	0.9186	0.7359	0.6546
F (3D)	0.5698	-	0.8076	-	-	0.7713	-	-

4.1.4 Hypothetical case IV

This a well-known case originally used by Yamagami & Ueta [200], and later by other researchers such as Greco [203] and Xie et al. [206], investigated the most critical sliding surface. The slope profile consists of 4 different horizontally layered lithological units (Figure 4.66 & Figure 4.67).

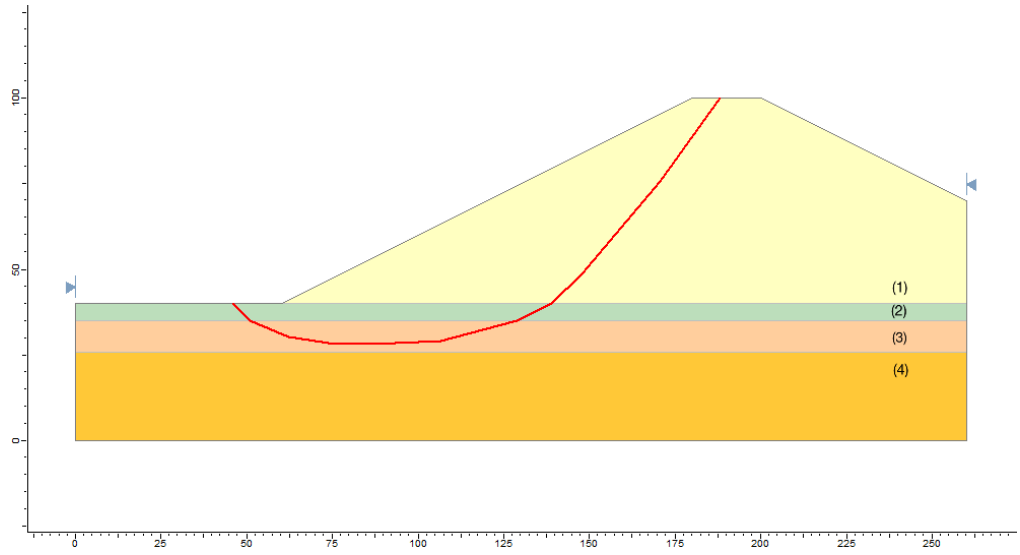


Figure 4.66 The cross-section of the investigated dam. The red line indicates the slip surface

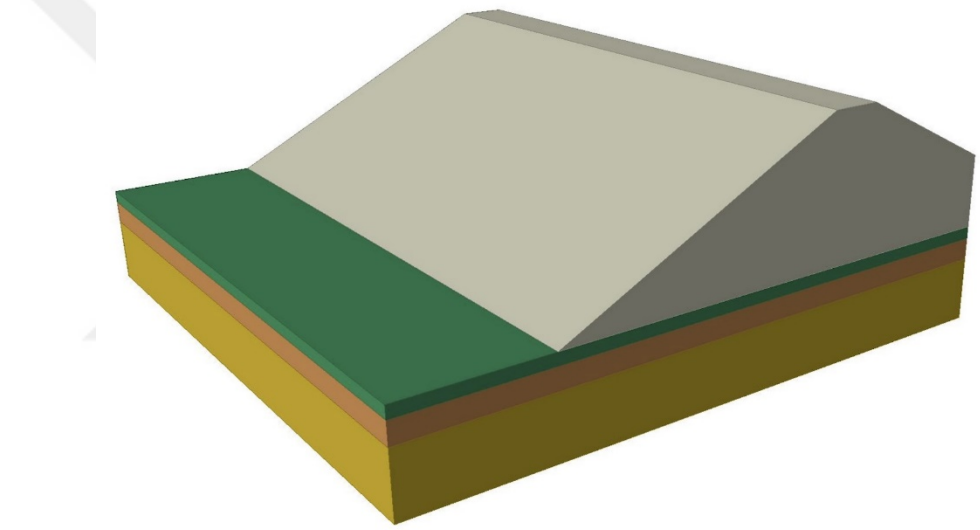


Figure 4.67 Three-dimensional model of the hypothetical case III.

Two of the soil materials have been assumed to have the same unit weight and relatively similar internal friction angles. Also, two of them have zero cohesion and one of them has relatively higher than the others (Table 4.83). This variety in geotechnical properties of the materials consequently formed a non-circular slip surface (Figure 4.66).

Table 4.83 Geotechnical properties of the materials.

Property	Material 1	Material 2	Material 3	Material 4
Dry unit weight (kN/m^3)	20.38	17.64	20.38	17.64
Cohesion (kPa)	49	0	7.84	0
Angle of internal friction (°)	29	30	20	30

The coordinates of the predefined non-circular slip surface and external boundary of the slope and the slope forming materials have been given in Cartesian coordinate system in Table 4.84 and Table 4.85, respectively.

Table 4.84 The location of the slip surface and external boundary.

Slip surface					External boundary				
2D		3D			2D		3D		
x-axis	*y*-axis	*x*-axis	*y*-axis	*z*-axis	*x*-axis	*y*-axis	*x*-axis	*y*-axis	*z*-axis
45.9772	40.0000	45.9772	0	40.0000	260	0	260	0	0
50.9499	35.0000	45.9772	260	40.0000	260	26	260	260	0
62.1700	30.4300	50.9499	0	35.0000	260	35	260	0	26
75.9410	28.2630	50.9499	260	35.0000	260	40	260	260	26
86.9060	28.2630	62.1700	0	30.4300	260	70	260	0	35
106.6880	29.2390	62.1700	260	30.4300	200	100	260	260	35
128.9760	35.0000	75.9410	0	28.2630	180	100	260	0	40
138.7510	40.0000	75.9410	260	28.2630	60	40	260	260	40
147.6370	48.8280	86.9060	0	28.2630	0	40	260	0	70
170.7400	75.7820	86.9060	260	28.2630	0	35	260	260	70
187.9200	100.0000	106.6880	0	29.2390	0	26	200	0	100
		106.6880	260	29.2390	0	0	200	260	100
		128.9760	0	35.0000			180	0	100
		128.9760	260	35.0000			180	260	100
		138.7510	0	40.0000			60	0	40
		138.7510	260	40.0000			60	260	40
		147.6370	0	48.8280			0	0	40
		147.6370	260	48.8280			0	260	40
		170.7400	0	75.7820			0	0	35
		170.7400	260	75.7820			0	260	35
		187.9200	0	100.0000			0	0	26
		187.9200	260	100.0000			0	260	26
							0	0	0
							0	260	0

Table 4.85 Coordinates of the material boundaries for the hypothetical case III.

Material boundary				
2D		3D		
x-axis	*y*-axis	*x*-axis	*y*-axis	*z*-axis
60	40	60	0	40
260	40	60	260	40
60	40	260	0	40
260	40	260	260	40
0	26	60	0	40
260	26	60	260	40
		260	0	40
		260	260	40
		0	0	26
		0	260	26
		260	0	26
		260	260	26

a – Fully drained slope profile

This analysis has been performed by assuming no pore-water pressures or any external forces due to the empty reservoir (Figure 4.66 & Figure 4.68). The corresponding factors of safety for various methods are given in Table 4.86.

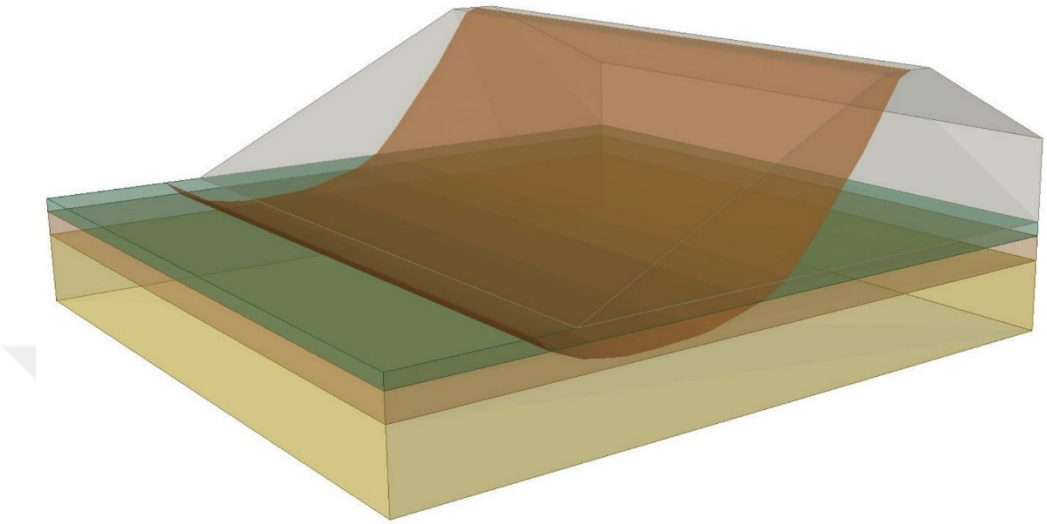


Figure 4.68 Three-dimensional profile of the hypothetical case IV. Brown area indicates the sliding surface.

Table 4.86 The results of the analysis for the scenario-*a.*

	JanbuS	JanbuC	Spencer	Corps.	L&K	GLE/MP	Sarma	SarmaNV
F (2D)	1.2869	1.3894	1.4874	1.6685	1.4347	1.4326	1.4532	1.4552
F (3D)	1.2896	-	1.4786	-	-	1.4186	-	-

b – Fully drained slope profile with seismic activity

In this analysis, earthquake-induced accelerations have been assumed to act on to the slope. The horizontal and vertical seismic coefficients have been taken as 0.1 and 0.025, respectively. The results of the analysis have been given in Table 4.87.

Table 4.87 The computed safety factors for the scenario-*b.*

	JanbuS	JanbuC	Spencer	Corps.	L&K	GLE/MP	Sarma	SarmaNV
F (2D)	1.0196	1.1008	1.3124	1.5230	1.1070	1.1473	1.2535	1.1678
F (3D)	1.0216	-	1.2888	-	-	1.1323	-	-

4.1.5 Hypothetical case V

This case is a two-stepped multi-layered slope which originally used by Chen & Shao [201] and later by Greco [203] to investigate the most critical slip surface. It consists of four different lithological units where two of them have a similar inclination, and one of them is parallel to the top of the slope (Figure 4.69 & Figure 4.70).

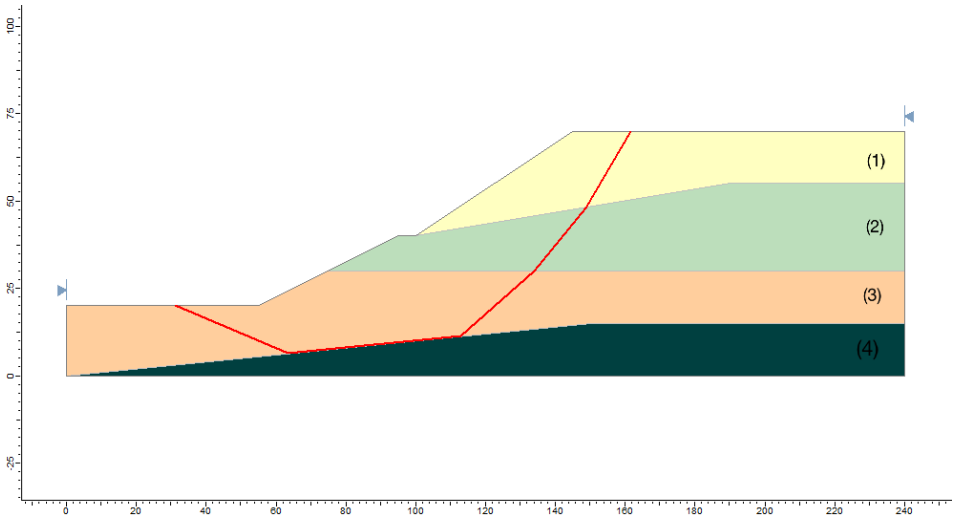


Figure 4.69 The slope profile of the case V.

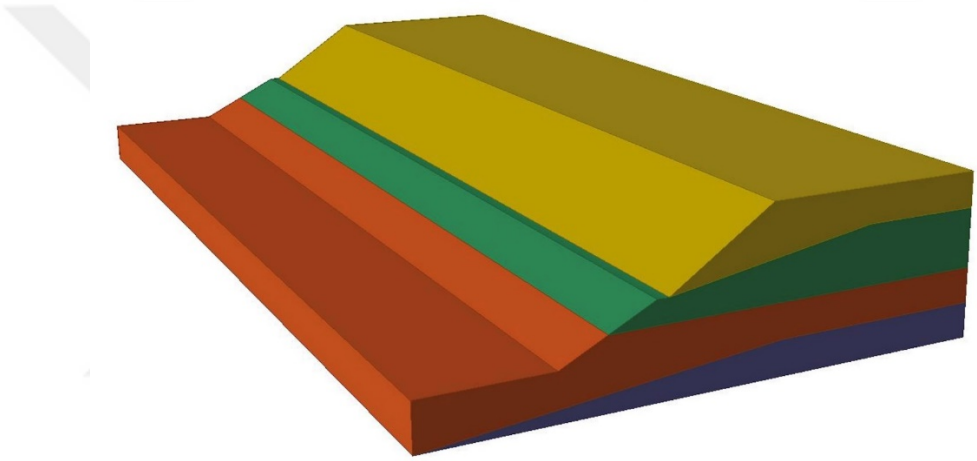


Figure 4.70 Three-dimensional model of the hypothetical case V.

Some of the soil materials have the same unit weight, cohesion or the internal friction angle and one them has a relatively higher strength (Table 4.88).

Table 4.88 Geotechnical properties of the materials for Case V.

Property	Material 1	Material 2	Material 3	Material 4
Unit weight (kN/m3)	19.62	18.64	21.09	21.09
Saturated unit weight (kN/m^3)	20.50	19.30	21.80	21.80
Cohesion (kPa)	9.8	58.8	19.8	9.8
Angle of internal friction (°)	35	25	30	16

The slip surface consists of five planar surfaces and assumed to slide along the bottom soil layer (Figure 4.69 & Figure 4.70). The coordinates of the slope geometry and material boundary, and the location of the slip surface were given in Cartesian coordinate system in Table 4.89 and Table 4.90, respectively.

Table 4.89 The coordinates of slope geometry.

External boundary					Material boundary				
2D		3D			2D		3D		
x-axis	*y*-axis	*x*-axis	*y*-axis	*z*-axis	*x*-axis	*y*-axis	*x*-axis	*y*-axis	*z*-axis
240	0	240	0	0	100	40	100	0	40
240	15	240	480	0	190	55	100	480	40
240	30	240	0	15	240	55	190	0	55
240	55	240	480	15	75	30	190	480	55
240	70	240	0	30	240	30	240	0	55
145	70	240	480	30	0	0	240	480	55
100	40	240	0	55	150	15	75	0	30
95	40	240	480	55	240	15	75	480	30
75	30	240	0	70			240	0	30
55	20	240	480	70			240	480	30
0	20	145	0	70			0	0	0
0	0	145	480	70			0	480	0
		100	0	40			150	0	15
		100	480	40			150	480	15
		95	0	40			240	0	15
		95	480	40			240	480	15
		75	0	30					
		75	480	30					
		55	0	20					
		55	480	20					
		0	0	20					
		0	480	20					
		0	0	0					
		0	480	0					

Table 4.90 Location of the slip surface for the hypothetical case V.

Slip surface				
2D		3D		
x-axis	*y*-axis	*x*-axis	*y*-axis	*z*-axis
31.01570	20.00000	31.01570	0	20.00000
63.45220	6.34522	31.01570	480.00000	20.00000
112.99200	11.29920	63.45220	0	6.345220
134.09300	30.00000	63.45220	480.00000	6.345220
148.65700	48.10940	112.99200	0	11.29920
161.43400	70.00000	112.99200	480.00000	11.29920
		134.09300	0	30.00000
		134.09300	480.00000	30.00000
		148.65700	0	48.10940
		148.65700	480.00000	48.10940
		161.43400	0	70.00000
		161.43400	480.00000	70.00000

a – Fully drained situation

This analysis has been performed by assuming no pore-water pressures exist through the slope (Figure 4.71). The corresponding results are given in Table 4.91.

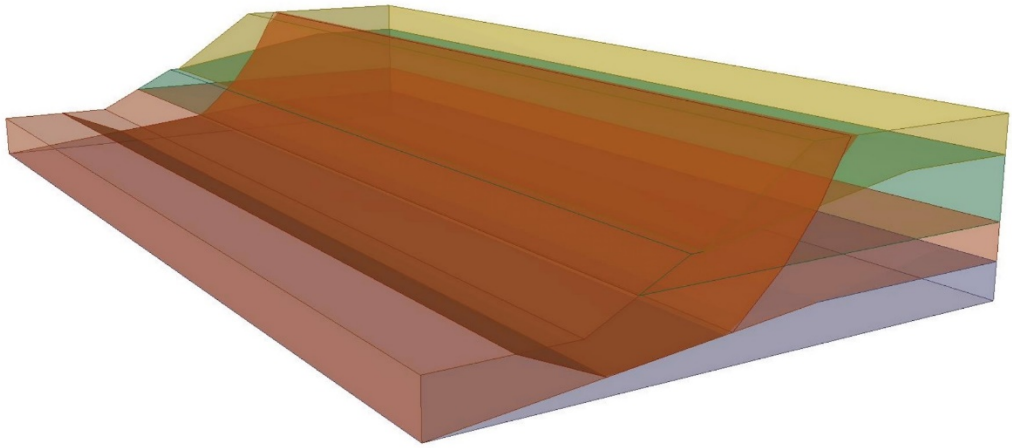


Figure 4.71 Three-dimensional profile of the scenario-*a*, hypothetical case V. Brown area indicates the slip surface

Table 4.91 Computed factors of safety for the scenario-*a*.

	JanbuS	JanbuC	Spencer	Corps.	L&K	GLE/MP	Sarma	SarmaNV
F (2D)	1.6658	1.8053	2.0625	2.1108	2.1790	2.0757	2.0490	1.9949
F (3D)	1.6513	-	2.0166	-	-	2.0138	-	-

b – Low elevation groundwater table

In this analysis, pore-water pressures exist from low elevation water table (Figure 4.72 & Figure 4.73). The coordinates of the water table and the results of the analysis are given in Table 4.92 and Table 4.93, respectively.

Table 4.92 The location of the groundwater table for the scenario-*a*, case V.

Groundwater table				
2D		3D		
x-axis	*y*-axis	*x*-axis	*y*-axis	*z*-axis
0	14.5060	0	0	14.5060
44.0665	14.5060	0	480.0000	14.5060
52.9000	15.8410	44.0665	0	14.5060
63.2910	17.4620	44.0665	480.0000	14.5060
71.5850	19.2730	52.9000	0	15.8410
82.9300	20.8940	52.9000	480.0000	15.8410
126.9480	23.6677	63.2910	0	17.4620
240.0000	23.6677	63.2910	480.0000	17.4620
		71.5850	0	19.2730
		71.5850	480.0000	19.2730
		82.9300	0	20.8940
		82.9300	480.0000	20.8940
		126.9480	0	23.6677

		126.9480	480.0000	23.6677
		240.0000	0	23.6677
		240.0000	480.0000	23.6677

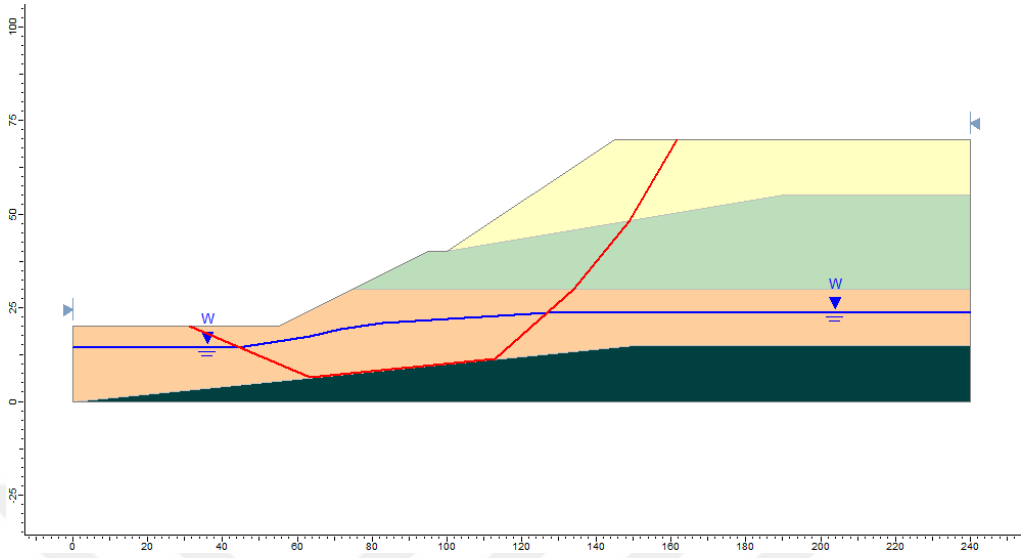


Figure 4.72 The cross-section of the slope. The blue line indicates the water table.

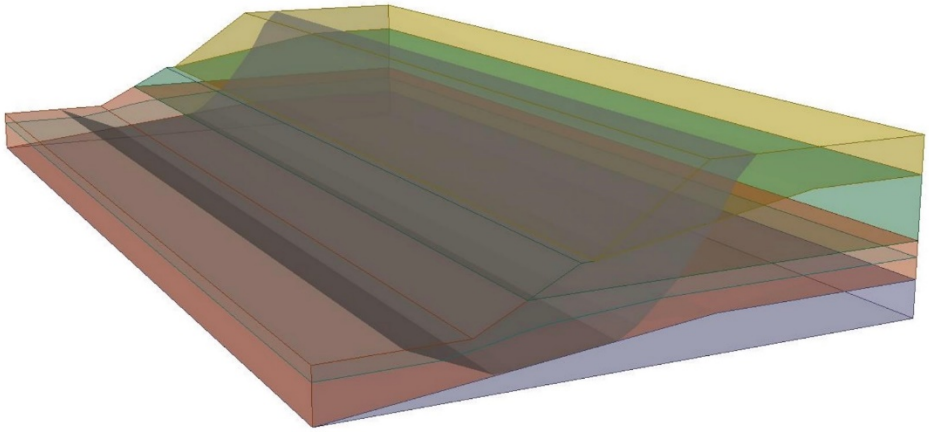


Figure 4.73 Three-dimensional model of the scenario-*b,* hypothetical case V.

Table 4.93 The results of the analysis for the scenario-*b,* case V.

	JanbuS	JanbuC	Spencer	Corps.	L&K	GLE/MP	Sarma	SarmaNV
F (2D)	1.4764	1.6001	1.8079	1.8671	1.9116	1.8178	1.8005	1.7781
F (3D)	1.4543	-	1.7561	-	-	1.7528	-	-

c - Low elevation groundwater table with external loadings on top of the slope

This analysis has been performed by assuming additional external loadings on top of the slope (Figure 4.74 & Figure 4.75). The location of the external loadings and the corresponding results of the analyses are given in Table 4.94 and Table 4.95, respectively.

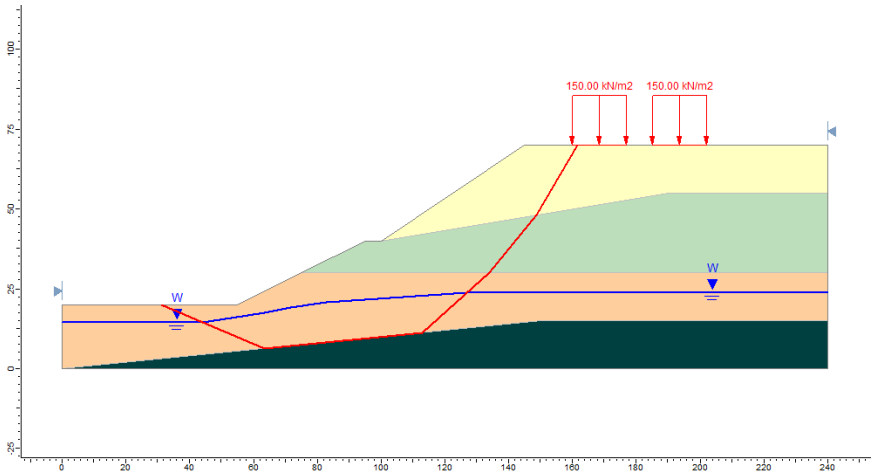


Figure 4.74 The location of the external loadings on top of the slope.

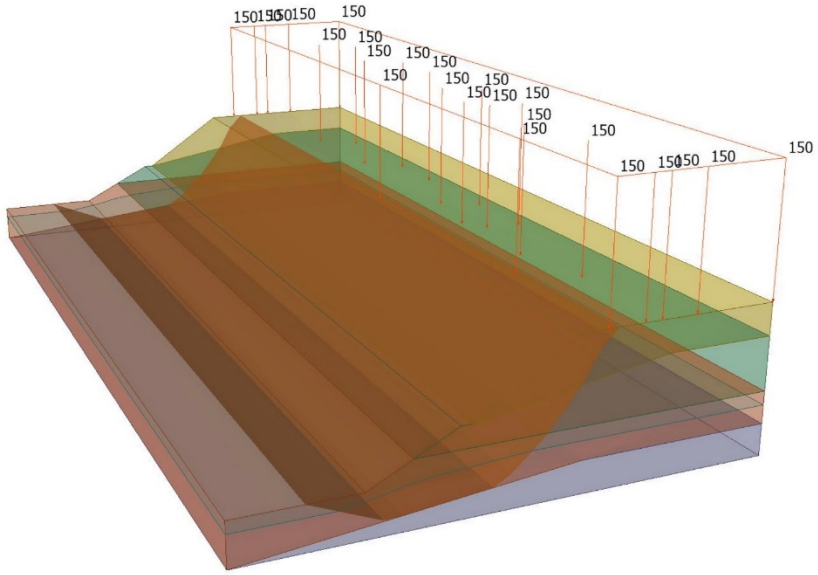


Figure 4.75 Three-dimensional model of the scenario-*c,* hypothetical case V.

Table 4.94 The coordinates of the external loadings for the scenario-*c,* case V.

External loadings				
2D		3D		
x-axis	*y*-axis	*x*-axis	*y*-axis	*z*-axis
177	70	177	0	70
160	70	177	480	70
202	70	160	0	70
185	70	160	480	70
		202	0	70
		202	480	70
		185	0	70
		185	480	70

Table 4.95 The computed safety factors for the scenario-*c,* case V.

	JanbuS	JanbuC	Spencer	Corps.	L&K	GLE/MP	Sarma	SarmaNV
F (2D)	1.4672	1.5902	1.8026	1.8551	1.8999	1.8136	1.7948	1.7781
F (3D)	1.4431	-	1.7301	-	-	1.7464	-	-

d - Low elevation groundwater table with seismic activity

This analysis has been performed by assuming the same conditions as the scenario-*b* with additional seismic activity. The horizontal and vertical seismic coefficients are taken as 0.1 and 0.025, respectively. The effect of such an activity can be seen in Table 4.96.

Table 4.96 Safety factors for the scenario-*d,* case V.

	JanbuS	JanbuC	Spencer	Corps.	L&K	GLE/MP	Sarma	SarmaNV
F (2D)	1.1814	1.2805	1.4828	1.4589	1.4702	1.4893	1.4676	1.4425
F (3D)	1.1578	-	1.4364	-	-	1.4250	-	-

e - Low elevation groundwater table with external loadings on top of the slope and seismic activity

In this analysis, the effect of pore-water pressures, external loadings and seismic activity has been investigated (Figure 4.76). The results of the analysis are given in Table 4.97.

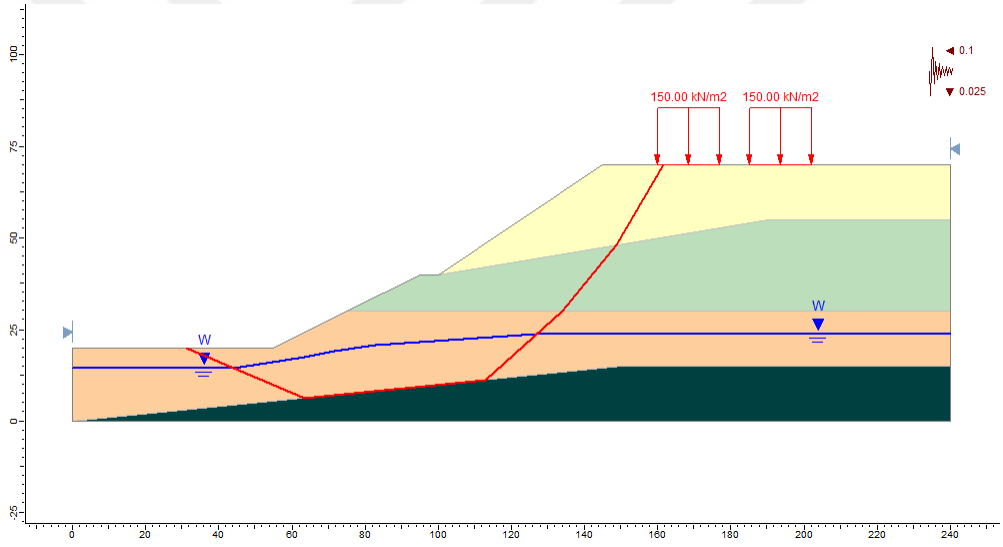


Figure 4.76 The investigated slope model for the scenario-*e,* case V.

Table 4.97 The computed safety factors for the scenario-*e,* case V.

	JanbuS	JanbuC	Spencer	Corps.	L&K	GLE/MP	Sarma	SarmaNV
F (2D)	1.1765	1.2751	1.4802	1.4528	1.4636	1.4870	1.4641	1.4425
F (3D)	1.1525	-	1.4318	-	-	1.4222	-	-

f - Low elevation groundwater table with ponded water at front of the slope

This analysis has been performed by assuming a direct resisting force from shallow ponded water at front of the slope (Figure 4.77 & Figure 4.78).

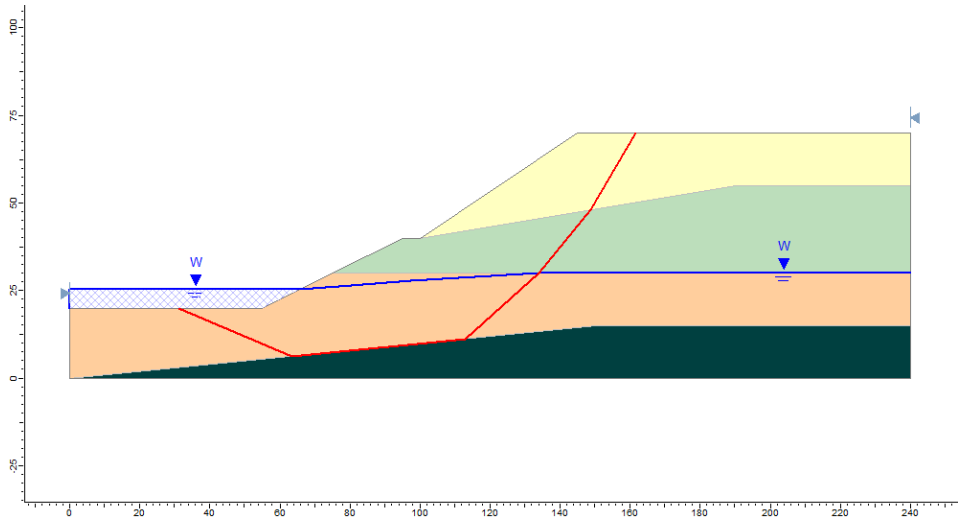


Figure 4.77 The cross-section of the slope for the scenario-*f*, hypothetical case V.

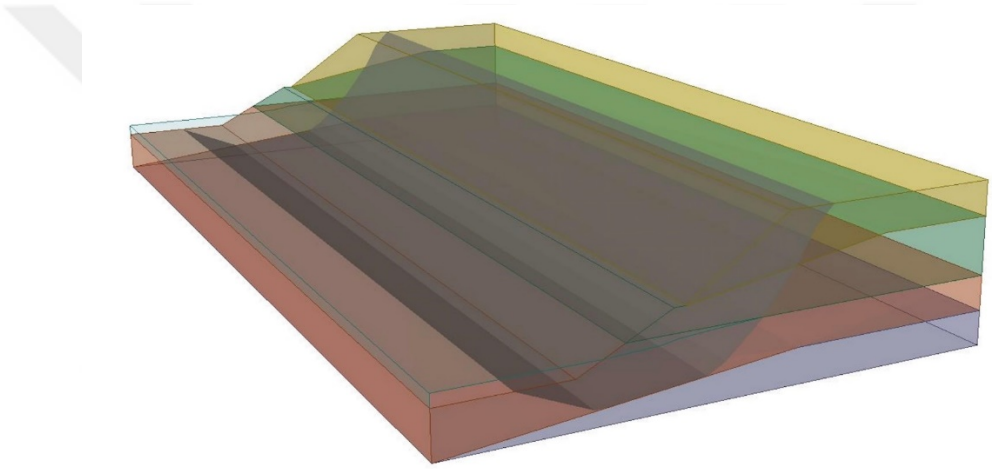


Figure 4.78 Three-dimensional model of the scenario-*f*, hypothetical case V.

The location of the water table and the results of the analysis are given in Table 4.98 and Table 4.99, respectively.

Table 4.98 The coordinates of the groundwater table.

Water table				
2D		3D		
x-axis	*y*-axis	*x*-axis	*y*-axis	*z*-axis
0	20.0000	0	0	20.0000
0	25.4920	0	480.0000	20.0000
65.9849	25.4925	0	0	25.4920
80.2870	26.4760	0	480.0000	25.4920
97.4470	27.8480	65.9849	0	25.4925
115.6370	29.0500	65.9849	480.0000	25.4925
134.0930	30.0000	80.2870	0	26.4760
240.0000	30.0000	80.2870	480.0000	26.4760
		97.4470	0	27.8480
		97.4470	480.0000	27.8480

		115.6370	0	29.0500
		115.6370	480.0000	29.0500
		134.0930	0	30.0000
		134.0930	480.0000	30.0000
		240.0000	0	30.0000
		240.0000	480.0000	30.0000

Table 4.99 The results of the analysis for the scenario-*f*, case V.

	JanbuS	JanbuC	Spencer	Corps.	L&K	GLE/MP	Sarma	SarmaNV
F (2D)	1.3832	1.4964	1.6922	1.7853	1.7282	1.7048	1.6715	1.6599
F (3D)	1.3536	-	1.6403	-	-	1.6336	-	-

g - Low elevation groundwater table with ponded water at the front and external loadings on top of the slope

This analysis consists of frontal water pressure and external loadings on top of the slope (Figure 4.79). The results of such effects are given in Table 4.100.

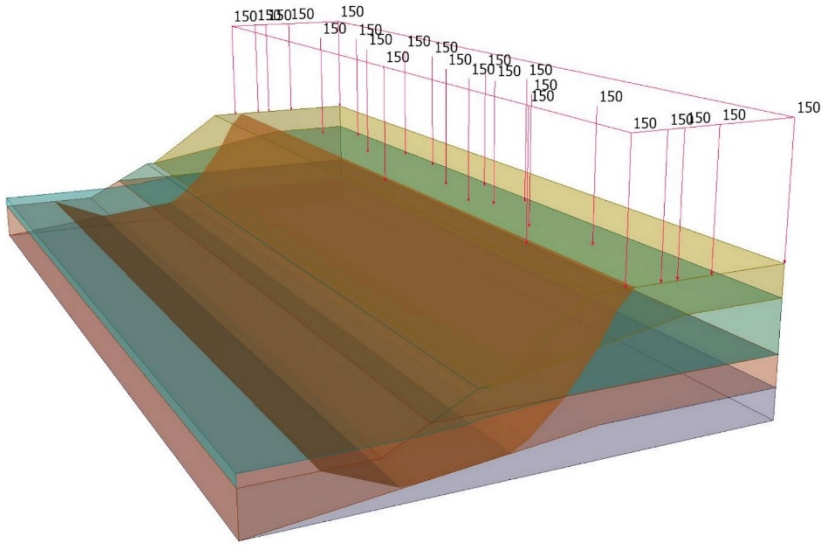


Figure 4.79 Three-dimensional model of the scenario-*g*, hypothetical case V.

Table 4.100 The computed safety factors for the scenario-*g,* case V.

	JanbuS	JanbuC	Spencer	Corps.	L&K	GLE/MP	Sarma	SarmaNV
F (2D)	1.3747	1.4872	1.6894	1.7734	1.7177	1.7006	1.6658	1.6599
F (3D)	1.3441	-	1.6320	-	-	1.6181	-	-

h - Low elevation groundwater table with ponded water at the front and seismic activity

In this analysis, earthquake-induced forces have been implemented into the analysis in addition to the scenario-*f.* The results of the computations are given in Table 4.101.

Table 4.101 The results of the analysis for the scenario-*h,* case V.

	JanbuS	JanbuC	Spencer	Corps.	L&K	GLE/MP	Sarma	SarmaNV
F (2D)	1.0954	1.1850	1.3817	1.3775	1.3142	1.3870	1.3633	1.3384
F (3D)	1.0737	-	1.3370	-	-	1.3259	-	-

i - Low elevation groundwater table with ponded water at the front, external loadings on top of the slope and seismic activity

This analysis includes the effects of frontal water pressure due to ponded water, external loadings on top and earthquake-induced forces (Figure 4.80). The results of the analyses are given in Table 4.102.

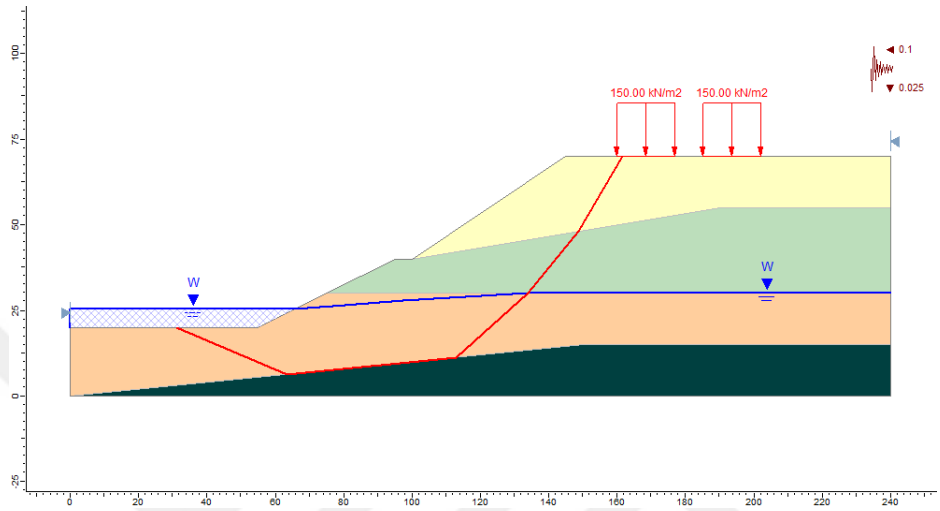


Figure 4.80 The cross-section of the investigated slope profile for the scenario-*i*, case V.

Table 4.102 The results of the analysis for the scenario-*i*, case V.

	JanbuS	JanbuC	Spencer	Corps.	L&K	GLE/MP	Sarma	SarmaNV
F (2D)	1.0910	1.1802	1.3788	1.3719	1.3093	1.3852	1.3604	1.3384
F (3D)	1.0695	-	1.3431	-	-	1.3234	-	-

j – High elevation groundwater table

In this analysis, the groundwater table has been raised to investigate the increased pore-water pressures (Figure 4.81 & Figure 4.82).

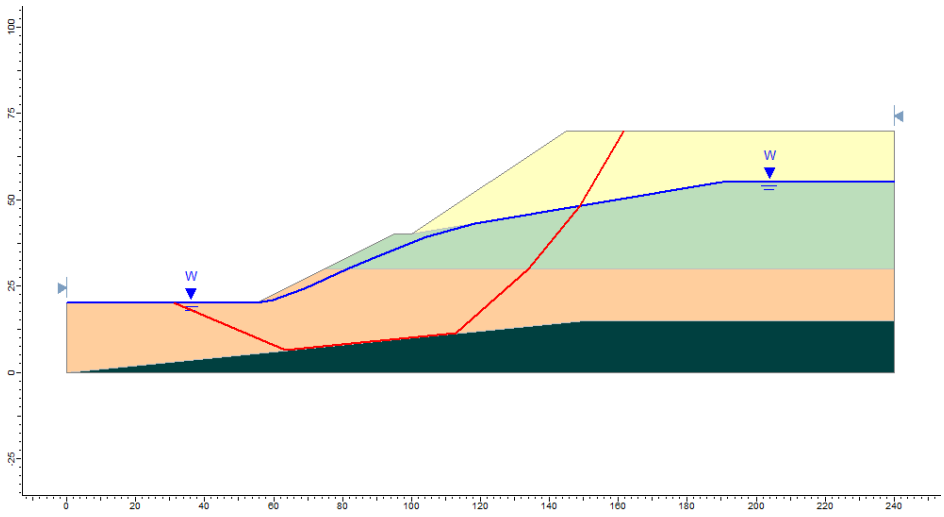


Figure 4.81 The analyzed slope model for the scenario-*j*, case V.

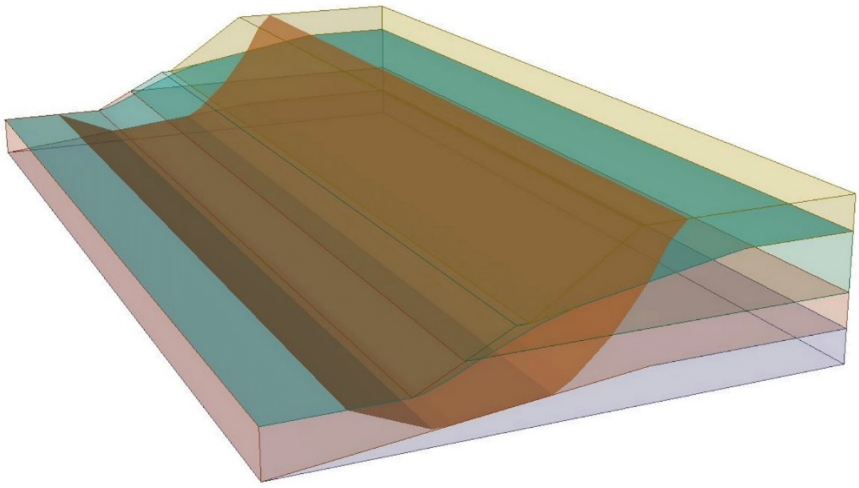


Figure 4.82 Three-dimensional model of the scenario-*j*, hypothetical case V.

The coordinates of the water table and the results of the analysis are given in Table 4.103 and Table 4.104, respectively.

Table 4.103 The coordinates of the groundwater table for the scenario-*j*.

Groundwater table				
2D		3D		
x-axis	*y*-axis	*x*-axis	*y*-axis	*z*-axis
0	20.0000	0	0	20.0000
55.0000	20.0000	0	480.0000	20.0000
59.8190	20.9690	55.0000	0	20.0000
68.9810	24.3250	55.0000	480.0000	20.0000
81.3979	30.0000	59.8190	0	20.9690
91.4020	34.0020	59.8190	480.0000	20.9690
104.4660	39.1800	68.9810	0	24.3250
118.2630	43.0439	68.9810	480.0000	24.3250
190.0000	55.0000	81.3979	0	30.0000
240.0000	55.0000	81.3979	480.0000	30.0000
		91.4020	0	34.0020
		91.4020	480.0000	34.0020
		104.4660	0	39.1800
		104.4660	480.0000	39.1800
		118.2630	0	43.0439
		118.2630	480.0000	43.0439
		190.0000	0	55.0000
		190.0000	480.0000	55.0000
		240.0000	0	55.0000
		240.0000	480.0000	55.0000

Table 4.104 The results of the analysis for the scenario-*j*, case V.

	JanbuS	JanbuC	Spencer	Corps.	L&K	GLE/MP	Sarma	SarmaNV
F (2D)	1.1358	1.2309	1.3939	1.4726	1.4929	1.3988	1.3785	1.3799
F (3D)	1.1102	-	1.3467	-	-	1.3365	-	-

k – High elevation groundwater table with external loadings on top of the slope

In this analysis, external loadings have been applied on top of the slope in addition to increased pore-water pressures (Figure 4.83). The corresponding results are given in Table 4.105.

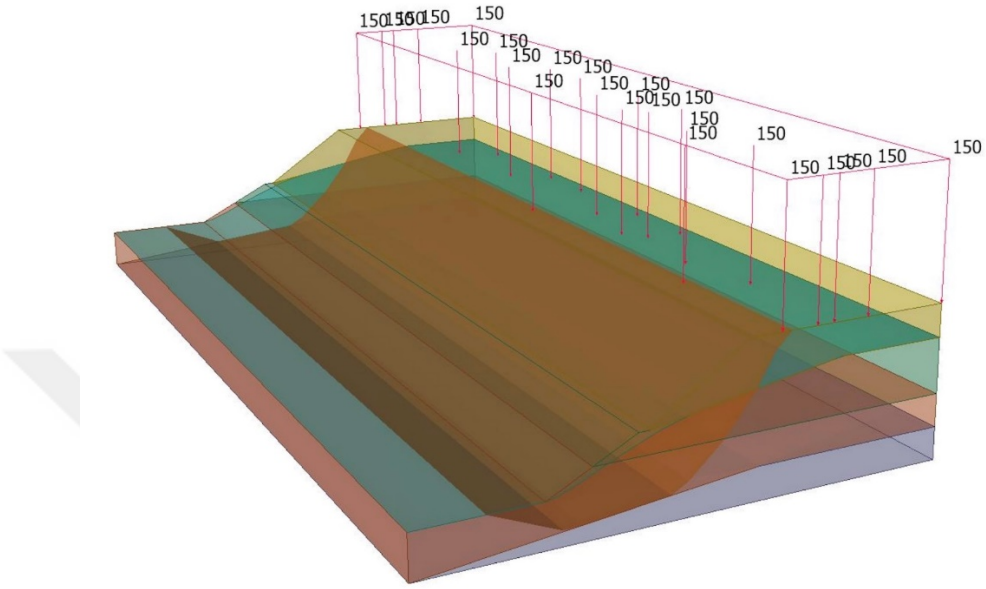


Figure 4.83 Three-dimensional model of the scenario-*k*, hypothetical case V.

Table 4.105 The computed safety factors for the scenario-*k*, case V.

	JanbuS	JanbuC	Spencer	Corps.	L&K	GLE/MP	Sarma	SarmaNV
F (2D)	1.1302	1.2248	1.3905	1.4648	1.4853	1.3967	1.3754	1.3799
F (3D)	1.1045	-	1.3429	-	-	1.3349	-	-

l - High elevation groundwater table with seismic activity

This analysis has been performed by assuming earthquake-induced forces acting on the slope. The results of the effects are given in Table 4.106.

Table 4.106 The results of the analysis for the scenario-*l*, case V.

	JanbuS	JanbuC	Spencer	Corps.	L&K	GLE/MP	Sarma	SarmaNV
F (2D)	0.9091	0.9852	1.1617	1.1655	1.1558	1.1624	1.1497	1.1329
F (3D)	0.8769	-	1.1066	-	-	1.0903	-	-

m - High elevation groundwater table with external loadings on top of the slope and seismic activity

In this analysis both the effects of high pore-water pressure, external loadings and seismic activity were taken into account (Figure 4.84). The results of such effects are given in Table 4.107.

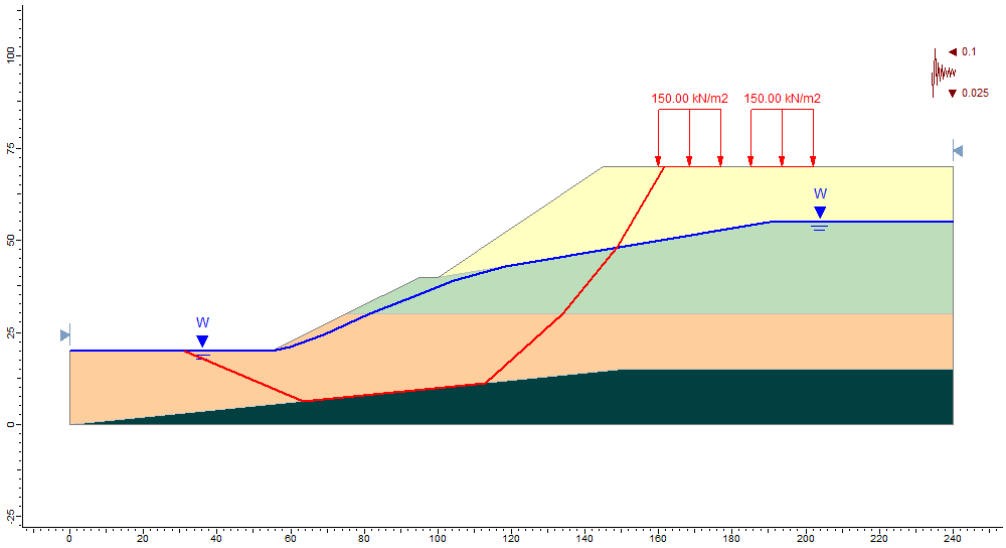


Figure 4.84 The cross-section of the scenario-*m*, case V.

Table 4.107 The computed safety factors for the scenario-*m*, case V.

	JanbuS	JanbuC	Spencer	Corps.	L&K	GLE/MP	Sarma	SarmaNV
F (2D)	0.9063	0.9822	1.1601	1.1618	1.1523	1.1619	1.1480	1.1329
F (3D)	0.8751	-	1.1047	-	-	1.0877	-	-

n - High elevation groundwater table with ponded water at the front of the slope

This analysis has been performed by assuming higher water pressure at front and higher inner pore-water pressure due to increased water table elevation (Figure 4.85 & Figure 4.86).

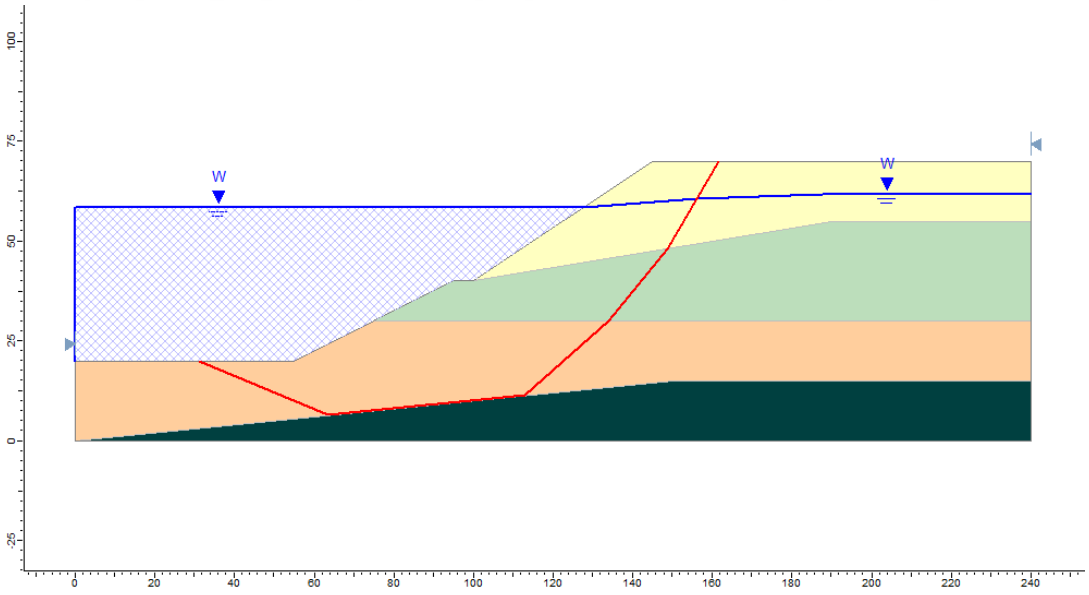


Figure 4.85 The cross-section of the slope for the scenario-n, case V.

The location of the water table and the computed factors of safety are given in Table 4.108 and Table 4.109, respectively.

Table 4.108 The coordinates of the water table for the scenario-n.

Water table				
2D		3D		
x-axis	*y*-axis	*x*-axis	*y*-axis	*z*-axis
0	20.0000	0	0	20.0000
0	58.5250	0	480.0000	20.0000
127.7880	58.5251	0	0	58.5250
155.9780	60.6520	0	480.0000	58.5250
187.6820	61.8067	127.7880	0	58.5251
240.0000	61.8067	127.7880	480.0000	58.5251
		155.9780	0	60.6520
		155.9780	480.0000	60.6520
		187.6820	0	61.8067
		187.6820	480.0000	61.8067
		240.0000	0	61.8067
		240.0000	480.0000	61.8067

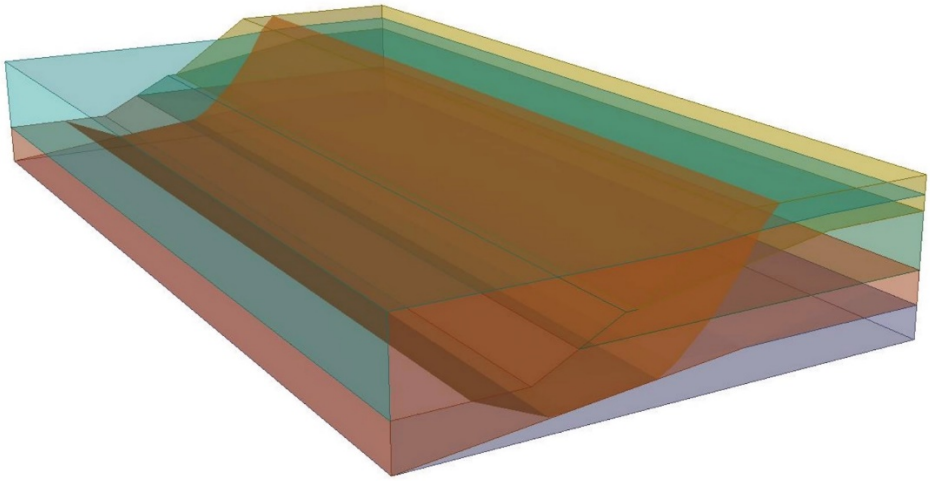


Figure 4.86 Three-dimensional model of the scenario-*n,* hypothetical case V.

Table 4.109 The results of the analysis for the scenario-*n*, case V.

	JanbuS	JanbuC	Spencer	Corps.	L&K	GLE/MP	Sarma	SarmaNV
F (2D)	1.6280	1.7644	2.0627	3.3365	2.1094	2.0794	2.0341	1.9778
F (3D)	1.6196	-	2.0373	-	-	2.0389	-	-

p - High elevation groundwater table with ponded water at the front and external loadings on top of the slope

This analysis has been performed by assuming the same conditions as the scenario-*n* with additional external loadings on top of the slope (Figure 4.87). The results of the analysis are given in Table 4.110.

Table 4.110 The computed safety factors for the scenario-*p*, case V.

	JanbuS	JanbuC	Spencer	Corps.	L&K	GLE/MP	Sarma	SarmaNV
F (2D)	1.6115	1.7466	2.0517	3.2698	2.0849	2.0717	2.0215	1.9778
F (3D)	1.5972	-	2.0208	-	-	2.0262	-	-

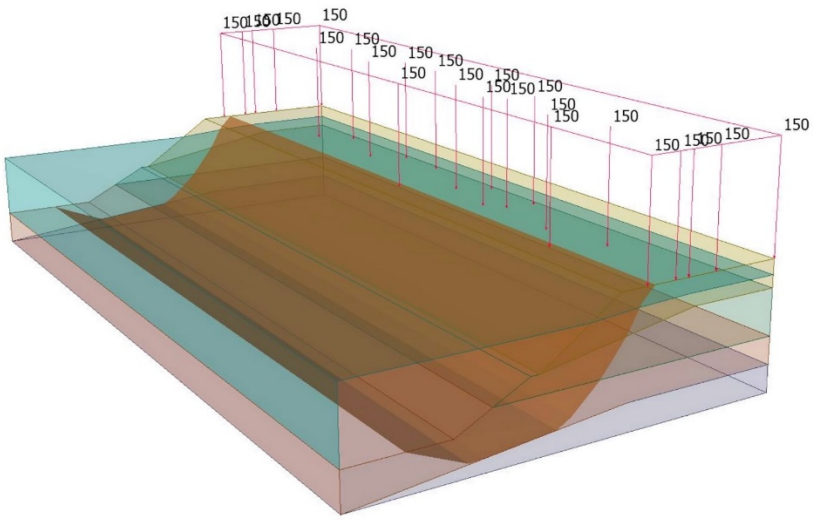


Figure 4.87 Three-dimensional model of the scenario-*p*, hypothetical case V.

r - High elevation groundwater table with ponded water at the front and seismic activity

Earthquake-induced forces have been implemented into the analysis. The results of the computations are given below. (Table 4.111)

Table 4.111 The computed safety factors for the scenario-*r*, case V.

	JanbuS	JanbuC	Spencer	Corps.	L&K	GLE/MP	Sarma	SarmaNV
F (2D)	1.1675	1.2653	1.5099	1.9943	1.4007	1.5173	1.4943	1.4420
F (3D)	1.1453	-	1.4729	-	-	1.4651	-	-

s - High elevation groundwater table with ponded water at the front, external loadings on top and seismic activity

In addition to increased frontal and inner water pressure, external loadings and seismic activity have been applied to the slope model (Figure 4.88). The results of the computations are given in Table 4.112.

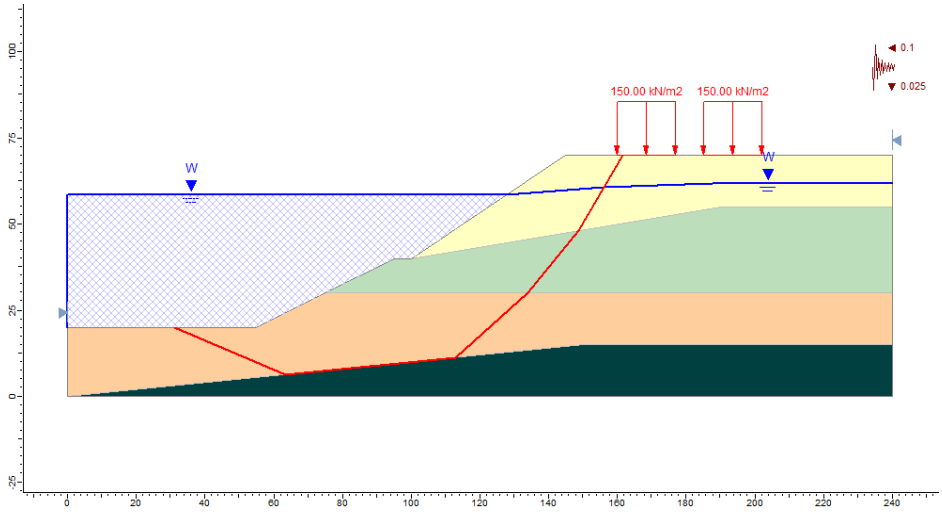


Figure 4.88 The investigated slope model for the scenario-*s*, case V.

Table 4.112 The results of the analysis for the scenario-*s*, case V.

	JanbuS	JanbuC	Spencer	Corps.	L&K	GLE/MP	Sarma	SarmaNV
F (2D)	1.1608	1.2581	1.5060	1.9767	1.3920	1.5144	1.4894	1.4420
F (3D)	1.1380	-	1.4652	-	-	1.4608	-	-

t – Fully drained slope with external loadings on top

This analysis has been performed by assuming no water pressure exists through the slope and only the effect of external loadings has been investigated (Figure 4.89). The results of the computation are given in Table 4.113.

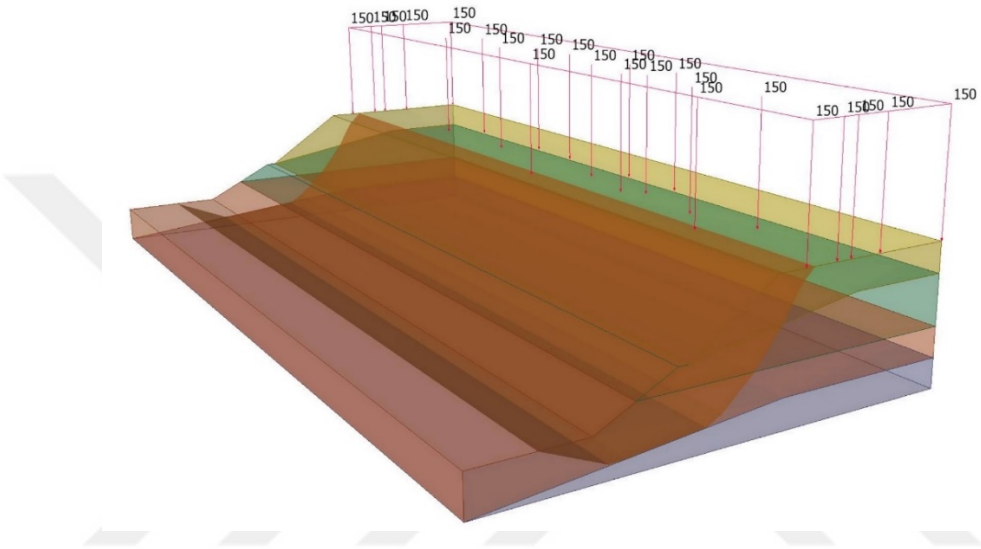


Figure 4.89 Investigated slope profile of the scenario-*t*, hypothetical case V.

Table 4.113 The results of the analysis for the scenario-*t*, case V.

	JanbuS	JanbuC	Spencer	Corps.	L&K	GLE/MP	Sarma	SarmaNV
F (2D)	1.6547	1.7933	2.0569	2.0962	2.1638	2.0708	2.0414	1.9949
F (3D)	1.6370	-	2.0042	-	-	2.0044	-	-

v – Fully drained slope with external loadings on top and seismic activity

In this analysis both the effect of external loadings and seismic activity have been investigated on a fully drained slope profile (Figure 4.90). The results of the analyses are given in Table 4.114.

Table 4.114 The computed safety factors for the scenario-*v*, case V.

	JanbuS	JanbuC	Spencer	Corps.	L&K	GLE/MP	Sarma	SarmaNV
F (2D)	1.3324	1.4440	1.6872	1.6432	1.6715	1.6964	1.6760	1.6203
F (3D)	1.3187	-	1.6487	-	-	1.6370	-	-

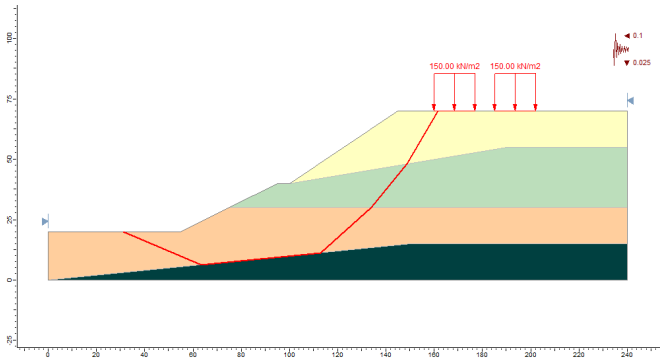


Figure 4.90 The slope model for the scenario-*v*, case V.

y – Fully drained slope with seismic activity

In this analysis, only the effect of earthquake-induced forces has been investigated on a fully drained slope profile. The results of the analysis are given below. (Table 4.115)

Table 4.115 The computed safety factors for the scenario-*y*, case V.

	JanbuS	JanbuC	Spencer	Corps.	L&K	GLE/MP	Sarma	SarmaNV
F (2D)	1.3385	1.4506	1.6918	1.6507	1.6788	1.6991	1.6806	1.6203
F (3D)	1.3259	-	1.6572	-	-	1.6430	-	-

4.1.6 Case VI

4.1.6.1 Introduction of the area

In this case, a recent and a paleo landslide was investigated in the same region. The investigation area was Denizkonak village of Cide district in Kastamonu city, south of the Black Sea, Turkey (Figure 4.91).

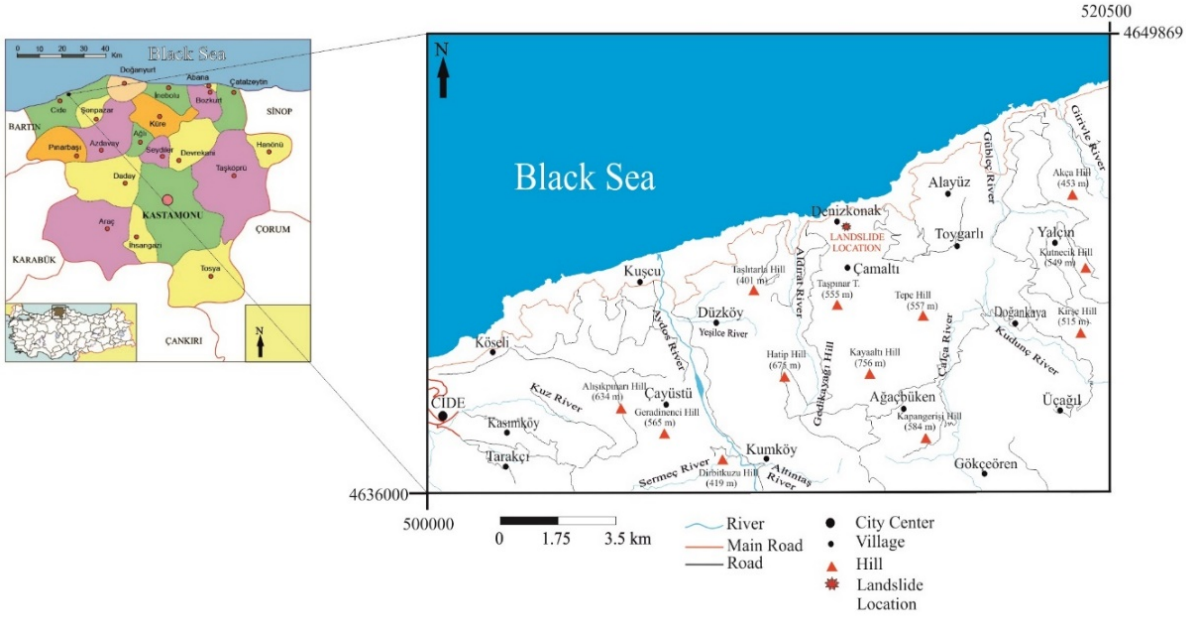


Figure 4.91 The location of the study area.

The area is highly vegetated with a variety of plants and trees which is very typical along the Black Sea region. The topography of the area is valley shaped with low to moderate inclination slopes in every direction (Figure 4.92). Also, the point with the highest elevation is approximately at 230 meters above the sea level (Figure 4.93).



Figure 4.92 Three-dimensional model of the investigated area.

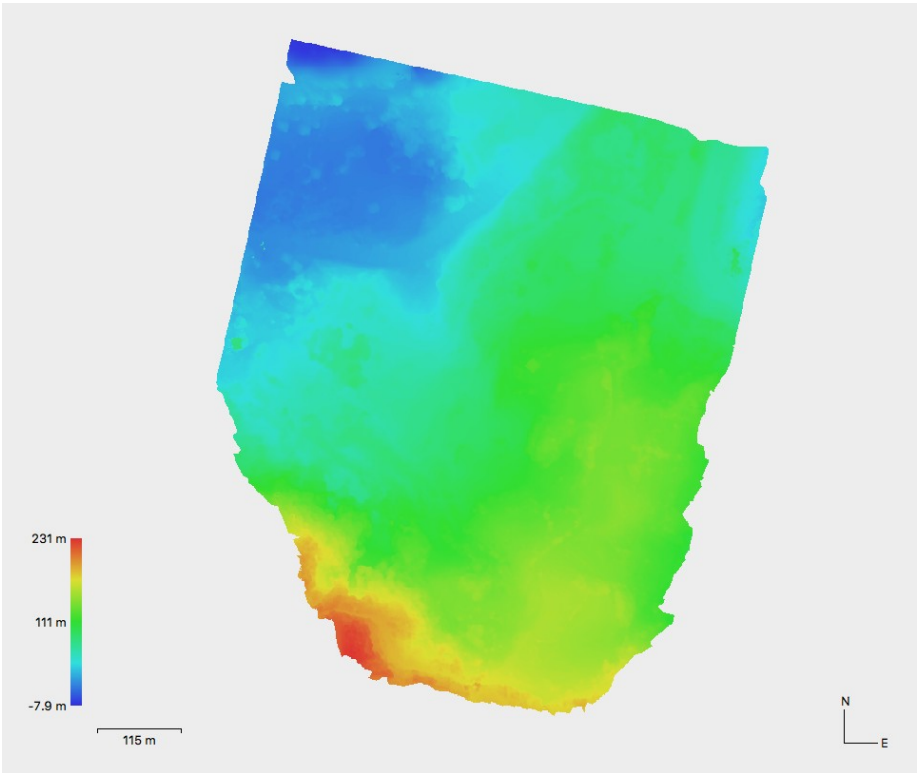
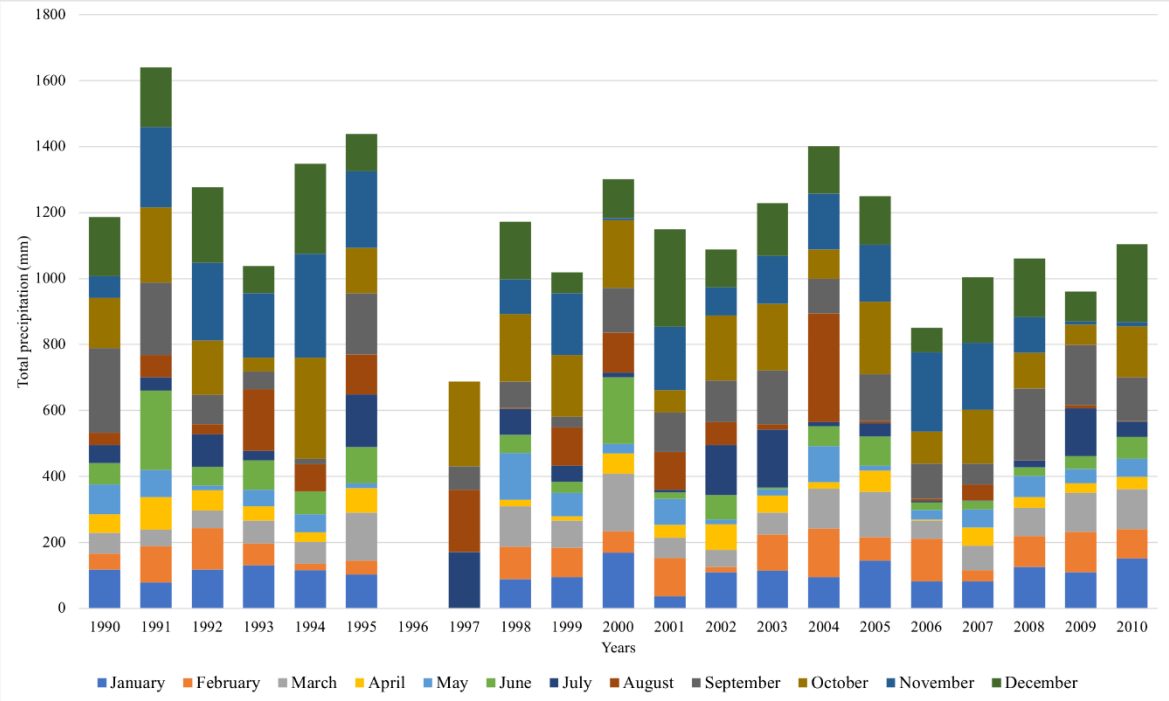


Figure 4.93 Elevation map of the inspected area.

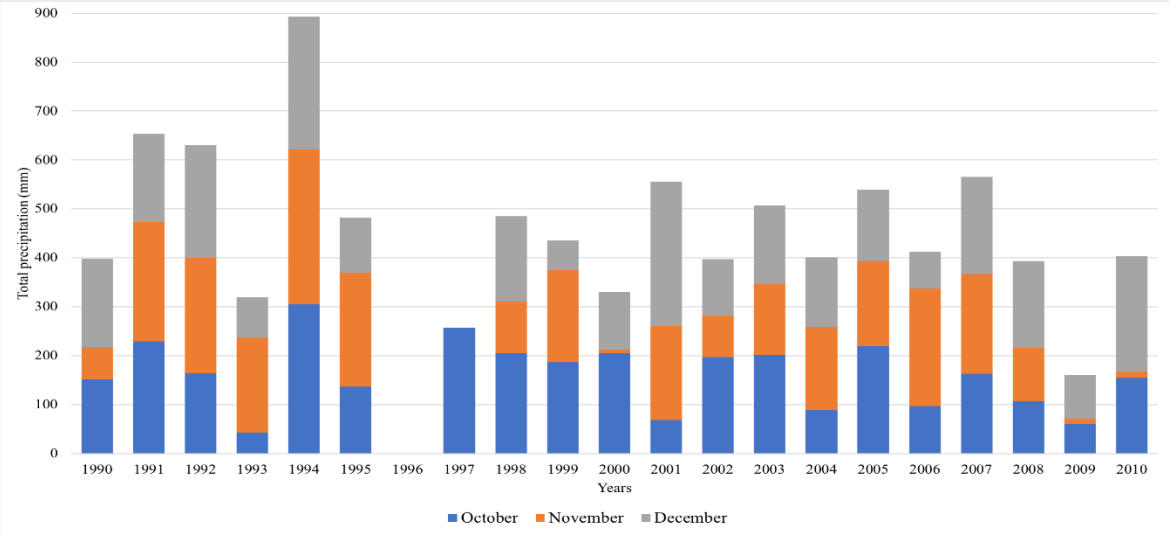
Several landslides have occurred at Denizkonak village in recent years. Some notable of them have taken place in the years 1992, 1994 and 2005. Also, the North of Kastamonu is known to be prone to landslides generally due to high precipitation. Monthly precipitation to the station at Cide district has been analyzed through the years 1990 to 2010 (Table 4.116). Some of the data for the years 1996 and 1997 wasn't found.

Table 4.116 Total precipitation from 1990 to 2010 for Cide district.



It is clear from the Table 4.116 that rainfall accumulation was at the highest level for the last three months of the year. Therefore, a separate investigation has been made for the specific months (Table 4.117).

Table 4.117 Total precipitation for the last three months of the years.



4.1.6.2 Field investigation

At the first point of the field investigation, two main scarps of previous landslides have been observed (Figure 4.94). The instabilities are named as Landslide #1 and Landslide #2 and the outcrops of them were shown as Scarp #1 and Scarp #2, respectively. One of the landslides (Scarp #2) has relatively fresher outcrop than the Scarp #1; which indicates that Landslide #2 has occurred more recently than the other one.



Figure 4.94 The outcrops of the two landslides.

The Landslide #1 is approximately 110 to 120 meters at the widest crown area while the other landslide is at about 50 to 60 meters. This difference can be easily seen in the aerial photograph taken by an unmanned aerial vehicle (UAV) (Figure 4.95). Also, the horizontal distance between the two scarps is approximately between 130 to 140 meters. These measurements can be easily done on an orthomosaic photograph which is a result of the alignment of numerous aerial photographs taken by a UAV.

The close-up investigation of the Landslide #1 indicates a non-uniform formation of the scarp area (Figure 4.96); which may be a result of a time-dependent erosion. Also, the general inclination of the outcrop of the Landslide #1 was steep (Figure 4.97 & Figure 4.98).



Figure 4.95 Aerial photograph of the two landslides.



Figure 4.96 Approximate scarp of the Landslide #1.



Figure 4.97 The outcrop of the Landslide #1. Showing a steeply inclined surface.



Figure 4.98 The steeply inclined outcrop of the Landslide #1.

In addition to the observation of scarps, a geological investigation has been also done. The ground and slope surfaces around the landslide area indicate a highly eroded and disintegrated flysch; which mainly composed of fine to very fine grained possible siltstone, claystone and marl (Figure 4.99 & Figure 4.100).



Figure 4.99 Highly disintegrated and eroded rocks at the ground surface.



Figure 4.100 Highly disintegrated and eroded rocks at the slope surface.

The public roads give geologists an advantage to investigate the geology of a site by examining the outcrops they yield. The investigated outcrops around the landslide area have indicated highly disintegrated, weathered, decomposed and eroded flysch. Disintegrated and weathered siltstones can be seen below in Figure 4.101, Figure 4.102 and Figure 4.103.



Figure 4.101 Disintegrated siltstones at the upper side of the photograph. Highly weathered soil-like siltstones at below.



Figure 4.102 Highly weathered and disintegrated layered siltstones.



Figure 4.103 Weathered and disintegrated layered siltstones.

Also, highly decomposed and weathered marl that can be easily disintegrated by hand were observed at the field and can be seen in Figure 4.104.



Figure 4.104 Decomposed and weathered marl.

Also, during the field investigation, it was spotted that many structures have been damaged by the earth movement. These included wooden electric poles that tilted over (Figure 4.105), village houses with minor cracks around the pillar and walls (Figure 4.106 and Figure 4.107), and severely damaged buildings (Figure 4.108, Figure 4.109, Figure 4.110 and Figure 4.111).



Figure 4.105 Tilted over a wooden electric pole.



Figure 4.106 Damaged house with minor cracks on the wall.



Figure 4.107 Minorly damaged building wall.



Figure 4.108 Severely damaged old village house.



Figure 4.109 Severely damaged village house due to the landslide.



Figure 4.110 Devastated building due to slope instability.



Figure 4.111 Severely damaged house pillars due to uplifting caused by the landslide. Red arrows indicate the area of vertical movement.

4.1.6.3 Laboratory testing

Three blocks of rock specimens had been acquired for laboratory testing to determine the unit weight and uniaxial compressive strength (UCS). The specimens were taken from outcrops that can be seen in Figure 4.101 and Figure 4.103. The block punch index (BPI) test apparatus was used to determine the UCS of the specimens (Figure 4.112). The BPI test apparatus was chosen by considering the fact that, the size of the specimens was not suitable for uniaxial compressive strength test (Figure 4.113). The blocks were cut into several cylindrical pieces with a diameter of approximately 52.5 mm and a width between of 5 mm to 15 mm (Figure 4.114). The preparation of the samples and the application of the test was done according to ISRM suggested methods [210].



Figure 4.112 The block punch index test apparatus.



Figure 4.113 Preparation of the block specimens.

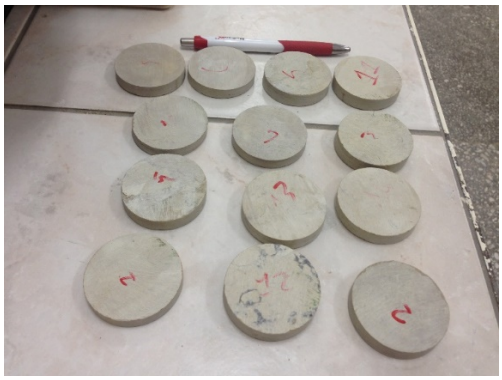


Figure 4.114 Prepared specimens for the BPI test.

The correction of the block punch index (BPI_c) with respect to thickness and the diameter of the specimen was done by using the equation (Equation 64) proposed by Ulusay et al. [211].

The conversion of BPI_c to UCS (Equation 65) with considering the type of rock material was done by using the conversion factor (Equation 66) proposed by Sonmez and Tunusluoglu [212]. The results of the laboratory tests can be seen in Table 4.118.

$$BPI_c = 3499D^{-1.3926}t^{-1.1265}F \quad 64$$

$$UCS = AxBPI_c \quad 65$$

$$A = 0.80x2.266(m_i)^{0.3824} \quad 66$$

Table 4.118 The results of the laboratory tests.

Specimen#	Diameter (mm)	Thickness (mm)	Fialure load (kN)	Weight (g)	Dry unit weigth (kN/m^3)	BPI_c (MPa)	σ_c (MPa)
1*	52.35	10.42	15	57.84	25.31	15.1232	50.73
2	52.5	9.28	18	51.4	25.11	20.5959	69.09
3	52.4	11.4	23.5	62.14	24.81	21.3830	71.73
4	52.49	9.18	22	50.62	25.01	25.4890	85.50
5	52.06	10.81	23	59.37	25.32	22.4214	75.21
6	52.7	8.9	20.5	49.85	25.20	24.4578	82.05
7	52.46	8.17	18	45.3	25.18	23.7994	79.84
8	52.55	9.9	23	54.51	24.92	24.4354	81.97
9	52.4	10.53	29.5	56.42	24.39	29.3535	98.47
10	52.54	8.41	13.5	44.95	24.20	17.2401	57.83
11*	52.49	10.84	20.5	59.85	25.04	19.6951	66.07
12	52.36	11.66	21.5	64.39	25.17	19.0927	64.05
13	52.4	10.41	29	57.76	25.25	29.2310	98.06
14	52.48	10.32	17	56.99	25.06	17.2671	57.92

*Invalid results according to failure pattern. [211]

4.1.6.4 The stability analyses

Limit equilibrium procedures have been applied to the landslides to acquire some knowledge about the conditions of failure. It is known that the studied area is highly prone to instabilities due to precipitation. Thus, during the analyses, special attention has been made to the pore-water pressures. During the field investigation, saturated ground soils were observed around the Landslide#1 crown area. Also, sounds of frogs were also present near the Scarp#1; which was a valuable information about the saturation of the material.

The study of the landslide area indicated that the instabilities have occurred in a heterogenous rock mass, flysch. Therefore, the Hoek-Brown criterion was chosen to define the rock mass strength of the area. Based on the study of Marinos & Hoek [214], the field observations Geological Strength Index (GSI) was taken as 20. The intact rock constant (m_i) was taken as 5.0, based on an estimation from the table proposed by Marinos & Hoek [79]. Unconfined compressive strength (UCS) and the unit weight of the material were found to be 76.81 MPa and 25 kN/m^3; which is the average of the laboratory test results (Table 4.118). However, this is the strength of an intact rock material and the investigated area was composed of highly disintegrated and weathered flysch, which cannot be represented by only siltstones as it also contained weathered clayey materials between the bedding planes. Therefore, the UCS determined from the laboratory cannot be applied to slope stability analyses. Other researches on the strength of weathered and saturated flysch near the city of Kastamonu indicate that the average UCS is 11.37 MPa [225]. This value found to be representative for the overall weathered heterogeneous flysch rock mass and therefore used in the analyses instead of the laboratory results. Although the disturbance factor (D_f) should not be assigned to the whole sliding mass, the landslide area was highly disintegrated and disturbed by possible tectonic activity. There was a sharp distinguishing difference between the landslide boundary and the surrounding area. Also, the first landslide has occurred 26 years ago at the time of this investigation. In addition, based on the visual interpretations gathered from the UAV photographs and field investigations, this region shows a typical paleolandslide topography. From these reasons, the disturbance factor was taken as 0.7. The summary of the input parameters used in the modelling of the landslides can be seen in Table 4.119.

Table 4.119 The input parameters used in the analyses.

γ (kN/m^3)	UCS (MPa)	GSI	m_i	D_f	m_b	s	a
25	11.37	20	5	0.7	0.0616571	92.194x10^{-7}	0.543721

A reasonable cross-section was taken from a current topographic map to investigate the possible pre-failure sections for the two landslides (Figure 4.115). However, besides of the present cross-section, the others were purely prepared by investigation of the current topography, considering the mechanics of the failures and the most importantly engineering instincts.

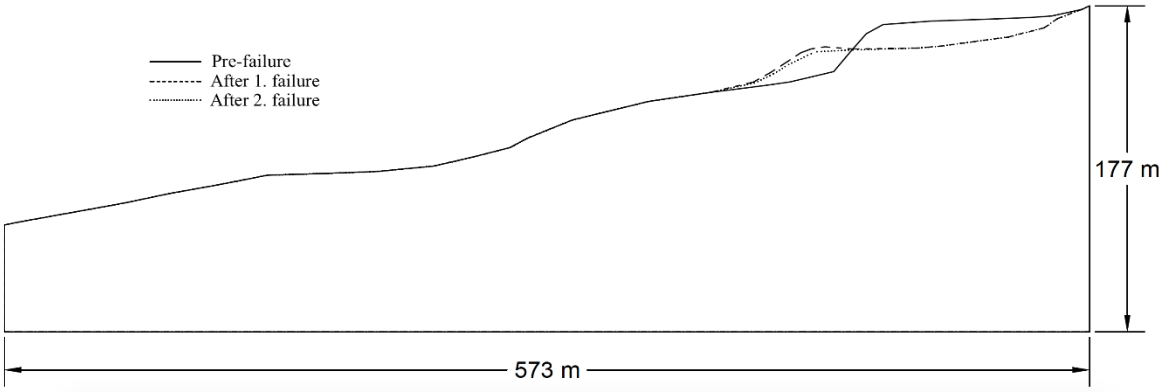


Figure 4.115 Cross-section of the investigated area. Dashed and dotted lines indicate post-failure 2D topography.

Back analyses from the very first topography (Figure 4.116), before any failure, was done to investigate the change between r_u [213] and F to determine the failure conditions. The location of the critical slip surface was estimated due to field observations and post-failure topography. The shape of the sliding surface was assumed to be circular based on the observations on Scarp#1, the lithology and post-failure topography. Morgenstern & Price's method was chosen for the rest of the analyses including three-dimensional models. The selected input parameters are the most reasonable values based on the field observations and the literature review.

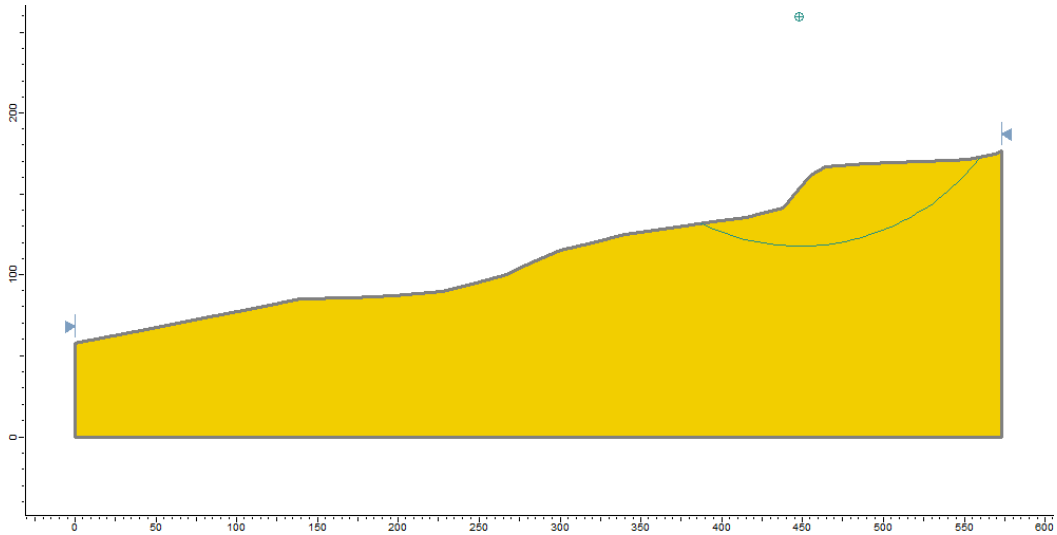


Figure 4.116 Pre-failure model of the investigated area.

According to the back analyses, the pre-failure two-dimensional topography was reconstructed (Figure 4.116) with considering the initial movement was started with GSI value of 20 and r_u of 0.44. The same parameters were integrated into three-dimensional analyses and for the same sliding surface, the factor of safety was found to be 1.0496 (Figure 4.117). The GSI value of 18.8 for three-dimensional failure was required to maintain the static equilibrium instead of 20 as in the two-dimensional model. The results of the back analyses for two and three-dimensional calculations can be seen in Figure 4.118.

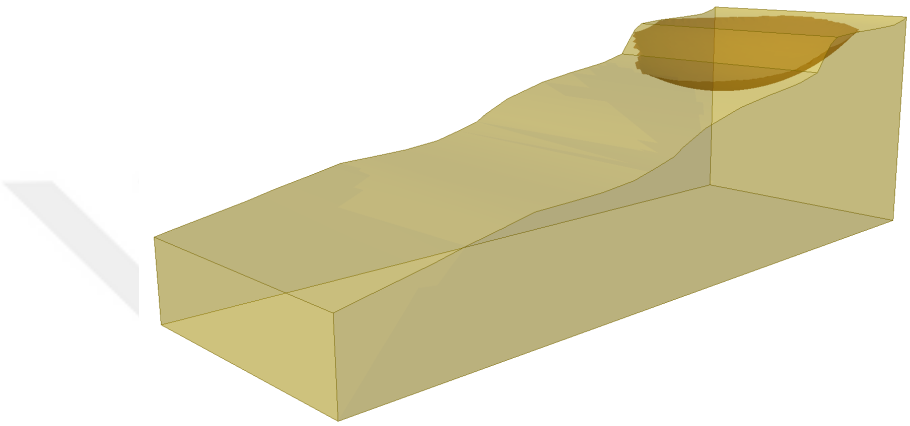


Figure 4.117 Three-dimensional model of the Landslide#1. Brown area indicates the sliding mass.

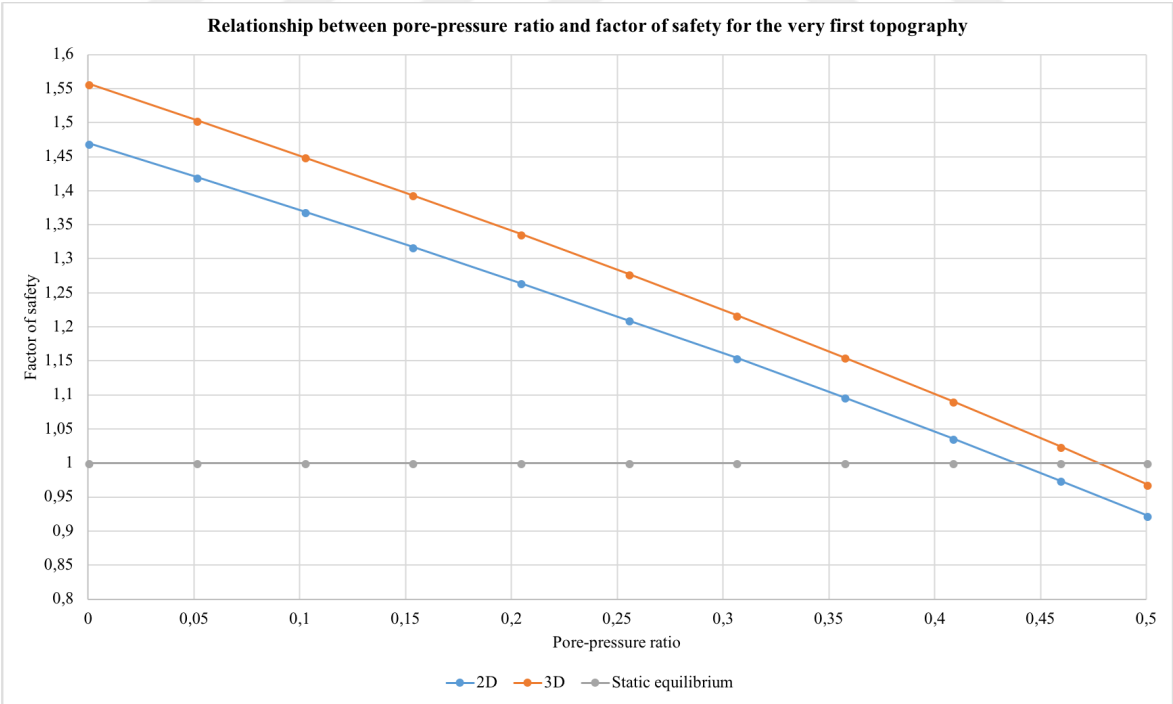


Figure 4.118 Back-analyses for the very first failure.

The coordinates of the center of the sliding surface in the Cartesian coordinate system for two and three-dimensional models, in (x, y) and (x, y, z) format, are (448.091, 259.298) and

(448.091, 100.000, 259.298), respectively. The radius of the slip surface is 141.395 meters. Also, the coordinates of the external boundary for two and three-dimensional models of the slope for further use was given in Table 4.120.

Table 4.120 The coordinates of the investigated landslide in two and three-dimensions.

External boundary				
2D		3D		
x-axis	*y*-axis	*x*-axis	*y*-axis	*z*-axis
573.000	177.000	573.000	0	177.000
569.000	175.000	573.000	200.000	177.000
553.036	171.405	569.000	0	175.000
542.069	170.634	569.000	200.000	175.000
522.919	169.824	553.036	0	171.405
489.768	168.667	553.036	200.000	171.405
463.935	166.736	542.069	0	170.634
455.083	161.755	542.069	200.000	170.634
447.047	152.428	522.919	0	169.824
437.838	141.225	522.919	200.000	169.824
424.627	138.009	489.768	0	168.667
414.901	135.678	489.768	200.000	168.667
404.684	134.112	463.935	0	166.736
394.426	132.730	463.935	200.000	166.736
373.000	130.000	455.083	0	161.755
340.000	125.000	455.083	200.000	161.755
320.000	120.000	447.047	0	152.428
300.000	115.000	447.047	200.000	152.428
288.000	110.000	437.838	0	141.225
276.000	105.000	437.838	200.000	141.225
267.000	100.000	424.627	0	138.009
248.000	95.000	424.627	200.000	138.009
227.000	90.000	414.901	0	135.678
197.000	87.000	414.901	200.000	135.678
171.000	86.000	404.684	0	134.112
139.000	85.000	404.684	200.000	134.112
114.000	80.000	394.426	0	132.730
87.000	75.000	394.426	200.000	132.730
64.000	70.000	373.000	0	130.000
37.000	65.000	373.000	200.000	130.000
10.000	60.000	340.000	0	125.000
0.000	58.000	340.000	200.000	125.000
0.000	0.000	320.000	0	120.000
573.000	0.000	320.000	200.000	120.000
		300.000	0	115.000
		300.000	200.000	115.000
		288.000	0	110.000
		288.000	200.000	110.000
		276.000	0	105.000

		276.000	200.000	105.000
		267.000	0	100.000
		267.000	200.000	100.000
		248.000	0	95.000
		248.000	200.000	95.000
		227.000	0	90.000
		227.000	200.000	90.000
		197.000	0	87.000
		197.000	200.000	87.000
		171.000	0	86.000
		171.000	200.000	86.000
		139.000	0	85.000
		139.000	200.000	85.000
		114.000	0	80.000
		114.000	200.000	80.000
		87.000	0	75.000
		87.000	200.000	75.000
		64.000	0	70.000
		64.000	200.000	70.000
		37.000	0	65.000
		37.000	200.000	65.000
		10.000	0	60.000
		10.000	200.000	60.000
		0.000	0	58.000
		0.000	200.000	58.000
		0.000	0	0.000
		0.000	200.000	0.000
		573.000	0	0.000
		573.000	200.000	0.000

The investigation of the second failure, the Landslide#2, consists of a back-analysis. At first, the most critical sliding surface was identified, then the corresponding safety factor was calculated (Figure 4.119). The previous input parameters were also used in this analysis including the pore-pressure ratio. The factor of safety in the two-dimensional analysis was calculated as 0.7561 for the most critical surface with r_u is equal to 0.44. From this point, it was obvious that the failure was not taken place while the pore-pressure ratio was 0.44. Therefore, a sensitivity analysis was done in both two and three-dimensions for the same slip circle to identify the critical pore-pressure ratio. Also, the three-dimensional model (Figure 4.120) was formed to compare the relationship between two-dimensional safety factor and the pore-pressure ratio.

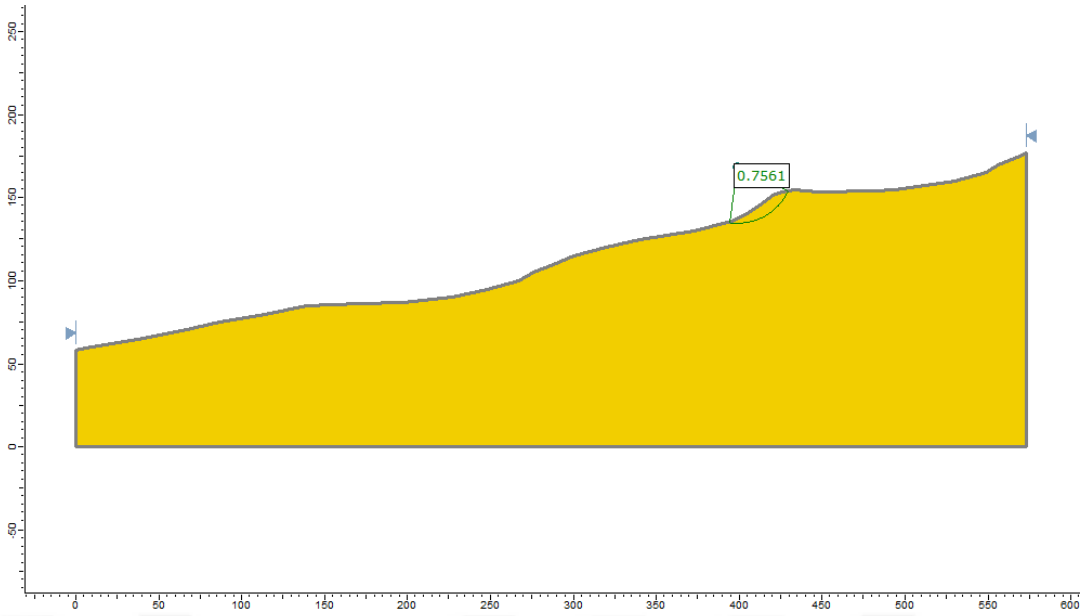


Figure 4.119 Cross-section of the topography before the second failure.

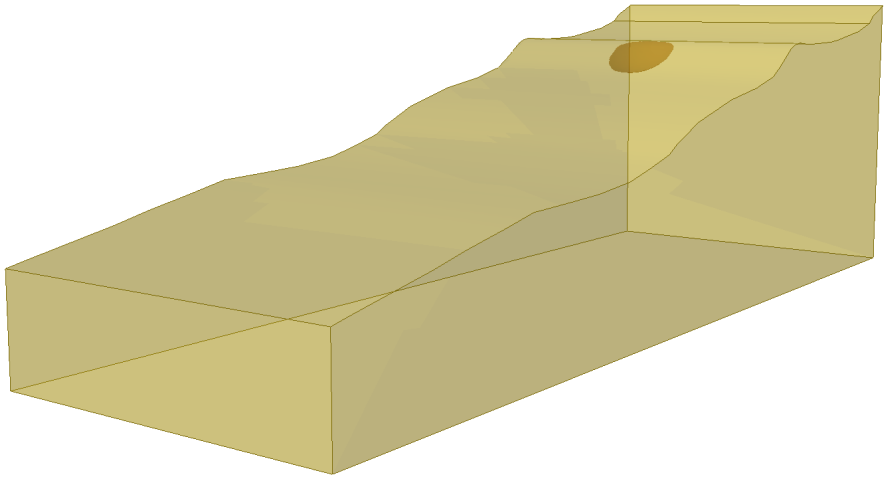


Figure 4.120 Three-dimensional model of the Landslide#2.

The sensitivity analysis shows that the instability has occurred while the pore-pressure ratio was equal to 0.24 and 0.28 for two and three-dimensional analyses, respectively (Figure 4.121). The table also indicates that the difference in two and three-dimensional factors of safety decreases with increasing pore-pressure ratio. In other words, the difference between 2D and 3D analyses, in terms of the safety factor, increases as the slope gets less saturated.

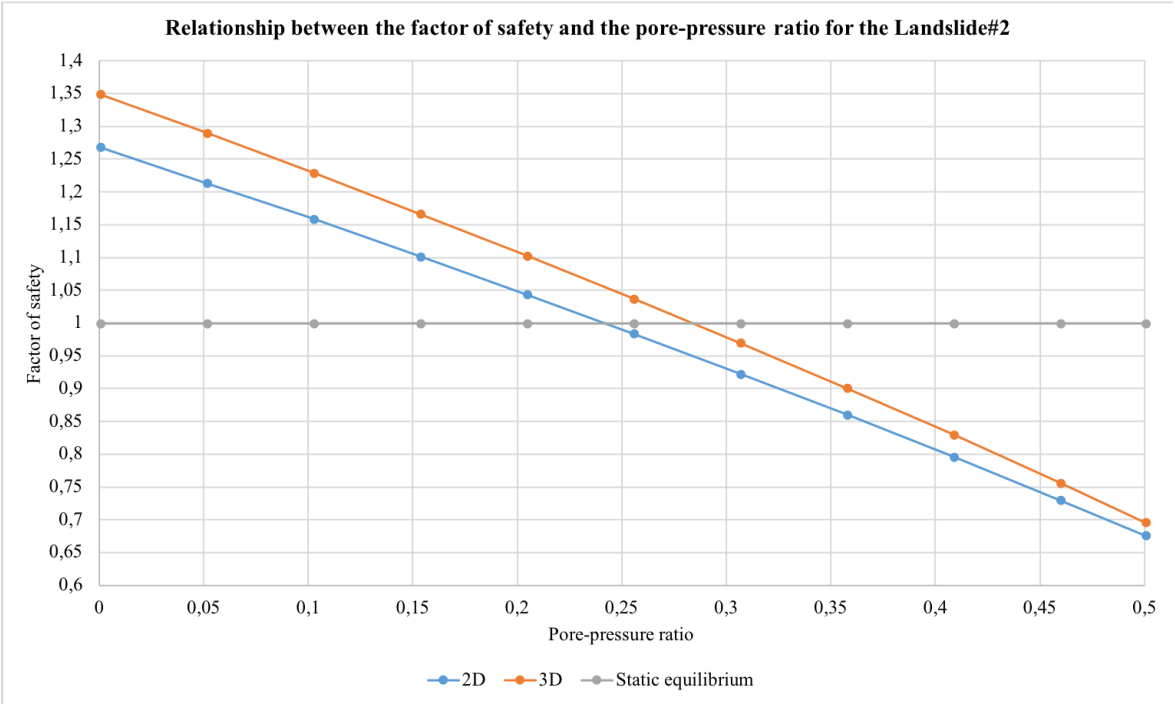


Figure 4.121 The relationship between the safety factors and the pore-pressure ratio.

The coordinates of the center of the sliding surface in the Cartesian coordinate system for two and three-dimensional models, in (x, y) and (x, y, z) format, are (399.014, 168.276) and (399.014, 100.000, 168.276), respectively. The radius of the sliding surface was 33.416 meters. Also, the coordinates of the external boundary were given for possible further use (Table 4.121).

Table 4.121 The coordinates of the Landslide#2 for modelling purpose.

External boundary				
2D		3D		
x-axis	*y*-axis	*x*-axis	*y*-axis	*z*-axis
573.000	177.000	573.000	0	177.000
569.000	175.000	573.000	200.000	177.000
556.000	170.000	569.000	0	175.000
549.000	165.000	569.000	200.000	175.000
530.000	160.000	556.000	0	170.000
494.000	155.000	556.000	200.000	170.000
482.000	154.000	549.000	0	165.000
447.980	153.457	549.000	200.000	165.000
433.299	154.697	530.000	0	160.000
425.858	153.506	530.000	200.000	160.000
420.561	151.495	494.000	0	155.000
412.222	145.805	494.000	200.000	155.000
404.472	140.704	482.000	0	154.000
395.496	135.554	482.000	200.000	154.000
373.000	130.000	447.980	0	153.457
340.000	125.000	447.980	200.000	153.457

320.000	120.000	433.299	0	154.697
300.000	115.000	433.299	200.000	154.697
288.000	110.000	425.858	0	153.506
276.000	105.000	425.858	200.000	153.506
267.000	100.000	420.561	0	151.495
248.000	95.000	420.561	200.000	151.495
227.000	90.000	412.222	0	145.805
197.000	87.000	412.222	200.000	145.805
171.000	86.000	404.472	0	140.704
139.000	85.000	404.472	200.000	140.704
114.000	80.000	395.496	0	135.554
87.000	75.000	395.496	200.000	135.554
64.000	70.000	373.000	0	130.000
37.000	65.000	373.000	200.000	130.000
10.000	60.000	340.000	0	125.000
0	58.000	340.000	200.000	125.000
0	0	320.000	0	120.000
573.000	0	320.000	200.000	120.000
		300.000	0	115.000
		300.000	200.000	115.000
		288.000	0	110.000
		288.000	200.000	110.000
		276.000	0	105.000
		276.000	200.000	105.000
		267.000	0	100.000
		267.000	200.000	100.000
		248.000	0	95.000
		248.000	200.000	95.000
		227.000	0	90.000
		227.000	200.000	90.000
		197.000	0	87.000
		197.000	200.000	87.000
		171.000	0	86.000
		171.000	200.000	86.000
		139.000	0	85.000
		139.000	200.000	85.000
		114.000	0	80.000
		114.000	200.000	80.000
		87.000	0	75.000
		87.000	200.000	75.000
		64.000	0	70.000
		64.000	200.000	70.000
		37.000	0	65.000
		37.000	200.000	65.000
		10.000	0	60.000
		10.000	200.000	60.000
		0	0	58.000
		0	200.000	58.000

		0	0	0
		0	200.000	0
		573.000	0	0
		573.000	200.000	0

The current topography after the previous landslides was also investigated for any prone-to-fail situation. “Auto Refine Search” method was performed to search for the most critical failure surface on the overall current cross-section. It was found that in the two-dimensional analysis the overall area was under static equilibrium while the pore-pressure ratio was equal to 0.33 (Figure 4.122). Three-dimensional analyses were also applied to the current topography by extending the cross-section 400 meters symmetrically (Figure 4.123). According to this result, the overall investigation area is prone to any failure if the pore-pressure ratio exceeds 0.33. This outcome can be an explanation for the previous several continuous landslides in the area, which they will continue to occur under these circumstances.

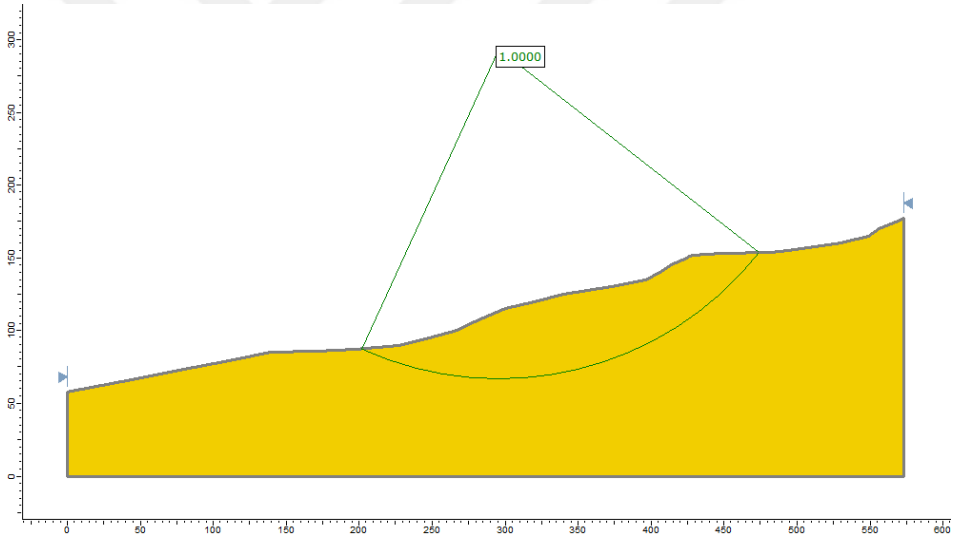


Figure 4.122 Two-dimensional model of the current topography.

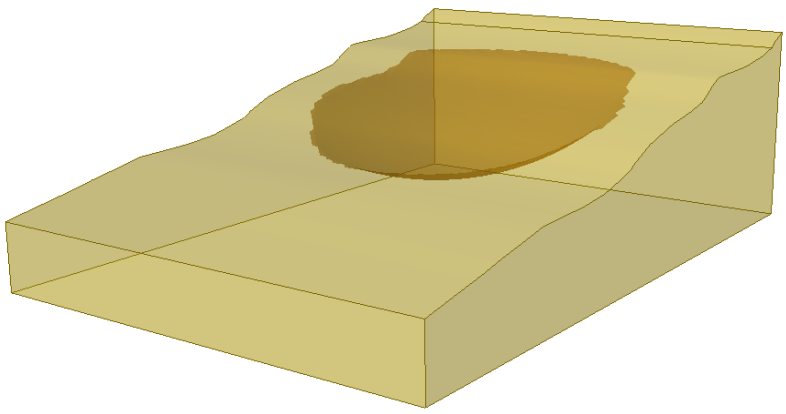


Figure 4.123 Three-dimensional model of the estimated current topography

Sensitivity analyses were also performed to investigate the relationship between the results of the two and three-dimensional analyses, and the pore-pressure ratio (Figure 4.124). The results were similar to the previous analysis; but the gap between the 2D and 3D safety factors was wider. This outcome means that to maintain the same factor of safety for the given cross-section in both 2D and 3D, much higher pore-pressure ratio is needed in three-dimensions. This can be seen clearly in Figure 4.124, where a safety factor of 1.3 was produced for unsaturated slope in two-dimensions, while a pore-pressure ratio of 0.12 was needed to maintain the same safety factor in three-dimension. Also, a pore-pressure ratio of 0.33 and 0.40 was needed to maintain the static equilibrium in two and three-dimensions, respectively. It is clear that two-dimensional analysis produced more conservative results than the three-dimensional analyses in terms of the safety factors.

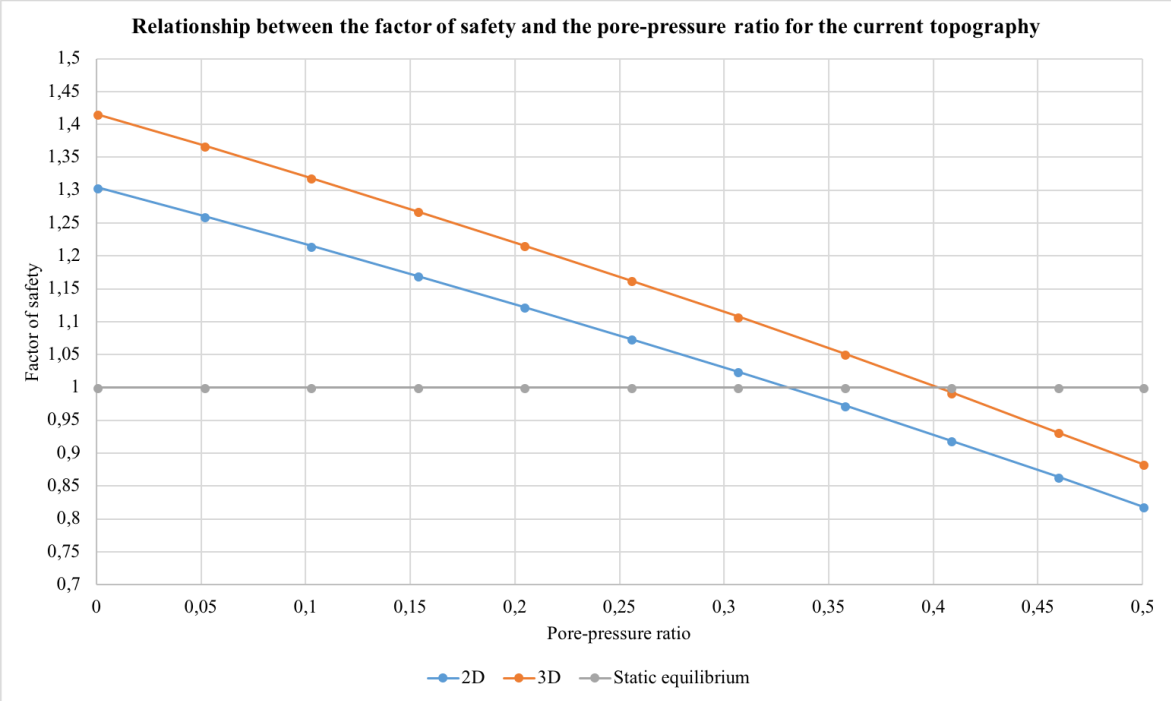


Figure 4.124 Comparing the safety factors with the pore-pressure ratio.

The coordinates of the center of the sliding surface in the Cartesian coordinate system for two and three-dimensional models, in (x, y) and (x, y, z) format, are (295.345, 293.748) and (295.345, 200.000, 293.748), respectively. The radius of the sliding surface was 226.625 meters. The coordinates of the current topography in two and three-dimensions were given in Table 4.122.

Table 4.122 The coordinates of up-to-date cross-section of the landslide area as the time of this work.

External boundary	
2D	3D

x-axis	*y*-axis	*x*-axis	*y*-axis	*z*-axis
573	177	573	0	177
569	175	573	400	177
556	170	569	0	175
549	165	569	400	175
530	160	556	0	170
494	155	556	400	170
482	154	549	0	165
448	153	549	400	165
429	152	530	0	160
426	151	530	400	160
424	150	494	0	155
414	145	494	400	155
406	140	482	0	154
396	135	482	400	154
373	130	448	0	153
340	125	448	400	153
320	120	429	0	152
300	115	429	400	152
288	110	426	0	151
276	105	426	400	151
267	100	424	0	150
248	95	424	400	150
227	90	414	0	145
197	87	414	400	145
171	86	406	0	140
139	85	406	400	140
114	80	396	0	135
87	75	396	400	135
64	70	373	0	130
37	65	373	400	130
10	60	340	0	125
0	58	340	400	125
0	0	320	0	120
573	0	320	400	120
		300	0	115
		300	400	115
		288	0	110
		288	400	110
		276	0	105
		276	400	105
		267	0	100
		267	400	100
		248	0	95
		248	400	95
		227	0	90
		227	400	90
		197	0	87

		197	400	87
		171	0	86
		171	400	86
		139	0	85
		139	400	85
		114	0	80
		114	400	80
		87	0	75
		87	400	75
		64	0	70
		64	400	70
		37	0	65
		37	400	65
		10	0	60
		10	400	60
		0	0	58
		0	400	58
		0	0	0
		0	400	0
		573	0	0
		573	400	0

5. DISCUSSIONS

In this chapter, summary and the results of the both two and three-dimensional analyses were given. Hypothetical cases were summarized by means of 2D and 3D effect and each individual limit equilibrium method was inspected for each case and as well as the scenarios. The comparison of methods was analyzed by assuming GLE/Morgenstern & Price's results as a reference value. This method is worldwide accepted for its accuracy in almost all instances.

The limit equilibrium procedures are well-known by convergence problems. Ching & Fredlund [215] has pointed out that inter-slice force function has a key role in convergence problems. Fan et al. [216] have developed a function that realistically approximates the in-situ stresses of a soil mass to overcome the convergence problems. Fredlund et al. [217] have demonstrated that the chosen axis of the moment may lead to convergence problems. Krahn [218] has proposed to implement stresses from finite element analysis to overcome the situation where the convergence problems appear as the base inclination of slice increases. Cheng et al. [219] have indicated that convergence problems may appear in slopes with external loadings and reinforcements as they induce local stress concentrations which eventually makes it difficult to acquire the safety factor with a simple inter-slice force function. Also, Cheng et al. [220] have implemented QR method [221] to evaluate the safety factor and internal forces from a matrix which eliminates the iteration procedure and eventually convergence problems due to iteration. In this thesis, non-converged safety factors are not included in the discussion and the corresponding tables and figures.

5.1 Hypothetical Case I

In 2D analyses, ordinary method of slices (OMS) have yielded the lowest factors of safety for all of the scenarios by as much as % 7.2. Inaccuracies for this method are expected due to being the most primitive method in limit equilibrium procedures and satisfying only overall moment equilibrium. Bishop's routine method gave similar results to the reference safety factors by less than % 1.25 for all of the scenarios. Although satisfying only overall moment and vertical force equilibrium Bishop's method is well-known for its accuracy, the reason is explained by Spencer [91] in his article. US Army Corps. of Engineer's method has generated the highest factors of safety in 12 of 20 scenarios. Especially in scenarios *n, p, r, s*; where the stability is controlled mainly by the high elevation water table and ponded water, the method has overestimated the safety factor as much as % 37.5. The overestimation of the factor of safety for homogeneous slopes has also been noted by Bowders & Lee [222].

Also, the method has generated up to % 3.1 lower factors of safety in scenarios where external loading is present without insignificant pore-water pressure. Lowe & Karafiath's method generally yielded insignificantly lower safety factors, only in scenario-*s* the difference is % 6. The differences between the results of the Spencer's and GLE/MP's method is less than % 0.35 as the slope was homogeneous and the methods satisfy all kind of static equilibrium, this outcome was expected. Janbu's simplified method has underestimated the factor of safety in all scenarios by up to % 20. Janbu's corrected method have generated more accurate results, although conservative safety factors still exist by up to % 14.7. The calculated factors of safety for Case I and the corresponding graph are also given in Appendix 1 and Appendix 2, respectively.

Three-dimensional analyses of the case I have been performed with four different limit equilibrium methods (Table 4.1). Convergence has been achieved for all of the scenarios. Janbu's simplified method has generated conservative factors of safety for all of the scenarios between % 7 and % 17.9 from GLE/MP's results. This outcome is also similar to two-dimensional analyses results. However, the safety factors of Bishop's and Spencer's method are in close agreement with GLE/MP's results. The computed three-dimensional factors of safety for all scenarios and corresponding column graph for comparison can be seen in Appendix 3 and Appendix 4, respectively.

Comparison of two and three-dimensional analyses in terms of the factor of safety has been made. The three-dimensional safety factors for each method and for all scenarios have been found to be higher than the two-dimensional analyses results (Appendix 5). Janbu's simplified method has achieved the least and the most difference by % 9.4 and % 59.7, respectively. Bishop's, Spencer's and GLE/MP's methods have produced % 12.6, % 11.4 and % 12.2 difference at the least, respectively. In scenario-*p*, where all of the methods generated the most difference, they are all in close agreement with Janbu's simplified method between % 53.0 and % 56.3. The difference is significantly higher if external loadings applied or high elevation water table with ponded water exist. The most difference has occurred in high elevation water table with ponded water at front and external loadings on top of the slope. Where the stability controlled only by seismic activity, the least difference between 2D and 3D was generated. Appendix 6 shows the percentage difference between two and three-dimensional analyses for all of the scenarios.

For 2D analyses, US Army Corps. of Engineers method have overestimated the safety factor by % 37.5 in scenario-*n*. Duncan et al. [85] have indicated that assumptions about interslice

forces affect the computed safety factors in some cases, drastically. This special case includes the representation of forces between slices as total or effective forces. In case of the total force, the effective stresses and the water pressure computed as a whole vector. While in case of the effective force, water pressure considered separately. The problem arises in force equilibrium methods such as US Army Corps. of Engineers when total forces are used in the stability analysis for simplicity. Normally, the inclination of water pressure is horizontal, therefore the assumption of inclined water pressure in total forces overestimates the factor of safety by up to % 60. However, using a rigorous method overcomes this problem [85]. Janbu's simplified method has generated underestimated safety factors by up to % 20. This method assumes that interslice forces act horizontally, thus shear forces between slices are not taking into account and overall moment equilibrium is not satisfied. These limitations of the method generate a conservative factor of safety. Janbu introduced correction factors to overcome the limitations; but in scenarios where external loadings applied on to the slope, the method still generated conservative results between % 7.8 and % 14.7.

5.2 Hypothetical Case II

In this case, the inclination of the failure surface from toe to crest is 15° steeper than the Case I. In 2D analyses, the differences for the factors of safety between Spencer's method and GLE/MP's method were found to be less than % 1 for all the scenarios. The ordinary method of slices (OMS) have generated up to % 4.9 less than the GLE/MP's method in 16 of 20 cases. However, in the other 4 cases which the stability of the slope generally controlled by high pore-water pressures, the OMS have overestimated the factor of safety between % 30.1 - % 33. Although Bishop's method does not satisfy all static equilibrium it has retained its accuracy by ± % 2.5 for all the scenarios. US Army Corps. of Engineers method has generated overestimated safety factors for the same scenarios as the Case I between % 23.8 - % 29.8 but the differences between the other scenarios are insignificantly small. Lowe & Karafiath's method has failed to converge in four of the scenarios and yielded % 32.5 more than the GLE/MP's result in only two scenarios; where Corps. of Engineer's method also overestimated the safety factor by % 23.8. Janbu's simplified method has generated underestimated factors of safety in all scenarios and it is most significant in scenario-*l* and *m* by % 10.4. However, Janbu's corrected method produced fairly accurate results for eighteen of the twenty scenarios; slightly lower safety factors by % 5.4 for scenario-*l* and *m* was produced. Also, the external loadings on top of the slope did not affect

the factors of safety for all the scenarios within % 0.01 accuracy. The results of the analyses and the corresponding graph of the safety factors versus scenarios are given in Appendix 7 and Appendix 8, respectively.

In three-dimensional analyses, Spencer's and GLE/MP's methods have failed to converge ten times while Bishop's and Janbu's methods converged in all of the scenarios. Spencer's and Bishop's method has generated similar values with GLE/MP's method. When high elevation water table with ponded water at front of the slope controls the overall stability of the slope, Bishop's method produced % 6.3 - % 6.7 higher safety factors. Janbu's simplified method has generated lower factors of safety in all scenarios. Especially, in scenarios with high elevation water table with ponded water at the front, the method has produced % 20.2 - % 34.1 lower factors of safety. The results of the computations for three-dimensional analyses and the corresponding column graph between each method were given in Appendix 9 and Appendix 10, respectively.

Comparison of factors of safety in two and three-dimensional methods for hypothetical case II has been made, and the results were somewhat intriguing. All of the four methods in three-dimensions have generated higher factors of safety than two-dimensional version; where drained condition with seismic activity or external loads controls the stability of the slope. Also, the same outcome is also valid in which low elevation water table exists. The difference was found to be between % 7.8 and % 16.7 higher than the results of two-dimensional analyses. However, when high elevation water table with ponded water was applied to the slope, the three-dimensional safety factors were found to be drastically higher than two-dimensional safety factors between % 327.5 and % 541.2. This outcome has decreased between % 218.7 and % 289.3 when earthquake-induced forces applied to the slope. These results were inspected carefully, and the analyses were repeated several times. However, the outcome was the same as before which is questionable because two-dimensional results were not increased drastically with increased elevation in ponded water as this was the situation with three-dimensional results. Also, when high elevation water table without ponded water applied, the three-dimensional factors of safety were found to be less than two-dimensional safety factors between % 4.1 and % 24.5, except Spencer's method. The computed two and three-dimensional factors of safety for each method and the difference in percentage between them has been given in Appendix 11 and Appendix 12, respectively.

US Army Corps. of Engineers method have overestimated the safety factor by up to % 29.8 in scenario-*n, p, r, s*. This result has generated from the same reason as the hypothetical case I; where the water pressure assumed to act at an angle between slices. The OMS also generated overestimated factors of safety between % 30 and % 33. The value of the base normal stress increased with steepening of the slice base, eventually overestimating the overall available shear strength; which resulted in a non-conservative factor of safety. The comparison of base normal & effective stresses and shear strengths & stresses between OMS and Morgenstern-Price's method has been given in Appendix 13 and Appendix 14, respectively. Janbu's simplified procedure satisfies only force equilibrium and interslice shear forces are not taken into account, which results in the underestimation of the safety factor in almost all of the scenarios. Lowe & Karafiath's method satisfy only force equilibrium condition and overestimated factors of safety by % 32.5 in scenarios where high pore-water pressure exists. The reason for that may be related to taking the forces between slices as total forces, and not as effective forces. However, the uncertainty for this overestimation remains.

5.3 Hypothetical Case III

For 2D analyses, Spencer's and GLE/MP's method did not yield close values as the previous cases. However, the difference is so small that it does not indicate a practical sense; with an average of % 2.4 and maximum of % 5.2. Janbu's simplified and corrected method has underestimated the safety factor in all scenarios by up to % 40 and % 37.2, respectively. US Army Corps of Engineers method has underestimated the factor of safety by up to % 20.3 when seismic activity applied to the slope. Also, the method has overestimated the safety of the slope by % 19 when only high elevation ponded water exists without external forces. Lowe & Karafiath's method has generated a similar pattern with US Army Corps of Engineer's method. The factor of safety has been underestimated between % 8.1 and % 10.9 under seismic activity. Also, the method has overestimated the safety factor by up to % 17.6 in scenarios with high elevation ponded water. Sarma's normal and non-vertical slices methods have generated underestimated safety factors in all of the scenarios by up to % 24.1 and % 35.9, respectively. The underestimation of the safety factor especially exists under seismic activity. The calculated safety factors for overall scenarios and the corresponding column graph are given in Appendix 15 and Appendix 16, respectively.

In three-dimensional analyses, Janbu's simplified method has generated underestimated safety factors in all of the scenarios by as much as % 30.4. However, the factors of safety

between GLE/MP's method and Janbu's simplified method are in relatively close agreement between % 2.3 and % 6.5; where high elevation water table controls the overall stability of the slope. Spencer's method has produced considerably similar results with GLE/MP's method. The most different results found to be in the scenario with only high elevation GWT (scenario-*j*) and high elevation GWT with ponded water in front under seismic activity (scenario-*r*); the outcome is % 9.5 and % 13.3 higher, respectively. The results of the computations for three-dimensional analyses and the corresponding column graph between each method were given in Appendix 17 and Appendix 18, respectively.

The outcomes of two and three-dimensional analyses have been compared (Appendix 19). All of the three-dimensional analyses have generated lower safety factors than the two-dimensional analyses. The least difference between 2D and 3D safety factors has been found in scenario-*c*; where low elevation GWT and external loadings applied to the slope. However, GLE/MP's method, Janbu's simplified and Spencer's method has generated underestimated safety factors in three dimensions by up to % 69.2, % 55.7 and % 69.6, respectively. The difference of the factors of safety in percentage between two and three-dimensional analyses has been given in Appendix 20.

US Army Corps of Engineers method has generated nonconservative safety factors for the same conditions applied to the previous cases. The assumption of total forces instead of effective forces between slices eventually caused the overestimation of the factors of safety. Sarma's non-vertical slices method yielded % 9 – 10 higher safety factors in all scenarios where the convergence has been achieved. This is the only case, the method has generated overestimated safety factors. Even though detailed investigations have been done about this outcome, no specific reasons have been detected. Although, the shape of the distribution of interslice shear forces is an assumption in this method [131], and its effects need to be investigated further. In addition, the non-vertical slices methods are known to generate incorrect answers if the direction of movement between slices are not considered properly, especially where the slip surface contains a reverse curvature [223].

5.4 Hypothetical Case IV

In this case, the static condition of the dam profile without the effect of pore-water pressure and external loadings has been investigated. The effect of an earthquake-induced forces has also been analyzed. In 2D analyses, the difference between Spencer's and GLE/MP's method has reached the maximum by % 14.4 when the seismic activity has been implemented. US Army Corps of Engineers have overestimated the factors of safety for

static and dynamic condition by up to % 16.5 and % 32.8, respectively. Sarma's method has generated similar results for the static condition but yielded % 9.3 higher safety factor for the dynamic condition. Janbu's corrected method has generated slightly lower values for both cases while Lowe & Karafiath's method yielded almost the same factor of safety for the static condition and similar value for the dynamic condition as Janbu's corrected. Janbu's simplified method has underestimated the safety factor between % 10.2 and % 11.1. However, Sarma's non-vertical slices method has generated almost the same value for both scenarios with % 1.7 difference from GLE/MP's solution. The column graph of methods versus factor of safety is given in Appendix 21.

In three-dimensional analyses, Janbu's simplified method has generated lower safety factors from GLE/MP's method between % 9.1 and % 9.8. Spencer's method has produced % 13.8 higher factor of safety under seismic activity. The outcome of 3D analyses in terms of percentage difference is quite similar to the two-dimensional analyses. The results of the computations have been given in column graph for better clarity in Appendix 22.

The results of the two and three-dimensional calculations have been compared (Appendix 23). The difference between both analyses is found to be quite similar. Janbu's simplified method has generated almost the same factor of safety as in two-dimensional analyses, only % 0.2 higher than 2D safety factor. Spencer's and GLE/MP's method has produced similar results with two-dimensional analyses; which is only % 1.8 and % 1.3 lower than 2D, respectively. The difference of factors of safety in percentage between two and three-dimensional analyses are given in a column graph in Appendix 24.

The safety factors between Morgenstern & Price's procedure and Spencer's method has reached the maximum difference by % 14.4 under dynamic condition. The reason is not clear as both methods satisfy all kind of equilibrium condition and this is the only case that showed up this outcome. US Army Corps. of Engineers method have overestimated the factor of safety under both static and dynamic condition due to high inclination of inter-slice forces. Janbu's simplified method has underestimated the factor of safety for both scenarios due to the assumption of horizontal inter-slice forces and lack of overall moment equilibrium.

5.5 Hypothetical Case V

For 2D analyses, the difference between Spencer's method and GLE/MP's method is insignificantly small, less than % 1. Sarma's normal and non-vertical slices method has generated slightly lower safety factors by an average of % 1.5 – % 3.3, respectively. Janbu's corrected and simplified methods have underestimated the factor of safety in all cases by up

to % 17, % 23 with an average of % 14, %21, respectively. Lowe & Karafiath's method has generated both lower and higher safety factors by % 8 and % 6.7, respectively. US Army Corps of Engineers method has overestimated the safety factor by up to % 60 in the same scenarios as before; where high elevation water table and ponded water control the overall stability of the slope. The calculated factors of safety and the corresponding graph are given in Appendix 25 and Appendix 26, respectively.

In three-dimensional analyses, Spencer's method has produced similar safety factors with GLE/MP's method with a maximum difference of % 1.6. Janbu's simplified method has underestimated the factor of safety in all of the scenarios. The maximum difference from GLE/MP's results was 22.1 per cent and with an average difference of 18.9 per cent. Also, the outcome is similar to 2D analyses in terms of percentage difference. The results of the computations and the corresponding column graph has been given in Appendix 27 and Appendix 28, respectively.

The computed factors of safety for two and three-dimensional analyses have been compared (Appendix 29). In all of the scenarios, three-dimensional computations have generated lower safety factors than the two-dimensional analyses. Janbu's simplified method has produced the least difference within three methods between % 0.5 and % 3.5. GLE/MP's has produced the most difference between % 2 and % 6.4. While Spencer's method has generated between % 1.2 and % 4.8 less than two-dimensional results. The difference in factors of safety between two and three-dimensional analyses has been given in a column graph in Appendix 30.

US Army Corps. of Engineers method have overestimated the factor of safety by up to % 60 for the same scenarios as previously. The assumption of total forces between slices instead of effective forces has generated high values for the safety factor. This outcome can be reduced by decreasing the inclination of forces between slices. Janbu's methods have underestimated the factors of safety in all scenarios. The assumption of forces between slices acting horizontally eventually caused the conservative factors of safety. Also, the slip surface has many planar sections instead of smooth circular regions, this condition is also known to exaggerate the outcome [85].

5.6 Case VI

Differing from the others, this case was a real case study from Denizkonak (Cide, Kastamonu) region at which an area exposed to a landslide. After the field observations and the inspection of the several photographs and models, it was determined that at least two

landslides occurred during the past years. Based on the laboratory testing, field observations and literature reviews, input parameters for the stability analyses were determined. The cross-section for the previous topography was estimated based on the field observations and the cross-section of the current time. The results of the two-dimensional analyses indicated that the very first instability has occurred at GSI value of 20 with a pore-pressure ratio of at least 0.44. However, according to the back analyses, the second landslide has not occurred at a pore-pressure ratio of 0.44. It was estimated that a ratio of 0.24 was enough for the second instability. The current topography was also investigated, and it was found that if the pore-pressure ratio exceeds 0.33, a relatively large landslide was expected. In both of the back analyses, 2D results have generated more conservative safety factors than the 3D outcomes, which eventually reflected as the difference in the pore-pressure ratios to maintain the static equilibrium.

6. CONCLUSIONS AND RECOMMENDATIONS

According to this thesis work, some recommendations for designing slopes using limit equilibrium procedures, in both two and three-dimensions, were made in this and the following paragraph. Planning of a men-made earthworks are generally done by using two-dimensional procedures. Within the scope of this thesis, this can be clearly said that for two-dimensional procedures, Spencer's and Morgenstern & Price's methods can be used with confidence in almost all instances with various types of slip surfaces and geological features. The same recommendation is also valid for Bishop's method but strictly restricted to circular slip surfaces. The remaining methods should only be used very cautiously.

Using three-dimensional methods for design purposes are not widely accepted in the time frame of this thesis work. Also, case studies with three-dimensional solutions are seldom seen in the literature. It will be much proper to judge three-dimensional analyses with increasing usage in practice. However, some notable conclusions can be made from this thesis. Three-dimensional analyses should be strictly avoided on slopes under the effect of high pore-water pressures with or without deep ponded water in front of the slope. Also, if any external loadings are present on a homogeneous slope, the three-dimensional methods should not be used. In addition, Spencer's, Bishop's and Morgenstern & Price's methods can be used in three-dimensional analysis, under the conditions of low or no pore-water pressure with or without ponded water in front of the slope. In general, the usage of three-dimensional methods should be preferably used in simple problems.

Also, based on the results of all slope stability analyses carried out in this thesis, to highlight some general issues, the following notable results and conclusions can be drawn. In addition, for each case, detailed results and discussions were also added to this section.

- Three-dimensional limit equilibrium analyses provide a more realistic approach to the slope stability problems. Slope and slip surface geometry including geological structures must be precisely determined in order to achieve an accurate result. However, this is not always possible in natural instabilities with a complex geology. If it is done so, the results from 3D analyses can be truly trusted and be more economical.
- In contrast to the literature, the factor of safety in the three-dimensional analysis was not always found to be unconservative. The reason for this outcome can be highly related to the assumption of the shear strength was zero, where tensile stresses occurred to avoid negative strength values.

- If external loading is not located on the sliding mass, its effects are impractically small or non-existent both in 2D and 3D.
- U.S. Army Corps. of Engineer's method should not be used where overall stability of a slope is controlled by ponded water since it exaggerates the safety factor.
- Fellenius's method is known to be very conservative, yet it has generated unconservative results where the inclination was steep and high pore-water pressures existed.
- Application of external loadings leads three-dimensional analyses to generate unconservative results.
- The effects of deep ponded water and high pore-water pressures were generally exaggerated in three-dimensional analyses.
- Only 4 out of 656 individual computations in two-dimensions and 14 out of 286 computations in three-dimensions had failed to converge within % 0.1 and % 1 accuracy.

7. REFERENCES

[1] Voight, B., "Time scale for the first movements of the May 18 eruption.," in *Prof. Pab. U.S. Geol. Surv.*, pp. 69–86, **1981.**

[2] Stoffel, D. B., and Stoffel, K. L, "Private communication with Voight, B.," **1980**.

[3] Voight, B., Glicken, H., Janda, R. J., and Douglas, P. M., "Catastrophic rockslide-avalanche of May 18.," in *Prof. Pab. U.S. Geol. Surv.*, pp. 347–377, **1981.**

[4] Voight, B., Janda, R. J., Glicken, H., and Douglas, P. M., "Nature and mechanics of the Mount St Helens rockslide-avalanche of 18 May 1980," *Géotechnique*, vol. 33, no. 3, pp. 243–273, **1983**.

[5] Lipman, P. W., Moore, J. G., and Swanson, D. A., "Bulging of the north flank before the May 18 eruption: geodetic data," in *Prof. Pab. U.S. Geol. Surv.*, pp. 143–156, **1981**.

[6] Hovland, H. J., "Three-dimensional slope stability analysis method.," *J. Soil Mech. Fdns. Div. Am. Soc. Civ. Engrs*, vol. 103, no. GT 9, pp. 971–986, **1977**.

[7] Kanamori, H. and Given, J. W. , "Analysis of long-period seismic waves excited by the May 18, 1980, eruption of Mount St. Helens - a terrestrial monopole," *J. Geophys. Res.*, vol. 87, no. B7, pp. 5422–5432, **1982**.

[8] Malone S. D., Endo, E.C., Weaver, S., and Ramey, J. W., "Seismic monitoring for eruption prediction," in *Prof. Pab. U.S. Geol. Surv.*, pp. 803–813, **1981.**

[9] Malone, S., "Private communication with Voight, B., from Broomhead [94]." **1982**.

[10] Malone, S., "Private communication with Voight, B. based on information supplied by Stewart Smith," **1980**.

[11] Genevois R., and Ghirotti, M., "The 1963 Vaiont Landslide," *G. di Geol. Appl.*, vol. 1, pp. 41–52, **2005**.

[12] Mencl, V., "Mechanics of Landslides with Non-Circular Slip Surfaces with Special Reference to the Vaiont Slide," *Géotechnique*, vol. 16, no. 4, pp. 329–337, **1966**.

[13] Hendron A. J., and Patton, F. D., "The Vaiont Slide, a Geotechnical Analysis Based on New Geologic Observations of the Failure Surface," Vicksburg, MS., **1985**.

[14] Semenza E., and Ghirotti, M., "History of the 1963 Vaiont slide: the importance of geological factors," *Bull. Eng. Geol. Environ.*, vol. 59, no. 2, pp. 87–97, **2000**.

[15] Loo, K. Y., Lee, C. F., and Gelinas, P., "Alternative Interpretation of the Vaiont Slide," in *Proc. 13th Symp. on Rock Mechanics*, pp. 595–623, **1972**.

[16] Janbu, N.,"Application of composite slip surface for stability analysis," in *European Conference on Stability of Earth Slopes*, **1954**.

[17] Chowdhury, R., "Analysis of the vajont slide - new approach," *Rock Mech. Felsmechanik Mec. des Roches*, vol. 11, no. 1, pp. 29–38, **1978**.

[18] Skempton A.W., and Vaughan, P.R., "The failure of Carsington Dam," *Géotechnique*, vol. 43, no. 1, pp. 151–173, **1993**.

[19] Vaughan, P.R., "Stability analysis of deep slides in brittle soils - lessons from Carsington," in *Slope Stability Engineering*, pp. 1–11, **1991**.

[20] Mitchell, J. K., Seed, R. B., and Seed, H. B., "Kettleman Hills Waste Landfill Slope

Failure. I: Liner-System Properties," *J. Geotech. Eng.*, vol. 116, no. 4, pp. 647–668, **1990**.

[21] Seed, R. B., Mitchell, J. K., and Seed, H. B., "Kettleman Hills Waste Landfill Slope Failure. II: Stability Analyses," *J. Geotech. Eng.*, vol. 116, no. 4, pp. 669–690, **1990**.

[22] Chang, M., "Three-dimensional stability analysis of the Kettleman Hills landfill slope failure based on observed sliding-block mechanism," *Comput. Geotech.*, vol. 32, no. 8, pp. 587–599, **2005**.

[23] Crosta, G. B., "Failure and flow development of a complex slide: The 1993 Sesa landslide," *Eng. Geol.*, vol. 59, no. 1–2, pp. 173–199, **2001**.

[24] Bromhead, E. N., Ibsen, M. L., Papanastassiou, X., and Zemichael, A. A., "Three-dimensional stability analysis of a coastal landslide at Hanover Point, Isle of Wight," *Q. J. Eng. Geol. Hydrogeol.*, vol. 35, pp. 79–88, **2002**.

[25] Hungr, O. "An Extension of Bishop's simplified method of slope stability analysis to three dimensions.," *Géotechnique*, vol. 37, No. 1, pp. 113–117, **1987**.

[26] Dapporto, S., Rinaldi, M., Casagli, N., and Vannocci, P., "Mechanisms of riverbank failure along the Arno River, Central Italy," *Earth Surf. Process. Landforms*, vol. 28, no. 12, pp. 1303–1323, **2003**.

[27] Koçkar, M., and Akgün, H., "Engineering geological investigations along the Ilıksu Tunnels, Alanya, southern Turkey," *Eng. Geol.*, vol. 68, no. 3–4, pp. 141–158, **2003**.

[28] Bieniawski, Z. T., *Engineering Rock Mass Classification*. New York: John Wiley and Sons, INC., **1989**.

[29] Leynaud, D. , Mienert, J., and Nadim, F., "Slope stability assessment of the Helland Hansen area offshore the mid-Norwegian margin," *Mar. Geol.*, vol. 213, no. 1–4, pp. 457–480, **2004**.

[30] Onder Cetin, K., Isik, N., and Unutmaz, B., "Seismically induced landslide at Degirmendere Nose, Izmit Bay during Kocaeli (Izmit)-Turkey earthquake," *Soil Dyn. Earthq. Eng.*, vol. 24, no. 3, pp. 189–197, **2004**.

[31] Işk, N. S., Doyuran, V., and Ulusay, R., "Assessment of a coastal landslide subjected to building loads at Sinop, Black Sea region, Turkey, and stabilization measures," *Eng. Geol.*, vol. 75, no. 1, pp. 69–88, **2004**.

[32] Kentli B., and Topal, T., "Assessment of rock slope stability for a segment of the Ankara-Pozant motorway, Turkey," *Eng. Geol.*, vol. 74, no. 1–2, pp. 73–90, **2004**.

[33] Teoman, M. B., Topal, T., and Işik, N. S., "Assessment of slope stability in Ankara clay: A case study along E90 highway," *Environ. Geol.*, vol. 45, no. 7, pp. 963–977, **2004**.

[34] Apuani, T., Corazzato, C., Cancelli, A., and Tibaldi, A. , "Stability of a collapsing volcano (Stromboli, Italy): Limit equilibrium analysis and numerical modelling," *J. Volcanol. Geotherm. Res.*, vol. 144, no. 1–4 SPEC. ISS., pp. 191–210, **2005**.

[35] Crosta, G. B., Imposimato, S., Roddeman, D., Chiesa, S., and Moia, F., "Small fast-moving flow-like landslides in volcanic deposits: The 2001 Las Colinas Landslide (El Salvador)," *Eng. Geol.*, vol. 79, no. 3–4, pp. 185–214, **2005**.

[36] Singh, R., Roy, D., and Jain, S. K. "Analysis of earth dams affected by the 2001 Bhuj Earthquake," *Eng. Geol.*, vol. 80, no. 3–4, pp. 282–291, **2005**.

[37] Neuffer D. P., and Schultz, R. A., "Mechanisms of slope failure in Valles Marineris, Mars," *Q. J. Eng. Geol. Hydrogeol.*, vol. 39, no. 3, pp. 227–240, **2006**.

[38] Gens, A. and Alonso, E. E., "Aznalcóllar dam failure. Part 2: Stability conditions and failure mechanism," *Géotechnique*, vol. 56, no. 3, pp. 185–201, **2006**.

[39] Bilgehan R. P., and Kiliç, R., "The landslides threatening Tasova town (Central Anatolia, Turkey) and their environmental impacts," *Environ. Geol.*, vol. 55, no. 1, pp. 179–190, **2007**.

[40] Chugh, A. K., Stark, T. D., and DeJong, K. A., "Reanalysis of a municipal landfill slope failure near Cincinnati, Ohio, USA," *Can. Geotech. J.*, vol. 44, no. 1, pp. 33–53, **2007**.

[41] Ulusay, R., Aydan, Ö., and Kilic, R., "Geotechnical assessment of the 2005 Kuzulu landslide (Turkey)," *Eng. Geol.*, vol. 89, no. 1–2, pp. 112–128, **2007**.

[42] Steiakakis, E., Kavouridis, K., and Monopolis, D. "Large scale failure of the external waste dump at the 'South Field' lignite mine, Northern Greece," *Eng. Geol.*, vol. 104, no. 3–4, pp. 269–279, **2008**.

[43] Özdemir, A., and Delikanli, M., "A geotechnical investigation of the retrogressive Yaka Landslide and the debris flow threatening the town of Yaka (Isparta, SW Turkey)," *Nat. Hazards*, vol. 49, no. 1, pp. 113–136, **2009**.

[44] Arikan, F., Yoleri, F., Sezer, S., Caglan, D., and Biliyul, B., "Geotechnical assessments of the stability of slopes at the Cakmakkaya and Damar open pit mines (Turkey): A case study," *Environ. Earth Sci.*, vol. 61, no. 4, pp. 741–755, **2009**.

[45] Kohv, M., Talviste, P., Hang, T., and Kalm, V., "Retrogressive slope failure in glaciolacustrine clays: Sauga landslide, western Estonia," *Geomorphology*, vol. 124, no. 3–4, pp. 229–237, **2010**.

[46] Sharifzadeh, M., Sharifi, M., and Delbari, S. M., "Back analysis of an excavated slope failure in highly fractured rock mass: The case study of Kargar slope failure (Iran)," *Environ. Earth Sci.*, vol. 60, no. 1, pp. 183–192, **2010**.

[47] Wei, L., Koutnik, T., and Woodward, M., "A slope stability case study by limit equilibrium and finite element methods," in *GeoFlorida 2010: Advanced in Analysis, Modeling & Design*, pp. 3090–3099, **2010**.

[48] Tutluoglu, L., Ferid Öge, I., and Karpuz, C., "Two and three dimensional analysis of a slope failure in a lignite mine," *Comput. Geosci.*, vol. 37, no. 2, pp. 232–240, **2011**.

[49] Xie, M., Wang, Z., Liu, X., and Xu, B., "Three-dimensional critical slip surface locating and slope stability assessment for lava lobe of Unzen volcano," *J. Rock Mech. Geotech. Eng.*, vol. 3, no. 1, pp. 82–89, **2011**.

[50] Kayabasi, A., and Gokceoglu, C., "Coal mining under difficult geological conditions: The Can lignite open pit (Canakkale, Turkey)," *Eng. Geol.*, vol. 135–136, pp. 66–82, **2012**.

[51] Leong, E. C., and Rahardjo, H., "Two and three-dimensional slope stability reanalyses of Bukit Batok slope," *Comput. Geotech.*, vol. 42, pp. 81–88, **2012**.

[52] Fellenius, W., "Calculation of the stability of earth dams," in *Transactions of the Second Congress on Large Dams, International Commission on Large Dams of the World Power Conference, Vol. 4*, pp. 445–462, **1936**.

[53] Bishop, A. W., "The use of the Slip Circle in the Stability Analysis of Slopes," *Géotechnique*, vol. 5, no. 1, pp. 7–17, **1955**.

[54] Janbu, B., Bjerrum, N., Kjaernsli, L., "Soil mechanics applied to some engineering problems," *Nor. Geotech. Institute, Publ. 16*, vol. Chapters 1, **1956**.

[55] Spencer, E., "Thrust line criterion in embankment stability analysis," *Géotechnique*, vol. 23, no. 1, pp. 85–100, **1973**.

[56] Morgenstern, N. R., and Price, V. E., "The Analysis of the Stability of General Slip Surfaces," *Géotechnique*, vol. 15, no. 1, pp. 79–93, Mar. **1965**.

[57] Fredlund, D. G., Krahn, J., and Pufahl, D. E., "The Relationship between Limit Equilibrium Slope Stability Methods," in *Proc. Int. Conf. Soil Mech. Found. Eng. Vol 3.*, pp. 409–416, **1981**.

[58] Singh, R., Umrao, R. K., and Singh, T. N., "Stability evaluation of road-cut slopes in the Lesser Himalaya of Uttarakhand, India: Conventional and numerical approaches," *Bull. Eng. Geol. Environ.*, vol. 73, no. 3, pp. 845–857, **2013**.

[59] Alemdag, S., Akgun, A., Kaya, A., and Gokceoglu, C., "A large and rapid planar failure: Causes, mechanism, and consequences (Mordut, Gumushane, Turkey)," *Arab. J. Geosci.*, vol. 7, no. 3, pp. 1205–1221, **2013**.

[60] Ozcan, N. T., Ulusay, R., and Isik, N. S., "A study on geotechnical characterization and stability of downstream slope of a tailings dam to improve its storage capacity (Turkey)," *Environ. Earth Sci.*, vol. 69, no. 6, pp. 1871–1890, **2013**.

[61] Ozbay A., and Cabalar, A. F., "FEM and LEM stability analyses of the fatal landslides at Çöllolar open-cast lignite mine in Elbistan, Turkey," *Landslides*, vol. 12, no. 1, pp. 155–163, **2014**.

[62] Alemdag, S., Kaya, A., Karadag, M., Gurocak, Z., and Bulut, F., "Utilization of the limit equilibrium and finite element methods for the stability analysis of the slope debris: An example of the Kalebasi District (NE Turkey)," *J. African Earth Sci.*, vol. 106, pp. 134–146, **2015**.

[63] Topsakal, E., and Topal, T., "Slope stability assessment of a re-activated landslide on the Artvin-Savsat junction of a provincial road in Meydancik, Turkey," *Arab. J. Geosci.*, vol. 8, no. 3, pp. 1769–1786, **2015**.

[64] Babanouri, N., and Dehghani, H., "Investigating a potential reservoir landslide and suggesting its treatment using limit-equilibrium and numerical methods," *J. Mt. Sci.*, vol. 14, no. 3, pp. 432–441, **2017**.

[65] Kliche, C. A., *Rock Slope Stability*. Littleton, CO, USA: Society for Mining, Metallurgy, and Exploration, Inc. (SME), **1999**.

[66] Ulusay, R., *Sevlerin Durayliligi ve Tasarimi, JEM619 Lecture Notes*. Ankara, **2008**.

[67] Lambe T. W., and Whitman, R. V., *Soil Mechanics*, SI Version. Singapore: John Wiley and Sons, INC., **1979**.

[68] Hoek E., and Brown, E. T., "Empirical Strength Criterion for Rock Masses," *Journal of the Geotechnical Engineering Division*, vol. 106, no. GT9. pp. 1013–1035, **1980**.

[69] Hoek, E., "Strength of jointed rock masses," *Geotechnique*, vol. 23, no. 3, pp. 187–223, **1983**.

[70] Hoek, E., and Brown, E. T., "The Hoek Brown failure criterion - a 1988 update,"

15th Canadian Rock Mechanics Symposium. pp. 31–38, **1988**.

[71] Hoek, E., Wood, D., and Shah, S., "Modified Hoek-Brown failure criterion for jointed rock masses," in *Proc. Rock Characterization, Symp. Int. Soc. Rock Mech.: Eurock '92*, pp. 209–214, **1992**.

[72] Hoek, E., "Strength of rock and rock masses," *ISRM News J.*, vol. 2, no. 2, pp. 4–16, **1994**.

[73] Hoek, E., and Brown, E. T., "Practical estimates of rock mass strength," *Int. J. Rock Mech. Min. Sci. Geomech. Abstr.*, vol. 34, no. 8, pp. 1165–1186, **1997**.

[74] Sonmez, H., and Ulusay, R., "Modifications to the geological strength index (GSI) and their applicability to stability of slopes," *Int. J. Rock Mech. Min. Sci.*, vol. 36, no. 6, pp. 743–760, **1999**.

[75] Sonmez, H., and Ulusay, R., "A discussion on the Hoek-Brown failure criterion and suggested modification to the criterion verified by slope stability case studies," *Yerbilim.*, vol. 26, pp. 77–99, **2002**.

[76] Hoek, E., Carranza, C., and Corkum, B., "Hoek-brown failure criterion – 2002 edition," in *Proc. Narms-Tac Conference*, pp. 267–273, **2002**.

[77] Hoek, E., Kaiser, P. K., and Bawden, W. F., *Support of underground excavations in hard rock*. Rotterdam, Balkema, **1995**.

[78] Hoek, E., Marinos, P., and Benissi, M., "Applicability of the geological strength index (GSI) classification for very weak and sheared rock masses. The case of the Athens Schist Formation," *Bull. Eng. Geol. Environ.*, vol. 57, no. 2, pp. 151–160, **1998**.

[79] Marinos, P., and Hoek, E., "GSI: A geologically friendly tool for rock mass strength estimation," *Proc. GeoEng2000 Conf.*, pp. 1422–1442, **2000**.

[80] Balmer, G., "A general analytical solution for Mohr's envelope," *Am. Soc. Test. Mat.*, vol. 52, pp. 1260–1271, **1952**.

[81] Huang, Y. H., *Slope Stability Analysis by the Limit Equilibrium Method: Fundamentals and Methods*. Reston, Virginia: American Society of Civil Engineers, **2014**.

[82] Fellenius, W., "Kaj-och jordrasen i Goteborg," *Tek. Tidskr. V.U.*, vol. 48, pp. 17–19, **1918**.

[83] Fellenius, W., "Staten Jarnjvagars Geoteknniska Commission," **1922**.

[84] Abramson, W. Lee, Lee, S. Thomas, Sharma, S., and Boyce, G. M., *Slope Stability and Stabilization Methods*. John Wiley and Sons, INC., **1996**.

[85] Duncan, J. M., Wright, S. G., and Brandon, T. L., *Soil Strenght and Slope Stability*, Second Edi. New Jersey: John Wiley and Sons, INC., **2014**.

[86] Fellenius, W., "Erdstatische Berechnungen mit Reibung und Kohasion," **1927**.

[87] Whitman, R. V., and Bailey, W. A., "Use of computers for slope stability analysis," *J. Soil Mech. Found. Div. Proc. ASCE*, vol. 93, no. SM4, pp. 475–498, Jul. **1967**.

[88] Turnbull, W. J., and Hvorslev, M. J., "Special problems in slope stability," *J. Soil Mech. Found. Div.*, vol. 93, no. SM4, pp. 499–528, Jul. **1967**.

[89] Bishop, A. W., "The Stability of Earth Dams," University of London, **1952**.

[90] Kenney, T. C., “An examination of the methods of calculating the stability of slopes.,” University of London, **1956**.

[91] Spencer, E., “A methof of analysis of the stability of embankments assuming parallel inter-slice forces,” *Géotechnique*, vol. 17, pp. 11–26, **1967**.

[92] Janbu, N., “Slope Stability Computations,” *Publ. Wiley Sons, Inc.*, pp. 47–86, **1973**.

[93] Sarma, S. K., “Stability analysis of embankments and slopes,” *J. Geotech. Eng. Div.*, vol. 105, no. GT-5, pp. 1511–1524, **1979**.

[94] Bromhead, E. N., *The Stability of Slopes*, Second Edi. Suffolk: Blackie Academic & Professional. An Imprint of Chapman & Hall, **1992**.

[95] Sarma, S. K., “Stability analysis of embankments and slopes,” *Géotechnique*, vol. 23, no. 3, pp. 423–433, **1973**.

[96] Chen, Z.-Y., and Morgenstern, N. R., “Extensions to the generalized method of slices for stability analysis,” *Can. Geotech. J.*, vol. 20, no. 1, pp. 104–119, **1983**.

[97] U.S. Army Corps. of Engineers, “Stability of slopes and foundations: Engineering manual.,” Viksburg, MS., **1967**.

[98] U.S. Army Corps. of Engineers, “Engineering and Design: Stability of Earth and Rock-Fill Dams, Engineer Manual EM 1110-2-1902,” Washington, DC, **1970**.

[99] U.S. Army Corps. of Engineers, “Engineering and Design: Slope Stability,” **2003**.

[100] Lowe, J., and Karafiath, L., “Stability of earth dams upon drawdown,” in *Proc. 1st Pan-American Conf. Soil Mech and Foundation Eng.*, pp. 537–552, **1960**.

[101] Maksumovic, M., “A new method of slope stability analysis. From a private communication with E. N. Bromhead.,” **1970**.

[102] Bailey, W. A., and Christian, J. T., “ICES-LEASE-I: A problem-oriented language for slope stability analysis.,” *MIT Soil Mech. Publ.*, no. No: 235, **1969**.

[103] Terzaghi, K., and Peck, R. B., *Soil Mechanics in Engineering Practice*. New York: Wiley, **1967**.

[104] Correia, R. M., “A limit equilibrium method for slope stability analysis.,” in *Proc. 5th Internatinal Symp. on Landslides Vol 1*, pp. 595–598, **1988**.

[105] Chugh, A. K., “Slope Stability Analaysis for Earthquakes.,” *Int. J. Numer. Anal. Methods Geomech.*, Vol 6, pp. 307–322, **1982**.

[106] Law, K. T., and Lumb, P., “A Limit Equilbirium Analysis of Progressive Failure in the Stability of Slopes” *Can. Geotech. J.*, Vol. 15, No. 1, pp. 113–122, **1978**.

[107] Leshchinsky, D., “Slope stability analysis: generalized approach,” *J. Geotech. Eng.*, vol. 116, no. 5, pp. 851–867, **1990**.

[108] Baker, R., and Garber, M., “Theoretical analysis of the stability of slopes.,” *Géotechnique*, vol. 28, no. 4, pp. 395–411, **1978**.

[109] Greenwood, J. R., “A Simple Approach to Slope Stability,” *Gr. Eng.*, vol. 16, no. 4, pp. 45–48, **1983**.

[110] Skempton, A. W., “The ϕ=0 analysis of stability and its theoretical basis.,” in *Proc. 2nd. Int. Conf. on Soil Mechanics and Foundation Eng. 1*, pp. 72–78, **1948**.

[111] Taylor, D. W., “Stability of earth slopes.,” *J. Bost. Soc. Civ. Engt.*, vol. 24, p. 197,

1937.

[112] Taylor, D. W., *Fundamentals of Soil Mechanics*. New York: Wiley, **1948**.

[113] Bell, J. M., "General slope stability and analysis," *J. Soil Mech. Fdns. Div. Am. Soc. Civ. Engrs*, vol. 94, no. SM6, pp. 1253–1270, **1968**.

[114] Nonveiller, E., "The stability analysis of slopes wih a slip surface of general shape.," in *Proc. 6th Int. Conf. Soil Mech. Found. Eng. 2*, pp. 522–525, **1965**.

[115] Terzaghi, K.V., *Theoretical Soil Mechanics*. John Wiley, **1943**.

[116] Frohlich, O. K., "The factor of safety with respect to sliding of a mass of soil along the arc of a logarithmic spiral.," in *Proc. 3rd. Int. Conf. on Soil Mechanics and Foundation Eng.*, vol. 2, pp. 230–233, **1953**.

[117] Yang, H., Wang, J., and Liu, Y., "A new approach for the slope stability analysis," *Mech. Res. Commun.*, vol. 28, no. 6, pp. 653–669, **2001**.

[118] Seed, H. B., and Sultan, H. A., "Stability analysis for a sloping core embankment.," *Proc. ASCE, Journal. Soil Mech. Found. Eng. Div.*, no. 93, pp. 69–84, **1967**.

[119] Li, K. S., and Lam, J., "Horizontal slice method of analysis," *Géotechnique*, vol. 51, no. 10, pp. 881–885, **2001**.

[120] Nouri, H., Fakher, A., and Jones, C. J. F. P., "Development of Horizontal Slice Method for seismic stability analysis of reinforced slopes and walls," *Geotext. Geomembranes*, vol. 24, no. 3, pp. 175–187, **2006**.

[121] Kumar, G. P., Das, A., Rai, R., and Jaiswal, A., "Slope Stability Analysis Using Radial Slices: A Mathematical Model," *J. Inst. Eng. Ser. D*, vol. 96, no. 2, pp. 189–193, **2015**.

[122] Patra, C. R., and Basudhar, P. K., "Generalized solution procedure for automated slope stability analysis using inclined slices," *Geotech. Geol. Eng.*, vol. 21, no. 3, pp. 259–281, **2003**.

[123] Fredlund, D. G., and Krahn, J., "Comparison of slope stability methods of analysis," *Can. Geotech. J.*, vol. 14, no. 3, pp. 429–439, **1977**.

[124] Duncan, J. M., and Wright, S. G., "The accuracy of equilibrium methods of slope stability analysis," *Eng. Geol.*, vol. 16, no. 1–2, pp. 5–17, **1980**.

[125] Espinoza, R. D., Bourdeau, P. L., and Muhunthan, B., "Unified Formulation for Analysis of Slopes with General Slip Surfaces," *J. Geotech. Eng.*, vol. 120, no. 7, pp. 1185–1204, **1994**.

[126] Zhu, D. Y., Lee, C. F., and Jiang, H. D., "Generalised framework of limit equilibrium methods for slope stability analysis.," *Géotechnique*, vol. 53, no. 4, pp. 377–395, 2003.

[127] Nash, D., "A comparative review of limit equilibrium methods of stability analysis.," *Slope Stab. Geotech. Eng. Geomorphol. John Wiley Sons, New York*, pp. 11–75, **1987**.

[128] Fredlund, D. G., "Analytical methods for slope stability analysis," *Proceedings of the 4th International Symposium on Landslides*. pp. 229–250, **1984**.

[129] Morgenstern, N. R., "The evaluation of slope stability—a 25-year perspective.," *Stab. Perform. slopes embankments II, Geotech. Spec. Publ. ASCE*, vol. 31, **1992**.

[130] Mostyn, G. R., and Small, J. C., "Methods of stability analysis," in *Soil Slope Instability and Stabilisation*, W. & Fell, Ed. Rotterdam, Balkema, pp. 71–120, **1987**.

[131] Cheng, Y. M., and Lau, C. K., *Slope Stability Analysis and Stabilization New Methods and Insight*, Second Edi. Boca Raton: CRC Press, Taylor & Francis Group, **2014**.

[132] Hoek, E., and Bray, J. W., *Rock Slope Engineering*. The Institute of Mining and Metallurgy., **1977**.

[133] Chen, Z. Y., Yin, J. H., and Wang, Y. J., "The Three-Dimensional Slope Stability Analysis: Recent Advances and a Forward Look," *Adv. Earth Struct. Res. to Pract.*, no. Gsp 151, pp. 1–42, **2006**.

[134] Huang, C.-C., and Tsai, C.-C., "New Method for 3D and Asymmetrical Slope Stability Analysis" *J. Geotech. Geoenvironmental Eng.*, Vol. 126, No. 10, pp. 917–927, **2000**.

[135] Azzouz, A. S., and Baligh, M. M., "Discussion on: Three-dimensional slope stability analysis method, by H.J. Hovland.," *J. Geotech. Eng. ASCE.*, vol. 104, no. GT9, pp. 1026–1028, **1978**.

[136] Chen, R. H., and Chameau, J. L., "Three-dimensional limit equilibrium analysis of slopes.," *Géotechnique*, vol. 32, no. 1, pp. 31–40, **1982**.

[137] Hutchinson, J. N., and Sarma, S. K., "Discussion on Three-dimensional limit equilibrium analysis of slopes.," *Can. Geotech. J.*, vol. 35, p. 215, **1985**.

[138] Cavounidis, S., "On the ratio of factors of safety in slope stability analyses," *Géotechnique*, vol. 37, no. 2, pp. 207–210, **1987**.

[139] Hungr, O., Salgado, F. M., and Byrne, P. M., "Evaluation of a three-dimensional method of slope stability analysis," *Can. Geotech. J.*, vol. 26, no. 4, pp. 679–686, **1989**.

[140] Lam, L., and Fredlund, D. G., "A general limit equilibrium model for three-dimensional slope stability analysis," *Can. Geotech. J.*, vol. 30, no. 6, pp. 905–919, **1993**.

[141] Huang, C., Tsai, C., and Chen, Y., "Generalized Method for Three-Dimensional Slope Stability Analysis," *J. Geotech. Geoenvironmental Eng.*, Vol. 128, No. 10, pp. 836–848, **2002**.

[142] Cheng, Y. M., and Yip, C. J., "Three-Dimensional Asymmetrical Slope Stability Analysis Extension of Bishop's, Janbu's, and Morgenstern–Price's Techniques," *J. Geotech. Geoenvironmental Eng.*, Vol. 133, No. 12, pp. 1544–1555, **2007**.

[143] Sherard, J. L., Woodward, R. J., Gizienksi, S. G., and Clevenger, W. A., *Earth-rock dams, engineering problems of design and construction.* New York: John Wiley and Sons, **1963**.

[144] Lambe, T. W., and Whitman, R. V., *Soil Mechanics*. New York: John Wiley and Sons, **1967**.

[145] Anagnosti, P., "Three-dimensional stability of fill dams," in *Proceeding of 7th International Conference on Soil Mechanics and Foundation Engineering*, pp. 275–280, **1969**.

[146] Baligh, M. M., and Azzouz, A. S., "End effects on the stability of cohesive soils.," *J.*

Geotech. Eng. Div. ASCE, vol. 101, no. GT11, pp. 1105–1117, **1975**.

[147] Azzouz, A. S., and Baligh, M. M., "Three-dimensional stability of slopes.," *MIT, Publ. No. R7B-8, Order No. 595, Natl. Tech. Inf. Serv. US Dep. Commer.*, p. 349 pp, **1978**.

[148] Azzouz, A. S., and Baligh, M. M., "Loaded areas on cohesive slopes.," *J. Geotech. Eng. ASCE.*, vol. 109, pp. 709–729, **1983**.

[149] Hutchison, B., "Three-dimensional slope stability analysis utilizing vertical column limiting equilibrium techniques. MSc Thesis," Imperial College of Science and Technology, London., **1981**.

[150] Humphrey, N. F., and Dunne, T., "Pore-pressures in debris failure initiation. Report 45.," Seattle, **1982**.

[151] Dennhardt, M., and Forster, W., "Problems of Three-Dimensional Slope Stability.," in *Proc. 11th. International Conference on Soil Mechanics and Foundations Engineering*, pp. 427–431, **1985**.

[152] Leshchinsky, D., Baker, R., and Silver, M. L., "Three-dimensional analysis of slope stability," *Int. J. Numer. Anal. Methods Geomech.*, Vol. 9, no. 3, pp. 199–223, **1985**.

[153] Kopacsy, J., "Three-dimensional stress distribution and slip surface in earth works at rupture.," in *Proc. 4th Int. Conf. Soil Mech. Found. Eng.*, pp. 339–342, **1957**.

[154] Leshchinsky, D., and Baker, R., "Three-dimensional Slope Stability: End Effects," *Soils Found.*, Vol 26, no. 4, pp. 98–110, **1986**.

[155] Baker, R., and Leshchinsky, D., "Stability Analysis of Conical Heaps.," *Soils Found.*, Vol. 27, no. 4, pp. 99–110, **1987**.

[156] Ugai, K., "Three-Dimensional Stability Analysis of Vertical Cohesive Slopes.," *Soils Found.*, Vol. 25, No.3, pp. 41–48, **1985**.

[157] Leshchinsky, D., and Mullet, T., "Design Charts for Vertical Cuts.," *J. Geotech. Geoenvironmental Eng.*, Vol. 114, no. 3, pp. 337–344, **1988**.

[158] Leshchinsky, D., and Mullet, T., "Stability of Vertical Corner Cuts.," in *Proceedings of the 6th International Conference on Numerical Methods in Geomechanics*, pp. 1249–1256, **1988**.

[159] Gens, A., Hutchinson, J. N., and Cavounidis, S., "Three-dimensional Analysis of Slides in Cohesive Soils.," *Géotechnique*, Vol. 38, no. 1, pp. 1–23, **1988**.

[160] Xing, Z., "Three-Dimensional Stability Analysis of Concave Slopes in Plan View," *J. Geotech. Eng.*, Vol. 114, No. 6, pp. 658–671, **1988**.

[161] Ugai, K., "Three-dimensional Slope Stability Analysis by Slice Methods.," in *Proceeding of the International Conference on Numerical Methods in Geomechanics*, pp. 1369–1374, **1988**.

[162] Ugai, K., and Hosobori, K., "Extension of simplified Bishop method, simplified Janbu method and Spencer method to three-dimensions.," in *Proc. Japanese Soc. of Civ. Engrs*, pp. 21–26, **1988**.

[163] Leshchinsky, D., and Huang, C.-C., "Generalized Slope Stability Analysis: interpretation, modification and comparsion.," *J. Geotech. Eng.*, Vol. 118, no. 10, pp. 1559–1576, **1992**.

[164] Leshchinsky, D., "Slope Stability Analysis: Generalized approach.," *J. Geotech. Eng.*, Vol. 116, no. 5, pp. 851–867, **1990**.

[165] Leshchinsky, D., and Huang, C.-C., "Generalized Three-Dimensional Slope Stability Analysis," *J. Geotech. Eng.*, Vol. 118, no. 11, pp. 1748–1764, **1992**.

[166] Cavounidis, S., and Kalogeropoulus, H., "End Effects on the Stability of Cuts in Normally Consolidated Clays.," *Riv. Ital. Gi Geotech.*, vol. 2, pp. 85–93, **1992**.

[167] Yamagami, T., and Jiang, J. C., "Determination of the Sliding Direction in Three-Dimensional Slope Stability Analysis.," in *Proceedings of the 2nd International Conference on Soft Soil Engineering*, pp. 567–572, **1996**.

[168] Yamagami, T., and Jiang, J. C., "A search for the critical slip surface in three-dimensional slope stability analysis," *Soils Found.*, Vol. 37, no. 3, pp. 1–16, **1997**.

[169] Jiang, J. C., and Yamagami, T., "Determination of the Sliding Direction in Three-Dimensional Slope Stability Analysis," in *Proceedings of 44th Symposium on Geotechnical Engineering*, pp. 193–200, **1999**.

[170] Chang, M., "A 3D slope stability analysis method assuming parallel lines of intersection and differential straining of block contacts," *Can. Geotech. J.*, vol. 39, no. 4, pp. 799–811, **2002**.

[171] Seed, R. B., Mitchell, J. K., and Seed, H. B., "Slope Stability Failure Investigation: Landfill Unit B-19, Phase I-A, Chemical Waste Management, Inc. Facility, Kettleman Hills, California, Vol. 1, Report of Investigation.," Berkeley, **1988**.

[172] Byrne, R. J., Kendall, J., and Brown, S., "Cause and mechanism of failure of Kettleman Hills Landfill B-19, Phase I-A," *Stab. Perform. Slopes Embankments - II, Am. Soc. Civ. Eng. Geotech. Spec. Publ.*, Vol. 2, No. 31, pp. 1188–1215, **1992**.

[173] Janbu, N., "Earth pressure and bearing capacity calculations by generalized procedure of slices," in *Proc. 4th Int. Conf. Soil Mech. Found. Eng.*, **1957**.

[174] Chen, Z., Mi, H., Zhang, F., and Wang, X., "A Simplified Method for 3D Slope Stability Analysis," *Can. Geotech. J.*, Vol. 40, no. 3, pp. 675–683, **2003**.

[175] Jiang, J. C., and Yamagami, T., "Three-dimensional slope stability analysis using an extended Spencer method," *Soils Found.*, Vol 44., no. 4, pp. 127–135, **2004**.

[176] Zheng, H., "A rigorous three-dimensional limit equilibrium method.," *Chinese J. Rock Mech. Eng.*, Vol. 26, no. 8, pp. 1529–1537, **2007**.

[177] Zheng, H., "Eigenvalue Problem from the Stability Analysis of Slopes," *J. Geotech. Geoenvironmental Eng.*, Vol. 135, no. 5, pp. 647–656, **2009**.

[178] Sun, G., Zheng, H., and Jiang, W., "A global procedure for evaluating stability of three-dimensional slopes," *Nat. Hazards*, vol. 61, no. 3, pp. 1083–1098, **2012**.

[179] Zheng, H., "A three-dimensional rigorous method for stability analysis of landslides," *Eng. Geol.*, vol. 144–145, pp. 30–40, **2012**.

[180] Zhu, D. Y., and Qian, Q. H., "Rigorous and quasi-rigorous limit equilibrium solutions of 3D slope stability and application to engineering.," *Chinese J. Rock Mech. Eng.*, Vol. 26, no. 8, pp. 1513–1528, **2007**.

[181] Zhou, X. P., and Cheng, H., "Analysis of stability of three-dimensional slopes using the rigorous limit equilibrium method," *Eng. Geol.*, vol. 160, pp. 21–33, **2013**.

[182] Lu, K. L., and Zhu, D. Y., "A three-dimensional rigorous method for stability analysis and its application," *Bull. Eng. Geol. Environ.*, vol. 75, pp. 1445–1457, **2016**.

[183] Feng, S. R., Feng, D. X., and Ge, X. R., "3D limit equilibrium method for slope stability and its application.," *Chinese J. Geotech. Eng.*, Vol. 21, no. 6, pp. 657–661, **1999**.

[184] Chen, Z. Y., Mi, H. L., and Wang, X. G., "A three-dimensional limit equilibrium method for slope stability analysis.," *Chinese J. Geotech. Eng.*, Vol. 23, no. 5, pp. 525–529, **2001**.

[185] Zhang, J. F., Wang, S. Y., and Qi, T., "Three-dimensional Spencer method for slope stability analysis.," *Chinese J. Rock Mech. Eng.*, Vol. 24, no. 19, pp. 3434–3439, **2005**.

[186] Zhang, J., Li, Z., and Qi, T., "An extension of 2D Janbu's generalized procedure of slices for 3D slope stability analysis II," *Eng. Mater. Sci.*, vol. 48, pp. 184–195, **2005**.

[187] Zhang, J., Qi, T., and Li, Z., "An extension of 2D Janbu's generalized procedure of slices for 3D slope stability analysis I," *Eng. Mater. Sci.*, vol. 48, pp. 171–183, **2005**.

[188] Cheng, Y. M., Li, D. Z., Li, L., Sun, Y. J., Baker, R., and Yang, Y., "Limit equilibrium method based on an approximate lower bound method with a variable factor of safety that can consider residual strength," *Comput. Geotech.*, vol. 38, no. 5, pp. 623–637, **2011**.

[189] Chakraborty, A., and Goswami, D., "State of the art: Three Dimensional (3D) Slope-Stability Analysis," *Int. J. Geotech. Eng.*, Vol. 10, No. 5, pp. 493–498, **2016**.

[190] Wines, D., "A comparison of slope stability analyses in two and three dimensions," *J. South. African Inst. Min. Metall.*, Vol. 116, no. 5, pp. 399–406, **2016**.

[191] Kalatehjari, R., and Ali, N., "A review of three-dimensional slope stability analyses based on limit equilibrium method," *Electron. J. Geotech. Eng.*, vol. 18 A, no. 1977, pp. 119–134, **2013**.

[192] Duncan, J. M., "State of the Art: Limit Equilibrium and Finite-Element Analysis of Slopes," *J. Geotech. Eng.*, vol. 122, no. 7, pp. 577–596, **1996**.

[193] Azzouz, A. S., Baligh, M. M., and Ladd, C. C., "Three dimensional stability analysis of four embankment failures.," in *Proc. 10th. International Conference on Soil Mechanics and Foundations Engineering*, pp. 343–346, **1981**.

[194] Giger, M. W., and Krizek, R. J., "Stability analysis of vertical cut with variable corner angle.," *Soils Found.*, Vol. 15, No. 2, pp. 63–71, **1975**.

[195] Giger, M. W., and Krizek, R. J., "Stability of vertical corner cut with concentrated surcharge load.," *J. Geotech. Eng.*, Vol. 102, No. 1, pp. 31–40, **1976**.

[196] Baligh, M. M., Azzouz, A. S., and Ladd, C. C., "Line loads on cohesive slopes.," in *Proc. 9th International Conference on Soil Mechanics and Foundations Engineering*, pp. 13–17, **1977**.

[197] Chen, R. H., and Chameau, J. L., "Three-dimensional Slope Stability Analysis," in *Proceedings of the 4th International Conference on Numerical Methods in Geomechanics*, pp. 671–677, **1982**.

[198] Michalowski, R. L., "Three-dimensional analysis of locally loaded slopes,"

Géotechnique, vol. 39, no. 1, pp. 27–38, **1989**.

[199] Arai, K., and Tagyo, K., "Determination of noncircular slip surface giving the minimum factor of safety in slope stability analysis," *Soils Found.*, vol. 25, no. 1, pp. 43–51, **1985**.

[200] Yamagami, T., and Ueta, Y., "Search for noncircular slip surfaces by the Morgenstern-Price method," in *Proc., 6th Int. Conf. Numer. Methods in Geomech.*, pp. 1219–1223, **1988**.

[201] Chen, Z.-Y., and Shao, C.-M., "Evaluation of minimum factor of safety in slope stability analysis," *Can. Geotech. J.*, vol. 25, pp. 735–748, **1988**.

[202] Sridevi, B., and Deep, K., "Application of global optimization technique to slope stability analysis," in *Proc., 6th Int. Symp. on Landslides*, pp. 573–578, **1992**.

[203] Greco, V. R., "Efficient Monte Carlo Technique for Locating Crtical Slip Surface," *J. Geotech. Eng.*, vol. 122, no. 7, pp. 517–525, **1996**.

[204] Husein Malkawi A. I., and Sarma, S. K., "Global search method for locating general slip surface using Monte Carlo techniques.," *J. Geotech. Geoenvironmental Eng.*, vol. 127, no. 8, pp. 688–698, **2001**.

[205] Zhu, D.-Y., "A method for locating critical slip surfaces in slope stability analysis," *Can. Geotech. J.*, vol. 38, no. 2, pp. 328–337, **2001**.

[206] Xie, M., Esaki, T., and Cai, M., "A GIS-based method for locating the critical 3D slip surface in a slope," *Comput. Geotech.*, vol. 31, no. 4, pp. 267–277, **2004**.

[207] Cheng, Y. M., Li, L., Lansivaara, T., Chi, S. C., and Sun, Y. J., "An improved harmony search minimization algorithm using different slip surface generation methods for slope stability analysis," *Eng. Optim.*, vol. 40, no. 2, pp. 95–115, **2008**.

[208] Sun, J., Li, J., and Liu, Q., "Search for Critical Slip Surface in Slope Stability Analysis by Spline-Based GA Method," *J. Geotech. Geoenvironmental Eng.*, vol. 134, no. 2, pp. 252–256, **2008**.

[209] Melo, C., and Sharma, S., "Seismic Coefficients for Pseudostatic Slope Analysis," *13th World Conf. Earthq. Eng.*, no. 369, p. 15, **2004**.

[210] Editors:, Ulusay, R., and Hudson, J. A., *ISRM: the complete ISRM suggested methods for rock characterization, testing and monitoring: 1974–2006*, April 2007. Ankara: Kozan ofset Matbaacılık San. ve Tic. Şti., **2007**.

[211] Ulusay, R., Gökçeoğlu, C., and Sülükçü, S., "Draft ISRM suggested method for determining block punch strength index test.," *Int. J. Rock Mech. Min. Sci.*, vol. 38, pp. 1113–1119, **2001**.

[212] Sonmez, H., and Tunusluoglu, C., "New considerations on the use of block punch index for predicting the uniaxial compressive strength of rock material.," *Int. J. Rock Mech. Min. Sci.*, vol. 45, pp. 1007–1014, **2008**.

[213] Morgenstern, N., and Bishop, A. W., "Stability Coefficients for Earth Slopes," *Géotechnique*, vol. 10, no. 4, pp. 129–153, **1960**.

[214] Marinos, P., and Hoek, E., "Estimating the geotechnical properties of heterogenous rock masses such as Flysch," *Bull. Eng. Geol. Environ.*, vol. 60, pp. 85–92, **2001**.

[215] Ching, R. K. H., and Fredlund, D. G., "Some difficulties associated with the limit equilibrium method of slices.," *Can. Geotech. J.*, vol. 20, pp. 661–672, **1983**.

[216] Fan, K., Fredlund, D. G., and Wilson, G. W., "An interslice force function for limit equilibrium slope stability analysis," *Can. Geotech. J.*, vol. 23, no. 1965, pp. 287–296, **1986**.

[217] Fredlund, D. G., Zhang, Z. M., and Lam, L., "Effect of the axis of moment equilibrium in slope stability analysis," *Can. Geotech. J.*, vol. 29, no. 3, pp. 456–465, **1992**.

[218] Krahn, J., "The 2001 R.M. Hardy Lecture: The limits of limit equilibrium analyses," *Can. Geotech. J.*, vol. 40, pp. 643–660, **2003**.

[219] Cheng, Y. M., Zhao, Z. H., and Sun, Y. J., "Evaluation of Interslice Force Function and Discussion on Convergence in Slope Stability Analysis by the Lower Bound Method," *J. Geotech. Geoenvironmental Eng.*, vol. 136, no. 8, pp. 1103–1113, **2010**.

[220] Cheng, Y. M., Lansivaara, T., and Siu, J., "Impact of convergence on slope stability analysis and design," *Comput. Geotech.*, vol. 35, no. 1, pp. 105–113, **2008**.

[221] Cheng, Y. M., "Location of critical failure surface and some further studies on slope stability analysis," *Comput. Geotech.*, vol. 30, pp. 255–267, **2003**.

[222] Bowders, J. J., and Lee, S. C., "Guide for selecting an approriate method to analyze the stability of slopes on reclaimed surface mines.," in *Proceedings America Society of Mining and Reclamation*, pp. 103–110, **1990**.

[223] Donald, I. B., and Chen, Z., "Slope stability analysis by the upper bound approach: fundamentals and methods," *Can. Geotech. J.*, vol. 34, no. 1983, pp. 853–862, **1997**.

[224] Terzaghi, K. V., "Mohr's diagram and the conditions for plastic equilibrium in ideal soils.," in *Theoretical Soil Mechanics*, 8th Printi., John Wiley and Sons, INC. New York., p. 16, **1956**.

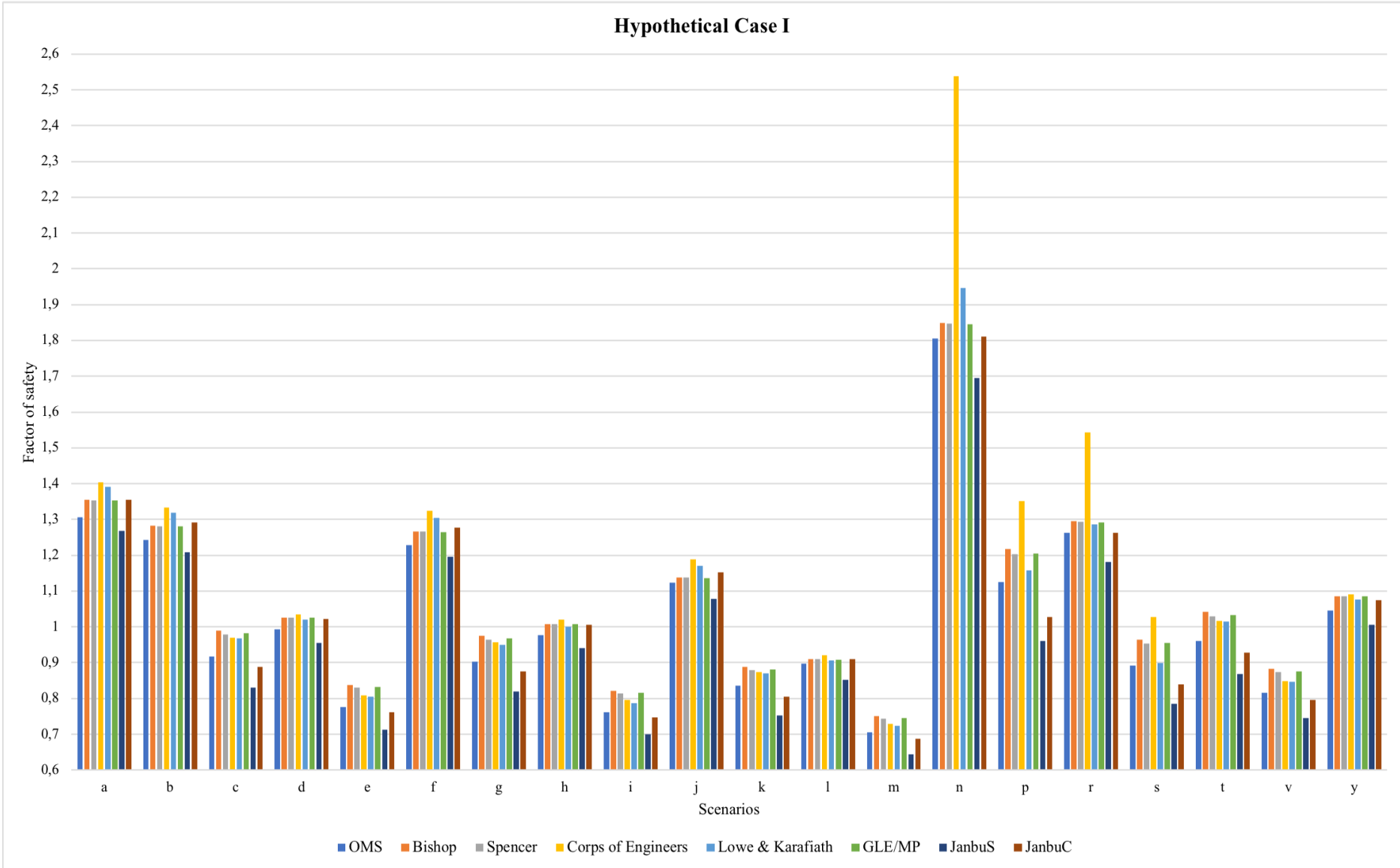
[225] Ersöz, T., and Topal, T., "Weathering and Excavation Effects on the Stability of Various Cut Slopes in Flysch-Like Deposits" *Geotechnical and Geological Engineering*, pp. 1-23, **2018.**

APPENDICES

APPENDIX – 1

Scenario	OMS	Bishop	Spencer	Corps. of Engineers	Lowe & Karafiath	GLE/MP	JanbuS	JanbuC
a	1.3070	1.3544	1.3526	1.4038	1.3915	1.3526	1.2685	1.3557
b	1.2428	1.2819	1.2801	1.3324	1.3193	1.2803	1.2077	1.2908
c	0.9170	0.9903	0.9791	0.9694	0.9670	0.9821	0.8310	0.8882
d	0.9937	1.0263	1.0255	1.0339	1.0196	1.0252	0.9559	1.0217
e	0.7768	0.8380	0.8300	0.8089	0.8045	0.8320	0.7119	0.7609
f	1.2292	1.2669	1.2662	1.3247	1.3051	1.2653	1.1951	1.2773
g	0.9027	0.9746	0.9640	0.9573	0.9502	0.9671	0.8186	0.8749
h	0.9774	1.0081	1.0077	1.0197	1.0001	1.0071	0.9407	1.0054
i	0.7621	0.8216	0.8141	0.7953	0.7877	0.8161	0.6992	0.7472
j	1.1231	1.1375	1.1371	1.1881	1.1696	1.1368	1.0783	1.1525
k	0.8351	0.8883	0.8788	0.8740	0.8708	0.8816	0.7529	0.8045
l	0.8969	0.9096	0.9097	0.9215	0.9056	0.9090	0.8520	0.9106
m	0.7062	0.7503	0.7443	0.7295	0.7229	0.7455	0.6432	0.6875
n	1.8059	1.8496	1.8463	2.5383	1.9469	1.8461	1.6947	1.8113
p	1.1244	1.2174	1.2027	1.3522	1.1582	1.2049	0.9614	1.0276
r	1.2631	1.2946	1.2926	1.5434	1.2857	1.2918	1.1806	1.2618
s	0.8922	0.9638	0.9540	1.0268	0.8989	0.9558	0.7848	0.8388
t	0.9611	1.0415	1.0301	1.0160	1.0142	1.0323	0.8682	0.9279
v	0.8152	0.8829	0.8733	0.8492	0.8458	0.8763	0.7449	0.7962
y	1.0463	1.0860	1.0858	1.0906	1.0760	1.0845	1.0057	1.0749

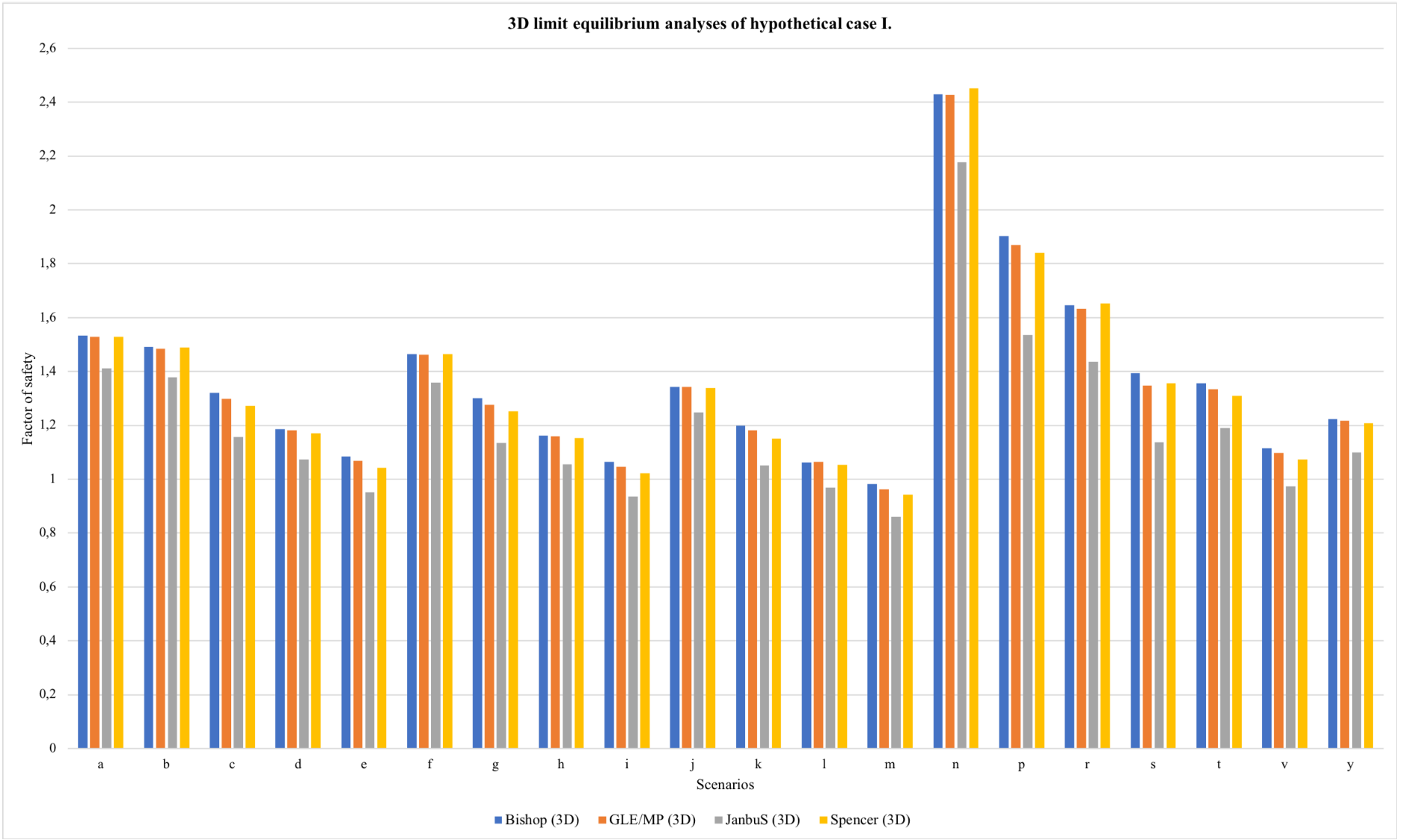
APPENDIX - 2


Hypothetical Case I
Factor of safety
2,6
2,5
2,4
2,3
2,2
2,1
2
1,9
1,8
1,7
1,6
1,5
1,4
1,3
1,2
1,1
1
0,9
0,8
0,7
0,6
a
b
c
d
e
f
g
h
i
j
k
l
m
n
p
r
s
t
v
y
Scenarios
OMS
Bishop
Spencer
Corps of Engineers
Lowe & Karafiath
GLE/MP
JanbuS
JanbuC

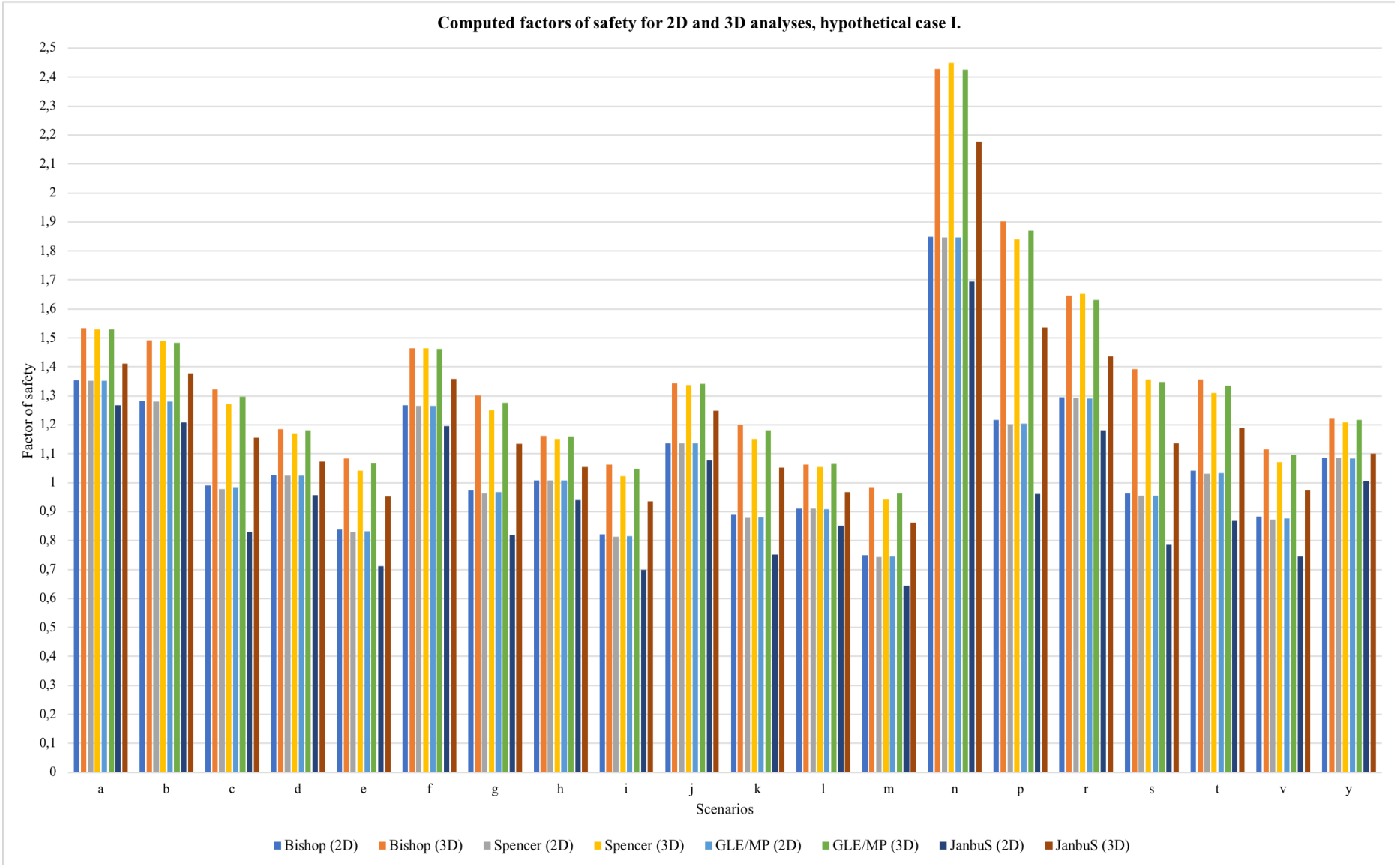
APPENDIX – 3

Scenario	Bishop (3D)	GLE/MP (3D)	JanbuS (3D)	Spencer (3D)
a	1.5330	1.5299	1.4124	1.5290
b	1.4922	1.4843	1.3776	1.4891
c	1.3219	1.2980	1.1566	1.2714
d	1.1858	1.1818	1.0734	1.1706
e	1.0835	1.0676	0.9519	1.0413
f	1.4652	1.4618	1.3576	1.4642
g	1.3007	1.2763	1.1352	1.2518
h	1.1625	1.1603	1.0551	1.1522
i	1.0633	1.0475	0.9357	1.0221
j	1.3435	1.3425	1.2486	1.3381
k	1.2002	1.1809	1.0516	1.1513
l	1.0623	1.0648	0.9685	1.0537
m	0.9819	0.9625	0.8617	0.9420
n	2.4285	2.4263	2.1769	2.4503
p	1.9029	1.8699	1.5356	1.8398
r	1.6456	1.6319	1.4365	1.6517
s	1.3928	1.3482	1.1370	1.3558
t	1.3568	1.3349	1.1902	1.3090
v	1.1152	1.0974	0.9744	1.0721
y	1.2225	1.2164	1.1002	1.2091

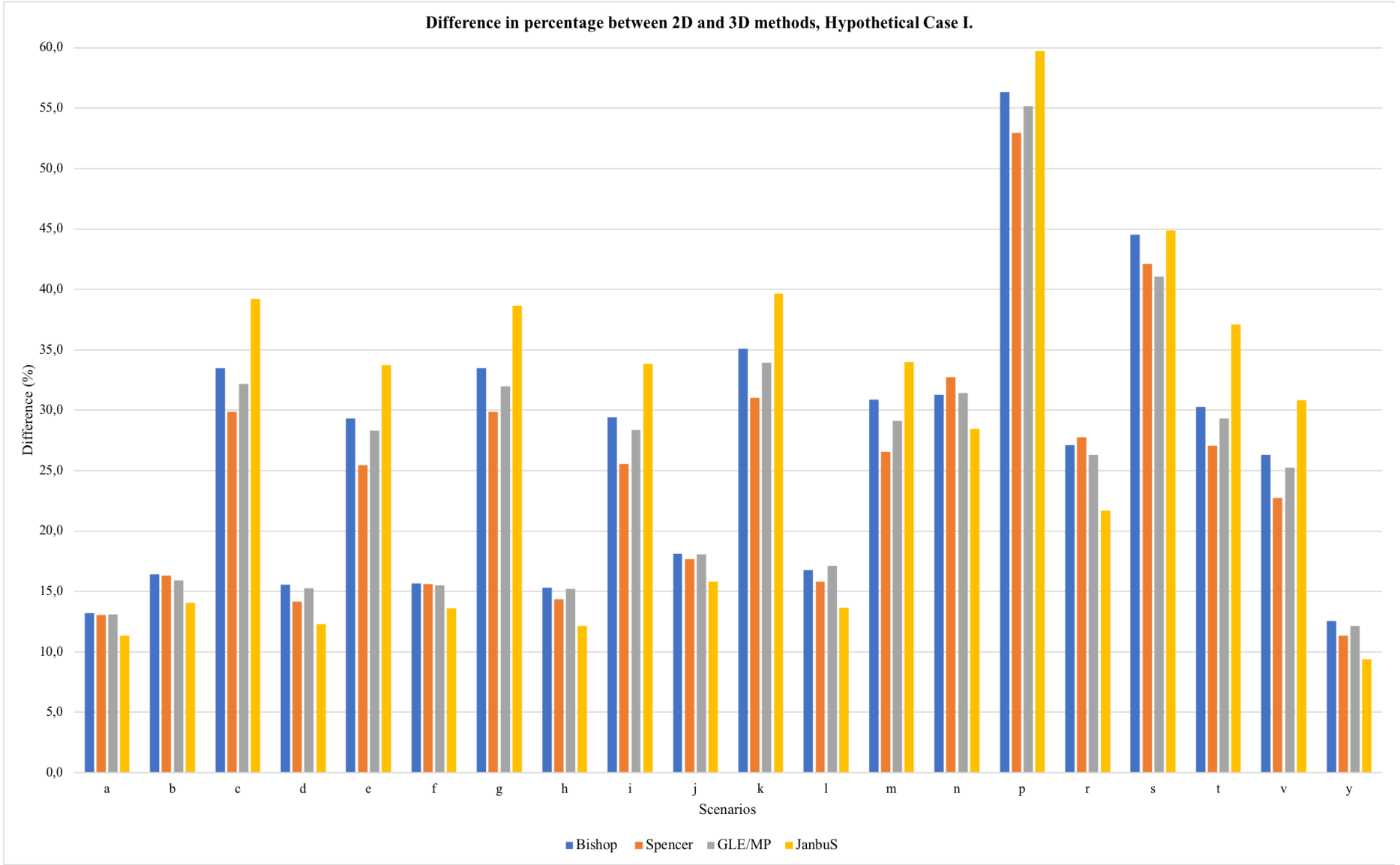
APPENDIX – 4


3D limit equilibrium analyses of hypothetical case I.
Factor of safety
2,6
2,4
2,2
2
1,8
1,6
1,4
1,2
1
0,8
0,6
0,4
0,2
0
a
b
c
d
e
f
g
h
i
j
k
l
m
n
p
r
s
t
v
y
Scenarios
Bishop (3D)
GLE/MP (3D)
JanbuS (3D)
Spencer (3D)

APPENDIX – 5


Computed factors of safety for 2D and 3D analyses, hypothetical case I.
Factor of safety
2,5
2,4
2,3
2,2
2,1
2
1,9
1,8
1,7
1,6
1,5
1,4
1,3
1,2
1,1
1
0,9
0,8
0,7
0,6
0,5
0,4
0,3
0,2
0,1
0
a
b
c
d
e
f
g
h
i
j
k
l
m
n
p
r
s
t
v
y
Scenarios
Bishop (2D)
Bishop (3D)
Spencer (2D)
Spencer (3D)
GLE/MP (2D)
GLE/MP (3D)
JanbuS (2D)
JanbuS (3D)

APPENDIX – 6

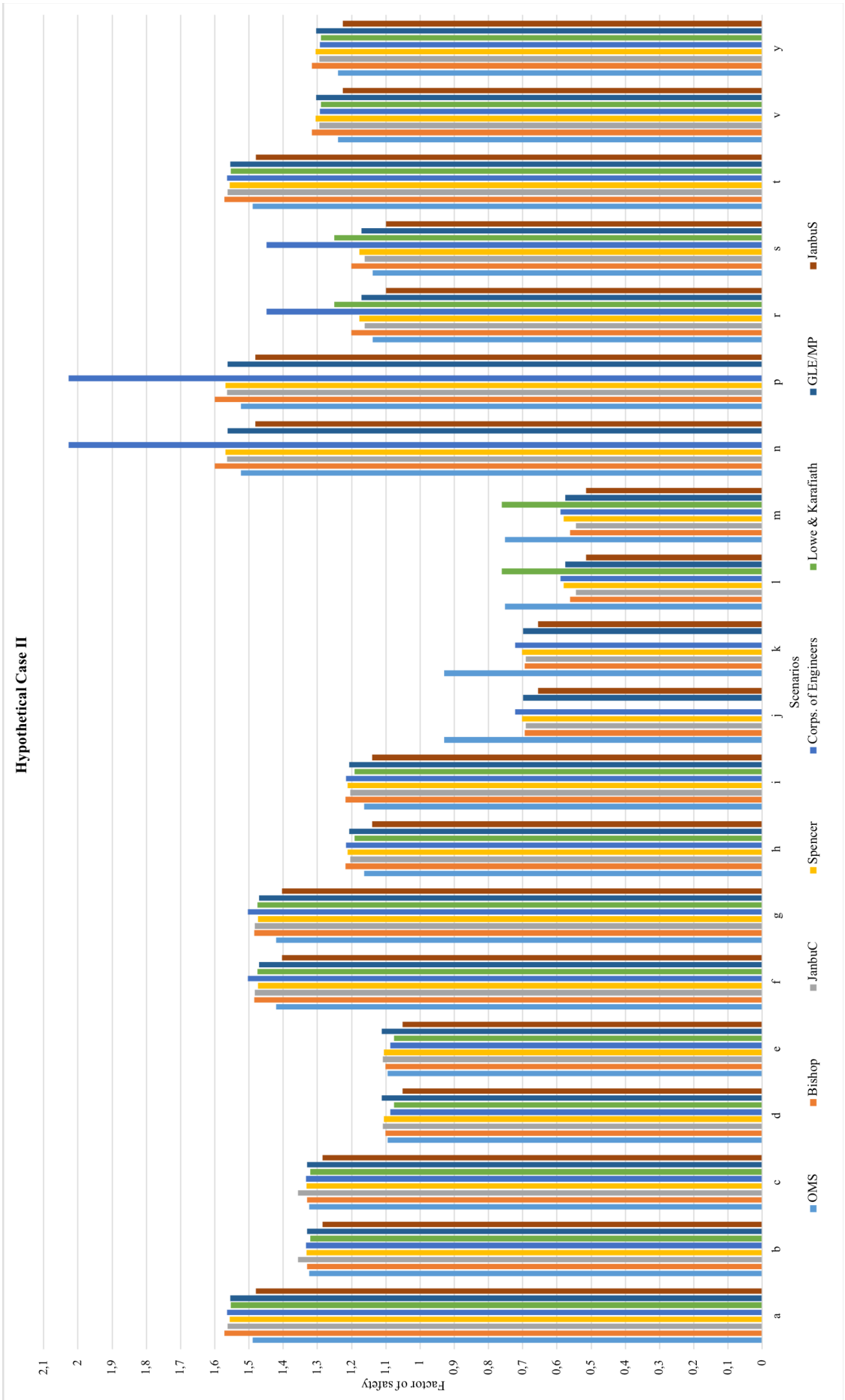

Difference in percentage between 2D and 3D methods, Hypothetical Case I.
Difference (%)
60,0
55,0
50,0
45,0
40,0
35,0
30,0
25,0
20,0
15,0
10,0
5,0
0,0
a
b
c
d
e
f
g
h
i
j
k
l
m
n
p
r
s
t
v
y
Scenarios
Bishop
Spencer
GLE/MP
JanbuS

APPENDIX – 7

Scenario	OMS	Bishop	Spencer	Corps. of Engineers	Lowe & Karafiath	GLE/MP	JanbuS	JanbuC
a	1.4897	1.5713	1.5568	1.5647	1.5529	1.5544	1.4795	1.5623
b	1.324	1.3300	1.3321	1.3334	1.3203	1.3308	1.2849	1.3568
c	1.324	1.3300	1.3321	1.3334	1.3203	1.3308	1.2849	1.3568
d	1.0948	1.1018	1.1052	1.0874	1.0762	1.1116	1.0508	1.1096
e	1.0948	1.1018	1.1052	1.0874	1.0762	1.1116	1.0508	1.1096
f	1.4212	1.4842	1.4734	1.5040	1.4751	1.4699	1.4038	1.4824
g	1.4212	1.4842	1.4734	1.5040	1.4751	1.4699	1.4038	1.4824
h	1.1639	1.2178	1.2124	1.2159	1.1913	1.2077	1.1407	1.2046
i	1.1639	1.2178	1.2124	1.2159	1.1913	1.2077	1.1407	1.2046
j	0.9291	0.6948	0.7017	0.7226	-*	0.6985	0.6549	0.6915
k	0.9291	0.6948	0.7017	0.7226	-*	0.6985	0.6549	0.6915
l	0.7524	0.5616	0.5808	0.5890	0.7619	0.5751	0.5153	0.5442
m	0.7524	0.5616	0.5808	0.5890	0.7619	0.5751	0.5153	0.5442
n	1.5237	1.6003	1.5683	2.0270	-*	1.5624	1.4817	1.5646
p	1.5237	1.6003	1.5683	2.0270	-*	1.5624	1.4817	1.5646
r	1.1378	1.2003	1.1778	1.4492	1.2505	1.1713	1.1000	1.1616
s	1.1378	1.2003	1.1778	1.4492	1.2505	1.1713	1.1000	1.1616
t	1.4897	1.5713	1.5568	1.5647	1.5529	1.5544	1.4795	1.5623
v	1.2398	1.3166	1.3053	1.2931	1.2891	1.3031	1.2253	1.2939
y	1.2398	1.3166	1.3053	1.2931	1.2891	1.3031	1.2253	1.2939

*did not converge.

APPENDIX - 8

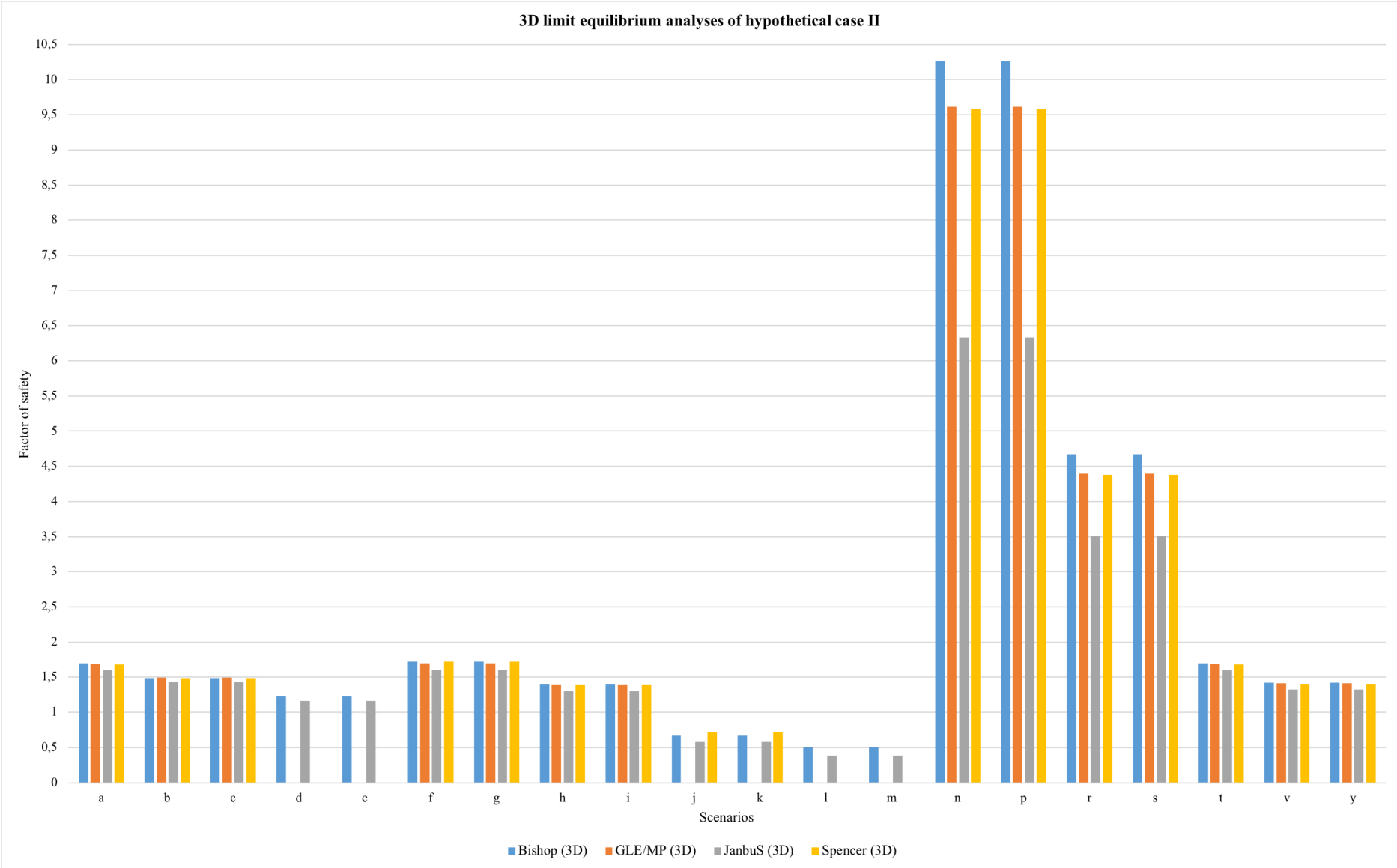

Hypothetical Case II
Factor of safety
2,1
2
1,9
1,8
1,7
1,6
1,5
1,4
1,3
1,2
1,1
1
0,9
0,8
0,7
0,6
0,5
0,4
0,3
0,2
0,1
0
a
b
c
d
e
f
g
h
i
j
k
l
m
n
p
r
s
t
v
y
Scenarios
OMS
Bishop
JanbuC
Spencer
Corps. of Engineers
Lowe & Karafiath
GLE/MP
JanbuS

APPENDIX – 9

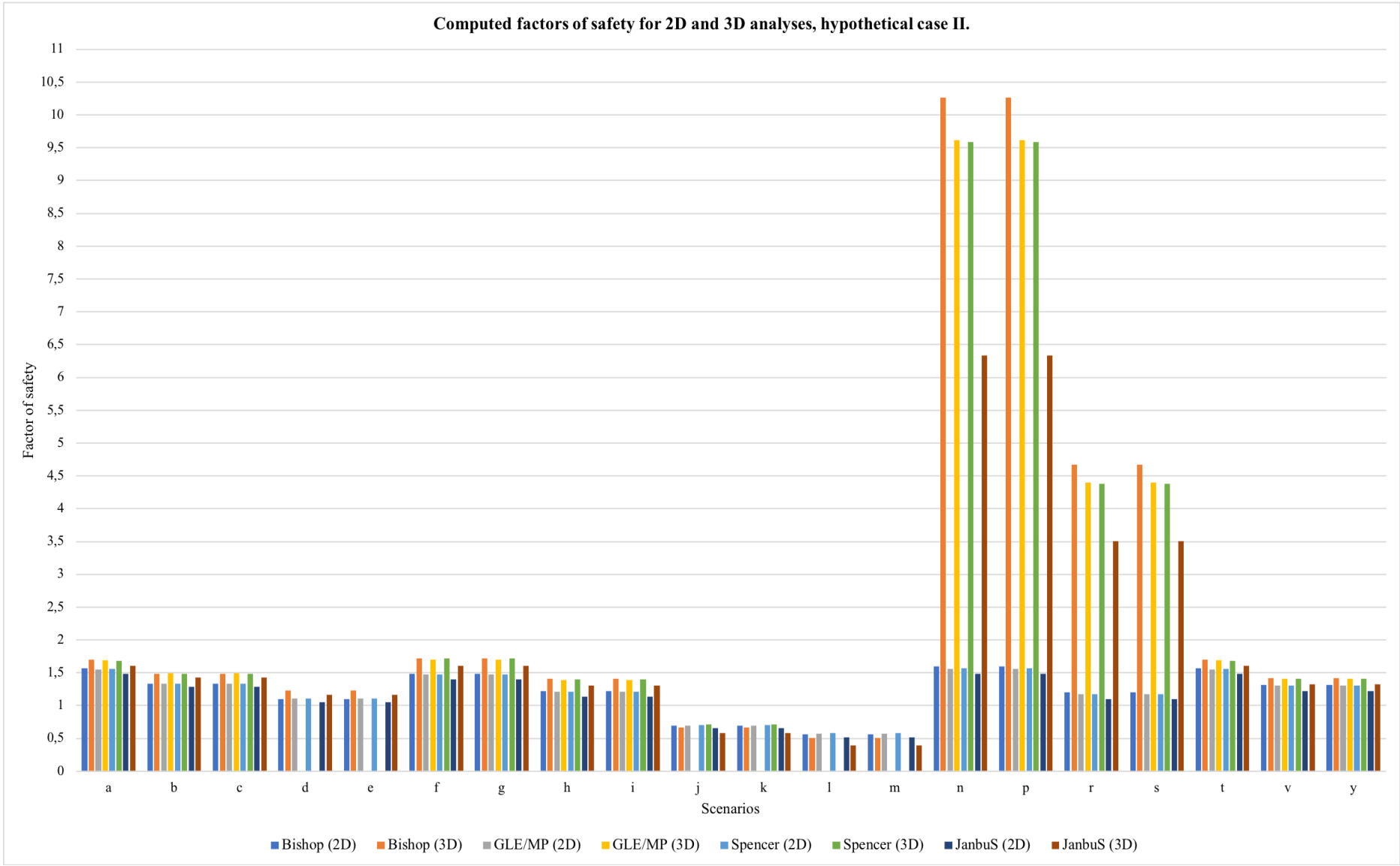
Scenario	Bishop (3D)	GLE/MP (3D)	JanbuS (3D)	Spencer (3D)
a	1.6977	1.6874	1.6041	1.6829
b	1.4860	1.4930	1.4299	1.4858
c	1.4860	1.4930	1.4299	1.4858
d	1.2290	-*	1.1631	-*
e	1.2290	-*	1.1631	-*
f	1.7191	1.6993	1.6098	1.7194
g	1.7191	1.6993	1.6098	1.7194
h	1.4068	1.3941	1.3012	1.3964
i	1.4068	1.3941	1.3012	1.3964
j	0.6661	-*	0.5823	0.7175
k	0.6661	-*	0.5823	0.7175
l	0.5094	-*	0.3891	-*
m	0.5094	-*	0.3891	-*
n	10.2607	9.6150	6.3338	9.5858
p	10.2607	9.6150	6.3338	9.5858
r	4.6725	4.3956	3.5059	4.3772
s	4.6725	4.3956	3.5059	4.3772
t	1.6977	1.6874	1.6041	1.6829
v	1.4189	1.4122	1.3222	1.4083
y	1.4189	1.4122	1.3222	1.4083

*did not converge.

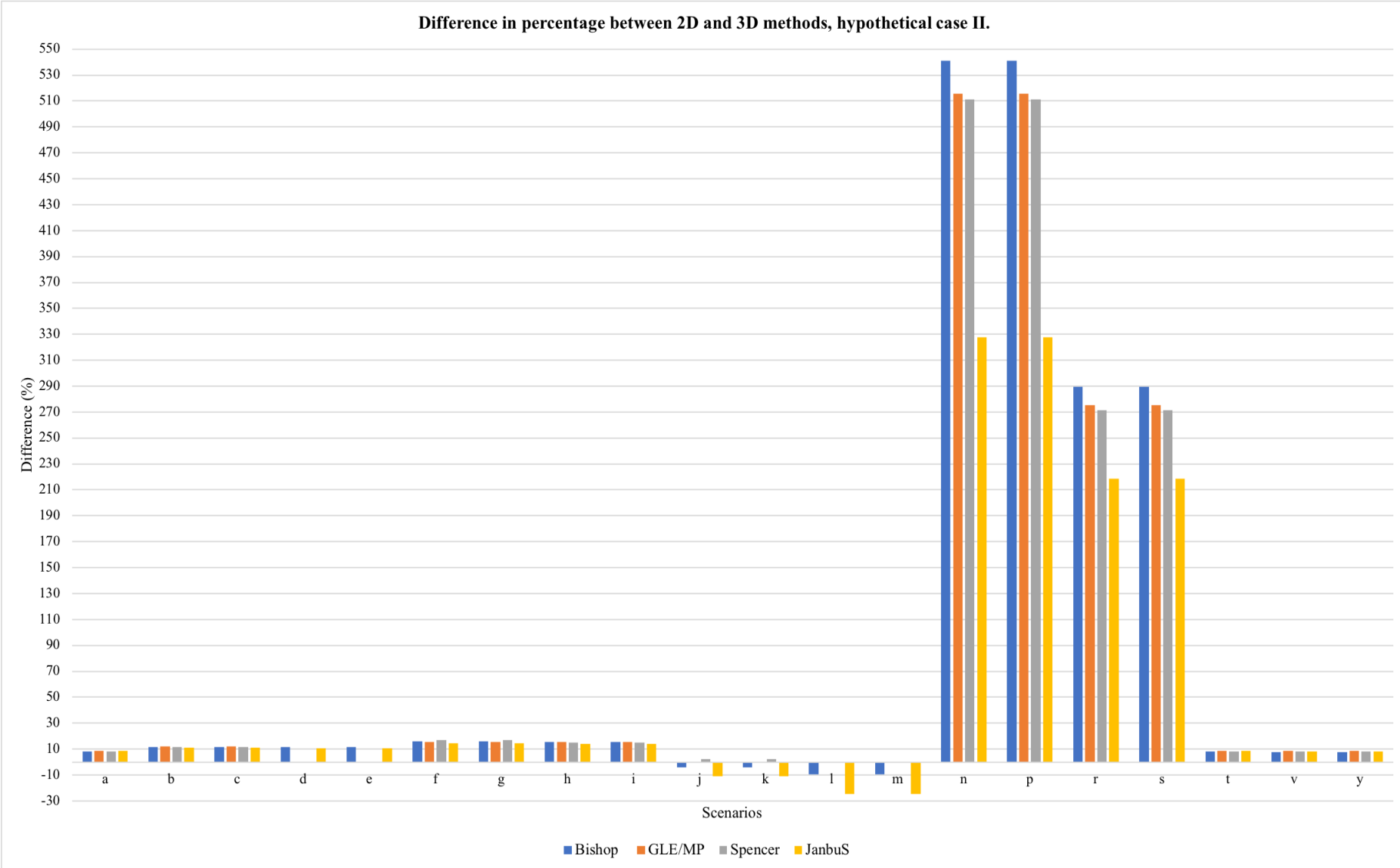
APPENDIX – 10


3D limit equilibrium analyses of hypothetical case II
Factor of safety
10,5
10
9,5
9
8,5
8
7,5
7
6,5
6
5,5
5
4,5
4
3,5
3
2,5
2
1,5
1
0,5
0
a
b
c
d
e
f
g
h
i
j
k
l
m
n
p
r
s
t
v
y
Scenarios
Bishop (3D)
GLE/MP (3D)
JanbuS (3D)
Spencer (3D)

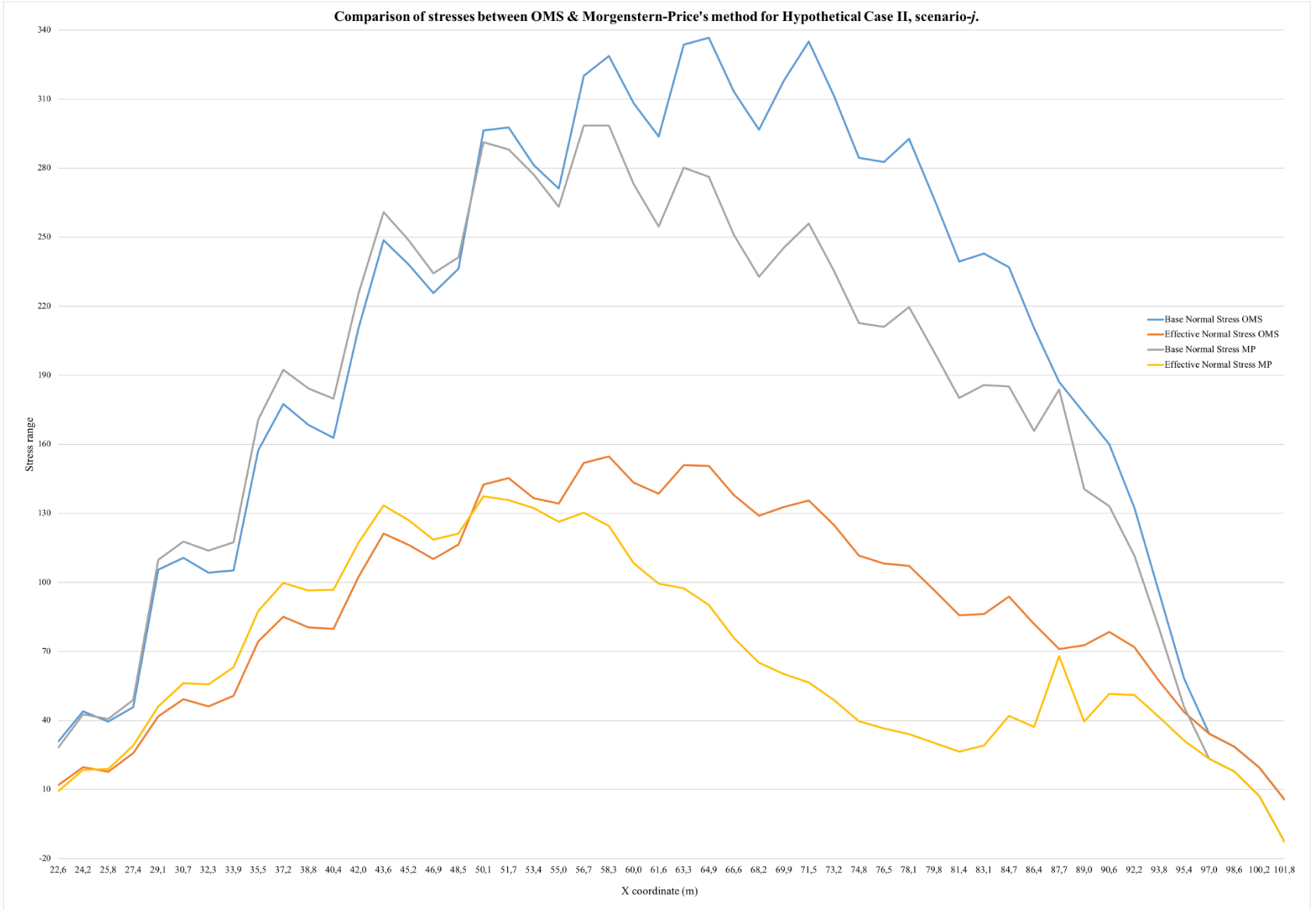
APPENDIX – 11


Computed factors of safety for 2D and 3D analyses, hypothetical case II.
Factor of safety
11
10,5
10
9,5
9
8,5
8
7,5
7
6,5
6
5,5
5
4,5
4
3,5
3
2,5
2
1,5
1
0,5
0
a
b
c
d
e
f
g
h
i
j
k
l
m
n
p
r
s
t
v
y
Scenarios
Bishop (2D)
Bishop (3D)
GLE/MP (2D)
GLE/MP (3D)
Spencer (2D)
Spencer (3D)
JanbuS (2D)
JanbuS (3D)

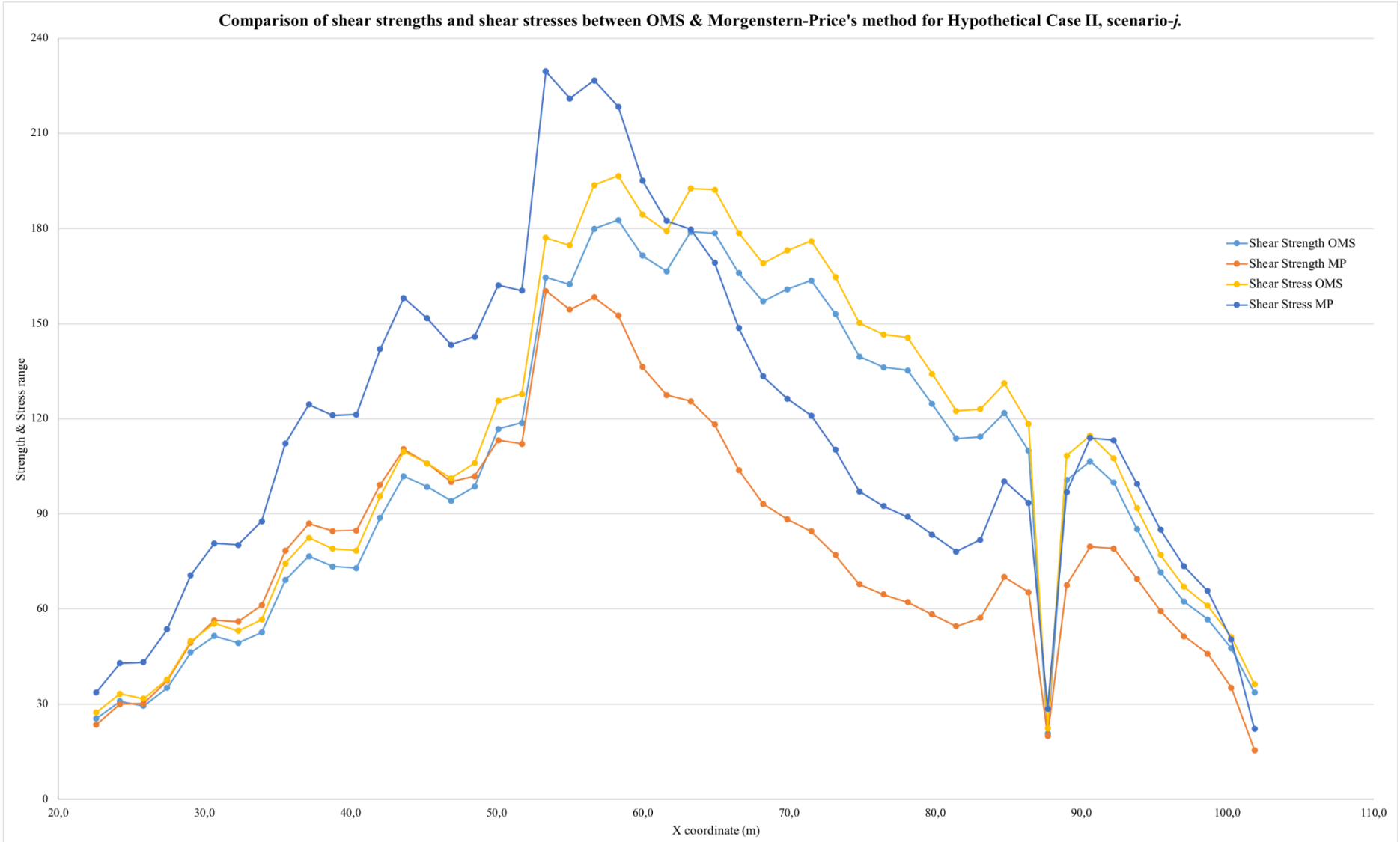
APPENDIX – 12


Difference in percentage between 2D and 3D methods, hypothetical case II.
Difference (%)
550
530
510
490
470
450
430
410
390
370
350
330
310
290
270
250
230
210
190
170
150
130
110
90
70
50
30
10
-10
-30
a
b
c
d
e
f
g
h
i
j
k
l
m
n
p
r
s
t
v
y
Scenarios
Bishop
GLE/MP
Spencer
JanbuS

APPENDIX – 13


Comparison of stresses between OMS & Morgenstern-Price's method for Hypothetical Case II, scenario-j.
Stress range
X coordinate (m)
Base Normal Stress OMS
Effective Normal Stress OMS
Base Normal Stress MP
Effective Normal Stress MP
340
310
280
250
220
190
160
130
100
70
40
10
-20
22,6 24,2 25,8 27,4 29,1 30,7 32,3 33,9 35,5 37,2 38,8 40,4 42,0 43,6 45,2 46,9 48,5 50,1 51,7 53,4 55,0 56,7 58,3 60,0 61,6 63,3 64,9 66,6 68,2 69,9 71,5 73,2 74,8 76,5 78,1 79,8 81,4 83,1 84,7 86,4 87,7 89,0 90,6 92,2 93,8 95,4 97,0 98,6 100,2 101,8

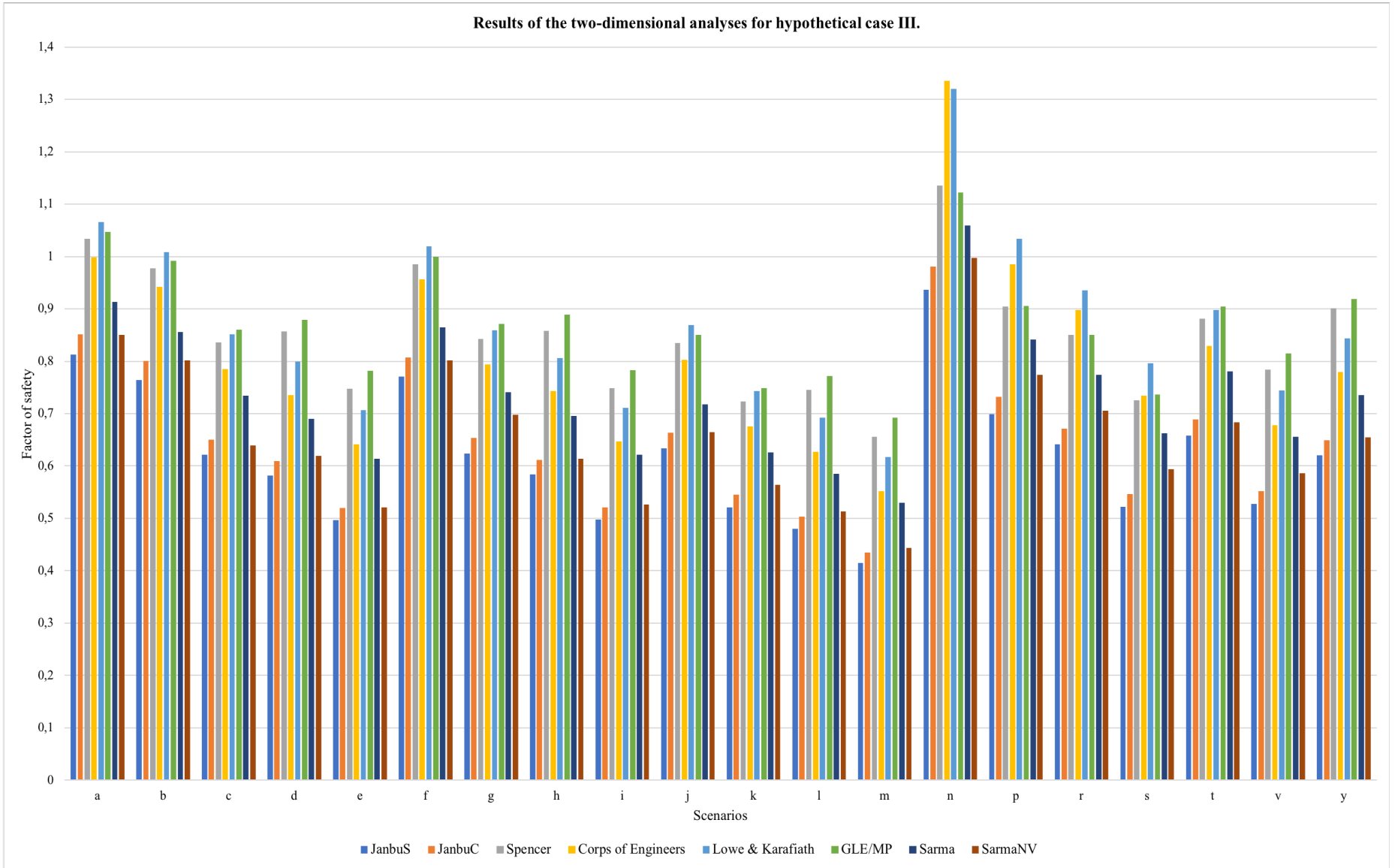
APPENDIX – 14


Comparison of shear strengths and shear stresses between OMS & Morgenstern-Price's method for Hypothetical Case II, scenario-j.
Strength & Stress range
X coordinate (m)
Shear Strength OMS
Shear Strength MP
Shear Stress OMS
Shear Stress MP
240
210
180
150
120
90
60
30
0
20,0
30,0
40,0
50,0
60,0
70,0
80,0
90,0
100,0
110,0

APPENDIX - 15

Scenario	JanbuS	JanbuC	Spencer	Corps of Engineers	Lowe & Karafiath	GLE/MP	Sarma	SarmaNV
a	0.8129	0.8512	1.0341	0.9982	1.0656	1.0473	0.9129	0.8505
b	0.7645	0.8006	0.9773	0.9424	1.0085	0.9915	0.8556	0.8021
c	0.6210	0.6502	0.8363	0.7851	0.8519	0.8606	0.7341	0.6392
d	0.5819	0.6094	0.8571	0.7356	0.8000	0.8786	0.6904	0.6192
e	0.4967	0.5201	0.7472	0.6411	0.7061	0.7814	0.6142	0.5214
f	0.7708	0.8071	0.9854	0.9559	1.0196	0.9995	0.8651	0.8013
g	0.6243	0.6537	0.8423	0.7942	0.8595	0.8717	0.7412	0.6977
h	0.5844	0.6119	0.8582	0.7431	0.8061	0.8895	0.6957	0.6142
i	0.4978	0.5213	0.7486	0.6466	0.7108	0.7832	0.6213	0.5263
j	0.6341	0.6640	0.8345	0.8028	0.8693	0.8498	0.7173	0.6649
k	0.5210	0.5455	0.7234	0.6758	0.7426	0.7487	0.6260	0.5637
l	0.4803	0.5030	0.7453	0.6270	0.6919	0.7714	0.5852	0.5134
m	0.4150	0.4345	0.6558	0.5515	0.6169	0.6920	0.5296	0.4433
n	0.9361	0.9802	1.1357	1.3352	1.3200	1.1224	1.0593	0.9969
p	0.6986	0.7315	0.9048	0.9856	1.0335	0.9050	0.8411	0.7736
r	0.6412	0.6714	0.8498	0.8977	0.9353	0.8498	0.7740	0.7050
s	0.5221	0.5467	0.7253	0.7345	0.7957	0.7367	0.6625	0.5938
t	0.6583	0.6893	0.8813	0.8291	0.8977	0.9047	0.7806	0.6838
v	0.5272	0.5521	0.7838	0.6780	0.7440	0.8154	0.6561	0.5860
y	0.6199	0.6491	0.9006	0.7798	0.8440	0.9186	0.7359	0.6546

APPENDIX - 16

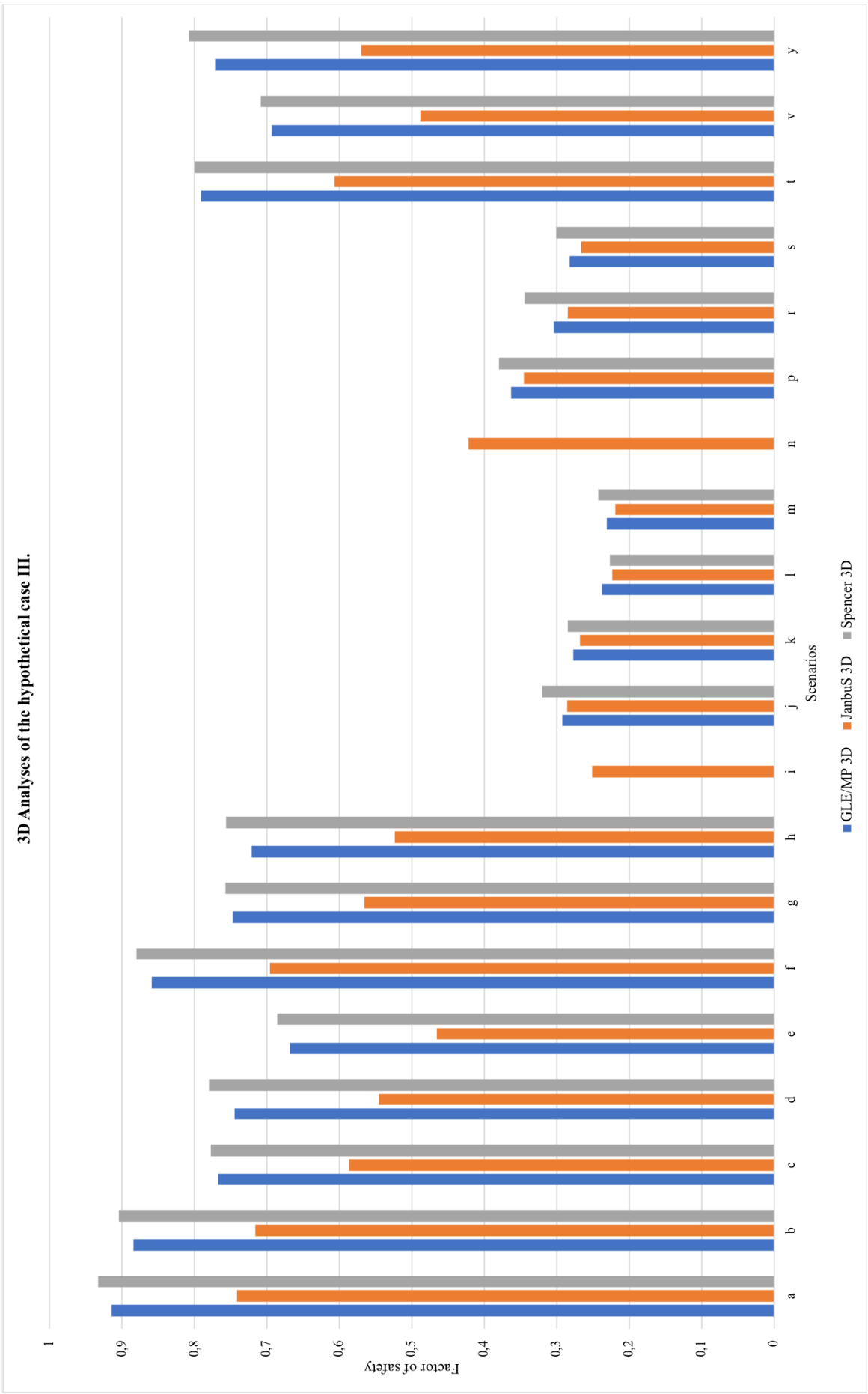

Results of the two-dimensional analyses for hypothetical case III.
Factor of safety
1,4
1,3
1,2
1,1
1
0,9
0,8
0,7
0,6
0,5
0,4
0,3
0,2
0,1
0
a
b
c
d
e
f
g
h
i
j
k
l
m
n
p
r
s
t
v
y
Scenarios
JanbuS
JanbuC
Spencer
Corps of Engineers
Lowe & Karafiath
GLE/MP
Sarma
SarmaNV

APPENDIX - 17

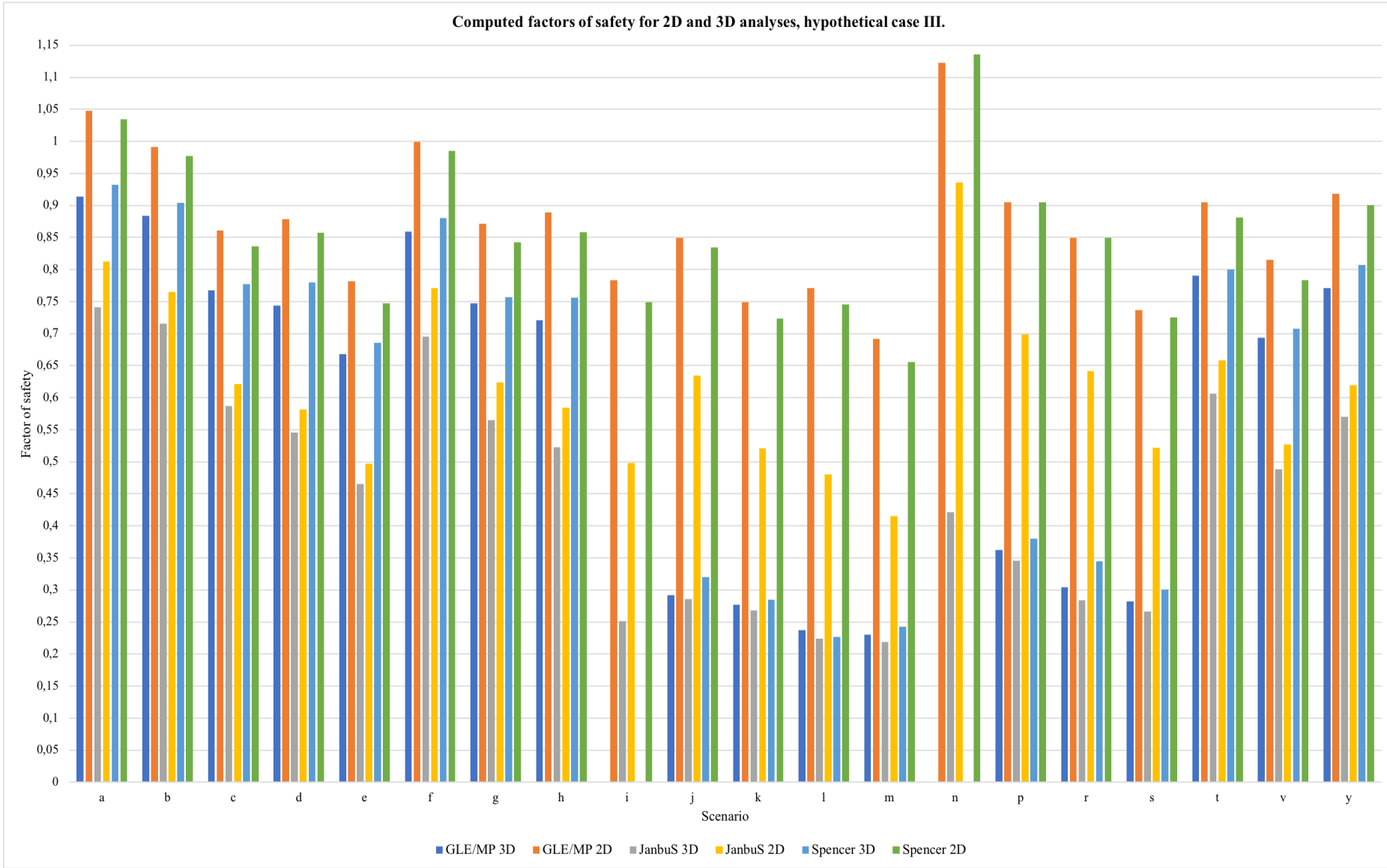
Scenario	GLE/MP 3D	JanbuS 3D	Spencer 3D
a	0.9139	0.7409	0.9323
b	0.8842	0.7158	0.9041
c	0.7673	0.5866	0.7774
d	0.7440	0.5454	0.7799
e	0.6682	0.4650	0.6857
f	0.8590	0.6953	0.8800
g	0.7473	0.5651	0.7572
h	0.7209	0.5231	0.7561
i	-*	0.2511	-*
j	0.2922	0.2856	0.3199
k	0.2771	0.2683	0.2849
l	0.2374	0.2237	0.2265
m	0.2305	0.2191	0.2427
n	-*	0.4215	-*
p	0.3627	0.3454	0.3797
r	0.3041	0.2843	0.3445
s	0.2822	0.2660	0.3004
t	0.7907	0.6064	0.8001
v	0.6935	0.4883	0.7079
y	0.7713	0.5698	0.8076

*did not converge.

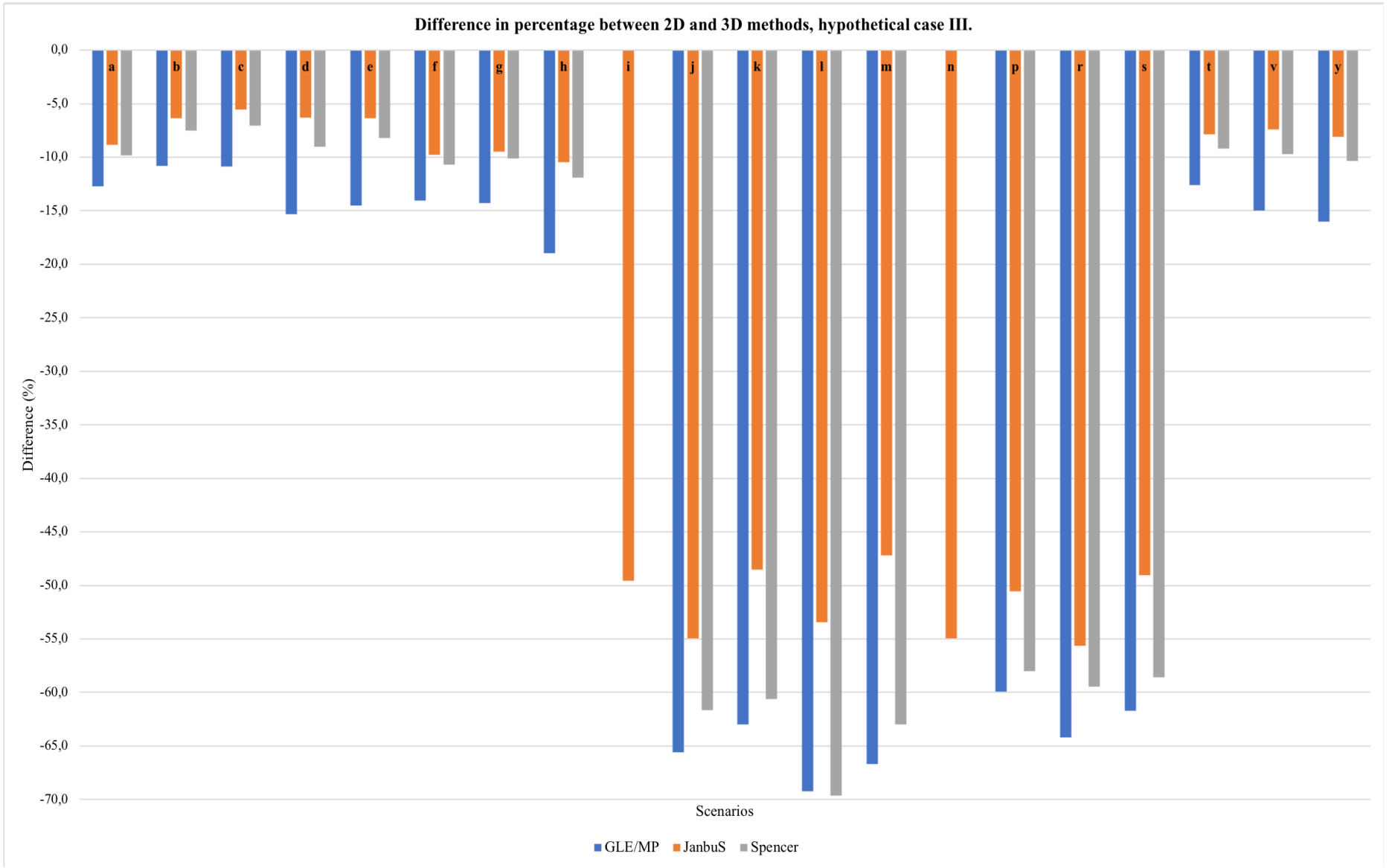
APPENDİX - 18


3D Analyses of the hypothetical case III.
Factor of safety
1
0,9
0,8
0,7
0,6
0,5
0,4
0,3
0,2
0,1
0
a
b
c
d
e
f
g
h
i
j
k
l
m
n
p
r
s
t
v
y
Scenarios
GLE/MP 3D
JanbuS 3D
Spencer 3D

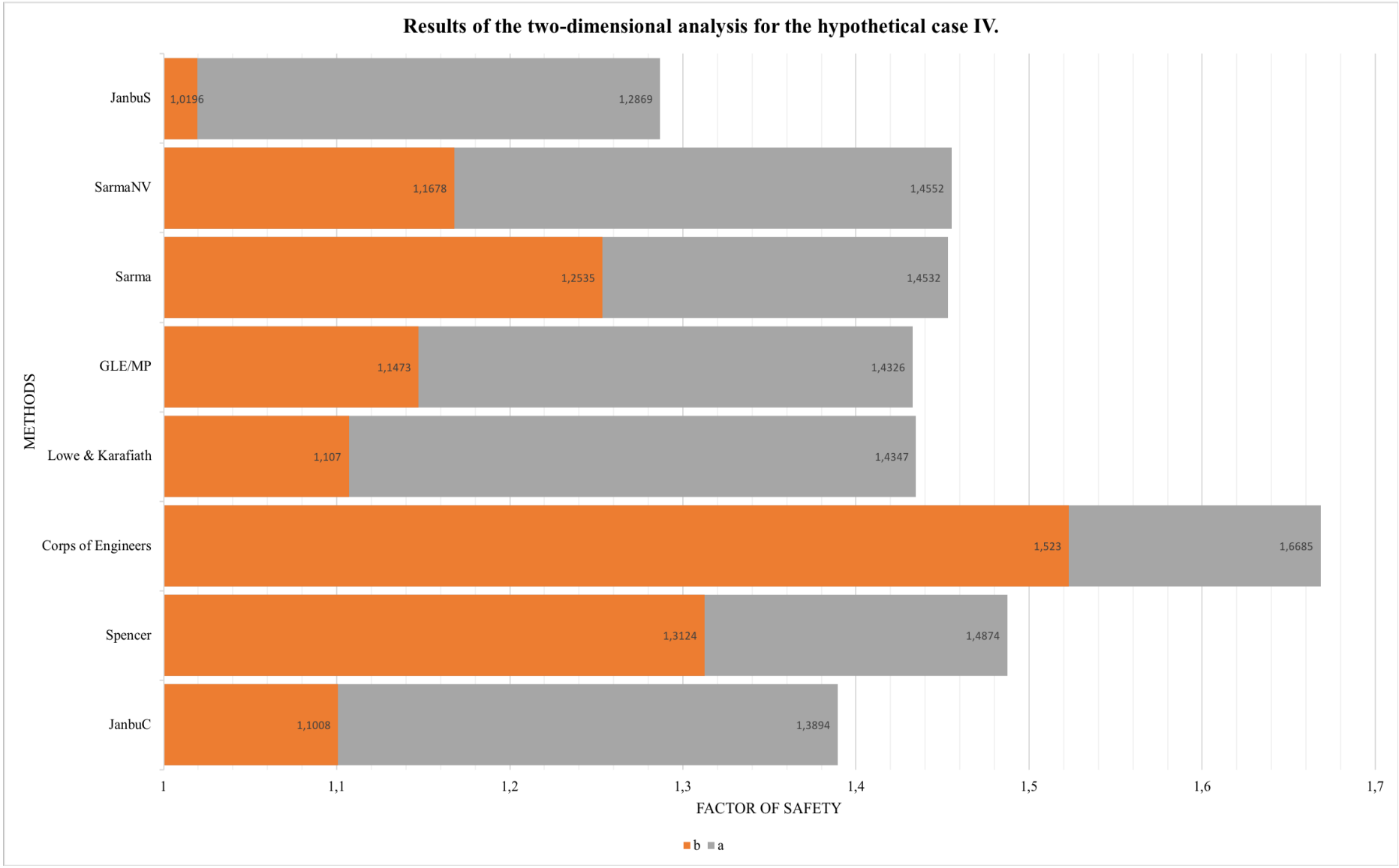
APPENDIX - 19


Computed factors of safety for 2D and 3D analyses, hypothetical case III.
Factor of safety
1,15
1,1
1,05
1
0,95
0,9
0,85
0,8
0,75
0,7
0,65
0,6
0,55
0,5
0,45
0,4
0,35
0,3
0,25
0,2
0,15
0,1
0,05
0
a
b
c
d
e
f
g
h
i
j
k
l
m
n
p
r
s
t
v
y
Scenario
GLE/MP 3D
GLE/MP 2D
JanbuS 3D
JanbuS 2D
Spencer 3D
Spencer 2D

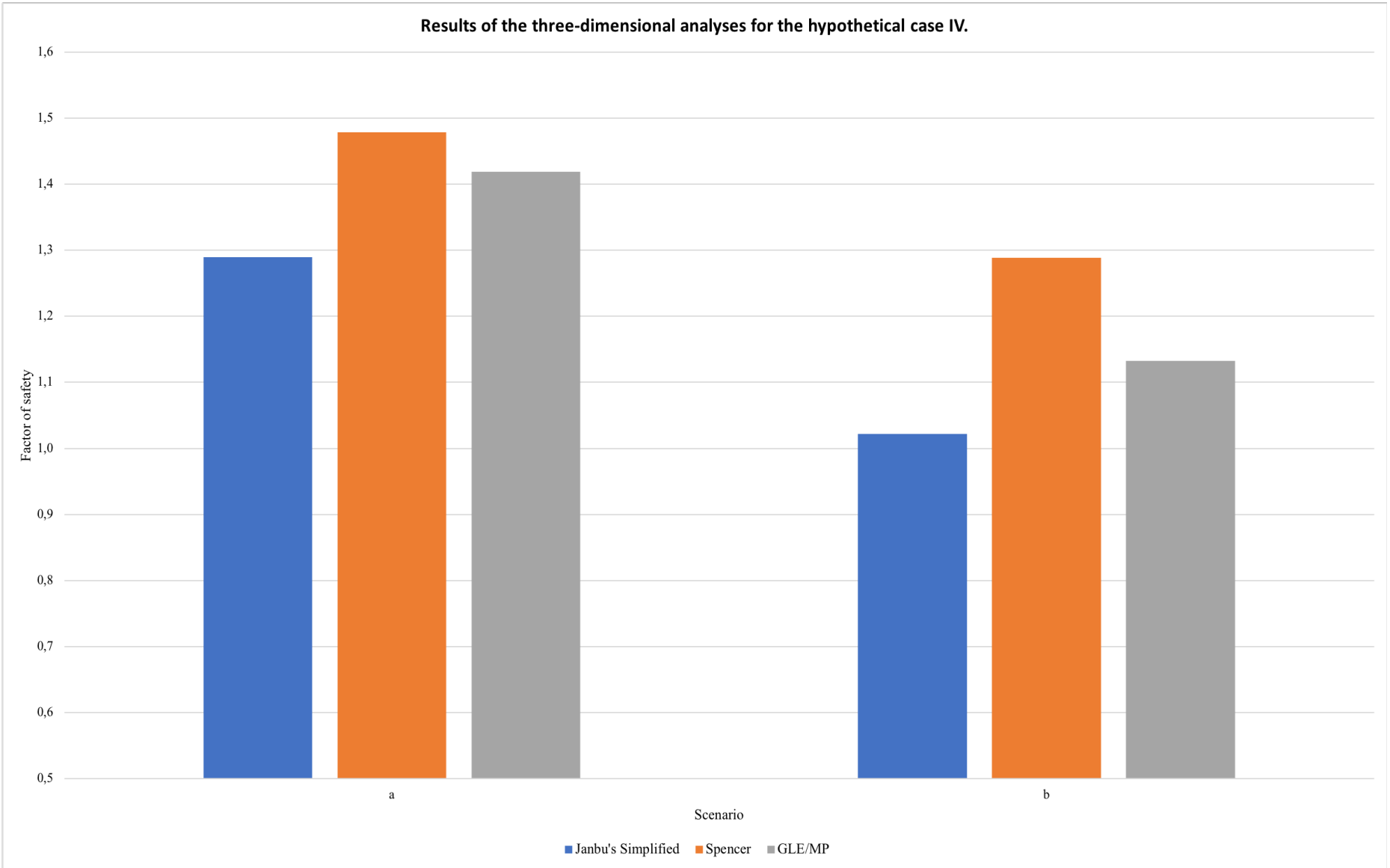
APPENDIX - 20


Difference in percentage between 2D and 3D methods, hypothetical case III.
0,0
-5,0
-10,0
-15,0
-20,0
-25,0
-30,0
-35,0
-40,0
-45,0
-50,0
-55,0
-60,0
-65,0
-70,0
Difference (%)
a
b
c
d
e
f
g
h
i
j
k
l
m
n
p
r
s
t
v
y
Scenarios
GLE/MP
JanbuS
Spencer

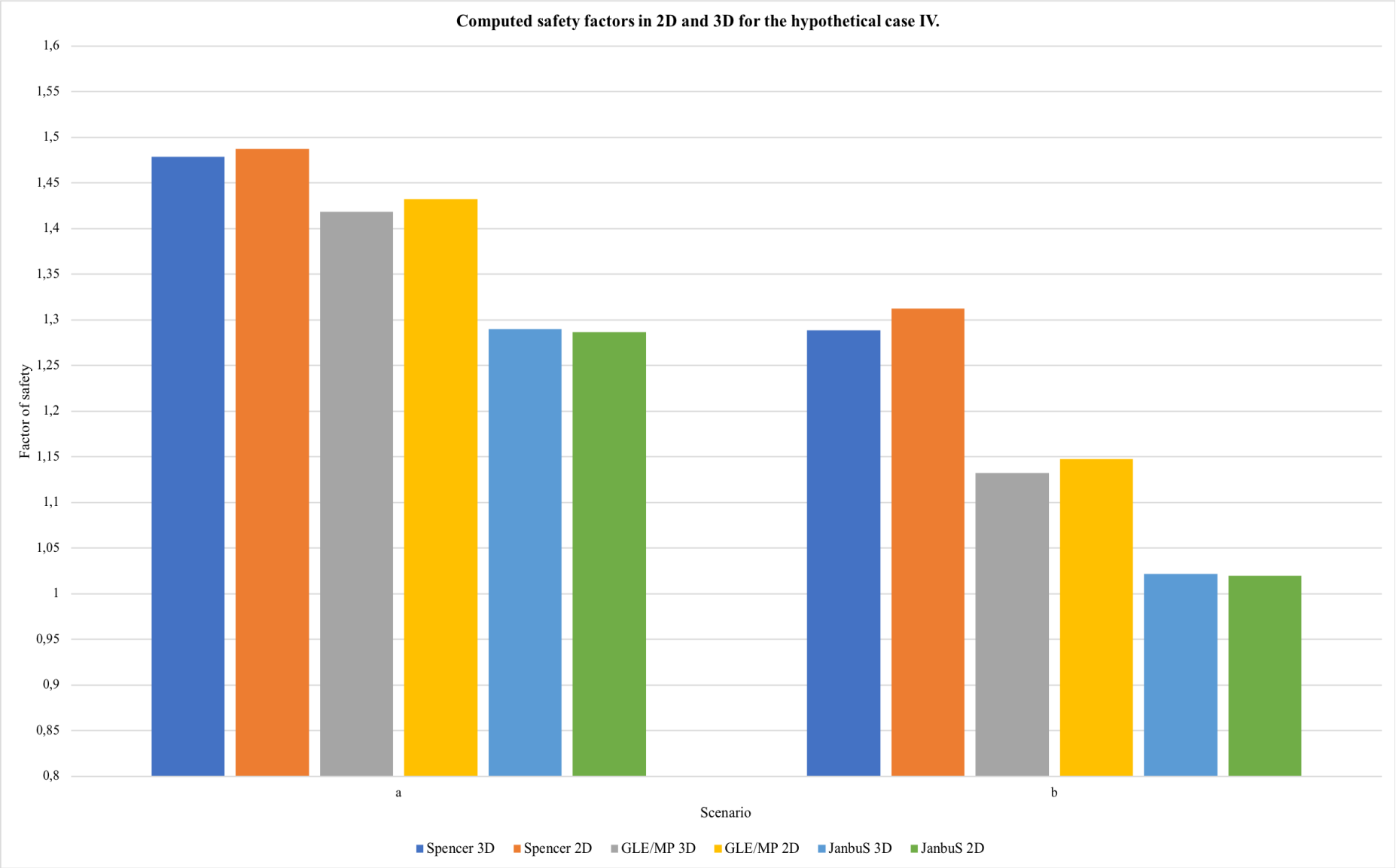
APPENDIX - 21


Results of the two-dimensional analysis for the hypothetical case IV.
METHODS
JanbuS
SarmaNV
Sarma
GLE/MP
Lowe & Karafiath
Corps of Engineers
Spencer
JanbuC
1,0196
1,2869
1,1678
1,4552
1,2535
1,4532
1,1473
1,4326
1,107
1,4347
1,523
1,6685
1,3124
1,4874
1,1008
1,3894
1
1,1
1,2
1,3
1,4
1,5
1,6
1,7
FACTOR OF SAFETY
b
a

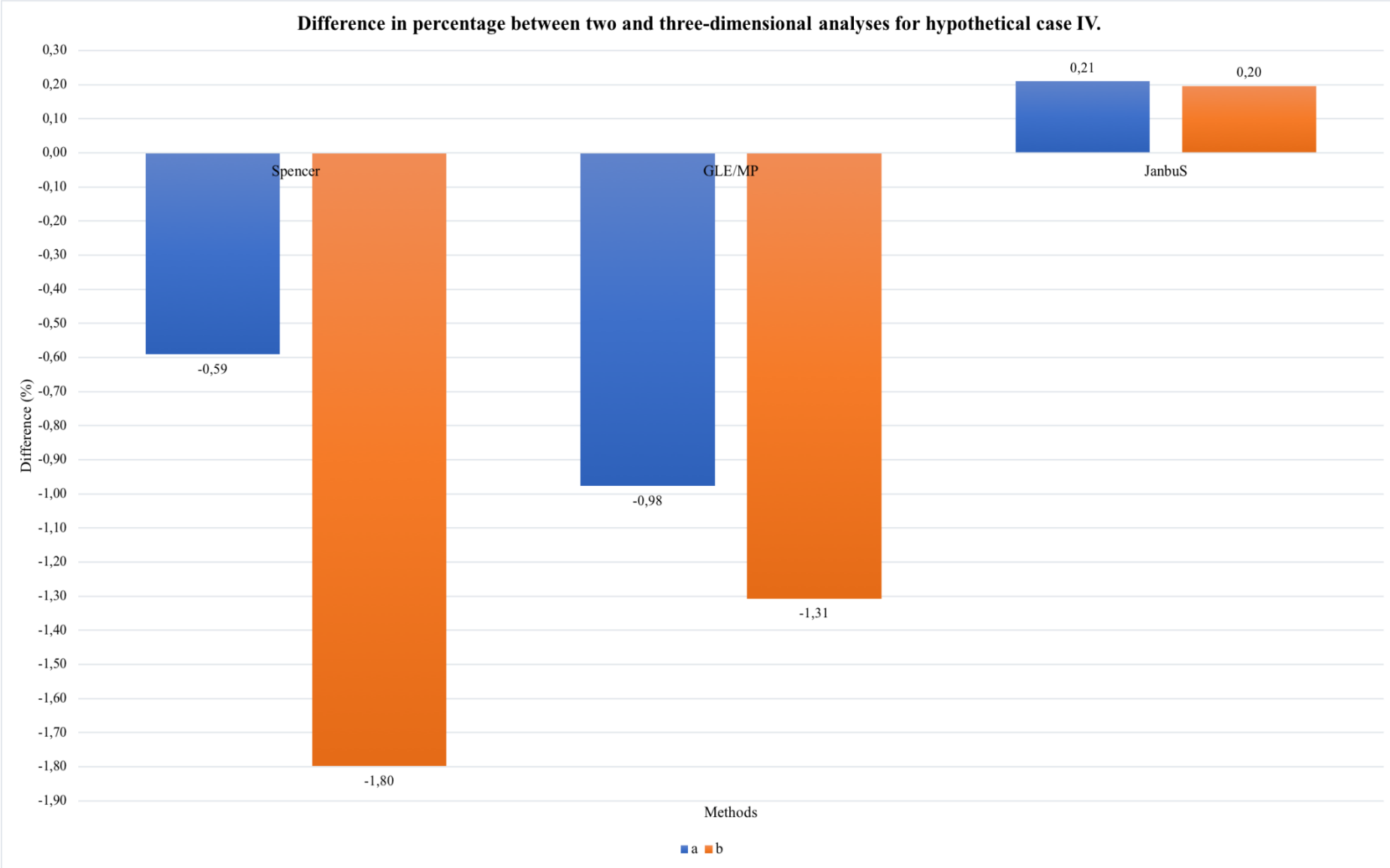
APPENDIX – 22


Results of the three-dimensional analyses for the hypothetical case IV.
1,6
1,5
1,4
1,3
1,2
1,1
1,0
0,9
0,8
0,7
0,6
0,5
Factor of safety
a
b
Scenario
Janbu's Simplified
Spencer
GLE/MP

APPENDIX – 23


Computed safety factors in 2D and 3D for the hypothetical case IV.
1,6
1,55
1,5
1,45
1,4
1,35
1,3
1,25
1,2
1,15
1,1
1,05
1
0,95
0,9
0,85
0,8
Factor of safety
a
b
Scenario
Spencer 3D
Spencer 2D
GLE/MP 3D
GLE/MP 2D
JanbuS 3D
JanbuS 2D

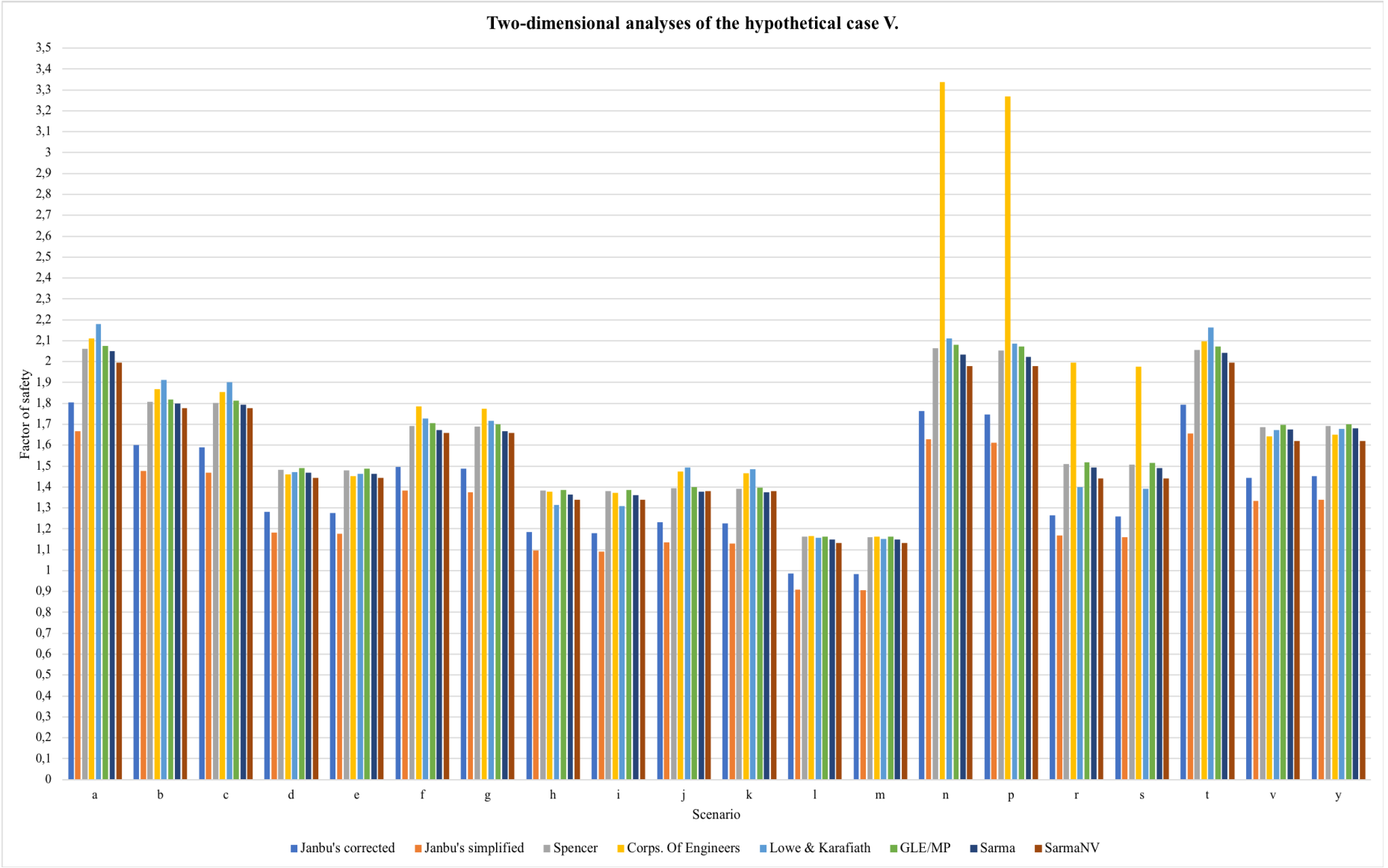
APPENDIX – 24


Difference in percentage between two and three-dimensional analyses for hypothetical case IV.
0,30
0,20
0,10
0,00
-0,10
-0,20
-0,30
-0,40
-0,50
-0,60
-0,70
-0,80
-0,90
-1,00
-1,10
-1,20
-1,30
-1,40
-1,50
-1,60
-1,70
-1,80
-1,90
Difference (%)
Spencer
GLE/MP
JanbuS
-0,59
-1,80
-0,98
-1,31
0,21
0,20
Methods
a
b

APPENDIX – 25

Scenario	JanbuC	JanbuS	Spencer	Corps. of Engineers	Lowe & Karafiath	GLE/MP	Sarma	SarmaNV
a	1.8053	1.6658	2.0625	2.1108	2.1790	2.0757	2.0490	1.9949
b	1.6001	1.4764	1.8079	1.8671	1.9116	1.8178	1.8005	1.7781
c	1.5902	1.4672	1.8026	1.8551	1.8999	1.8136	1.7948	1.7781
d	1.2805	1.1814	1.4828	1.4589	1.4702	1.4893	1.4676	1.4425
e	1.2751	1.1765	1.4802	1.4528	1.4636	1.4870	1.4641	1.4425
f	1.4964	1.3832	1.6922	1.7853	1.7282	1.7048	1.6715	1.6599
g	1.4872	1.3747	1.6894	1.7734	1.7177	1.7006	1.6658	1.6599
h	1.1850	1.0954	1.3817	1.3775	1.3142	1.3870	1.3633	1.3384
i	1.1802	1.0910	1.3788	1.3719	1.3093	1.3852	1.3604	1.3384
j	1.2309	1.1358	1.3939	1.4726	1.4929	1.3988	1.3785	1.3799
k	1.2248	1.1302	1.3905	1.4648	1.4853	1.3967	1.3754	1.3799
l	0.9852	0.9091	1.1617	1.1655	1.1558	1.1624	1.1497	1.1329
m	0.9822	0.9063	1.1601	1.1618	1.1523	1.1619	1.1480	1.1329
n	1.7644	1.6280	2.0627	3.3365	2.1094	2.0794	2.0341	1.9778
p	1.7466	1.6115	2.0517	3.2698	2.0849	2.0717	2.0215	1.9778
r	1.2653	1.1675	1.5099	1.9943	1.4007	1.5173	1.4943	1.4420
s	1.2581	1.1608	1.5060	1.9767	1.3920	1.5144	1.4894	1.4420
t	1.7933	1.6547	2.0569	2.0962	2.1638	2.0708	2.0414	1.9949
v	1.4440	1.3324	1.6872	1.6432	1.6715	1.6964	1.6760	1.6203
y	1.4506	1.3385	1.6918	1.6507	1.6788	1.6991	1.6806	1.6203

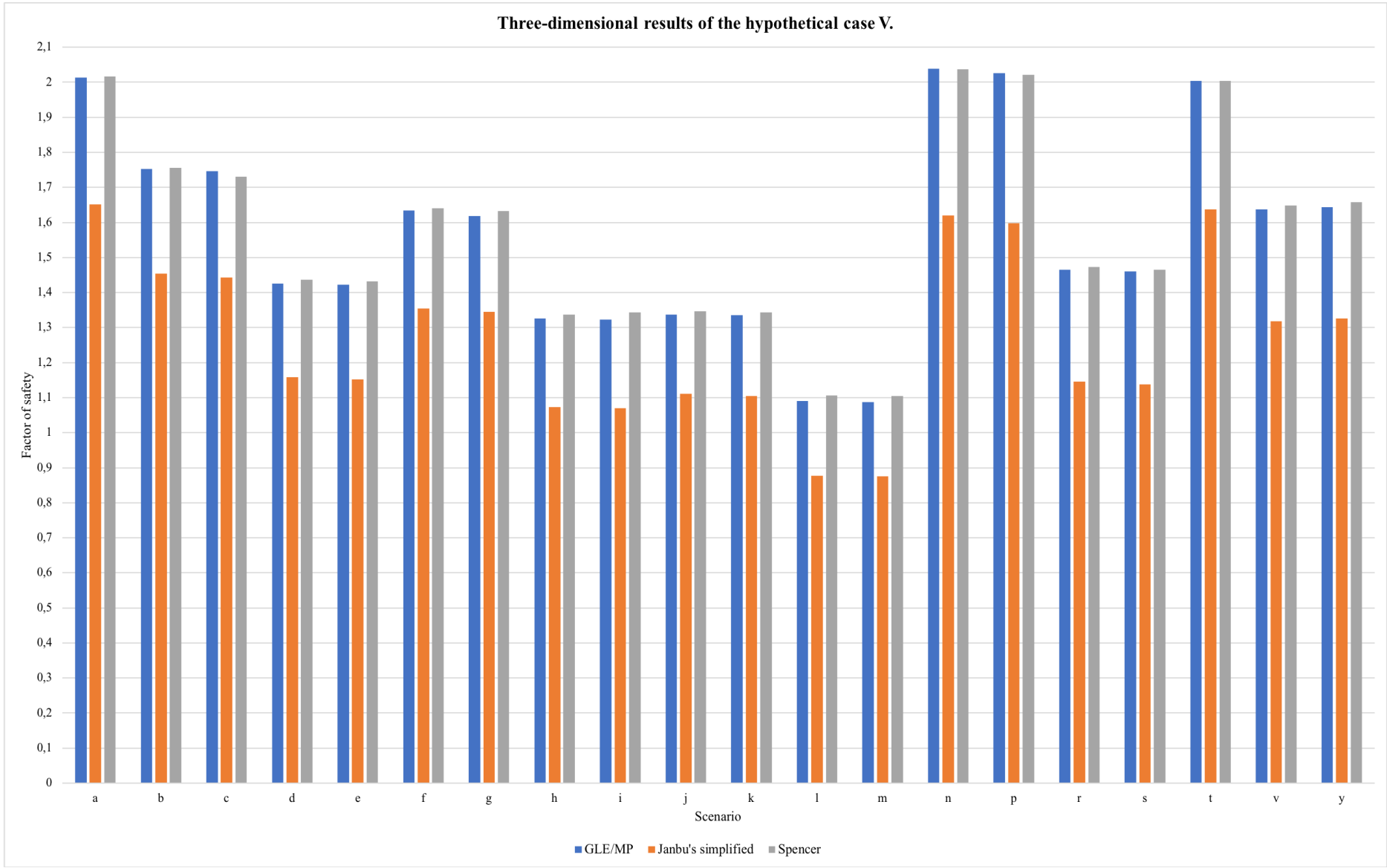
APPENDIX - 26


Two-dimensional analyses of the hypothetical case V.
Factor of safety
3,5
3,4
3,3
3,2
3,1
3
2,9
2,8
2,7
2,6
2,5
2,4
2,3
2,2
2,1
2
1,9
1,8
1,7
1,6
1,5
1,4
1,3
1,2
1,1
1
0,9
0,8
0,7
0,6
0,5
0,4
0,3
0,2
0,1
0
a
b
c
d
e
f
g
h
i
j
k
l
m
n
p
r
s
t
v
y
Scenario
Janbu's corrected
Janbu's simplified
Spencer
Corps. Of Engineers
Lowe & Karafiath
GLE/MP
Sarma
SarmaNV

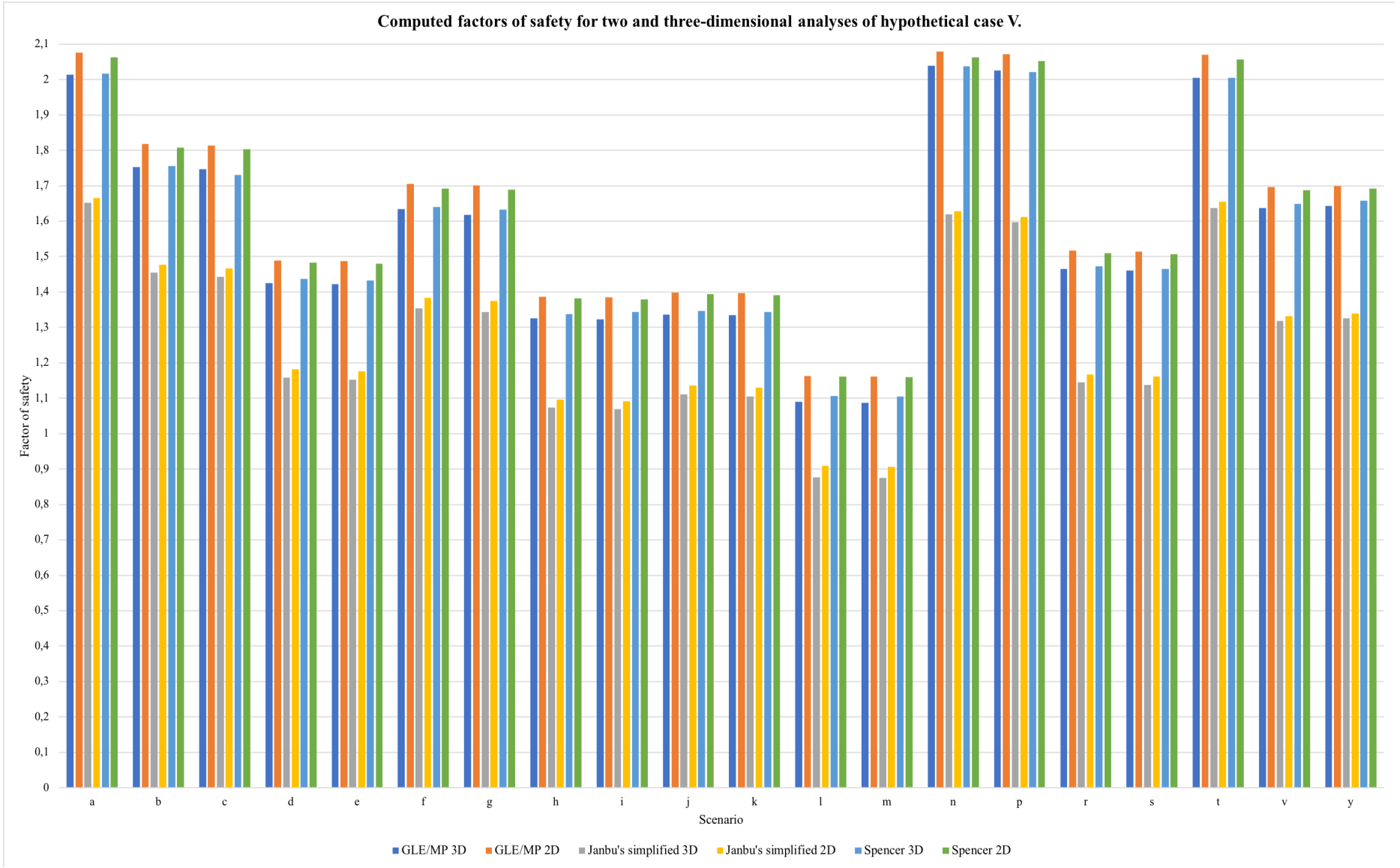
APPENDIX – 27

Scenario	GLE/MP	Janbu's simplified	Spencer
a	2.0138	1.6513	2.0166
b	1.7528	1.4543	1.7561
c	1.7464	1.4431	1.7301
d	1.4250	1.1578	1.4364
e	1.4222	1.1525	1.4318
f	1.6336	1.3536	1.6403
g	1.6181	1.3441	1.6320
h	1.3259	1.0737	1.3370
i	1.3234	1.0695	1.3431
j	1.3365	1.1102	1.3467
k	1.3349	1.1045	1.3429
l	1.0903	0.8769	1.1066
m	1.0877	0.8751	1.1047
n	2.0389	1.6196	2.0373
p	2.0262	1.5972	2.0208
r	1.4651	1.1453	1.4729
s	1.4608	1.1380	1.4652
t	2.0044	1.6370	2.0042
v	1.6370	1.3187	1.6487
y	1.6430	1.3259	1.6572

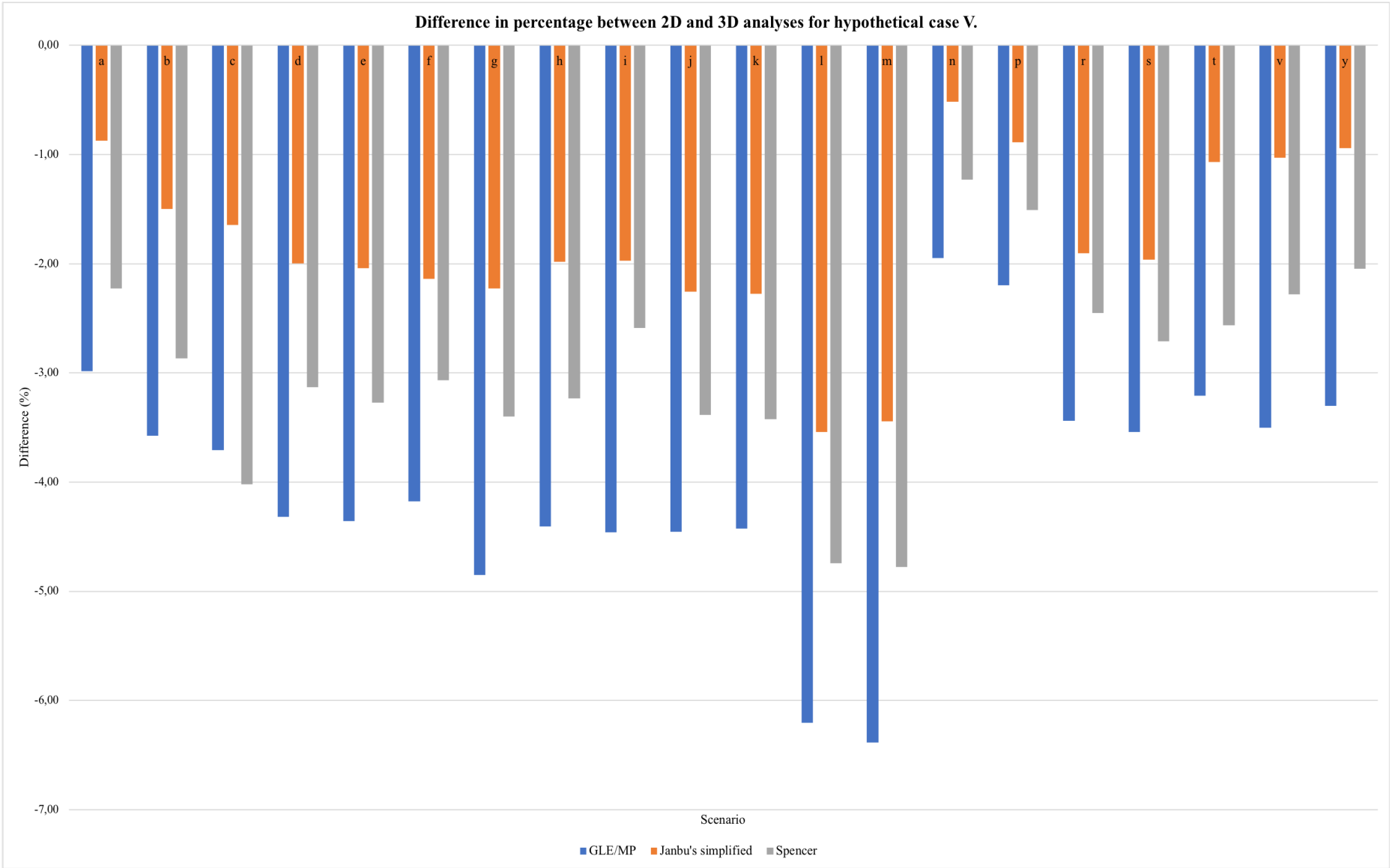
APPENDIX – 28


Three-dimensional results of the hypothetical case V.
Factor of safety
2,1
2
1,9
1,8
1,7
1,6
1,5
1,4
1,3
1,2
1,1
1
0,9
0,8
0,7
0,6
0,5
0,4
0,3
0,2
0,1
0
a
b
c
d
e
f
g
h
i
j
k
l
m
n
p
r
s
t
v
y
Scenario
GLE/MP
Janbu's simplified
Spencer

APPENDIX – 29


Computed factors of safety for two and three-dimensional analyses of hypothetical case V.
Factor of safety
2,1
2
1,9
1,8
1,7
1,6
1,5
1,4
1,3
1,2
1,1
1
0,9
0,8
0,7
0,6
0,5
0,4
0,3
0,2
0,1
0
a
b
c
d
e
f
g
h
i
j
k
l
m
n
p
r
s
t
v
y
Scenario
GLE/MP 3D
GLE/MP 2D
Janbu's simplified 3D
Janbu's simplified 2D
Spencer 3D
Spencer 2D

APPENDIX – 30


Difference in percentage between 2D and 3D analyses for hypothetical case V.
0,00
-1,00
-2,00
-3,00
-4,00
-5,00
-6,00
-7,00
Difference (%)
a
b
c
d
e
f
g
h
i
j
k
l
m
n
p
r
s
t
v
y
Scenario
GLE/MP
Janbu's simplified
Spencer

CURRICULUM VITAE

Credentials

Name. Surname	:	Bekir Salih Fırıncıoğlu
Place of Birth	:	Nicosia/TRNC
Marital Status	:	Single
E-mail	:	bekir.firincioglu@yahoo.com
Address	:	Manolya street No: 11 Bogazköy/Kyrenia TRNC

Education

Middle & High school:		19 Mayıs Türk Maarif Koleji
BSc.	:	Geological Engineering/Hacettepe University
MSc.	:	Geological Engineering/Hacettepe University

Foreign Languages

English (Advanced level)

Work Experience

Intern Engineer at: TRNC Geology and Mining Department 06.2015 – 08.2015
Geoteam Ltd. Şti 06.2015 – 08.2015
Geo Survey Ltd. Şti. 06.2015 – 08.2015

Areas of Experiences

Determination of stability and design of slopes. Limit equilibrium procedure. Geotechnical laboratory techniques. Intermediate level GIS applications.

Projects and Budgets

Fast funding project under Hacettepe University Scientific Research Projects Coordination Unit. Project#: FHD-2018-16818

HACETTEPE UNIVERSITY
GRADUATE SCHOOL OF SCIENCE AND ENGINEERING
THESIS/DISSERTATION ORIGINALITY REPORT

HACETTEPE UNIVERSITY
GRADUATE SCHOOL OF SCIENCE AND ENGINEERING
TO THE DEPARTMENT OF Geological Engineering

Date: 29/05/2018

Thesis Title / Topic: AN INVESTIGATION ON THE APPLICATION OF TWO AND THREE DIMENSIONAL LIMIT EQUILIBRIUM ANALYSES IN SLOPE STABILITY

According to the originality report obtained by myself/my thesis advisor by using the *Turnitin* plagiarism detection software and by applying the filtering options stated below on 29/05/2018 for the total of 177 pages including the a) Title Page, b) Introduction, c) Main Chapters, d) Conclusion sections of my thesis entitled as above, the similarity index of my thesis is 9 %.

Filtering options applied:

1. Bibliography/Works Cited excluded
2. Quotes excluded / ~~included~~
3. Match size up to 5 words excluded

I declare that I have carefully read Hacettepe University Graduate School of Sciene and Engineering Guidelines for Obtaining and Using Thesis Originality Reports; that according to the maximum similarity index values specified in the Guidelines, my thesis does not include any form of plagiarism; that in any future detection of possible infringement of the regulations I accept all legal responsibility; and that all the information I have provided is correct to the best of my knowledge.

I respectfully submit this for approval.

Date and Signature

29.05.2018

Name Surname:	Bekir Salih Fırıncıoğlu
Student No:	N16124161
Department:	Geological Engineering
Program:	Geological Engineering
Status:	☒ Masters ☐ Ph.D. ☐ Integrated Ph.D.

ADVISOR APPROVAL

APPROVED.

(Prof. Dr. Murat Ercanoğlu)